POSGRADO EN CIENCIAS APLICADAS

A Multidisciplinary Study of Carbon Nanotube Structures: From Inorganic to Biological Systems

Tesis que presenta

Ana Laura Elías Arriaga

Para obtener el grado de

Doctor en Ciencias Aplicadas

En la opción de

Nanociencias y Nanotecnología

Codirectores de la Tesis:

Dr. Mauricio Terrones Maldonado

Dr. Humberto Terrones Maldonado

San Luis Potosí, S.L.P., 16 de julio de 2006

IPICYT

Constancia de aprobación de la tesis

La tesis "*A Multidisciplinary Study of Carbon Nanotube Structures: From Inorganic to Biological Systems*" presentada para obtener el Grado de Doctora en Ciencias Aplicadas en la opción de Nanociencias y Nanotecnología fue elaborada por **Ana Laura Elías Arriaga** y aprobada el **10 de julio de 2006** por los suscritos miembros de la División de Materiales Avanzados para la Tecnología Moderna quienes fungieron como supervisores de dicho trabajo.

Prof. Dr. Mauricio Terrones Maldonado
(Codirector de la tesis)

Prof. Dr. Humberto Terrones Maldonado
(Codirector de la tesis)

IPICYT

Instituto Potosino de Investigación Científica y Tecnológica, A.C.

Acta de Examen de Grado

COPIA CERTIFICADA

El Secretario Académico del Instituto Potosino de Investigación Científica y Tecnológica, A.C., certifica que en el Acta 016 del Libro Primero de Actas de Exámenes de Grado del Programa de Doctorado en Ciencias Aplicadas en la opción de Nanociencias y Nanotecnología está asentado lo siguiente:

En la ciudad de San Luis Potosí a los 16 días del mes de julio del año 2006, se reunió a las 17:00 horas en las instalaciones del Instituto Potosino de Investigación Científica y Tecnológica, A.C., el Jurado integrado por:

Dr. Humberto Terrones Maldonado	**Presidente**	**IPICYT**
Dr. Mauricio Terrones Maldonado	**Secretario**	**IPICYT**
Dr. Emilio Muñoz Sandoval	**Sinodal**	**IPICYT**
Dr. Pulickel M. Ajayan	**Sinodal externo**	**Resselaer Polytechnic Institute**

a fin de efectuar el examen, que para obtener el Grado de:

DOCTORA EN CIENCIAS APLICADAS
EN LA OPCIÓN DE NANOCIENCIAS Y NANOTECNOLOGÍA

sustentó la C.

Ana Laura Elías Arriaga

sobre la Tesis intitulada:

A Multidisciplinary Study of Carbon Nanotube Structures: From Inorganic to Biological Systems

que se desarrolló bajo la dirección de

Dr. Humberto Terrones Maldonado
Dr. Mauricio Terrones Maldonado

El Jurado, después de deliberar, determinó

APROBARLA

Dándose por terminado el acto a las 19:05 horas, procediendo a la firma del Acta los integrantes del Jurado. Dando fé el Secretario Académico del Instituto.

A petición de la interesada y para los fines que a la misma convengan, se extiende el presente documento en la ciudad de San Luis Potosí, S.L.P., México, a los 16 días del mes julio de 2006.

Dr. Marcial Bonilla Marín
Secretario Académico

L.C.C. Ivonne Lizette Cuevas Velez
Jefa del Departamento de Asuntos Escolares

INSTITUTO POTOSINO DE INVESTIGACIÓN CIENTÍFICA Y TECNOLÓGICA, A.C.
IPICYT
SECRETARIA ACADEMICA

A Multidisciplinary Study of Carbon Nanotube Structures: From Inorganic to Biological Systems

Abstract

The aerosol pyrolysis technique was used to produce carbon based nanostructures. Monocrystalline FeCo nanowires encapsulated inside multi-walled carbon nanotubes (MWNTs), centimeter-long strands of wide single walled carbon nanotubes (SWNTs), undoped MWNTs (PCMWNTs) and nitrogen doped multi walled carbon nanotubes (CN_x MWNTs) were fabricated. Strong capillary forces driven by the interaction of PCMWNTs and CN_x MWNTs with organic solvents produced self-assembled nanotube cellular foams. The toxicological effects of PCMWNTs and CN_x MWNTs in biological systems (mice and amoebas) were tested. CN_x MWNTs appeared to be more biocompatible than undoped MWNTs, which exhibited an amoebicidal condition. These results encourage further studies testing CNx MWNTs as drug deliveries and cell transporters. Other applications of the synthesized nanomaterials will be discussed, such as the usage of FeCo filled MWNTs in the fabrication of high density magnetic storage devices.

Key Words: FeCo alloys | Biocompatibility | Aerosol Pyrolysis | N-doped MWNTs | Cell Viability

Contents

List of Figures

1. Introduction

1.1 Identification of C_{60} and Carbon Nanotubes

Thirty years ago, Oberlin, Endo and Koyama [1], identified what they called filamentous growth of carbon and performed a high resolution transmission electron microscopy (HRTEM) analysis of those structures. The fibers consisted of concentric sheets of carbon, compared by these authors to "*the annual rings of a tree*". Each fiber had a hollow core in the inside with diameters ranging from 20 to 500 Å. They pyrolyzed mixtures of benzene and hydrogen at temperatures of c.a. 1100 °C and optimized the experimental parameters in order to obtain carbon filaments of less than 8000 Å (800 nm) in diameter; reaction time and benzene concentration were reduced, because these authors observed that an increase in those parameters increase the thickness of the carbon fibers. These authors were interested in those days in small diameter microfibers. Probably, they also provided the first image of a single walled carbon nanotube (SWNT) ever published (figure 1.1).

In the mid 80's, Kroto and coworkers [2] reported the discovery of a new carbon cage molecule named "Buckminsterfullerene", composed of 60 carbon atoms. These authors' goal was to synthesize in the laboratory long carbon chains (polyynes) which were observed in the interstellar space. In these experiments, a rotating graphite disk was the target of a pulsed laser beam of 30 to 40 mJ, with a wavelength of 532 nm. The target vaporization was carried out under a helium atmosphere (760 atm) which carried the carbon species that reacted to form carbon molecules. A time-of-flight mass spectrometer detected the novel molecular species; spectrum shown in figure 1.2. In the cluster mass distribution, the C_{60} signal was

clearly outstanding. The authors proposed that the existence of 6 and 5 memebered carbon rings collisions resulted in the formation of a perfect truncated icosahedros containing 60 vertices. Inspired in Buck-minster Fuller's domes, these authors proposed that the new C_{60} molecule should be named it "buckminsterfullerene". Their proposal was certain and Kroto, Curl and Smalley were awarded with the Nobel Prize in Chemistry for the discovery of the fullerenes in 1996.

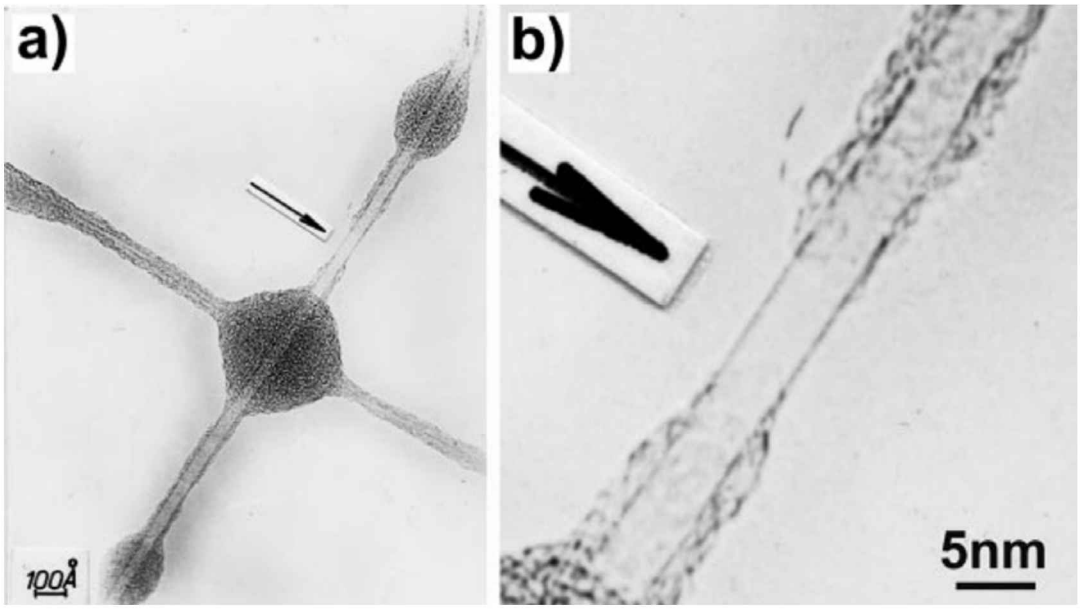

Fig. 1.1. *HRTEM images of two SWNTs produced by pyrolysis of benzene at 1100 °C. (a) First published HRTEM image of SWNTs ever. (b) Inset shows the a higher magnification image, depicting the SWNT and the amorphous-like material that partially cover it. The nanotube diameter is high, about 4 nm (obtained from Oberlin's report [1]).*

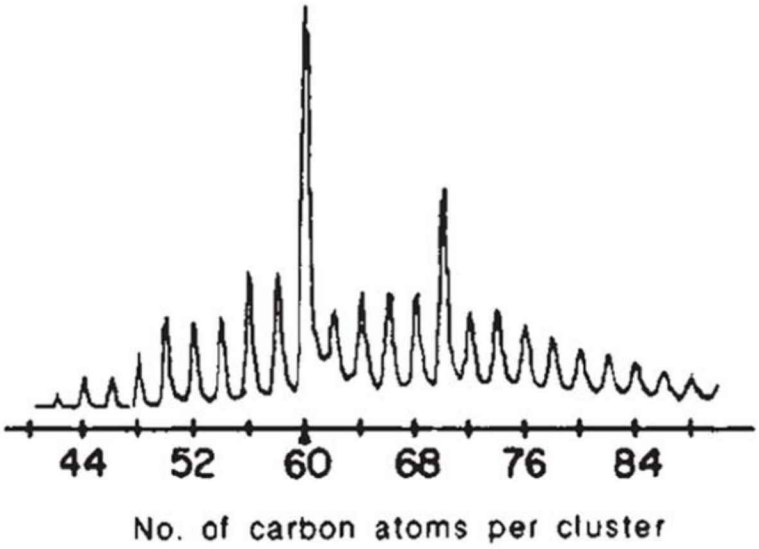

Fig. 1.2. *A time-of-flight mass spectrum of laser vaporized graphite in helium atmosphere, at 760 torr. C_{60} signal is outstanding and constituted the first evidence of the existence of fullerenes (obtained from Kroto's [2]).*

In 1990, Krätschmer and coworkers [3] reported the synthesis of a solid and new form of carbon based on C_{60} molecules. These authors demonstrated that carbon soot produced in a carbon arc experiment contained C_{60} molecules that could be dissolved in benzene. The C_{60}-benzene solution adopted a magenta color. C_{60} crystals obtained from this procedure were subsequently characterized using electron diffraction, time-of-flight mass spectroscopy, X-ray diffraction, TEM and infrared absorption spectroscopy [3]. This crystal is nowadays called fullerite and, together with graphite (figure 1.3a) and diamond (figure 1.3b), constitutes the third allotropic form of carbon. Fullerite has an fcc structure, decorated with C_{60} molecules and it is depicted in figure 1.3c.

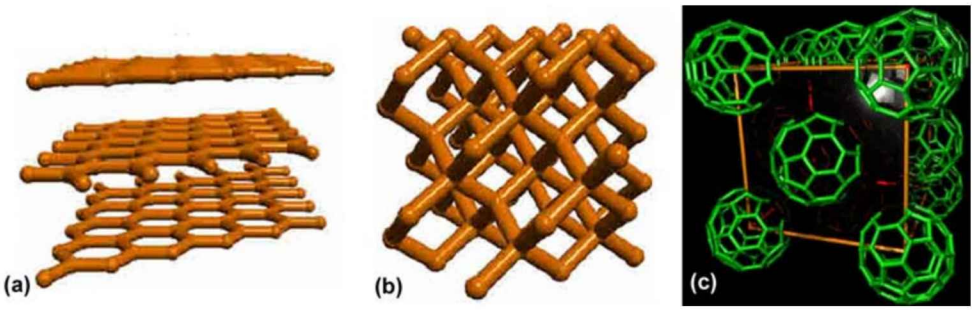

Fig. 1.3. *Molecular models of the three known allotropic forms of carbon. (a) Graphite. (b) Diamond. (c). Fullerite (Images obtained from Terrones's report [17])*

One year later, in 1991, Iijima [4] reported the electron microscopy characterization of what he called helical microtubules of graphitic carbon. Samples were synthesized by an arc discharge evaporation of carbon rods, in an Ar atmosphere and a pressure of 100 torr (similar to the experimental set up used for Krätschmer and coworkers [3] to obtain C_{60}). Figure 1.4 depicts a HRTEM of three different individual carbon nanotubes published by Iijima. The number of layers within the tubes was reported to vary from 2 to 50. The coaxial arrangement of these structures was confirmed by electron diffraction patterns that exhibited the hexagonal symmetry and strong (00ℓ) spots, corresponding to the spacing of graphitic cylinders.

A large scale production of multi-walled carbon nanotubes (MWNTs) was reported by Ebbesen and Ajayan [5] in 1992. These authors performed an arc discharge of graphite electrodes under a helium atmosphere. MWNTs were deposited on the cathode and an optimization of experimental parameters was carried out, using different inert gases, and applying various voltages and pressures. TEM characterization was used to analyze the samples obtained under different conditions. It was found that a pressure of 500 torr, a potential of 18 V (direct

current) under helium were the best conditions for obtaining high yields of MWNTs.

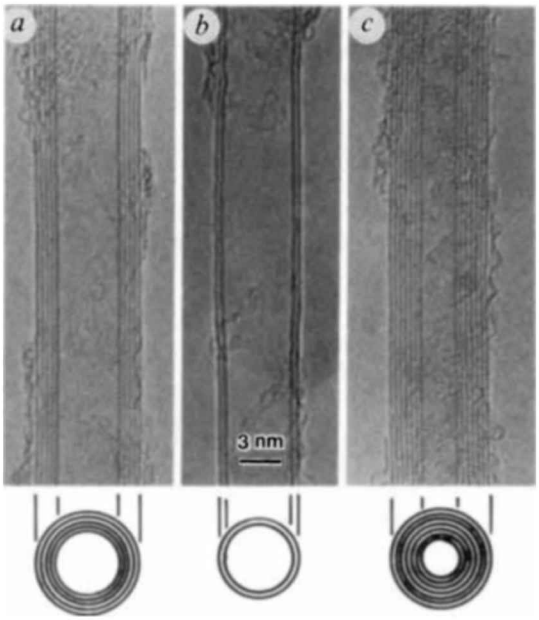

Fig. 1.4. *HRTEM images of MWNTs synthesized by arc discharge method in an Ar atmosphere. At the bottom of real images, schematics of them are shown, to exhibit the number of layers in each case. (a) 5-walled carbon nanotube, with an outer diameter of 6.7 nm. (b) Double walled carbon nanotube, whit an outer diameter of 5.5 nm. (c) 7-walled carbon nanotube, with an inner diameter of 2.2 nm (obtained from Iijima's report [3]).*

Soon after, Iijima and Ichihashi [6] reported the synthesis of SWNTs. These authors used the carbon arc chamber with a 10 mm graphitic anode and a 20 mm cathode with a piece of iron located in the core. The experiment was carried out in a 10 torr methane atmosphere [6]. They generated an arc by applying a voltage of 20 V and a direct current of 200 A. These authors proposed that iron melted and reacted to form iron carbide particles above the cathode, simultaneously with the carbon vaporization. The SWNT sample was collected on the electrodes's surface and was analyzed with TEM and electron diffraction. Figure 1.5 exhibits a representative TEM image of SWNTs, entangled with iron carbide particles. The diameters of

individual nanotubes were measured. 1 nm was found to be the average diameter within the nanotubes. These authors believed that iron catalyzed the SWNT growth, although they could not find those catalytic particles at the tips of nanotubes.

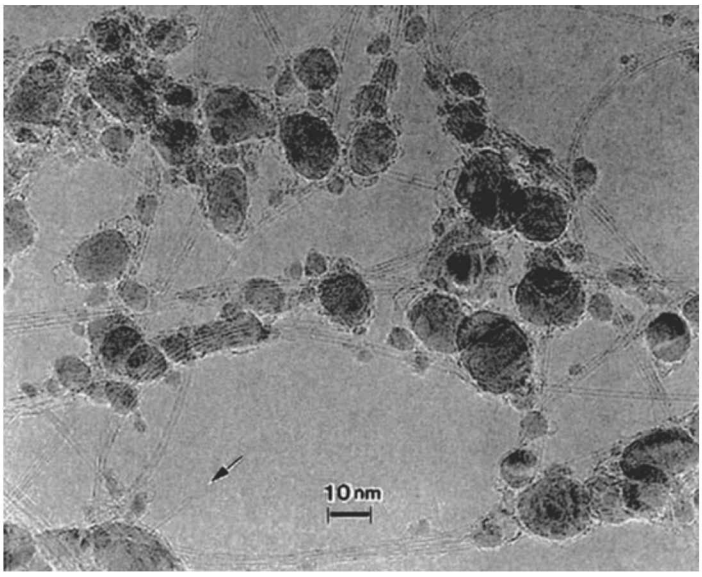

Fig. 1.5. *TEM image of SWNTs produced by the arc discharge technique. SWNTs are entalngled with cementie particles, which assist the growth. The arrow indicates the termination of an individual SWNT (obtained from Iijima's report [4]).*

1.2 Structure and Properties of Carbon Nanotubes

In order to analyze the structure of SWNTs, researchers have considered them as rolled graphene sheets [7-9]. The chirality of SWNTs can be determined in terms of the chiral vector C_n,

$$\mathbf{C}_n = m\mathbf{a}_1 + n\mathbf{a}_2$$

where $\mathbf{a}_1$ and $\mathbf{a}_2$ vectors and lattice points (m, n) are defined in figure 1.6. The rolling direction of the graphene sheet, and diameter of a SWNT, are determined by this chiral vector. In order to form a tube, the lattice point (m, n) need to be superimposed with the origin (0,0) (see figure 1.6). When the C-C bonds are located perpendicular to the nanotube axis, the nanotube is called "*armchair*". In order to obtain an armchair SWNT, the origin and a lattice point (m, n) where $m = n$ or $m = -2n$, have to be superimposed. For C-C bonds located parallel to the SWNT axis, the nanotube is called "*zigzag*". In terms of the chiral vector, a zigzag tube is formed by superimposing the lattice point (m, *0*) with the origin (see figure 1.6). All other possible configurations are called chiral, whereas the previous two (armchair and zigzag) are known as non-chiral. Figure 1.7 depicts examples of the three types of nanotubes described above: figure 1.7a exhibits an armchair SWNT, figure 1.7b depicts a zigzag nanotube and figure 1.7c provides an example of a chiral SWNT.

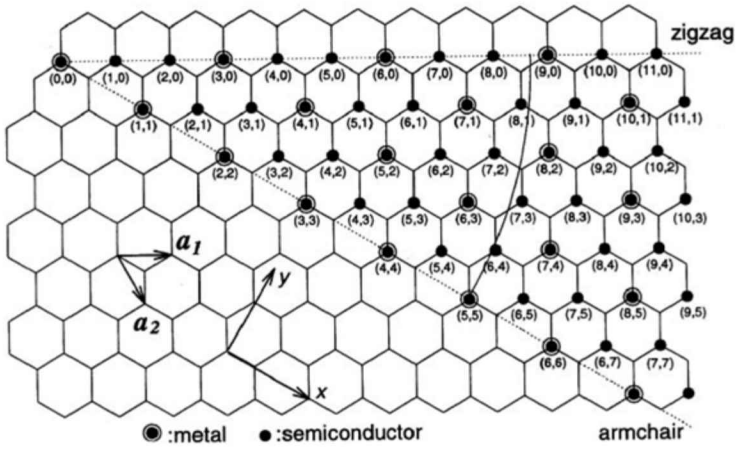

Fig. 1.6. *A graphene sheet that can be rolled in different ways. A chiral vector C_n is a convention that indicates any given lattice point and it is defined in terms of two unitary vectors a_1 and a_2. The scheme also provides information on the electronic properties of nanotubes, being metallic or semiconductor, depending on their chirality (obtained from Terrones' review [7]).*

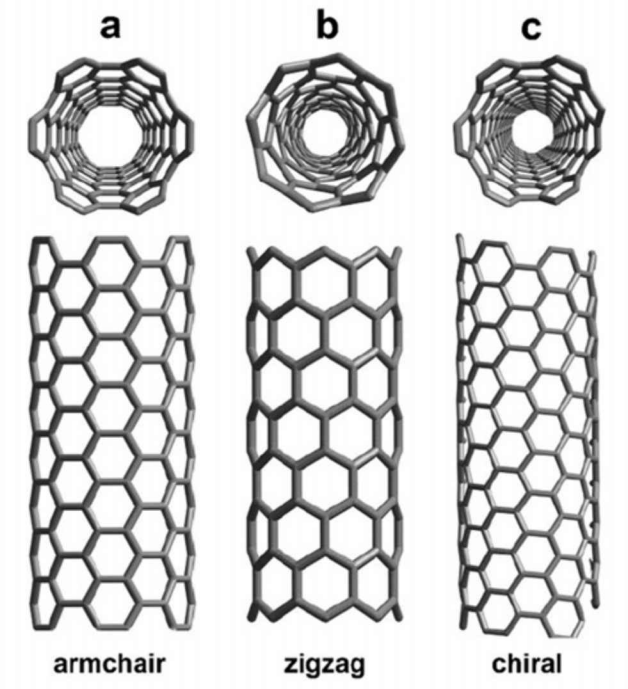

Fig. 1.7. *Schematic molecular model of three types of nanotubes. (a) Arm chair nanotube, where C-C bonds are normal to the tube axis. (b) Zigzag nanotube, where C-C bonds are parallel to the nanotube axis. (c) Chiral configuration (obtained from Terrones' review [7]).*

Multi-walled carbon nanotubes consist on several concentric cylinders made of graphene sheets. Figure 1.8 exhibits a molecular model of both structures.

Following the publication by Iijima in 1991, theoretical predictions and measurements of their properties started. One of the first calculations related to the electronic properties of SWNTs was reported by Hamada et al. [8]. These authors performed tight binding calculations, and calculated the total energy and band structures of different types of nanotubes. They found metallic or semiconductor behaviors with SWNTs of different chiralities. Armchair nanotubes were found to be metallic, whereas zigzag nantoubes could exhibit a narrow band-gap or a moderate semiconductor band gap, depending on their diameter. Simultaneously, Saito and coworkers [8] studied the electronic structure of SWNTs with different chiralities. Using the tight-binding framework, they calculated band structures and

studied their instabilities, and demonstrated that nanotubes could be either metallic or semimetallic, in agreement with Hamada's report [8].

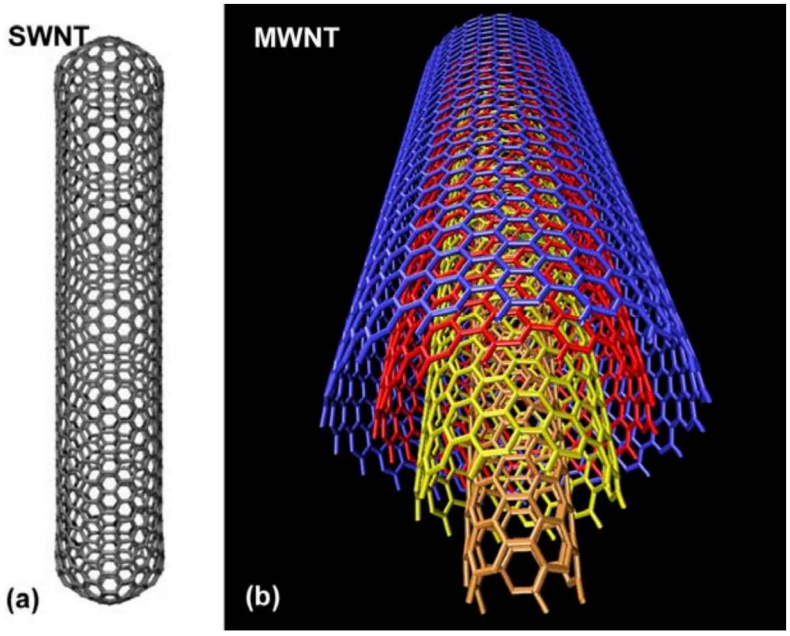

Fig. 1.8 *(a) Molecular model of an armchair SWNT [16]. (b) Molecular model of a MWNT, exhibiting four concentric graphene layers [27].*

Electronic structure calculations [7-9] allowed to determine the metallicity of nanotubes in terms of the lattice point (m, n) as follows:

$$(2m + n) / 3 = \textbf{integer}$$

Wildöer and coworkers [10], experimentally tested the electronic properties of individual SWNTs using scanning tunneling microscopy (STM) and spectroscopy (STS). As established by previous theoretical calculations [7-9], some SWNTs were metallic while others semiconducting. SWNT samples were synthesized by the laser vaporization technique. The STM imaging of SWNTs was capable of showing the chirality associated with each carbon nanotube tested, providing diameter and

wrapping angle. Figure 1.9 depicts 5 different analyzed nanotubes named no.10, no.11, no.1, no.7 and no.8 [10]. The dashed arrow represents the chiral vector C_n, defined previously, whereas the solid arrow represents the nearest neighbor carbon atoms row, which appear in the images as black dots. SWNT No.10 has a 1.3 nm diameter and its lattice point corresponds to (11, 7); a chiral nanotube. N Nanotubes No.11 and no.1 are also chiral nanotubes. A zigzag SWNT, named no.7, is depicted in figure 6. An armchair nanotube is also shown (named no.8) and a hexagonal lattice scheme was superimposed on this image to clarify its hexagonal structure.

STS was used to record the current (I) as a function of the bias voltage (V) applied to the sample, and the differential conductance (dI/dV) was shown; a value that is proportional to the density of states (DOS). Form the chiral nanotubes analyzed, two main categories were found : one with a well defined gap of c.a. 0.5-0.6 eV and other with much larger gaps, such as 1.7-2.0 eV. The first group corresponds to the theoretically predicted gaps of semiconducting tubes, whereas the second group corresponded to predicted metallic tubes. Simultaneously, Lieber's group [11] reported a very similar study related to the electronic properties and atomic structure of SWNTs, which was in agreement with Wildöer's [10] report and theroretical predictions [8-9].

The mechanical properties of carbon nanotubes have also been tested [12-13]. Treacy et al. [12], reported for the first time an experimental estimation of the Young's modulus of an individual MWNT syntesized by the arc discharge method [5]. A TEM assisted method was used by these authors to determine the Young's modulus as a function of the MWNT intrinsic thermal vibrations. Bundles of MWNTs were attached to the edge of a nickel ring to perform TEM observations. The free tips of the bundle were shredded with tweezers to isolate some nanotubes. At room temperature, the free tip of MWNTs was vibrating, thus focus was not

possible. When increasing the temperature to 600 K, the tips became more blurried. These authors related the Young's modulus (Y) and the vibration energy (W_n) to the amplitude of the tip vibration. They found and average Y value of 1.8 TPa, which could be 3 orders of magnitude higher than the values for carbon fibers.

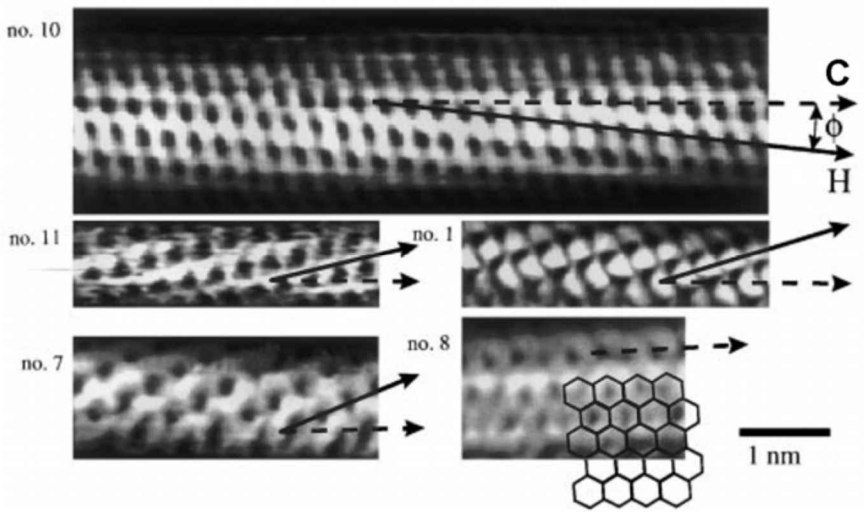

Fig. 1.9. *STM images of 5 individual SWNTs which exhibit the chirality of each of them. The dashed arrow represents the chiral vector C_n, and the solid arrow represent the nearest neighbor carbon atoms row. No.10 has a 1.3 n, diameter and its lattice point is (11, 7), being a chiral nanotube. No.11 and no.1 are also chiral nanotubes. No.7 is a zigzag SWNT, whereas an armchair nanotube is depicted in no.8 and a hexagonal lattice scheme was superimposed (obtained from Wildöer's report [10]).*

Falvo and coworkers [13] reported the AFM tip assisted bending and buckling of MWNTs under large strain. In this study, carbon nanotubes were placed onto mica substrates and the authors applied lateral stresses that produced bends and translations to the tubes. Some carbon nanotubes were bent into many configurations. MWNTs resulted to be extraordinarily flexible under large strains, and did not fail under repeating bending, thus these authors demonstrated that MWNTs posses an outstanding flexural strength.

Both MWNTs and SWNTs have also been subject to thermal properties characterization [14-15]. Both theoretical and experimental approaches have been obtained by Hone et al. [14], who measured the thermal conductivity $\kappa(T)$ of SWNT ropes form 350 to 8 K. The tested SWNT samples were synthesized by arc discharge method, with a Ni and Y catalyst. The obtained SWNT bundles were composed by hundreds of several micron long SWNTs, exhibiting a diameter of 1.4 nm. SWNT bundles were mounted in series with a constant rod and differential thermocouples were attached to the nanotubes. These authors affirmed that the thermal conductivity is dominated by phonons at all temperatures, this indicated by the ratio of thermal to electrical conductance from the different samples. Figure 1.10 depicts the $\kappa(T)$ against T. The thermal conductivity decreases smoothly form 350 to 8 K, but a change in the slope appears at about 30 K. Below this value, the behavior is linear and the magnitude of $\kappa(T)$ implied an energy-independent of the phonon mean free path (*c.a.* 0.5 to 1.5 μm).

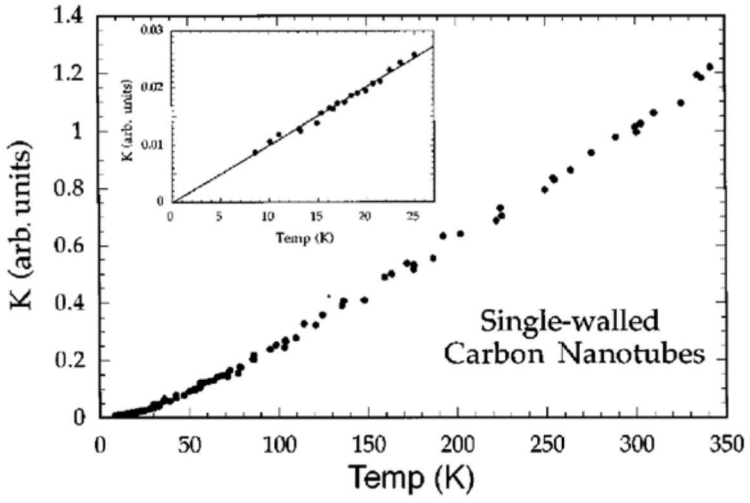

Fig. 1.10. *Thermal conductivity κ(T) in SWNT bundles, which decreases smoothly form 350 to 8 K, but changes at about 30 K. Inset show the behavior of thermal conductivity at low temperatures. The solid line corresponds to fitted curve, to extrapolate κ(T) at 0 K (obtained from Hone's [14]).*

Kim and coworkers [15] designed a device to measure thermal properties on individual MWNTs. The suspended a micro-device that was fabricated on an etched nitride/silicon oxide/silicon multilayer (figure 1.11). The device possessed silicon nitride islands suspended with silicon nitride beams (200 μm long). A Pt thin film resistor served as a heater in each island. After the complete fabrication of the micro-device, MWNTs were placed on it and bridged between two islands. The inset in figure 1.11, exhibits a higher magnification of the central area of the device, were a MWNT was placed. The thermal conductivity at room temperature is larger than 3000 W/K m, which is two orders of magnitude higher than previous values obtained from macroscopic MWNT samples. This value is in agreement with theoretical predictions [15]. In addition, the thermoelectric power displayed a linear temperature dependence at room temperature.

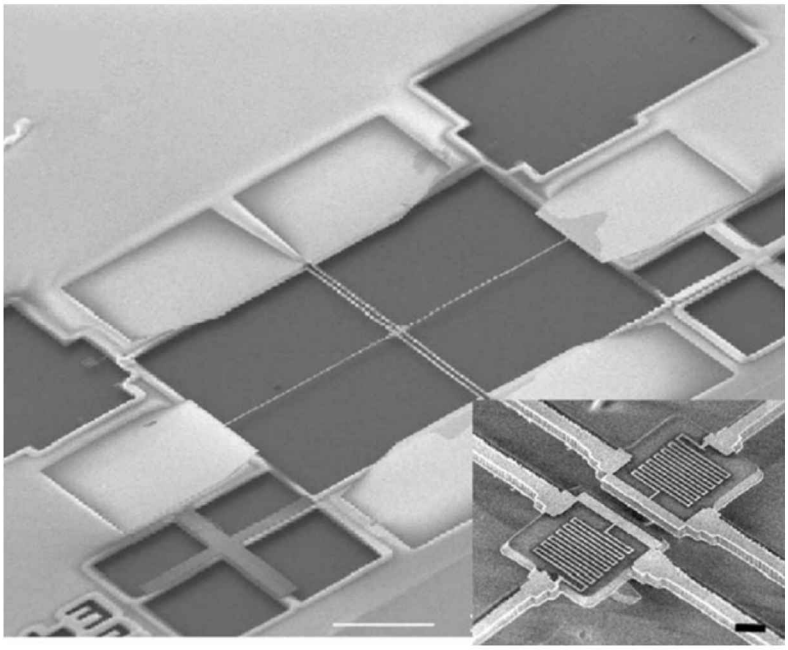

Fig. 1.11. *SEM image of a measurement device of individual MWNT's thermal properties, on individual MWNTs. Inset presents a higher magnification image, exhibiting the central area of the device, where a MWNT is suspended (obtained from Kim's [15]).*

1.3 Methods for producing Carbon Nanotubes

The most important methods for producing SWNTs and MWNTs are: arc discharge, laser vaporization, electrolysis and hydrocarbon pyrolisis [16]. The arc discharge method was employed by Iijima when he identified carbon nanotubes in 1991 [4]. An experimental set up is depicted in figure 1.12. A high direct current travels through a pair of graphitic electrodes. During the experiment, the electrodes are separated by a constant distance of *c.a.* 1 or 2 mm, which was controlled in order to avoid the cease of the arc. The anode is consumed and the material is deposited on the cathode. The experiment is carried out under a helium atmosphere at a pressure of 500 torr. A water cooling system roughly controls the chamber's temperature. After the experiment, the chamber is allowed to cool to room temperature and is opened to extract the cathode material.

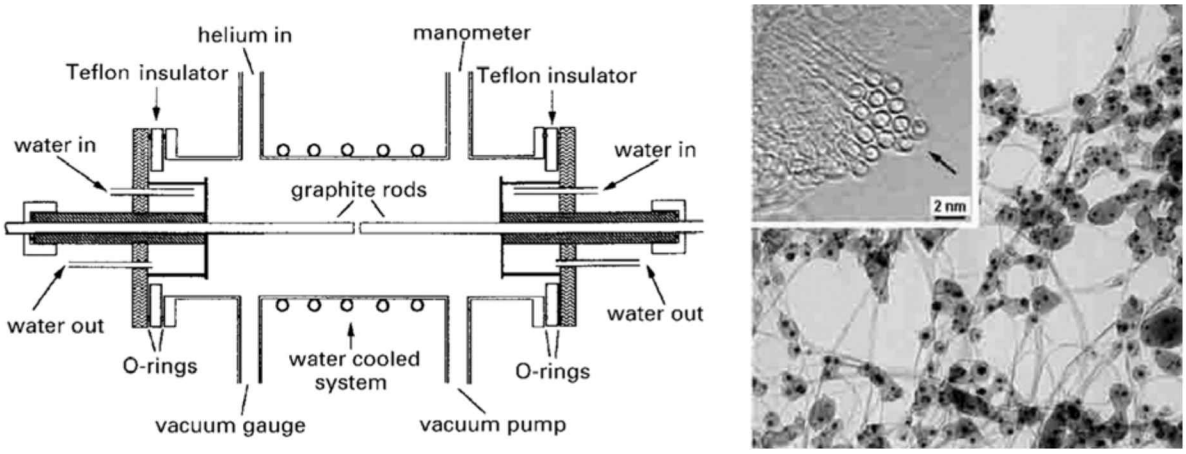

Fig. 1.12. *Left. An schematic image of the arc discharge experimental set up. Two graphitic rods serve as electrodes and remain separated by 1 or 2 mm. The anode is consumed and the produced nanomaterial is deposited on the cathode. The chamber has a pressure of 500 torr ad the atmosphere is controlled (He). A water cooling system controls the chamber's temperature. Right. TEM image of arc discharge produced SWNTs (obtained from Terrones' review [16]).*

For producing SWNTs, a metal catalyst is required inside the graphite anode. Ususally, the electrode is dug and filled with a carbon-metal powder compound. Fe, Co, Ni and Y are commonly used to synthesize SWNTs.

SWNTs and MWNTs can also be synthesized by the laser vaporization method [10]. The experimental set up is depicted in figure 1.13. A graphite target is vaporized by a powerful laser (NdY) placed in one end of a silica tube [16]. The silica tube is placed in a furnace at a temperature of 1200 °C. A Cu cooled needle is placed at the other end of the silica tube, which collects the produced nanotubes. Again, for synthesizing SWNTs, a metal responsible of catalyzing the growth needs to be present. Commonly, a graphite-Co-Ni target is used [10].

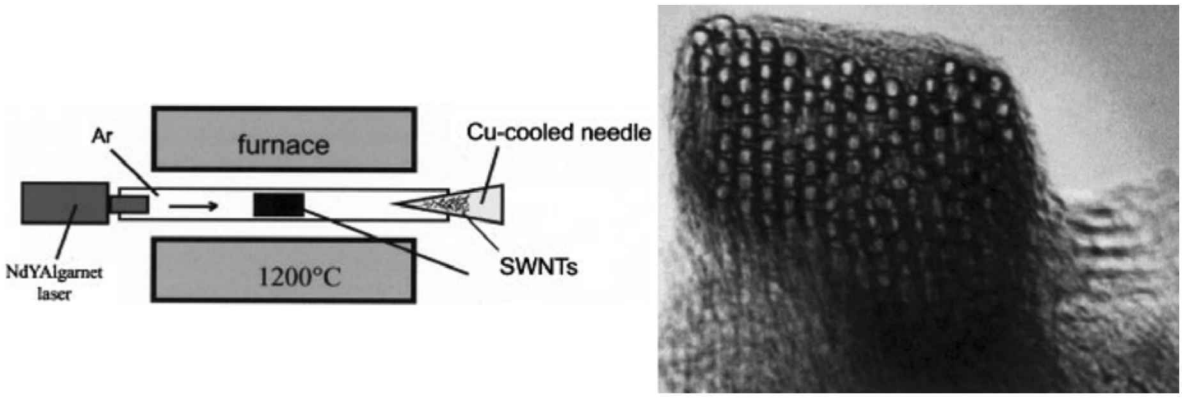

Fig. 1.13. *Left. Schematic of the laser vaporization method for producing carbon nanotubes. A graphite target placed at the center of the device is vaporized by a laser. A silica serves as support and the temperature of reaction is c.a. 1200 °C. A Cu needle placed at the end of the silica tube collects the produced nanotubes. Right. A TEM image of SWNTs produced by this technique (obtained from Terrones' review [16]).*

Electrolysis is another versatile technique that can be used to produce mainly MWNTs [16]. Here, graphite electrodes are immersed in molten LiCl under an Ar atmosphere and a potential was applied between two electrodes. A schematic

diagram of the experimental set up is shown in figure 1.14. After the electrolysis, the system was allowed to cool at room temperature. Subsequently, the salt is dissolved in distilled water and filtered to separate the nanotube material.

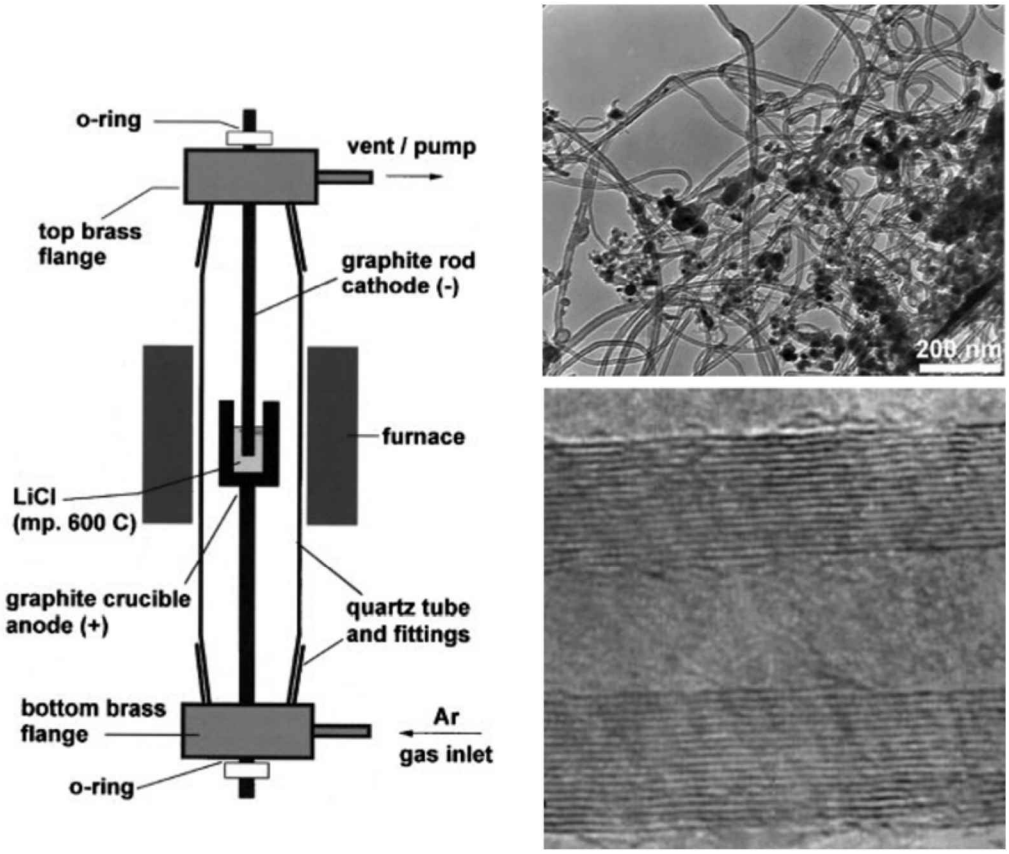

Fig. 1.14. *Schematic view of the electrolysis production system for. Graphitic electrodes are immersed in molten LiCl under an Ar atmosphere and a potential is applied between the electrodes. The chamber where this synthesis is carried out remains sealed. On the right, TEM and HRTEM images of multi-walled nanotubes are shown (obtained from Terrones' reviews [7,16]).*

Hydrocarbon pyrolysis or chemical vapor deposition (CVD), is a versatile method for producing carbon nanotubes [16]. A metal catalyst, such as Fe, Co, Pt or Ni, among others is deposited onto a substrate. That substrate is placed iside a furnace and a hydrocarbon (toluene, benzylamine, xylene, methane, acetylene, etc), is thermolized on the substrate in an inert atmosphere. An example of a CVD system

is shown in figure 1.15 [17]. In this case, the hydrocarbon is not a gaseous or liquid precursor but a solid. An organometallic compound could be used as both carbon source and catalyst. The CVD method could be used for producing high yields of aligned MWNTs and SWNTs. This method will be discussed in more detail in chapters 2 and 3.

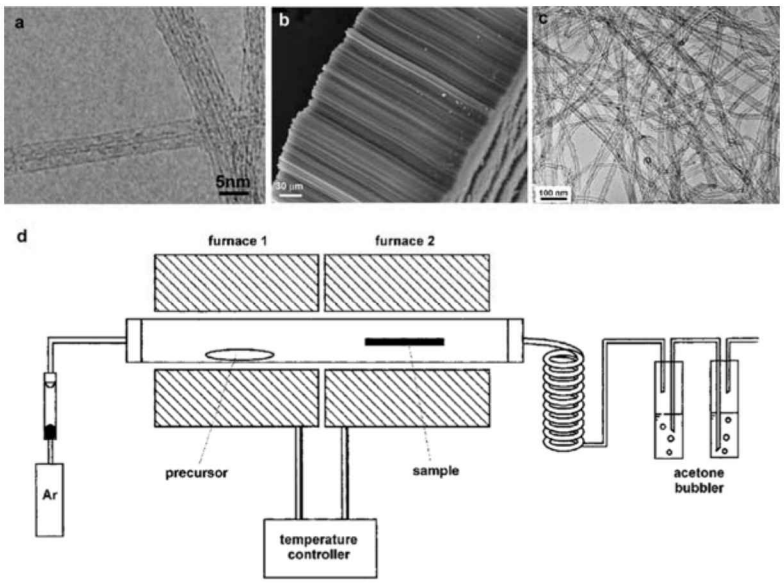

Fig. 1.15. (d) *Schematic of the hydrocarbon pyrolysis experimental set up. Both carbon precursor and catalyst are located inside at the first furnace, in a silica tube that serves as a substrate for the reaction. Ar gets into de system through an inlet located in one end of the silica tube. At the other end, a water cooler and acetone bubblers are located (obtained from Terrones' publication [17]). (a) HRTEM image of SWNTs produced by CVD technique. (b) SEM image of MWNTs produced by pyrolysis. (c) TEM of thermolysis produced MWNTs.*

1.4 Applications of Carbon Nanotubes

A wide variety of applications of carbon nanotubes has been proposed since their identification and characterization [1,4]. For instance, they could be used as field

emission sources [7], in the production of lithium ion batteries and electrochemical devices [20], as molecular sensors [18-19,23], for storage of gas and hydrogen [16], for scanning probe tips [16,18], for the fabrication of nanotube electronic devices [20], as polymer composite fillers [21], as drug delivery agents [24-26], for producing nanotube based filters [22], and so forth.

When a potential is applied between a carbon nanotube surface and an anode, electrons can be emitted from carbon nanotube tips [7]. Therefore, they could be used as light sources, flat panel displays and X-ray sources. Nanotubess are advantageous because of their stable field emission over long time, high current densities, long life time and because they would not require an ultra high vacuum [7]. Figure 1.16 depicts a representation of a carbon nanotube based flat panel display. This would be an application of the outstanding field emission properties of carbon nanotubes. Li^+ ions can be intercalated within the graphitic layers of carbon nanotubes. This allows the migration of Li^+ ions form graphitic anode to a cathode, such as $LiCoO_2$ or $LiMn_2O_4$. Arrays of MWNTs could be used in the anode fabrication for Li^+ batteries, duplicating the capacity of standard carbon [7].

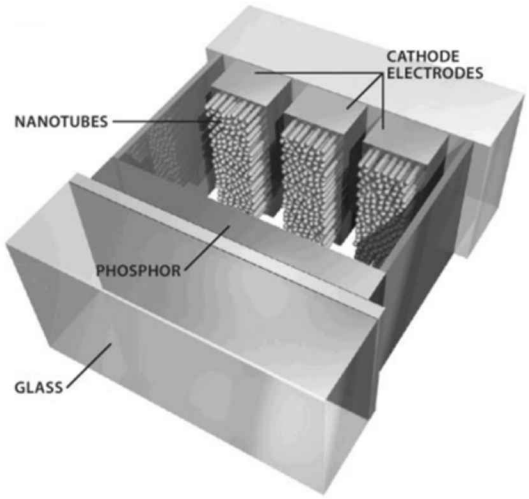

Fig. 1.16. *Schematic representation of a carbon nanotube based flat panel display (obtained from Terrones' report [17]).*

Due to the large surface area of MWNTs and MWNT bundles [add value], nanotubes could be used in electrochemical applications [20]. In order to increase the image resolution, carbon nanotubes have been used as scanning probe microscopy tips. Figure 1.17 exhibits an atomic force microscope (AFM) tip with an attached nanotube, which could enhances the resolution [17]. For instance, Wong and coworkers [18] proposed the usage of covalently functionalized nanotubes as nanometre-sized probes in chemistry and biology. These authors explored the possibility for creating nanotube probes that could sense and manipulate matter at the molecular level, because of their high aspect ratio and outstanding mechanical properties and they demonstrated that carbon nanotubes are capable of chemical and biological discrimination [18].

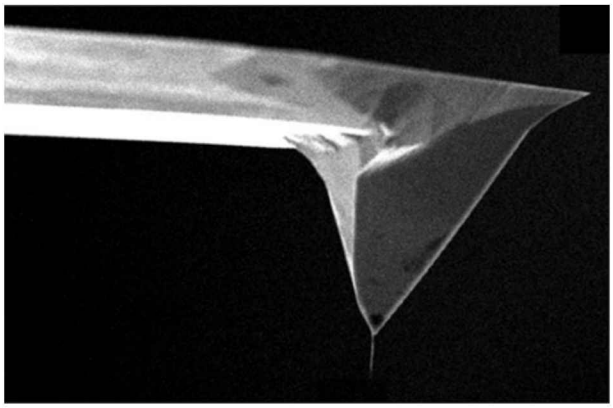

Fig. 1.17. *SEM image of an atomic force microscope (AFM) tip with an attached MWNTs, which enhances the image resolution (obtained from Terrones' review [17]).*

The closed cage structure of carbon nanotubes suggests that they could be used for the storage of a variety of molecules. Ar and N_2 have been successfully store into nanotubes [16]. Hydrogen storage could be advantageous, for fabrication of fuel cells. Kong et al. [23], fabricated a nanotube chip by synthesizing high quality SWNTs by pyrolisis of methane on silicon-dioxide susbtrates on controlled regions

using patterned catalytic islands. Subsequently, microfabrication techniques were used to connect the nanotubes obtaining a low resistance.

According to Bogunia-Kubik and Sugisaka [24], not only carbon nanotubes, but different kinds of nanoparticles could be used as carriers of therapeutical molecules or even as drug delivery matrices. In 2004, Bianco and coworkers [25], reported the effective usage of carbon nanotubes as plasmid DNA gene deliver. These authors characterized mammalian HeLa cells, after incubation with nanomaterials. TEM showed that the carbon nanotubes had been introduced into the cell, preferentially cell nucleus, by an unknown mechanism. They suggested that nanotubes could spontaneously cross the cell membrane. Correa Duarte et al. [26] proposed a different application for carbon nanotubes in cell culture. Aligned MWCNTs on silicon substrates were acid treated and annealed to produce three dimensional arrays, called cellular carbon nanotube foams. The formed micro cavities are successfully used as scaffolds for cell seeding and growth.

Carbon nanoscience and nanotechnology have attracted the attention of numerous researches world wide and the number of publications in the field has increased enormously. Although many of the envisaged applications for carbon nanotubes are still far from becoming a reality, a considerable step forward the crystallization of many of them has been already made. It is important to mention that this chapter does not intend to cover all the progress made in nanotube research to date. The intention is only to provide brief review of some of the most remarkable advances in the field.

Add motivation of the thesis work and a brief summary, with the most relevant results. HTM

References

1. Oberlin, A., Endo, M., Koyama, T. "Filamentous growth of carbon through benzene decomposition" *J. Cryst. Growth* **32**, 335-349 (1976).
2. Kroto, H. W., Heath, J. R., O'Brien, O., Curl, R. F., Smalley, R. E. "C60: Buckminsterfullerene" *Nature* **318**, 162-163 (1985).
3. Krätschmer, W., Lamb, L. D., Fostiropoulos, K., Huffman, D. R. "Solid C60: a new form of carbon" *Nature* **347**, 354-358 (1990).
4. Iijima, S. "Helical microtubules of graphitic carbon" *Nature* **354**, 56-58 (1991).
5. Ebbesen, T. W., Ajayan, P. M. "Large synthesis of carbon nanotubes" *Nature* **358**, 220-221 (1992).
6. Iijima, S., Ichihashi, T. "Single-shell cabrbon nanotubes of 1-nm diameter" *Nature* **363**, 603-5 (1993).
7. Terrones M. "Science and Technology of the Twenty-First Century: Synthesis, Properties and Application of Carbon Nanotubes" *Annu. Rev. Mater. Res.* **33**, 419-501 (2003).
8. Hamada, N., Sawada, S., Oshiyama, A., "New One-Dimensional Conductors: Gaphitic Microtubules" *Phys. Rev. Lett.* **68**, 1579-1582 (1992).
9. Saito, R., Fujita, M., Dresselhaus, G., Dresselhaus, M. S. "Electronic structure of graphene tubules based on C_{60}" *Phys. Rev. B* **46**, 1804-1811 (1992).
10. Wildöer, J. W. G., Venema, L. C., Rinzler, A. G., Smalley, R. E., Dekker, C. "Electronic structure of atolically resolved carbon nanotubes" *Nature* **391**, 59-62 (1998).
11. Odom, T. W. O., Huang, J. L-., Kim, P., Lieber, C. M. "Atomic structure and electronic properties of single-walled carbon nanotubes" *Nature* **391**, 62-64 (1998).
12. Treacy, M. M. J., Ebbesen, T. W., Gibson, J. M. "Exceptionally High Young's modulus observed for individual carbon nanotubes" *Nature* **381**, 678-680 (1996).

13. Falvo, M. R., Clary, G. J., Taylor II, R. M., Chi, V., Brooks Jr., F. P., Washburn, S., Superfine, R. "Bending and buckling of carbon nanotubes under large strain" *Nature* **389**, 582-584 (1997).

14. Hone, J., Whitney, M., Piskoti, C., Zettl, A. "Thermal conductivity of single-walled carbon nanotubes" *Phys. Rev. B* **59**, 2514-2516 (1999).

15. Kim, P., Shi, L., Majumdar, A., McEuen, P. L. "Thermal Transport Measurements of Individual Multiwalled Nanotubes" *Phys. Rev. Lett.* **87**, 215502 (2001).

16. Terrones, M. "Carbon nanotubes: synthesis and properties, electronic devices and other emerging applications" *International Materials Reviews* **49**, 325-377 (2004).

17. Terrones, H., Terrones, M. "Curved nanostructured materials" *New Journal of Physics* **5**, 126.1-126.37 (2003).

18. Wong, S.S.; Joselevich, E.; Woolley, A.T.; Cheung, C.L.; Lieber, C.M. "Covalently functionalized nanotubes as nanometre-sized probes in chemistry and biology" *Nature* 1998, **394**, 52-55.

19. Kong, J.; Franklin, N.R.; Zhou, C.W.; Chapline, M.G.; Peng, S.; Cho, K.J.; Dai, H.J. *Science* 2000, **287**, 622-625.

20. Baughman, R.H.; Zakhidov, A.A.; De Heer, W.A. *Science* 2002, **297**, 787-792.

21. Harris, P.J.F. *Int. Mater. Rev.* 2004, **49** (1): 31-43.

22. Viswanathan, G.; Kane, D.B.; Lipowicz, P.J. *Adv. Mater.* 2005, **16**, 2045-2049.

23. Kong, J., Zhou, C., Morpurgo, A., Soh, H. T., Quate, C. F., Marcus, C., Dai, H. "Synthesis, integration, and electrical properties of individual single-walled carbon nanotubes" *Appl. Phys. A* **69**, 305-308 (1999).

24. Bogunia-Kubik, K., Sugisaka, M. "From molecular biology to nanotechnology and nanomedicine" *BioSystems* **65**, 123-138 (2002).

25. Pantarroto, D., Singh, R., McCarthy, D., Erhardt, M., Briand, J.P., Prato, M., Kostarelos, K., Bianco, A. "Functionalized Carbon Nanotubes for Plasmid DNA Gene Delivery" *Angew. Chem.* **116**, 5354-5358 (2004).

26. Correa-Duarte, M.A., Wagner, N., Rojas-Chapana, J., Morsczeck, C., Thie, M., Giersig, M. "Fabrication and Biocompatibility of Carbon Nabotube-Based 3D Networks as Scaffolds for Cell Seeding and Growth" *Nano Lett.* **4**, No. 11, 2233-2236 (2004).

27. http://www.nanotech-now.com/images/multiwall-large.jpg

2. Production of Carbon Nanotubes and alloyed Nanowires using the aerosol pyrolysis technique

This chapter describes the aerosol pyrolysis technique as a versatile method to produce carbonaceous nanostructures. Encapsulated alloyed metallic nanowires inside multi walled carbon nanotubes (MWNTs) were synthesized using this framework and both parameters and precursors to produce such a nanomaterial are given in detail in the present chapter. The obtained samples were characterized with different techniques and interesting and novel results were obtained. Applications of the synthesized materials are also discussed in the following sections.

2.1 Description of the Aerosol Pyrolysis Method; conditions and operation

Hydrocarbon pyrolysis or chemical vapor deposition (CVD) is a widely used technique to produce carbon nanotubes [1]. It has some advantageous characteristics, such as versatility, and low cost. The thermolized material can be either solid or a liquid hydrocarbon and requires the presence of a metal catalyst (usually Fe, Co or Ni). Mayne-L'Hermite and coworkers [2,3] reported for the first time a novel variation of the pyrolysis technique to produce carbon nonotubes from an aerosol. In the present section this technique is described in detail.

The simplest variation of CVD technique in the production of carbon nanostructures is called powder pyrolysis. An organometallic compound is thermolyzed at 700 °C to 950 °C in an inert atmosphere to produce carbon nanotubes. For instance, Grobert et al. [4] deposited several alternated layers of C_{60} molecules and Ni thin films onto a silica substrate and the coated plate was then pyrolyzed at 950°C. These authors obtained needle-like nanotubes from this procedure. Rao and coworkers [5] pyrolyzed $FeCp_2$ and $FeCp_2$-acetylene mixtures to obtain aligned nanotubes filled with Fe. Later, organic solvents were incorporated into the process and that improved its versatility. Mayne-L'Hermite et al. [2] reported the pyrolysis of aerosols in order to produce aligned carbon nanotubes. These authors provided a schematic view of their experimental set up, which consisted of an atomizer, furnace, water cooler and acetone trap (figure 2.1). The solution, in this case ferrocene dissolved in benzene (2.5 - 5 wt%), was placed in the atomizer that atomized the solution due to a pressure difference. The spray was distributed within a quartz tube placed inside a tubular furnace. The products deposited in the quartz tube were collected and consisted of nanotube-containing dark powders. The size of the droplets generated (estimated in the order of hundreds of microns) and the carrier gas flow are very important experimental parameters that affect the final features of the samples [2].

An improvement of the floating catalyst CVD system, for producing carbon nanotubes, came with a better control of the generated aerosol. It was described for Mayne-L'Hermite and coworkers [3,6] and is the one used in the present work. A photograph of the experimental set up is shown in figure 2.2. For the reaction to take place, it is necessary to pyrolyze a solution that contains a carbon source (hydrocarbon) and a catalyst (metallocene). That solution (usually 300 ml) is placed into the container of an ultrasonic sprayer. At the bottom of the container, there is a ceramic piezoelectric. When a voltage is applied to this piezoelectric with certain

frequency, the piezoelectric vibrates ultrasonically, turning the initial solution into a mist. This mist is then transported to a reaction zone, where carbon nanotubes or nanowires could grow.

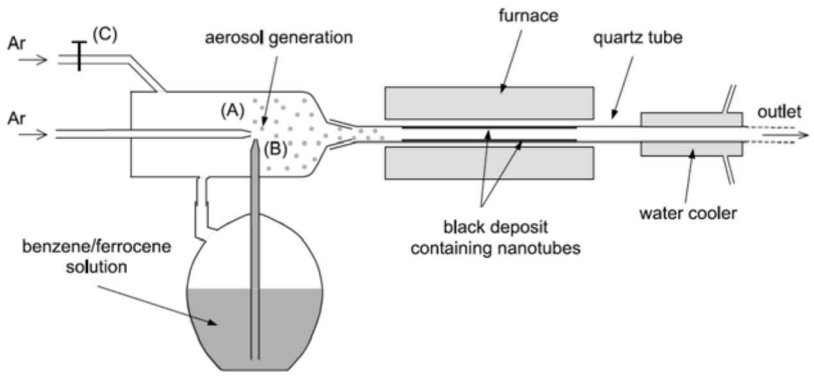

Fig. 2.1. *Experimental set up of the spray pyrolysis system. The solutionof ferrocene and benzene is placed in a container that atomized the solution due to a pressure difference. The generated spray is distributed within a quartz tube placed inside a tubular furnace. At the end of the furnace, a water cooler is placed (obtained form Mayne's report [2]).*

The container is provided with a gas inlet that works as a carrier of the mist (aerosol) into the furnace, where the pyrolysis will take place (figure 2.2). When the aerosol is formed, and the gas is flowing, both the catalyst and the carbon source reach the tubular furnace, which was already heated up to a temperature ranging between 600 °C to 1100 °C. A quartz tube is used as a substrate and the produced material is deposited on its wall. The quartz tube is joined to a condenser and acetone trap, which cool down and trap the hydrocarbons resulting from the reaction occurring inside the furnace. After the reaction, the whole system is allowed to cool to room temperature, and the sample is extracted from the quartz tube walls by scratching with a metallic tool. Before and after the reaction, the carrier gas (Argon) should flow in the whole system, but with a reduced rate (0.2 L/min).

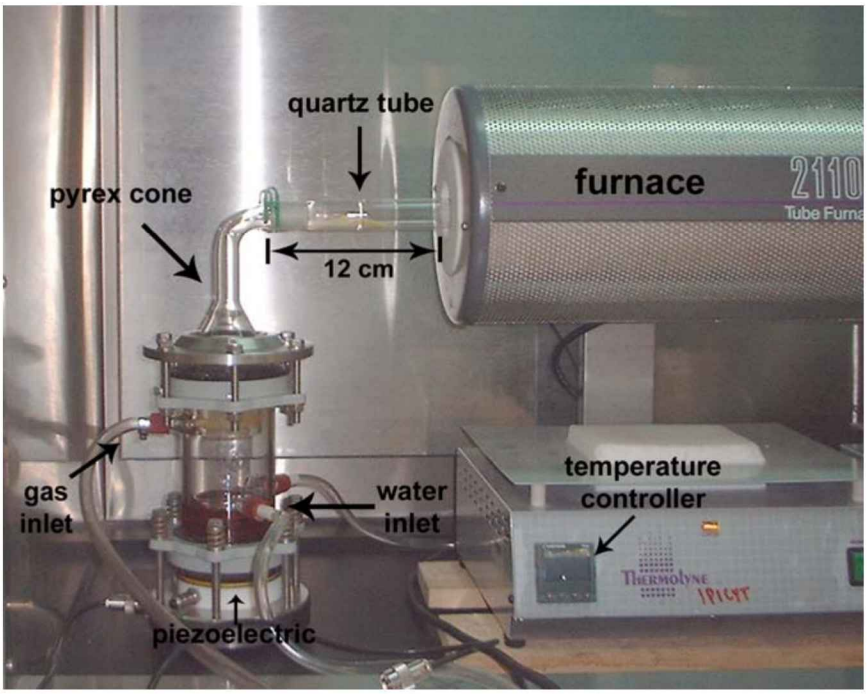

Fig. 2.2. *Photograph of the aerosol pyrolysis method experimental set up used in this work. The main components of the system are labeled and pointed with arrows: piezoelectric, water inlet, gas inlet, pyrex cone, quartz tube, furnace, temperature controller. The reservoir is filled with a hydrocarbon/catalyst solution. An applied voltage causes the ultrasonic vibration of the piezoelectric, so the solution turns into a mist. The carrier gas that enters the system through the gas inlet, travels with the aerosol along the pyrex cone and quartz tube, which is the substrate of the reaction. The mist reaches the hot zone of the tubular furnace and the formation of carbon nanotubes takes place.*

The solution container is made of pyrex. Due to the piezoelectric vibrations, the solution temperature increases (above 50 °C). Therefore, the pyrex container includes a water inlet that forms a spiral, which cools down the solution to prevent any accident or reaction; there is also a water outlet, so water should be flowing during the aerosol generation.

Argon is commonly used as a carrier gas. Its flow is a very important experimental

parameter. In order to grow carbon nanotubes inside of the quartz tube, the flow should range from 0.6 to 5.0 L/min. The reaction temperature is also crucial. One could produce nanotubes at a temperature as low as 650 °C, as it is described in section 2.2 but the formation of carbon nanotubes could also take place at 1050 °C.

A large series of experiments was performed in order to determine the optimal conditions of the operation of the ultrasonic sprayer. For producing undoped MWCNTs (deposited inside the quartz tube) the optimal temperature is 800 °C, whereas the optimal temperature to produce nitrogen doped MWCNTs (CN_x MWNTS) is 50 °C higher, 850 °C. Usually, an Ar flow of 3.7 L/min works well for both experiments.

The furnace position is another important parameter to take into account. The aerosol formation takes place far away form the furnace, at the lower part of the container. The aerosol is then carried through the cone and tube by the inert gas, and travels a long way before reaching the furnace, thus the mist could condense and the nanotube growth may be inhibited. In order to optimize these conditions, the position of the furnace was varied and it was found that the furnace should be at 12 cm from the left extreme of the quartz tube (figure 2.2), for obtaining the best nanotube growing conditions.

The referred pyrolysis system can also be operated with two furnaces. The temperature and position of the second oven is also crucial to enhance the nanotube growth. After a large number of trial experiments, it was found that the distance between the furnaces should be 4.2 cm for the production of CN_x MWNTs and 5 cm for MWCNTs.

The ceramic piezoelectric is placed at the bottom of the solution container (see

Figure 2.2) and is connected to an item called ultrasonic generator. The user interface (not shown here) allows changing the frequency; different solutions may have different frequencies at which the aerosol can be produced efficiently. For these reason, every time a new solution is placed inside the container to perform an experiment, the appropriate frequency should be found by varying this parameter. The appropriate frequency is the one that turns a particular solution into a mist. There is another parameter that can be adjusted in the ultrasonic generator: the power. An excessive volatile aerosol not necessarily leads to a large production of carbon nanotubes. Therefore, the power can be lowered or raised, at the scale of 0 to 10 units, depending on the particular experimental needs. For almost all the experiments carried out in this wok, a power of 5 units is adequate. The power is proportional to the amplitude of the ultrasonic wave that generates the electric signal, responsible of the piezoelectric vibrations.

The running time is a very important condition that can also be varied in the experiments. The most common values (in this thesis) were 15 minutes for producing MWCNT's and 30 minutes for SWCNT's (see chapters 3 and 4). The length of the nanotubes does not dependent linearly with time, but if the experiment is performed for 30 seconds, the obtained nanotubes (about 20 μm in length) become shorter than those obtained for a one hour experiments (up to 300 μm).

The ceramic piezoelectric is a delicate item. After every experiment, the whole system needs to be cleaned. The container should be emptied and cleaned in order to remove completely the solution residues. Usually organic solvents help to clean the container, but it is important to take into account that some solvents could damage the system. For instance, the container should not be cleaned with acetone, because that can deteriorate the piezoelectric component.

After a large number of experiments are carried out, the piezoelectric performance could decrease. For example, the amount of aerosol produced could be diminished using the same operating conditions. Therefore, it may be necessary to increase the power form the preset value. The piezoelectric component can fail and stop producing aerosol when long reaction times occur, such as 45 or 60 minutes. When this happens, the generator should be turned off and after a few seconds turned on again.

The aerosol pyrolysis method presented here can now be used to produce MWCNT's, CNxMWNT's, encapsulated nanowires inside MWCNT's and even SWCNT's. In the following sections the production and characterization of these nanostructures is discussed in detail (see chapters 3 and 4 as well).

2.2 Production and Characterization of Single-crystal FeCo Nanowires inside Carbon Nanotubes

In this section, the synthesis of novel monocrystalline FeCo nanowires encapsulated inside multi-walled carbon nanotubes (MWNTs) is described. These FeCo nanowires exhibit homogenous Fe and Co concentrations and do not contain an external oxide layer due to the presence of insulating carbon shells. The method involves the aerosol thermolysis of toluene-ferrocene-cobaltocene solutions in inert atmospheres. The materials have been carefully characterized using high-resolution transmission electron microscopy (HRTEM), electron-energy-loss spectroscopy (EELS), scanning electron microscopy (SEM), energy dispersive X-ray analysis (EDX), electron diffraction, HREELS-STM elemental mapping, X-ray powder diffraction and SQUID magnetometry. The formation of FeCo alloys (γ-phase, bcc lattice) occurs at relatively low temperatures (e.g. 650 – 750 °C). These single-crystal

nanowires, always exhibit the FeCo (110) plane normal to the carbon nanotube axis. The FeCo nanomaterials have shown large coercive fields at room temperature (e.g. 900 Oe). It is possible that these aligned ferromagnetic nanowires could be used in the fabrication of high density magnetic storage devices and magnetic composites.

2.2.1 Filling Carbon Nanotubes with Solid Materials

Because carbon nanotubes are hollow, it is possible to introduce metals inside their core. Ajayan and Iijma first demonstrated in 1993 that carbon nanotubes could be filled with Pb [7]. These authors dispersed multi-walled carbon nanotubes were sonicated in ethanol and a then pipetted on carbon TEM grids. Lead particles were subsequently deposited on the grid, which was annealed at 400 °C in air for 30 minutes. Detailed TEM characterization of the grid showed that the hollow cavitiy of some MWCNTs was filled with solid Pb material, as can be observed in figure 2.3. Lead particles were found decorating the surface of nanotubes before annealing and also on the closed tips of the nanotubes. After annealing, these tips became open and strong irradiation of them induced Pb material to melt and enter the nantoube.

Soon after this discovery, various groups managed to introduce "foreign" materials inside carbon nanotubes, such as metals, carbides, oxides and even proteins using thermal and chemical methods [1,8,9]. As reviewed by Banhart and coworkers, Pb_3O_4 and Bi encapsulation into nanotubes was reported, following a similar procedure than that reported in [7]. Cs, S, Se, $AgNO_3$ and Ag were also successfully introduced into MWCNTs.

The arc discharge method was also used to achieve the goal of introducing foreign materials into carbon nanotubes. Ruoff and coworkers [10] used C anodes filled

with metals and metal carbides, which were then found into the produced carbon nanotubes. After this report, many metals were used in arc discharge experiments so that they could be introduced inside carbon nanotubes. It is important to note that this is a one step method, and the synthesis occurs at ca. 3000 °C.

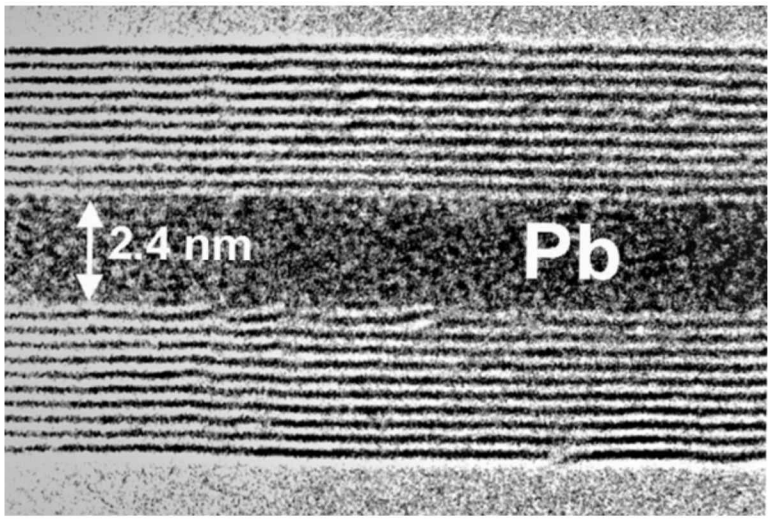

Fig. 2.3. *HRTEM image of a carbon nanotube filled with a Pb nanowire (obtained from Ajayan's report [7]).*

Wet chemical techniques have been also used to fill nanotubes, as reported by Tsang and coworkers [11]. They opened MWCNTs caps by treatment in nitric acid; after that, the metal oxides were successfully introduced into nanotubes. Sloan and coworkers [9] reviewed the structural chemistry of a range of binary halide crystals (NaCl, AgCl, AgBr, CsCl, CsBr, SrI_2, BaI_2, $LnCl_3$, UCl_4, $ThCl_4$, TeI_4) encapsulated in SWCNTs. The synthesis method is at least a two step method. For instance, to introduce Ru into SWCNTs, the synthesized tubes were acid treated (HCl) in order to open their tips; subsequently, they were immersed in a saturated solution of $RuCl_3$, and Ru metal was found inside the nanotubes, after H_2 reduction. The authors reported the formation and growth of atomically regulated KI crystals within SWCNTs, which have been recalled as Feynman crystals, using a method

involving the heat treatment of the halide and the SWCNT material in a vacuum sealed quartz ampoule (see figure 2.4).

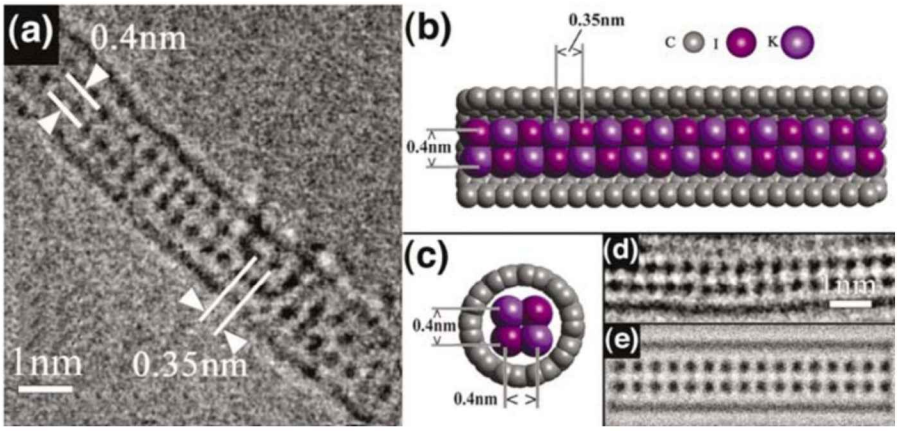

Fig. 2.4. *(a) HRTEM image of a 1.4 nm diameter SWNT filled with a KI crystal. (b) Molecular simulation of the HRTEM shown in (a), exhibiting the KI crystal inside an armchair (10,10) SWNT. (c) End view of (b). (d) Real HRTEM image and (e) calculated Scherzer focus image (obtained from Sloan's report [9]).*

Hsu et al [12] produced Sn-Pb nanowires within a carbon shell by the electrolysis method. A graphite cathode was depth in an electrolyte of LiCl, mixed with a very small amount of Sn and Pb (1 wt%). The applied voltage varied form 0 to 20 V and the current from 3 to 7 A. The obtained sample was analyzed by HRTEM equipped with an X-ray detector. 40 to 60% of the products consisted on SnPb nanowires, with diameters ranging form 40 – 90 nm. EDX and XRD techniques provided information on the stoichiometry of the nanowires, which was found to vary along the nanowire axis. Variations of these experiments were performed in order to produce Bi-Pb and Sn-Bi nanowires [12], but the yield was quite smaller (5%).

It is noteworthy that ferromagnetic materials are mainly introduced inside MWNTs via one-step thermolytic routes involving organometallic compounds containing Co [13], Ni [4] and Fe [5,14]. Terrones et al. [13] pyrolyzed 2-amino-4,6-dichloro-s-

triazine on a thin Co film deposited onto a silica plate as a substrate, using laser ablation. The substrate was etched to create linear patterns before pyrolysis. SEM and TEM and characterizacion showed that aligned carbon nanotubes were grown on the cobalt etched sustrate and a carefull HRTEM analysis exhibited cobalt-filled nanotubes among this sample (see figure 2.5). The Co nanowires produced inside the nantoubes were monocrystalline and the graphene layers exhibited good crystallinity, as can be seen in figure 2.5(b).

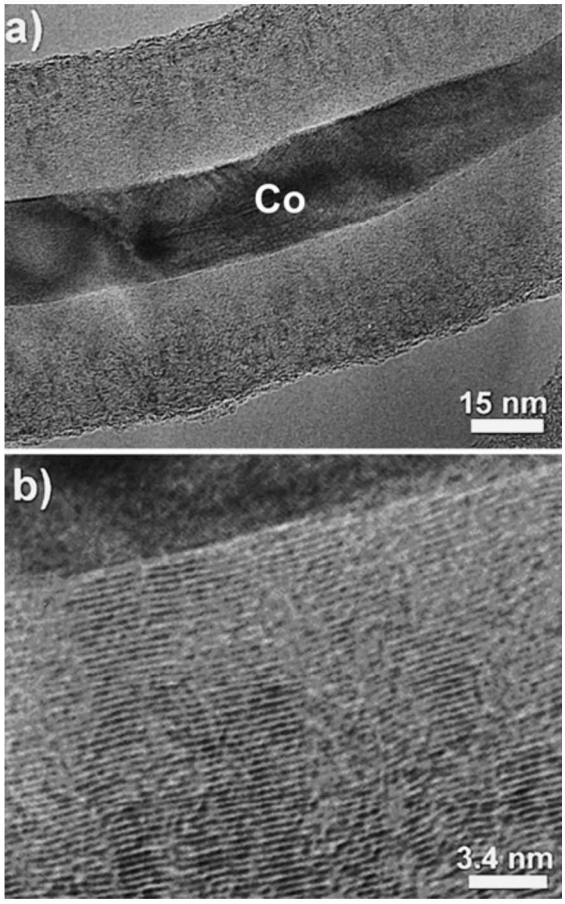

Fig. 2.5. *(a) HRTEM image of a cobalt-filled multi walled carbon nanotube. (b) Higher magnification of (a), exhibiting clearly the cobalt-graphite interface. The cobalt planes correspond to the (002) reflections separated by 2.35 Å (obtained from Terrones' report [13]).*

Similarly, Grobert et al. [4] used the pyrolysis technique to produce Ni-filled carbon nanotubes. They deposited several alternated layers of C_{60} molecules and Ni thin films onto a silica substrate. The coated plate was then pyrolyzed at 950°C under an inert atmosphere. Needle-like nanotubes were obtained from this procedure and Ni crystals were found in their cavities, as can be observed in Figure 2.6. Rao et al. [5] pyrolyzed $FeCp_2$ and $FeCp_2$-acetylene mixtures to obtain aligned nanotubes filled with Fe. Grobert and coworkers [14] reported that pyrolysis of C_{60}-$FeCp_2$ mixtures under argon atmosphere could also lead to aligned MWCNTs filled with Fe crystalline nanowires (figure 2.7(a)). The nanomaterial was magnetically characterized, proving that coercive fields decrease linearly as temperature increases (see figure 2.7(b)). The external magnetic field was applied parallel and perpendicular to the nanotube axis. The highest H_c obtained was 1070 Oe, for a very low temperature, and the lowest value (430 Oe) was obtained at room temperature, the latter higher than that corresponding to the bulk Fe (H_c=0.68 Oe, according to [15]).

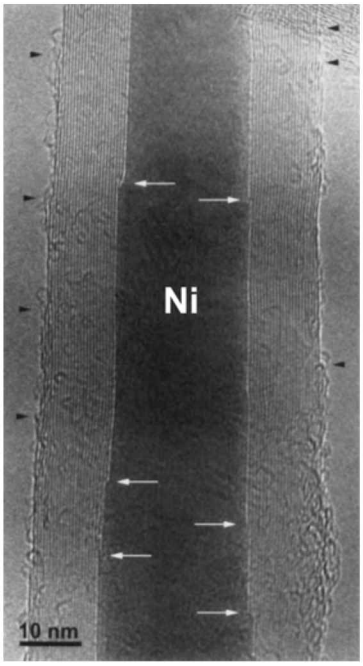

Fig. 2.6. *HRTEM image of a needle-like carbon nanotube, filled with crystalline Ni (obtained from Grobert's report [4]).*

The same group [16], reported the synthesis of alloyed nanowires inside carbon nanotubes. In this case, solutions of $NiCp_2$-$FeCp_2$ (ferrocene:nickelocene) where prepared, using benzene (C_6H_6) as a solvent. This solution was then placed in a reservoir and dropped into a capillary, from where they were atomized into the quartz tube. The experiments were carried out in an Ar atmosphere; this gas served as a carrier as well. The samples were characterized by XRD and EELS line scans, to determine the $Fe_{65}Ni_{35}$ alloy, also known as invar. SEM and HRTEM images are shown in figure 2.8. The products obtained from Grobert's experiments consist of aligned multiwalled nanotubes arrays, as can be observed in figure 2.8 (b). Figure 2.8(a) shows a HRTEM image of the as grown material, where the $Fe_{65}Ni_{35}$ single crystal is contained by the carbon nanotube walls.

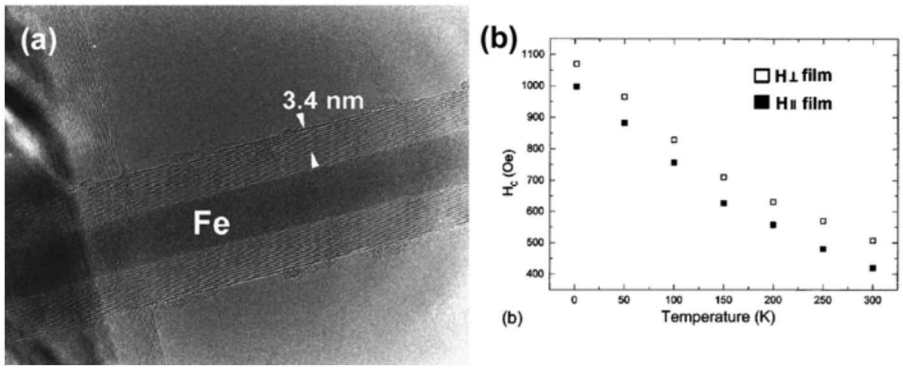

Fig. 2.7. *(a) HRTEM image of two crossed Fe-filled MWNTs exhibiting different diameters. (b) Plot shows the variations on the obtained coercive fields while varying temperature. Hc diminishes linearly as temperature increases. The external magnetic field was applied in two directions; perpendicular and parallel to the nanotube axis (obtained from Grobert's report [14]).*

As described above, several approaches have been used to produce nanowires. However, the introduction of monocrystalline ferromagnetic alloy nanowires with superior magnetic properties in MWNTs is a major achievement in the fabrication of high density magnetic storage devices, such as the quantum magnetic disk

(figure 2.9), achieving densities in the order of Tbits/in^2.

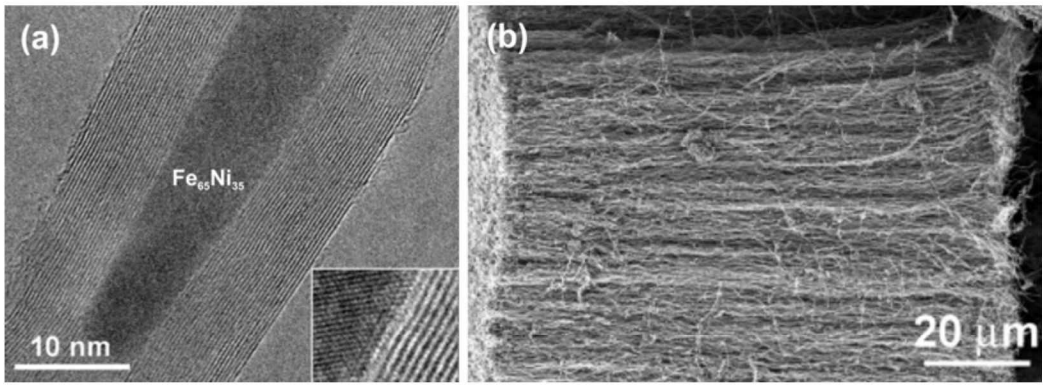

Fig. 2.8. *(a) HRTEM image of an Invar-filled MWNT. Inset shows the crystallinity of both the alloy and the nanotube. (b) SEM image of aligned nanotube arrays, showing the purity of the sample. (obtained from Grobert's report [16]).*

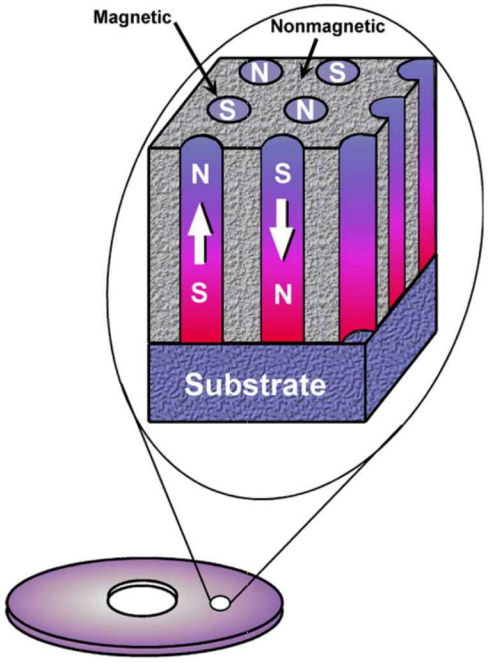

Fig. 2.9. *Schematic diagram of quantized magnetic disk, consisting of single magnetic domain bit uniformly embedded in non-magnetic material: each bit could possess two possible magnetizations, ideally equal in magnitude but opposite in direction (adapted from S. Y. Chou [17])*

2.2.2 Bare Ferromagnetic Nanowires: An Overview

Periodic arrays of ferromagnetic nanostructures could be used in the fabrication of high density magnetic storage devices [17]. In the past, it has been demonstrated that Fe-filled carbon nanotubes could exhibit large magnetic coercivities at room temperature (e.g. 430 Oe) [14], greater than those reported for Ni and Co nanowires [18]. However, FeCo alloy nanowires offer an attractive alternative for magnetic data storage since they could exhibit even larger coercive fields at room temperature [19]. Due to their robustness, FeCo alloys are also useful for developing high temperature magnetic applications (*e.g.* high temperature space power systems [20], wiring materials for audio and radio frequency transformers, magnetic bearings, magnetomechanical actuators, etc.). Nanowire arrays may have significant potential in magnetic data storage devices -such as the quantum magnetic disk, first proposed by Chou and coworkers, in 1993- due to their size and anisotropic behavior, which permits the use of smaller bit size (one per nanowire, see figure 2.9), thus increasing the attainable recording density [21].

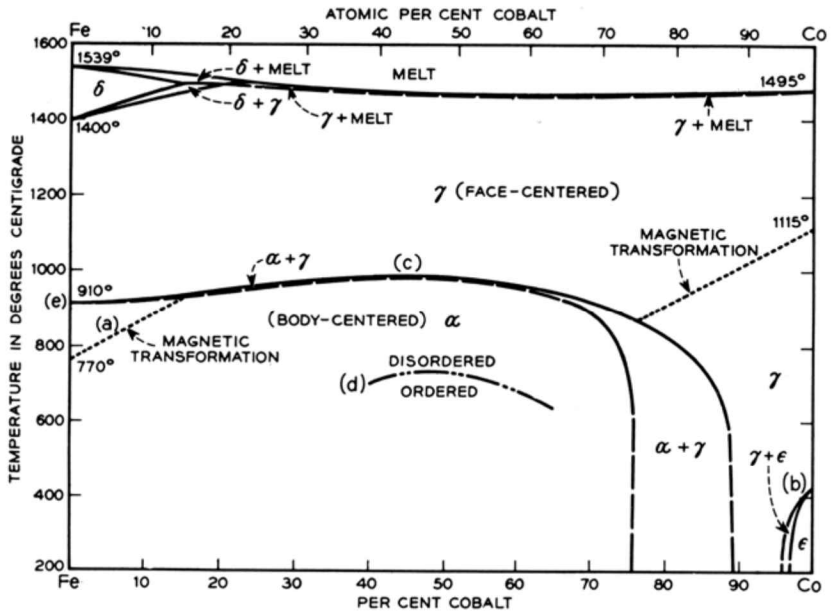

Fig. 2.10. *Iron-Cobalt phase diagram (obtained from Bozorth [15]).*

According to the phase diagram (figure 2.10), the FeCo crystalline lattice is bcc (α phase), at synthesis temperatures lower than 1000 °C. Thus, monocrystalline FeCo nanowires could grow in different crystallographic orientations; for instance, in figure 2.11 the molecular models of two nanowires grown with their axis perpendicular to FeCo (1-10) and (100) planes are depicted. Crystallographic planes can be observed, such as the FeCo (111), which is facing the reader in the lateral view (figure 2.11(a)). Several views of another FeCo nanowire grown normal to the (100) plane are shown in figure 2.11(b); the top view clearly exhibits the growth direction (100) and, in the lateral view, the direction (010) can also be appreciated.

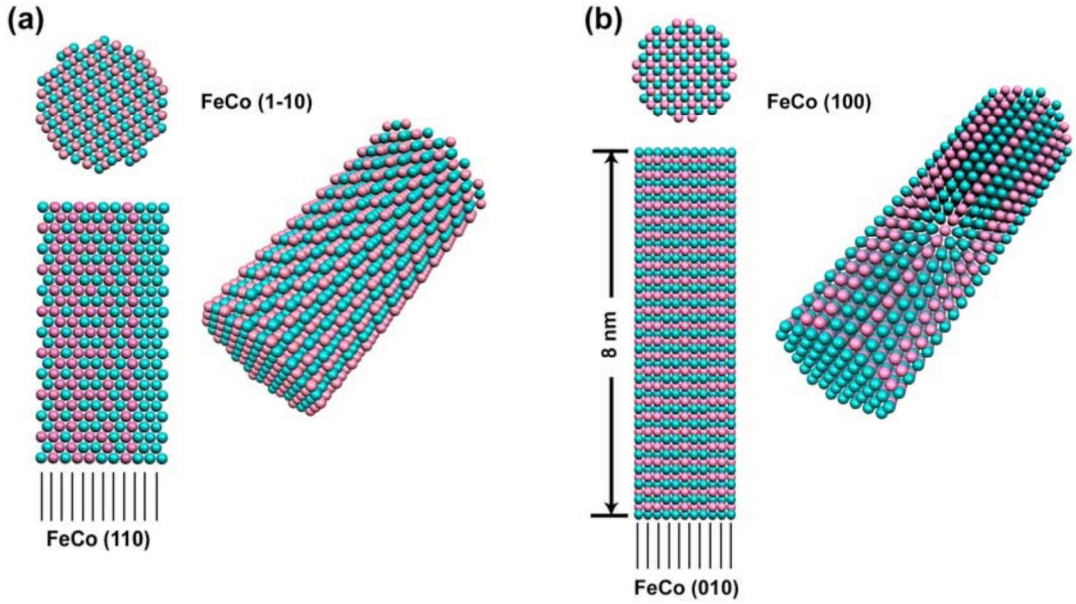

Fig. 2.11. *Molecular models of two nanowires grown perpendicular to (a) FeCo (110) and (b) (100) planes are depicted. (a) Crystallographic planes can be observed, such as the FeCo (111), which is facing the reader in the lateral view. (b) Several views of another FeCo nanowire grown normal to the (100) plane; the top view clearly exhibits the growth direction (100) and, in the lateral view, the direction (110) can also be appreciated.*

In the past, different groups have tried to produce $Fe_{(1-x)}Co_x$ nanowires of different stoichiometries [22-29]. Polycrystalline $Fe_{1-x}Co_x$ ($0.0 \leq x \leq 0.92$) nanowires were

synthesized depositing Fe and Co atoms on anodic aluminum oxide (AAO) templates by Chen et al. [22]. The pore size of the alumina template determined the diameter of the nanowires (about 20 nm). Their length (~7.5 μm) depended on the depositing time. TEM characterization and electron diffraction showed the dimensions and plycristalline condition of the synthesized nanowires (figure 2.12). Chen and coworkers found a bcc $Fe_{1-x}Co_x$ structure for $x \leq 0.82$ and a mixture of bcc and fcc for $0.82 \leq x \leq 0.92$. From Mössbauer spectroscopy, they concluded that the internal field of arrays was randomly oriented, either parallel or antiparallel to the nanowire axis. They reported that the energetically favorable direction of spontaneous magnetization of nanowires (known as easy axis) was [110], which differs from the bulk alloy [100].

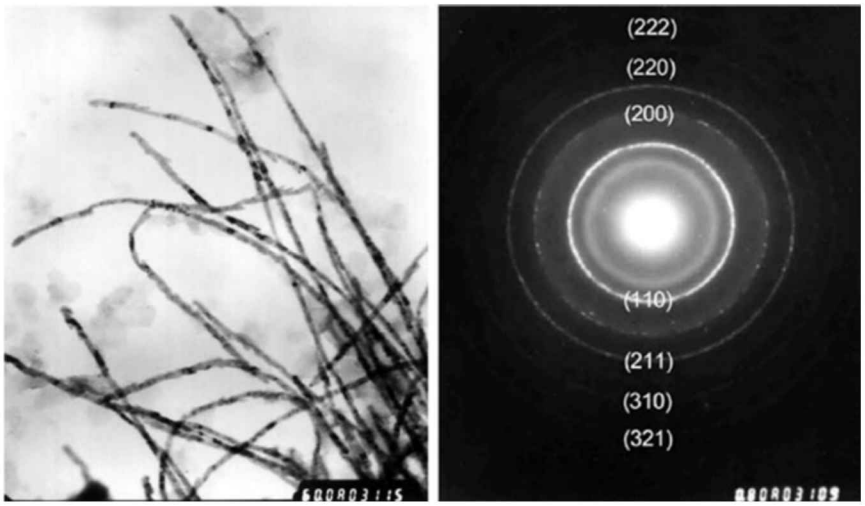

Fig. 2.12. *TEM image of $Fe_{0.56}Co_{0.44}$ nanowires and their corresponding electron-diffraction pattern (obtained from Chen's report [22]), which evidences the polycrystalline feature of these alloyed nanostructures.*

Zhan et al. [23] reported the synthesis of $Fe_{1-x}Co_x$ ($0.0 \leq x \leq 1.0$) arrays of polycrystalline nanowires, following Chen's approach [22]. Different stoichiometries resulted in different crystalline structure of the nanowires. For

instance they obtained XRD patterns and found a bcc structure for nanowires with $x \leq 0.82$, with a [110] preferred orientation; when $x=0.92$, samples exhibited a mixture of bcc and fcc, with a [110] orientation. When they measured the inter-planar spacing along the preferred orientation, they found values slightly larger than those corresponding to the bulk (table 1). Hysteresis loops were also obtained (figure 2.13) at 5 and 300 K and the easy magnetization axis was the one parallel to the nanowires' axis. At both temperatures, when the magnetic field was applied orthogonal to the nanowire axis, they found a much smaller H_c, compared to the latter one. For instance, at 300 K, the H_c obtained for the $Fe_{0.38}Co_{0.62}$ sample applying the magnetic field perpendicular to the wire axis was about 680 Oe, while the resulting H_c applying the magnetic field parallel to the nanowire axis was larger than 2500 Oe (see figure 2.13). They complemented the experimental procedure applying the "chains-of-spheres model", which helped them to study the magnetization reversal process. They found an approximate coincidence between the theoretical and the experimental values of the coercivity.

TABLE I. The XRD data for the $Fe_{1-x}Co_x$ nanowires. d is the average interplanar spacing along the preferred orientation.

x	0.00	0.22	0.44	0.62	0.82	0.92	1.00
(hkl)	(110)	(110)	(110)	(110)	(110)	(111)	(1000)
d(Å)	2.027	2.033	2.025	2.022	2.011	2.049	2.181

Fodor et al. [24] reported $Co_{1-x}Fe_x$ nanowires ($0.0 \leq x \leq 1.0$) fabricated with the same method described above. The pore diameter was 40 nm, thus the nanowire diameter, and the inter-pore distance corresponded to 95 nm. The length of the wires was reported to be 290 ± 20 nm. In this case, two crystallographic transitions

were found when varying the x parameter. For pure Co wires, the structure displayed the hcp packing. For x = 0.1, they reported the coexistence of hcp and fcc phases. When $x \geq 0.15$, the structure was bcc (α). They performed a magnetic characterization of the samples at different concentrations of Fe and Co within the nanowires (figure 2.14). The maximum value for the coercive field (parallel to wire axis) was about 2150 Oe in the range of $0.5 \leq x \leq 0.6$, as shown in figure 2.14. However, higher aspect ratio nanowires [4,25] reported more prominent coercive fields for x = 0 and $0.5 \leq x \leq 0.6$. These authors reported coercive fields ranging from 450 to 750 Oe when the magnetic field is applied perpendicular to the nanowire axis. The magnetic characterization was performed at room temperature (private communication with Prof. Wenger)

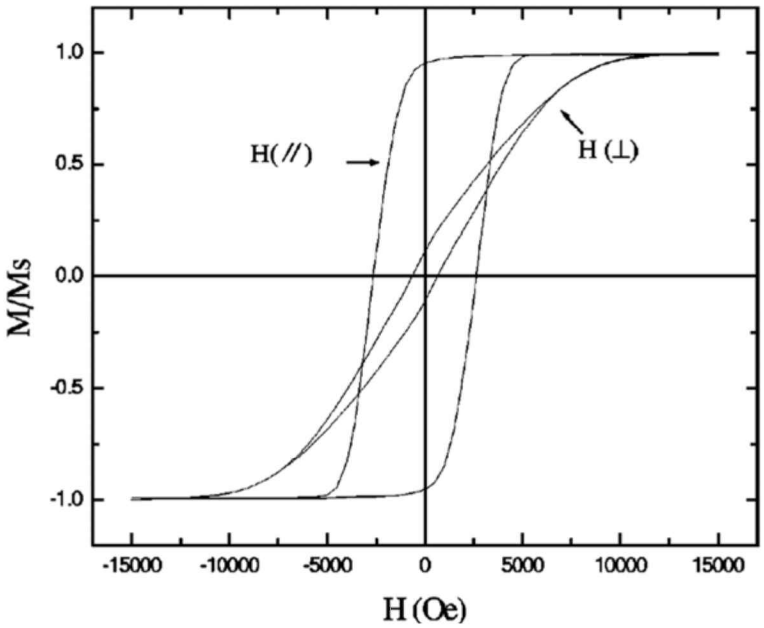

Fig. 2.13. *The hysteresis loops of the $Fe_{0.38}Co_{0.62}$ AAO film at room tempreature. H(//) indicates that the applied field is parallel to the nanowires, while H(⊥) indicates that the applied field is perpendicular to the nanowires (obtained from Zhan's report [23]).*

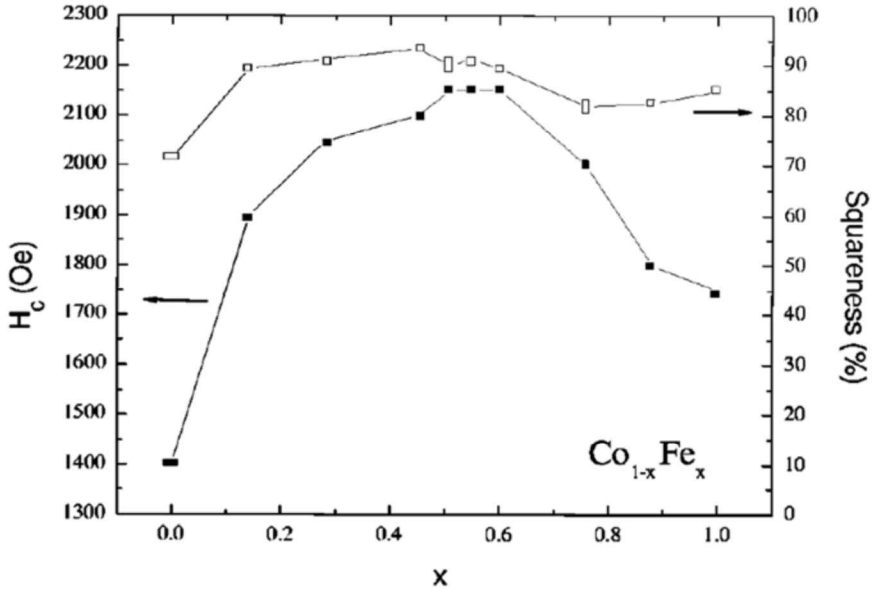

Fig. 2.14. *Plot showing the Co1-xFex concentration dependence of the coercivity field Hc (white square) and squareness (black square). Both curves belong to data obtien while applying the external magnetic field along the nanowire axis (obtained from Fodor's report [24]).*

Smaller aspect ratio nanowires (diameter of 18 nm and length of 2 μm) were reported by Tang et al. [27]. The synthesis method used was the deposition of an Fe-Co alloy into anodic aluminum oxide (AAO) templates, with a fixed stoichiometry of $Fe_{69}Co_{31}$. After synthesis, samples were annealed and characterized. XRD patterns revealed a bcc structure and a (110) preferred orientation (parallel to the nanowire axis); the annealed sample behaved similarly, but the (110) peak was sharper and the general signal less noisy. The annealed samples also exhibited larger diameters (~25 nm). Annealing driven structural changes were also studied using HRTEM. Figure 2.15(a) exhibits an image of an as produced nanowire, while figure 2.15(b) shows an annealed nanowire HRTEM image. It is important to notice the amorphous-like material surrounding both samples. H_c and M_r/M_s were monitored during annealing (see figure 2.15(c)), and

the authors found an optimal annealing temperature of 550 °C, with H_c = 3650 Oe and M_r/M_s ~ 0.95 (corresponding values before annealing were 2300 and also 0.95). The improvement of the magnetic properties after annealing was studied with the sphere chain approximation, supposing that the chain was made up of prolate ellipsoids. It was concluded that annealing improves the magnetic signal of the sample because this treatment results in an increase of crystallite size along the wire axis and reduces the amount of defects; Ms is increased. Parallel and orthogonal hysteresis loops were obtained, and the easy axis was parallel to the wires (for the orthogonal one H_c was about 1200 Oe).

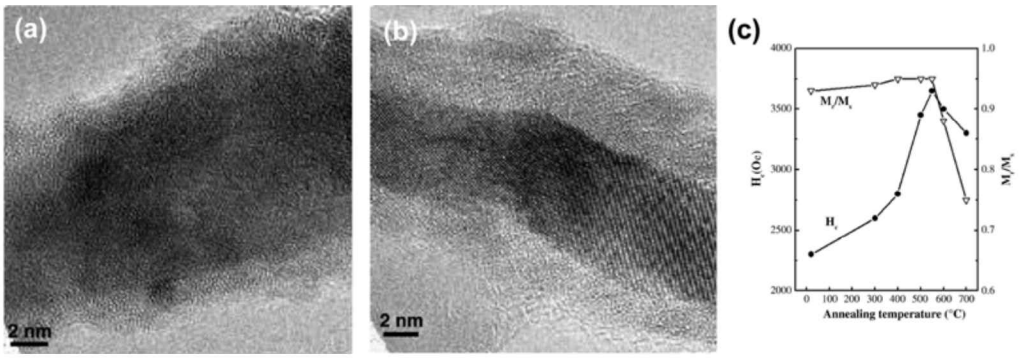

Fig. 2.15. *HRTEM images of $Fe_{69}Co_{31}$ nanowires (a) as deposited; (b) annealed in 550 °C for 20 min. (c) Dependence of coercivity and remanence ratio M_r/M_s with annealing temperature (obtained from Tang's report [27]).*

A different approach was used by Pierce, Plummer and Shen [28] to synthesize $Fe_{1-x}Co_x$ nanowires along the step edges of a tungsten (110) surface. The average step height was about 8.5 nm, and the edges were parallel to the [001] direction. Surface magneto-optical Kerr effect (SMOKE) measurements were performed varying the Fe-Co ratio. It was found that the easy magnetization lied along the [1-10] direction, perpendicular to the wires. The Curie temperature decreased as the Co concentration was increased, and falls rapidly after x=0.3, which is an opposite behavior compared to the bulk (see figure 2.16). Therefore, these authors concluded

that the addition of Co inhibits the magnetic order in the system.

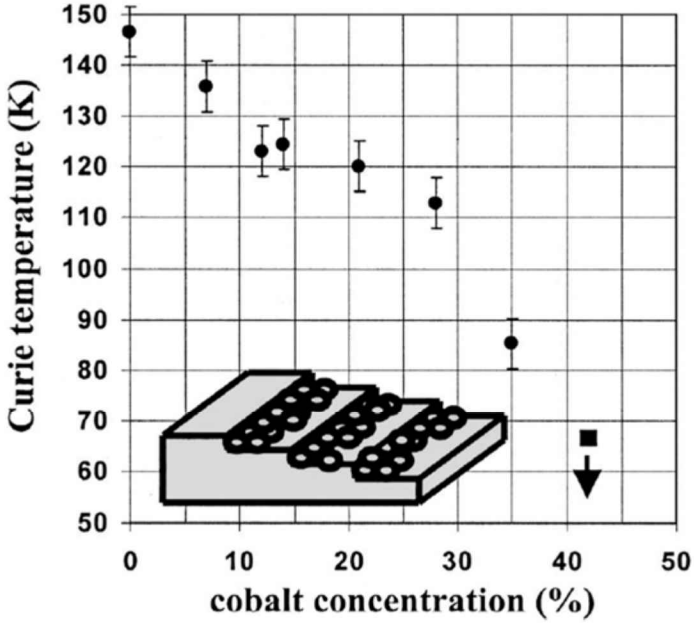

Fig. 2.16. *Dependence of the Curie temperature of the $Fe_{1-x}Co_x$ alloy nanowire system on the Co concentration. The Curie temperature that corresponds to the last (black square) data point must lie below the temperature shown (obtained from Tang's report [28]).*

Arrays of FeCo binary nanocluster wires were synthesized by thermal decomposition of Fe $(CO)_5/Co_2(CO)_8$ metal carbonyl vapors [29]. The first produced nanoclusters were piled up by a magnetic field in order to produce arrays of nanowires. It was assumed that Fe and Co mixed almost completely due to their high solubility. The compactness of the wires decreased as the Fe mole % increased. From XRD patterns, the authors determined that bcc was the structure of pure Fe nanowires and fcc for the pure cobalt ones. Unfortunately, this study does not include magnetic characterization of the samples.

The previous research described above, refers to the generation of nanowires exhibiting amorphous-like materials on their surface, such as carbon, oxides, etc., as can be appreciated in figure 2.15 [24,27]. In addition, the nanowires were

polycrystalline [22,27-29] (see figure 2.12 and 2.15). In order to circumvent these problems, carbon nanotubes may be used as templates in order to promote the formation of single-crystalline wires coated by perfect graphene cylinders.

In the following section, the production and characterization of aligned MWNTs filled with monocrystalline FeCo nanoalloys is described in detail. Interestingly, the FeCo materials exhibited large magnetic coercivities at room temperature (e.g. 928 Oe).

2.2.3 Synthesis of single crystal FeCo nanowires inside carbon nanotubes using the aerosol pyrolysis method

Solutions of ferrocene ($FeCp_2$) in toluene (C_7H_8; 2.5 % by weight, Aldrich) and cobaltocene ($CoCp_2$) in toluene (C_7H_8; 2.5 % by weight, Aldrich) were mixed in 1:1 and 3:1 proportions. This solution was then transferred to the reservoir of an atomizer (described in figure 2.2). The solutions were then atomized and pyrolyzed in a two stage furnace system at temperatures varying from 600 to 800°C; all experiments were carried out for 15 min. The aerosol generator operation was then terminated and a low argon flow (0.36 l/min) was kept until the furnace reached room temperature. Table 2 shows a list of the preformed experiments.

$FeCp_2$ [wt%]	$CoCp_2$ [wt%]	Toluene [wt%]	Temperature [°C]
1.25	1.25	97.5	600
1.25	1.25	97.5	650
1.25	1.25	97.5	700
1.25	1.25	97.5	750
1.25	1.25	97.5	800
1.875	0.625	97.5	600
1.875	0.625	97.5	650
1.875	0.625	97.5	700
1.875	0.625	97.5	750
1.875	0.625	97.5	800

Table 2*: Table of the experimental parameters of the carried out experiments. A mixture of ferrocene and cobaltocene (ratios indicated) in toluene were atomized and pyrolyzed at the temperatures indicated.*

2.2.4 Characterization of FeCo nanowires inside carbon nanotubes

The soot deposited on the walls of the quartz tube was scratched and analyzed by scanning electron microscopy (SEM) using a JEOL-JSM 6300F operated at 2-10 kV and a Philips FEG-XL30, operated at 5-10 kV. The as-grown products were also characterized using an X-ray powder diffractometer (XRD; RINT 2200) with Cu *Kα* radiation. Samples for HRTEM studies were prepared by dispersing the powders (1 mg) in acetone (10 ml) in an ultrasonic bath for 1 minute, and one drop of the suspension was then placed onto a holey-carbon grid and left to dry. HRTEM studies were performed with a Field emission JEOL-JEM-3000F operated at 300kV, equipped with a Gatan 766 2D-DigiPEELS, a JEOL-JEM 4000EX HRTEM , operated at 400 kV, and a JEOL JEM-2010F, operated at 200kV, equipped with thin-window light-element-sensitive X-ray detector, and a Gatan Enfina EELS for high spatial resolution microanalysis. EELS studies and Elemental mapping were carried out

using: (a) 300 kV field emission JEM-3010F microscope equipped with an Omega Energy Filter, (b) Philips CM200-FEG system equipped with a PEELS detector, and (c) Tecnai F20 HRTEM equipped with a post-column Gatan Imaging Filter (GIF).

d

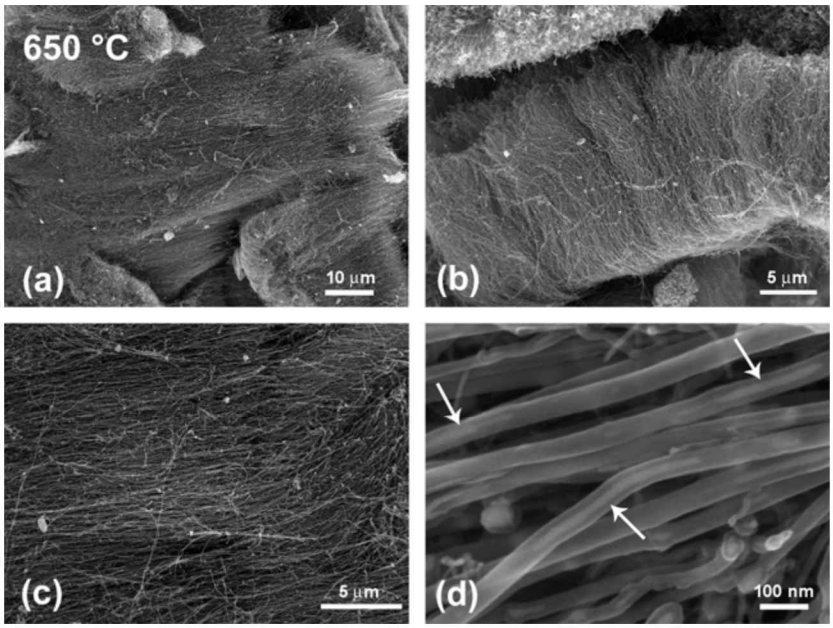

Fig. 2.17. *Representative SEM images of bulk carbon material produced at 650 °C (a)-(b)-(c) Low magnification images of FeCo filled MWNT bundles. (d) High magnification SEM image of individual nanotubes. Contrast allows to observe some FeCo nanowires inside MWNTs, pointed with arrows.*

Magnetization measurements [M(H)] were performed using a quantum designed SQUID (superconducting quantum interference device) system (MPMS) at two different temperatures (5 K and 300 K). A small quantity of synthesized carbon nanotubes, obtained from the quartz tube, was wrapped in a plastic film to make a small pellet. This pellet was introduced into the MPMS to carry out magnetization measurements at 300 K. The temperature was then lowered to 5 K and magnetization measurements were repeated.

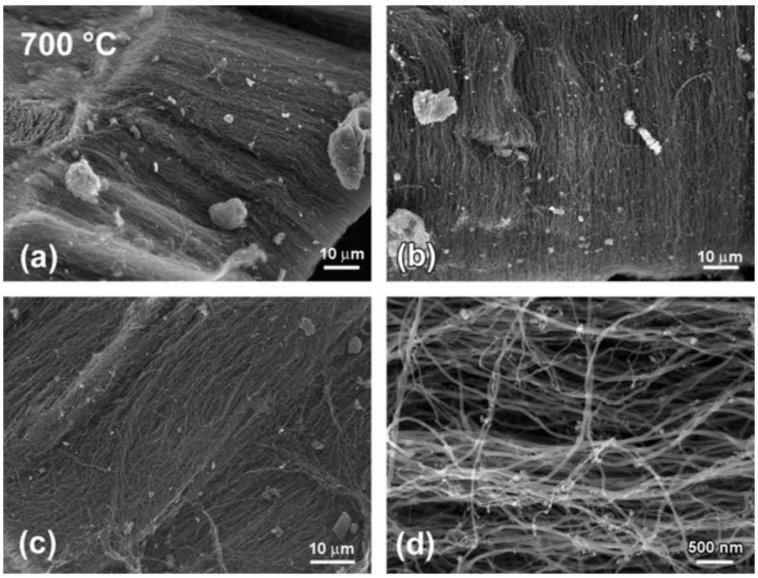

Fig. 2.18. *Representative SEM images of bulk carbon material produced at 700 °C (a) to (c) Low magnification images of FeCo filled MWNT bundles of 60-70 □m in length. (d) Higher magnification of panel (c), exhibiting individual MWNTs.*

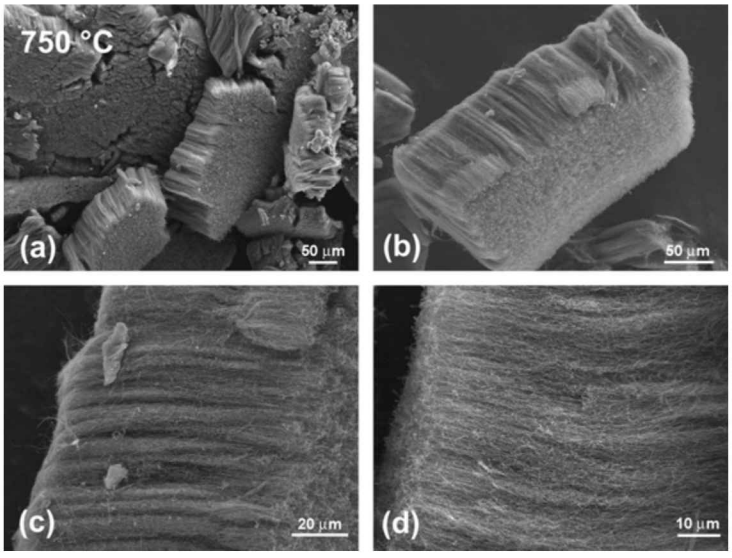

Fig. 2.19. *Representative SEM images of bulk carbon material produced at 750 °C (a) Very low magnification image of several FeCo filled MWNT bundles. (b) Image of an individual bundle of MWNTs filled with the FeCo alloy. (c) and (d) Higher magnifications of (b).*

SEM images of the products obtained at reaction temperatures of 650, 700, 750 and

800 °C are shown in figures 2.17, 2.18, 2.19 and 2.20, respectively, while experiments carried out at 600 °C did not produce any material. At low magnifications, these images revealed the presence of bundles of well aligned carbon nanotubes. At this magnification it is possible to determine the length of the bundles, which ranges from 20 up to 300 microns, and appears to increase with the reaction temperature (figures 2.17(b), 2.18(b), 2.19(b), 2.20(b)). At very high magnifications, such as 150 kX, it is possible to observe in detail the nanomaterial. In figure 2.17(d), the contrast allows to see some encapsulated nanowires within the nanotubes (see arrows); the signal coming from heavier atoms, such as Fe and Co, is stronger than the one coming form lighter atoms, such as C, and that provides the contrast. It is important to note that all samples consisted mainly of carbon nanotubes and contained almost no foreign particles such as amorphous carbon or encapsulated metal particles (see arrows in figure 2.17(d)).

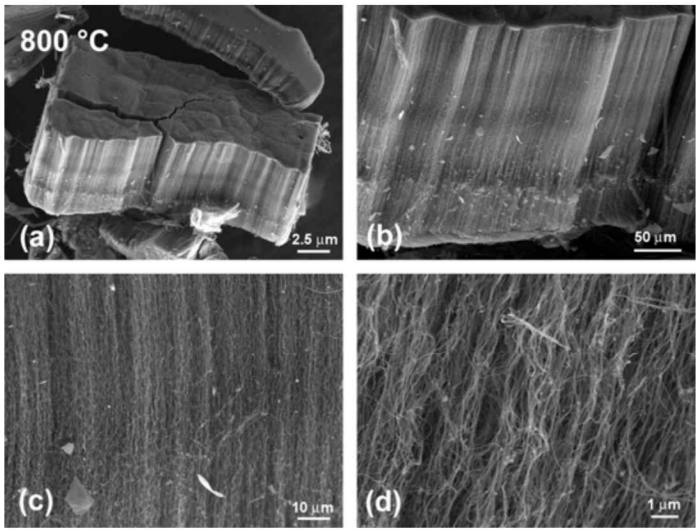

Fig. 2.20. *Representative SEM images of bulk carbon material produced at 800 °C (a) and (b) Low magnification images of FeCo filled MWNTs. The length of these samples is bigger compared to samples synthesized at lower temperatures (200 □m). (c) and (d) Higher magnification of (b) panel.*

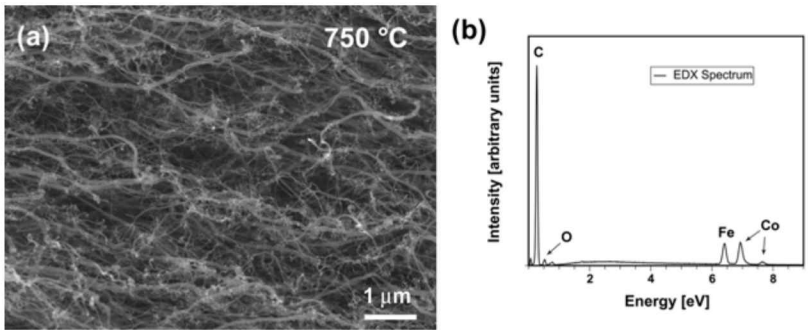

Fig. 2.21. *(a) Low magnification SEM image of encapsulated nanowires, synthesized at 750 °C. (b) EDX spectrum obtained from the region depicted in (a). The signal corresponding to Fe localizes at 6.4 eV, where as the Co signal appears at 6.93 eV. Fe:Co weight percent ratio corresponds to 2.53:2.75, very close to that of FeCo. A weak peak in the spectrum also exhibits the presence of O, at 0.52 eV. The most important signal depicted in the spectrum is attributed to the C (0.28 eV), which is the main element in the sample.*

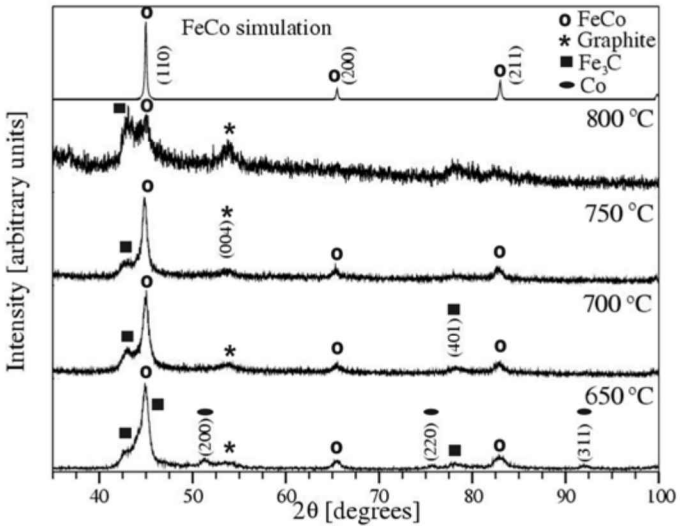

Fig. 2.22. *X-Ray diffraction patterns of nanotube materials produced at temperatures between 650 and 800 °C. The formation of FeCo alloys inside the MWCNT's is clearly observed from 650 to 750 °C. In addition, Fe_3C reflections appear at all temperatures. At 800°C, we observed a drastic decrease in intensity of the FeCo alloy, which could be due to the amorphization of Fe, Co and C phases (see text). A simulation of the FeCo alloys X-ray pattern is shown for comparison.*

Figure 2.21 shows a SEM image of encapsulated nanowires, synthesized at 750 °C,

and its corresponding EDX spectrum. At the energy of 6.4 eV localizes the peak corresponding to Kα energy of Fe. The Kα Co signal is located at 6.93 eV. A roughly calculation performed by the software indicates what the Fe:Co ratio corresponds to 2.53:2.75, very close to that of FeCo.

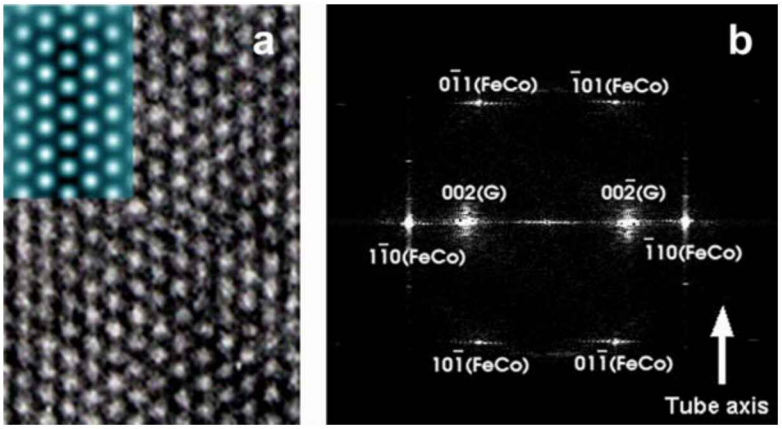

Fig. 2.23. *(a) HRTEM images of a monocrystalline FeCo nanowire viewed along the [111] direction; blue inset shows simulated HRTEM image of FeCo nanocrystal, with FeCo (110) plane parallel to the nanotube axis and G(002) planes; (b) Fast Fourier Transform (FFT) from the image shown in figure 2.29a, exhibiting the G(002) and the FeCo (110) planes. Note that epitaxial relationship between the FeCo (110) and the G (002) planes; planes are parallel.*

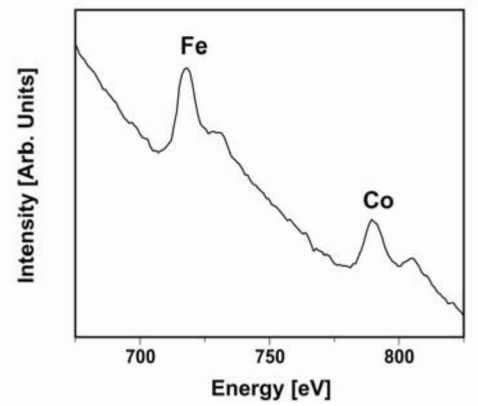

Fig. 2.24. *EELS spectra from a sample produced at 750 °C. It exhibits the presence of Fe and Co, represented by sharp core-ionization edges located at ca. 708 eV and 779 eV, respectively.* Check PLOT mtm

XRD studies revealed the presence of an FeCo alloy for samples prepared between

650 and 750 °C (Fig. 2.22). The presence of Fe_3C (cementite) and the interlayer graphite reflections (000ℓ) was also noted. Interestingly, fcc-Co (γ-Co) is also present at 650 °C. For preparation temperatures higher than 800 °C, the FeCo alloy disappeared almost completely (Fig. 2.22). It is noteworthy that the amount of material produced at 650 °C was extremely small relative to that obtained at temperatures higher than 750 °C (e.g. 1:15), whereas at 600 °C no products were obtained. XRD simulations clearly confirmed that an FeCo alloy was obtained at pyrolytic temperatures between 650 and 750 °C. For 800 °C, the FeCo (110) reflection was extremely low in intensity, but reflections corresponding to turbostratic graphite remained intense (as revealed by the presence of the graphite (0002) peak; not shown in Fig. 2.22). The crystallinity of graphene layers obtained at 800 °C appeared to be better when compared with lower temperatures. According to the phase diagram shown in figure 2.10, This drastic reduction in concentration of FeCo at 800 °C could be due to amorphization of the materials caused by the interaction of Fe, Co and C atoms induced by an order-disorder transition occurring at temperatures above 730 °C (see figure 2.10 phase diagram). This observation is also consistent with the Fe-Co phase diagram [17, 23,24]. FeCo alloy was found in its bcc phase (space group Im-3m (229) and lattice parameter a = 2.85 Å). The strongest reflection for the FeCo alloy corresponded to the (110) lattice plane. Reflections from Fe_3C (cementite) were also observed, with the strongest peak superimposing the (110) reflection of FeCo. Besides, the (401) Fe_3C reflexion was present in all patterns, especially at 650 and 700 °C, but with a week intensity At 650 °C, they were observed three of the characteristic reflections for the gamma phase of Co (Fig. 2.22). γ-Co (200) and (220) were the most intense, followed by (311). However, the peak intensities of γ-Co reflexions were much weaker than those from FeCo, Fe, Fe_3C and graphite.

HRTEM images revealed the presence of carbon nanotubes with metal inside their

cores (Figures 2.25-2.29). EDX spectra (not shown here) of samples prepared at 700 and 750 ° C displayed both Fe and Co within the carbon-coated nanowires (close to 1:1 ratio), suggesting the formation of an FeCo alloy phase. Closer inspection on the nanowires indicated that they were monocrystalline. Figures 2.25a and 2.26a exhibit low aspect ratio nanowires encapsulated in MWCNTs. Insets presented in figures 2.25b and 2.26b show a higher magnification detail of crystallographic planes, corresponding to graphite and the FeCo alloy. Both samples were synthesized at 750 °C. The electron diffraction pattern from figure 2.26 showed an epitaxial relationship between the (111) plane of the metallic alloy and the (002) plane of graphite (G). Figure 2.27 exhibits two parallel MWNTs synthesized at 700 °C, which possess higher aspect ratio when compared to those in figures 2.25 and 2.26. In the case of figure 2.28, two different encapsulated nanowires, produced at 700 °C, are depicted. The diameter in the carbon nanotube in figure 2.28a is remarkably large (close to 100 nm in outer diameter).

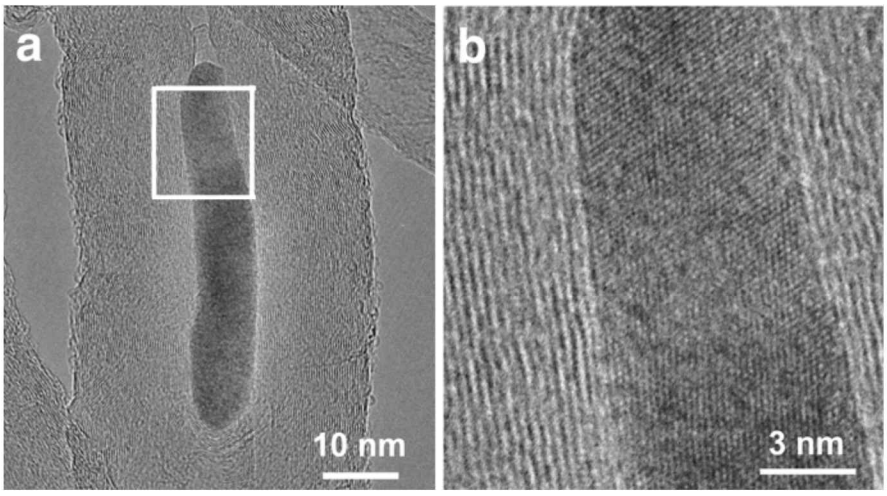

Fig. 2.25. *(a) HRTEM micrograph of an FeCo nanowire encapsulated inside a MWCNT. The sample was synthesized at 750 °C (b) Inset shows a detailed image of the inter-atomic planes from both the nanowire and nanotube.*

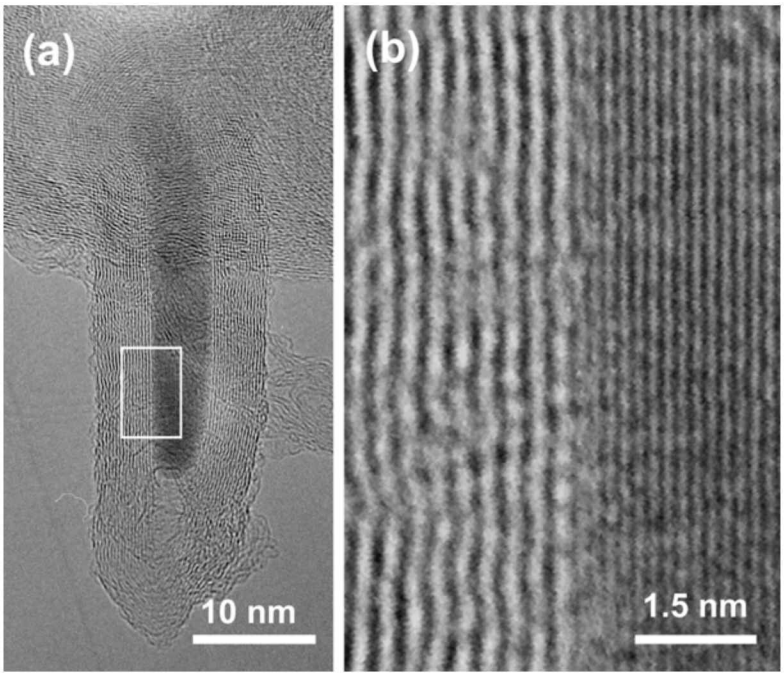

Fig. 2.26. *(a) HRTEM image of an encapsulated FeCo nanowire synthesized at 750°C. (b) Higher magnification image of (a). The panel depicts the epitaxial relationship between planes graphite (002) and FeCo (110).*

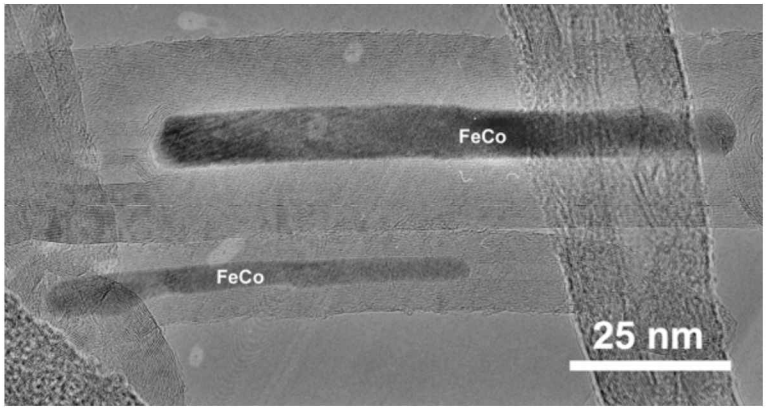

Fig. 2.27. *HRTEM image of two aligned FeCo nanowires. The alloyed nanomaterial is labeled and it is surrounded by the graphitic layers of the MWNTs. This sample was synthesized at 700 °C.*

Figure 2.23a depicts a HRTEM simulation of an FeCo crystal viewed along the [111] direction (see inset). By comparing the experimental and simulated HRTEM

images, clear match is observed, thus confirming that the FeCo (110) plane is indeed parallel to the G (002) plane. The Fast Fourier Transform (FFT) from the image shown in Fig. 2.29a, also exhibits the G (002) and the FeCo (110) lattice spacings. The presence of the hexagonal pattern created by the FeCo (101), FeCo (110) and FeCo (011) lattice planes indicates that the crystal is oriented along the [111] direction. Therefore, an epitaxial relationship between the FeCo (110) and the G (002) planes occurs in the nanowires studied. It is likely that these results would motivate further studies on the magnetic properties of FeCo nanowires oriented along the (110) plane from both the theoretical and experimental stand points.

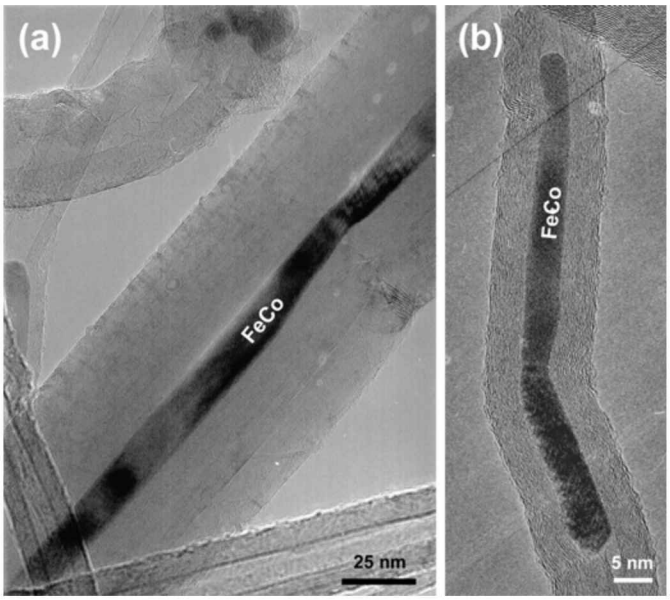

Fig. 2.28. *HRTEM images of alloyed FeCo nanowires synthesized at 750 °C. (a) Long FeCo nanowire inside a very thick MWNT (75 nm OD). (b) FeCo nanowire inside a bended MWNT.*

EELS spectra of samples produced at 700 and 750 °C always revealed the presence of Fe and Co, represented by sharp core-ionization L edges located at *ca.* 708 eV and 779 eV, respectively, as can be observed in Figure 2.24. In order to study the homogeneity of the FeCo alloy nanowires, EELS line-scans across individual wires

were performed. Figure 2.30a shows the Fe and Co concentrations across a nanowire produced at 750 °C. The profile demonstrates that the Fe and Co intensities are correlated and correspond to 1:1 stoichiometries. It is also interesting to notice that the "quasispherical" particle, located at the tip of the tube, also exhibits uniform concentrations of Fe and Co (Fig. 2.30b). Figure 2.31a shows the corresponding line scan from a nanowire synthesized at 700 °C. The profile exhibited in figure 2.31b corresponds to a nanowire synthesized at 750 °C, such as figure 2.26. In general, samples produced at 700 °C and 750 °C displayed stoichiometries close to 1:1 ratios. However, the best conditions for obtaining perfect FeCo stoichiometry were usually observed for 750 °C. ***

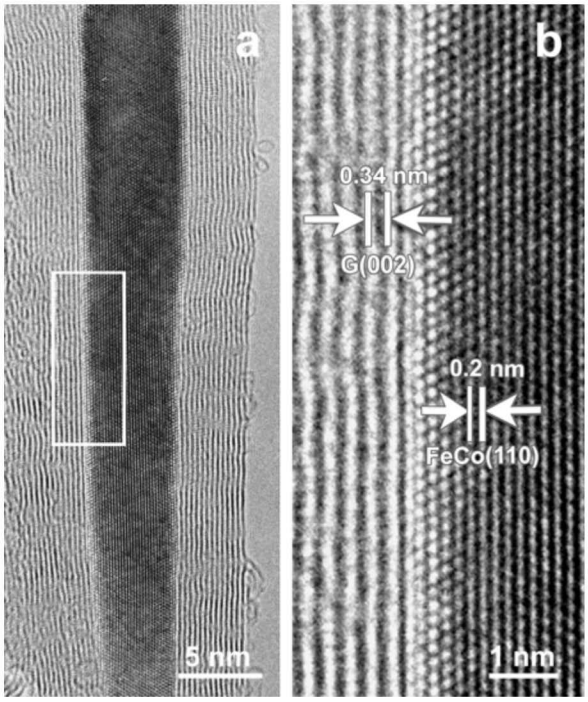

Fig. 2.29. *(a) HRTEM image of FeCo-filled MWCNT's produced at 700 °C. (b) Inset showing magnified view of the iron-cobalt alloy inside the carbon nanotube. The alloy nanowires (5-30 nm) are monocrystalline and always exhibit the FeCo (110) parallel to the carbon nanotube axis; G(002) (see figure 2.23).*

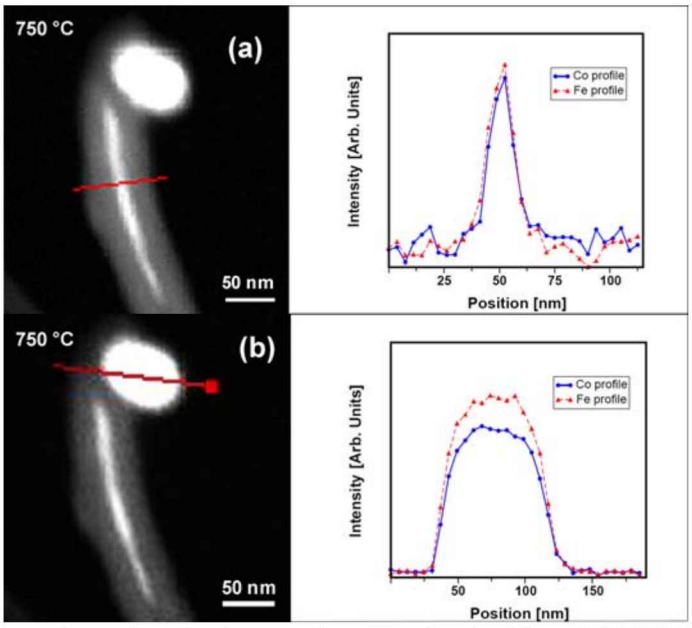

Fig. 2.30. *Linear mapping of a single metal nanowire inside a MWCNT. This sample was synthesized at 750ºC. (a) Concentration profile of Iron and Cobalt across the nanotube, derived from EELS line scans. (b) Concentration profile from the particle located at the tip of the same nanotube.*

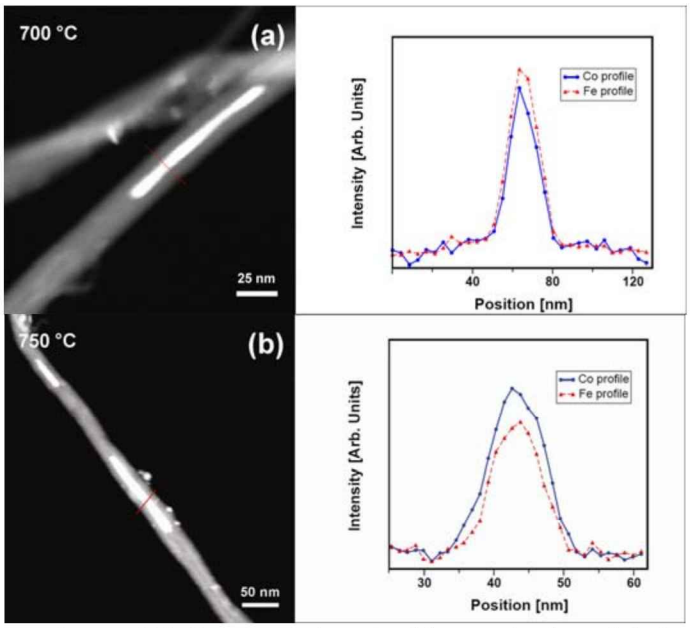

Fig. 2.31. *Linear mappings of FeCo nanowires inside nantoubes. (a) Sample synthesized at 700°C exhibits an equilibrated concentration profile of both metals, Co and Fe. (b) Nanotube synthesized at 750°C that contains several alloyed nanowires in its cavity. The concentration profile exhibits FeCo stoichiometry of the wire.*

EELS mapping studies on various samples indicated the uniform presence of Fe and Co within the same nanowire (Fig. 2.32a-d and Fig. 2.33a-d). At 650 °C, pure Co nanowires presence was noted (Fig. 2.32e-h and Figure 2.33e-h)). This observation is consistent with the XRD patterns, which indicated the formation of γ-Co in addition to cementite (Fe_3C) and FeCo.

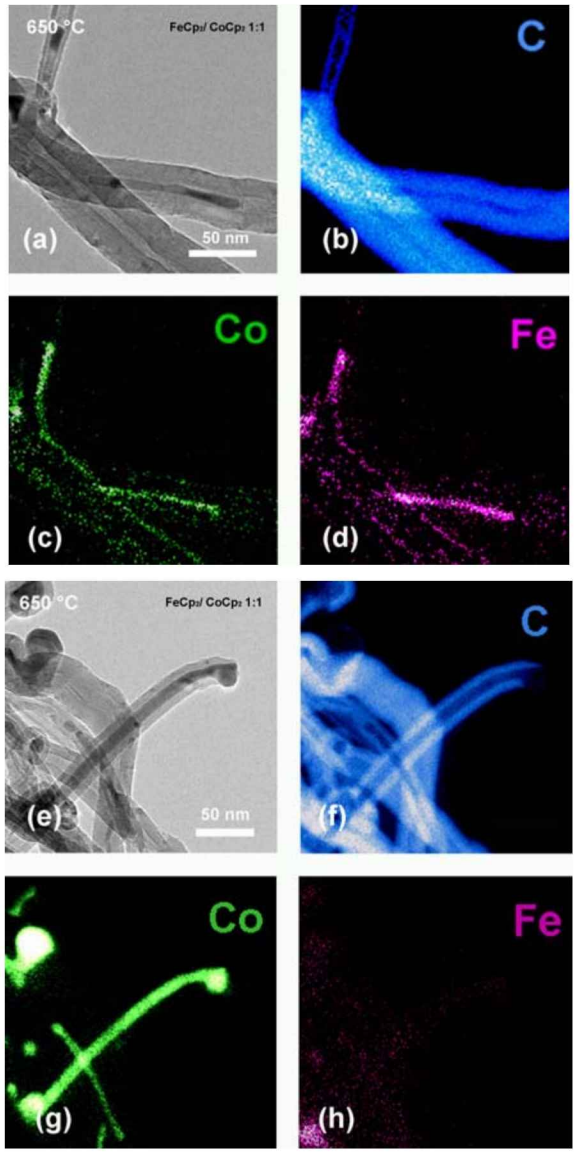

Fig. 2.32. *Elemental mapping of nanowires synthesized at 650 °C. (a) and (e) Bright field images; (b) and (f) Carbon maps; (c) and (g) Cobalt maps; (d) and (h) Iron maps. Notice the existence of an FeCo alloy in figures (a) to (d) and the segregation phenomena in (e) to (h), consistent with the XRD pattern (see figure 2.22).*

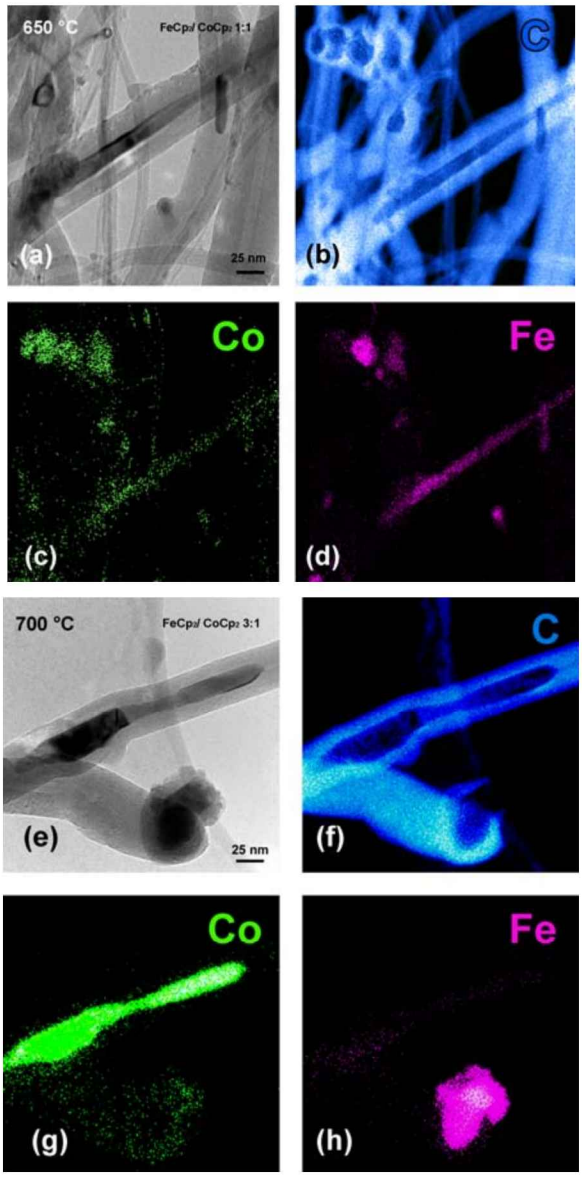

Fig. 2.33. *Elemental mapping of nanowires synthesized at 650 and 700 °C. (a) Bright field image of nanowires synthesized at 650 °C; (b) Carbon map obtained from elemental mapping; (c) Cobalt map; (d) Iron map. (e)-(h) Segregation phenomenon present in a sample synthesized at 750 °C; nanowires synthesized pyrolyzing a 3:1 mixture of $FeCp_2$ and $CoCp_2$ in toluene. (a) Bright field image. Elemental mapping of the nanomaterial shows (b) carbon, (c) cobalt and (d) iron maps.*

The prepared solutions of $FeCp_2$ and $CoCp_2$ in toluene were also mixed in 3:1 ratio,

to be pyrolyzed. The results were similar to those reported for the 1:1 mixture. Figure 2.33e-h shows one of these samples, synthesized at 700 °C. It is clear that the encapsulated nanowire is formed by Co, so it is concluded that the segregation phenomena presented in figure 2.32e-h is taking place in this sample as well, which is consistent with the phase diagram (figure 2.6). The encapsulated particle that appears in figure 2.33(e) is formed of pure Fe as it can be observed in figure 2.33(h).

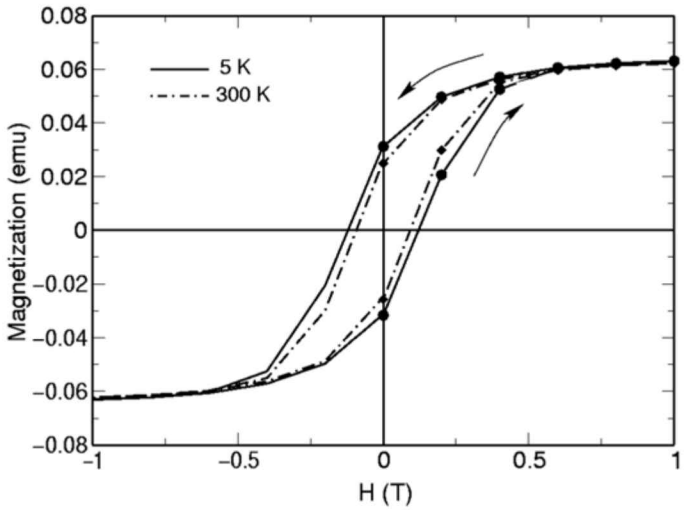

Fig. 2.34. *Hysteresis loops for bulk iron-cobalt nanowire(s) synthesized at 700 °C. The coercive field at 5 K is 0.12 T (1212 Oe) and decreases to 0.09 T (928 Oe) at 300 K. Note that the hysteresis curve at negative applied field is not from the experiment but from the mirror of the experimental point obtained at H > 0.*

SQUID magnetization measurements were performed on the synthesized products. In particular, randomly distributed nanotubes with FeCo nanocrystals, produced at 750 °C, revealed typical soft ferromagnetic behavior. The hysteresis loops exhibited coherent rotation upon demagnetization (Fig. 2.34). It is important to note that the coercive fields obtained in this sample were large at room temperature (ca. 928 Oe) when compared to bulk phases of FeCo (H_c=0.68 Oe) [15]. At 5 K, the coercive field did not vary significantly and stabilized at *ca.* 1212 Oe. These results indicate that

these materials should have potential value for the fabrication of magnetic devices operating at room temperature. It is worth mentioning that pure Fe-filled carbon nanotubes exhibited large differences in coercivities at different temperatures; varying from 450 Oe at room temperature to 2000 Oe at 5 K [14].

2.2.5 Discussion and possible growth mechanism of FeCo nanowires inside nanotubes and Perspectives

It is important to note that the presence of Fe and Co during thermolysis always results in high yields of carbon nanotubes with a low concentration (< 5% by volume) of unwanted carbon impurities (e.g. encapsulated metal particles, amorphous carbon, etc.) (Fig. 2.17-2.20). The FeCo alloy formation is consistent with the phase diagram of bulk Fe-Co (Fig. 2.10). Detailed characterization allows to conclude that a metal catalytic particle (either Co, Fe or FeCo) was always responsible for the nanotube growth.

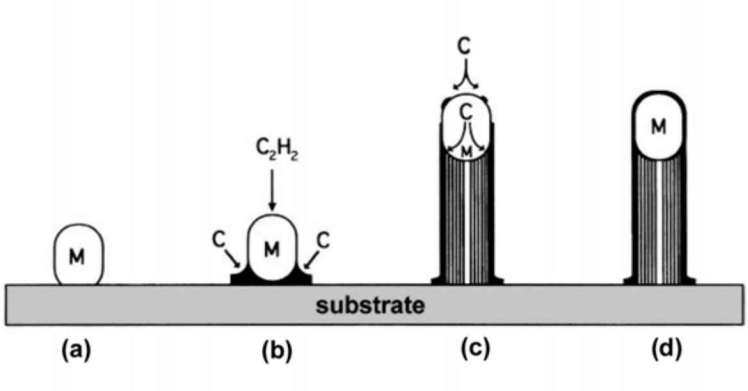

Fig. 2.35. *Scheme of the carbon filament growth mechanism first proposed by Baker [32]. In this experiment, acetylene (C_2H_2) was used as a carbon source. The metal catalyst particle helps acetylene to decompose and carbon species diffuse through it and precipitate at the bottom of the particle, forming the carbon fiber [32].*

In the past, possible carbon filament growth mechanisms have been described. There are three main mechanisms regarding the growth of carbon fibers. One was named top carbon diffusion through catalytic particles [32]. It was first proposed by Baker et al. [32] and other authors subsequently. Here, the metal catalyst is placed on the substrate (figure 2.35(a)) and the carbon source (acetylene) reacts with it, forming C_n and H_2 species (figure 2.35(b)). Subsequently, C_n fragments diffuse through the metal catalyst and precipitate, starting the formation of the carbon filament layers (figure 2.35(c)). The catalyst activity stops when there are no more carbon species to react with it, or when the metal particle is neutralized (figure 2.35(d)).

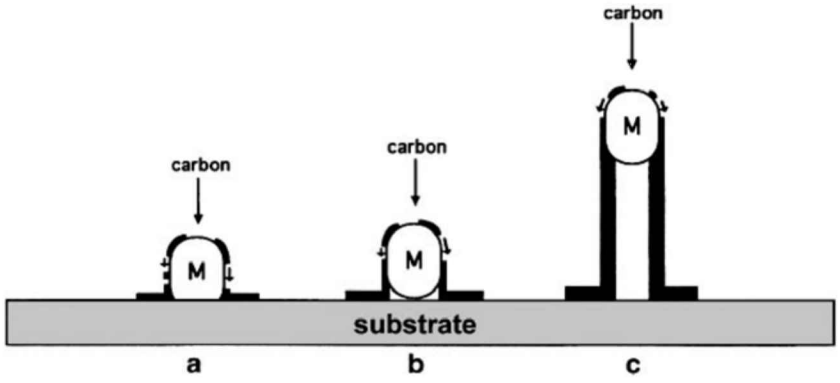

Fig. 2.36. *Carbon fibers growth mechanism, called "top carbon diffusion on catalytic particle". The catalyst is deposited on the substrate en carbon diffuses on its surface and precipitates to the lower part of the catalyst, constituting the carbon fiber [32].*

A similar mechanism to the previous is named top carbon diffusion on catalytic particles [32]. This was proposed for the first time by Baker and coworkers [32]. Again, the metal catalyst particle is placed on the surface of the substrate and there are carbon species surrounding it (figure 2.36(a)). Carbon fragments travel on the

catalyst particle surface, from the top to the bottom and they accumulate below the catalysts, starting the formation of the carbon filament (figure 2.36(b)). Carbon species continue to diffuse on the catalyst and it goes up while the carbon filament grows (figure 2.36(c)).

The third mechanism is called bottom carbon diffusion through catalytic particles [32]. In this mechanism, Fe catalyst particle are placed on Pt substrates (figure 2.37(a)). Acetylene was used as carbon source in CVD experiments explained by this model and C_2H_2 molecules make contact with the catalysts (figure 2.37(b)); carbon fragments diffuse through the particle and start the growth of the carbon filament upwards while the catalysts remains on the substrate (figure 2.37(c)). When the catalysts activity stops, the carbon filament growth finishes (figure 2.37(d)).

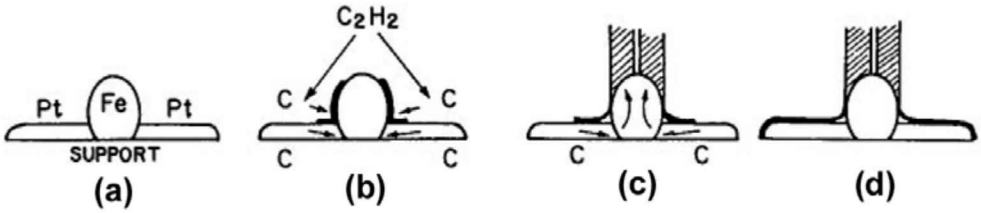

Fig. 2.37. *Base growth carbon filament mechanism. In this case Fe-Pt catalysts remains in the surface of the substrate during the formation of the carbon cylinder; acetylene decomposes and carbon diffuses through it, from the bottom to the top, forming the carbon fiber [32].*

Recent in situ TEM observations [31,32] have demonstrated that these mechanisms

could take place during NT growth. However it is not the scope of this chapter to discuss individually each of them.

Based in growth mechanisms for carbon filament described above, here it is proposed a formation mechanism of alloyed nonowires inside carbon nanotubes is modeled in figure 2.38. Fine and uniform droplets of $FeCp_2$, $CoCp_2$ and C_7H_8 molecules (Figure 2.38(a)) fragment rapidly forming Fe and/or Co clusters, H_2 molecules, as well as C_x species in the gaseous phase (Figure 2.38(b)). Depending on the temperature, these clusters could either generate FeCo phases or segregate into Fe and Co (Figure 2.38(b)). Subsequently, any of these clusters continue growing in diameter and start condensing on the quartz (SiO_x) substrate forming nanoparticles (5 - 20 nm in diameter), which react with gaseous molecules and species present in the environment (Figure 2.38(b)). At this point, the exposed metallic particles start to react exothermally with C_x species (Figure 2.38(c)). Most of the times, the metal particles are well fixed to the substrate, and the C_x species are extruded upwards, in the form of crystalline carbon cylinders (Figure 2.38(d)). During precipitation, additional metal clusters coming from the gas phase could be coalescing with the base metal particle (Figure 2.38(e)), thus resulting in the formation of a metal nanowire (Figure 2.38(f)) (Fe, Co or FeCo, depending on the reaction temperature). The use of two metals possibly enhances the formation of nanotubes due to the high surface activity of the various metallic clusters.

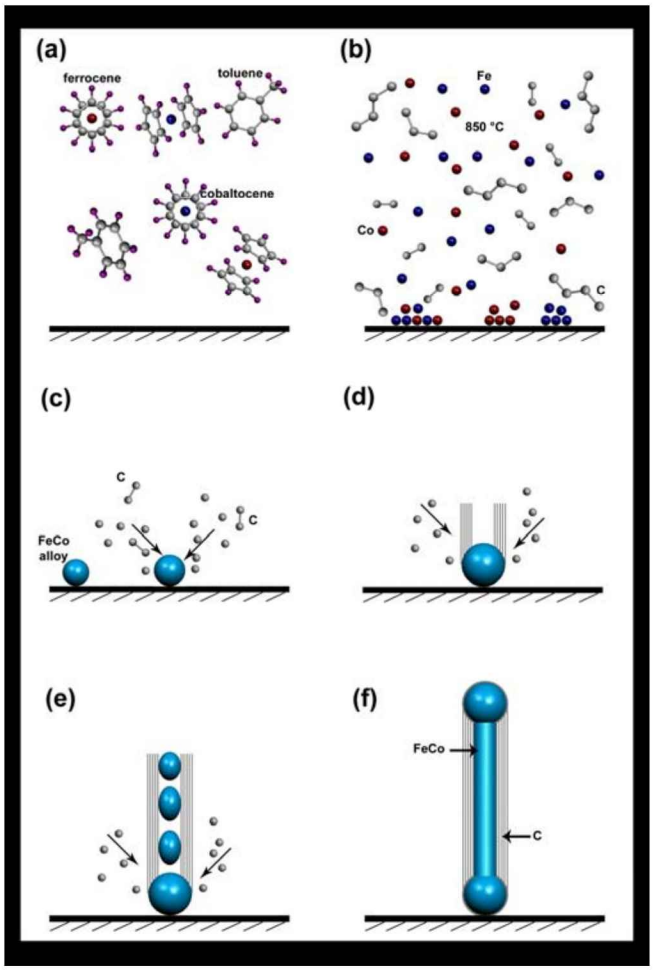

Fig. 2.38. *The formation mechanism of alloyed nonowires inside carbon nanotubes. (a) Model of the molecules present in the reaction ($FeCp_2$, $CoCp_2$ and C_7H_8). (b) With temperature, $FeCp_2$, $CoCp_2$ and C_7H_8 molecules fragment rapidly forming Fe and/or Co clusters, H_2 molecules, as well as C_x species in the gaseous phase. Depending on the temperature, these clusters could either generate FeCo phases or segregate into Fe and Co. Subsequently, any of these clusters continue growing in diameter and start condensing on the quartz (SiO_x) substrate forming nanoparticles (5 - 20 nm in diameter). (c) The exposed metallic particles start to react exothermally with C_x species. (d) Metal particles are well fixed to the substrate, and the* C_x species are extruded upwards, in the form of crystalline carbon cylinders. (e) Additional metal clusters coming from the gas phase could be coalescing with the base metal particle t*hus resulting in the formation of a metal nanowire. (f) Model of an FeCo nanowire inside a MWCNT.*

2.2.6 Conclusions

In summary, it has been described the production of single-crystal FeCo nanowires inside multi-walled carbon nanotubes using the aerosol pyrolysis method. The products were analyzed by diverse electron microscopy and allied studies. TEM, SEM and associated analytical techniques demonstrated that the alloyed wires were uniform, monocrystalline, and exhibited homogenous Fe and Co concentrations within the wire. The optimal temperatures in order to obtain stoichiometric FeCo alloy nanowires (1:1 ratio) were found between 700 and 750 °C. The high coercive fields of the nanowires obtained at room temperature (ca. 928 Oe) are unusual when compared with Fe-filed carbon nanotubes. Note that the most stable phase was FeCo and other stoichiometries were not successfully obtained, even when changing the ratios of ferrocene and cobaltocene in the starting solutions.

The achievement of synthesizing isolated ferromagnetic nanowires inside MWCNTs is important for their application in the quantum magnetic disk, first proposed by Chou et al [17]. A schematic view of this storage device is depicted in Figure 2.9. Film structures of this kind, based on single-domain elements, could exhibit the best available storage densities [35]. The presence of carbon nanotubes does not affect the magnetic or mechanical properties of the wires and it is even positive, since protects the nanowires form oxidating agents that could diminish their magnetic properties.

Magnetization measurements [M(H)] were performed as described above. It was reported a high coercive field at room temperature but the sample at this point was randomly oriented. From the experiments reported in this chapter came out aligned carbon nanotubes. Therefore, by placing removable substrates inside the quartz tube during pyrolysis, it is possible to obtain intact arrays that can be placed into a

SQUID system, in order to perform a more complete magnetic characterization, which includes the determination of H_c vs. temperature plots for different angles of application of the external magnetic field.

Since the FeCo nanowires produced are single crystals, one envisages that these materials could have enhanced mechanical properties when compared to polycrystalline wires. For instance, it is possible to predict a significant improvement of the material strength. These findings may expand the applications of FeCo nanoalloys in the fabrication of magnetic power generating systems, operating at high temperatures under high mechanical stress. In addition, the fact that the FeCo (110) planes are usually oriented perpendicular to the wire axis, should stimulate theoretical determination of their magnetic properties.

References

[1] Terrones, M. "Carbon nanotubes: synthesis and properties, electronic devices and other emerging applications" *Int. Mat. Rev.* **2004**, 49(6), 325-377.

[2] Mayne, M., Grobert, N., Terrones, M., Kamalakaran, R., Rühle, M., Kroto, H. W., Walton, D. R. M. "Pyrolytic production of aligned carbon nanotubes from homogeneously dispersed benzene-based aerosols" *Chem. Phys. Lett.* **338**, 101-107 (2001).

[3] Pinault, M., Mayne-L'Hermite, M., Reynaud, C., Pichot, V., Launois, P., Ballutaud, D. "Growth of multiwalled carbon nanotubes during the initial stages of aerosol-assitedCCVD" *Carbon* **43**, 2968-2976 (2005).

[4] Grobert, N., Terrones, M., Osborne, O.J., Terrones, H., Hsu, W. K., Trasobares, S., Zhu, Y. Q., Hare, J. P., Kroto, H. W., Walton, D. R. M. "Thermolysis of C_{60} thin film yields Ni-filled tapered nanotubes" *Appl. Phys. A* **67**, 595-598 (1998).

[5] Rao, C. N. R., Sen, R., Satishkumar, B. C., Govindaraj, L. "Large aligned-nanotube bundles from ferrocene pyrolysis" *Chem. Commun*. **15**, 1525-1526 (1998).

[6] Mayne-L'Hermite, M., Armand, X., Porterat, D., Reynaud, C. "Pyrolysis od mixed aerosols: a versatile CVD-based process to produce clean and long aligned multi-walled carbon nanotubes" *Procedings of chemical vapor deposition-XVI and EUROCVD-14* **Vol**. **2003-2008**, 549-56 (2003).

[7] Ajayan, P. M., Iijima, S. "Capillarity-induced filling of carbon nanotubes" *Nature* **361**, 333-334 (1993).

[8] Banhart, F., Grobert, N., Terrones, M., Charlier, J. C., Ajayan, P. M. "Metal Atoms in Carbon Nanotubes and Related Nanoparticles" *Int. J. of Modern Physics B* **15**, 4037-4069 (2001).

[9] Sloan, J., Kirkland, A. I., Hutchison, J. L., Green, M. L. H. "Integral atomic

layer architectures of 1D crystals inserted into single walled carbon nanotubes" *Chem. Commun.* **13**, 1319-1332 (2002).

[10] Ruoff, R.S., Lorents, D.C., Chan, B.C., Malhotra, R., Subramoney, S. "Single Crystals Metals Encapsulated in Cabon Nanoparticles" ***Science*** **259**, 346-348 (1993).

[11] Tsang, S.C., Chen, T.K., Harris, P.J.F., Green, M.L.H. "A simple chemical method of opening and filling carbon nanotubes" *Nature* **372**, 159 (1994).

[12] W K Hsu, S Trasobares, H Terrones, M Terrones, N Grobert, Y Q Zhu, W Z Li, R Escudero, J P Hare, H W Kroto and D R M Walton "Electrolytic formation of carbon-sheathed mixed Sn-Pb-nanowires" *Chem. Mater.*, **11**, 1747-1751 (1999).

[13] Terrones, M., Grobert, N., Zhang, J. P., Terrones, H., Olivares, J., Hsu, W. K., Hare, J. P., Cheetham, A. K., Kroto, H. W., Walton. D. R. M. "Preparation of aligned carbon nanotubes catalysed by laser-etched cobalt thin films" *Chem. Phys. Lett.* **285**, 299-305 (1998).

[14] Grobert, N., Hsu, W. K., Zhu, Y. Q., Hare, J. P., Kroto, H. W., Walton, D. R. M., Terrones, M., Terrones, H., Redlich, P., Rühle, M., Escudero, R., Morales F. "Enhanced magnetic coercivities in Fe nanowires" *Appl. Phys. Lett.* **75**, 3363-3365 (1999).

[15] Bozorth, R. M. *Ferromagnetism*; IEEE Press: New York, 1993; pp. 190,199.

[16] Grobert, N., Mayne, M., Terrones, M., Sloan, J., Dunin-Borkowski, R.E., Kamalakaran, R., Seeger, T., Terrones, H., Rühle, M., Walton, D.R.M., Kroto, H.W., Hutchison, J.L. "Alloy nanowires: Invar inside carbon nanotubes" *Chem. Comm.* **5**, 471-472 (2001).

[17] Chou, S. Y., Wei, M. S., Krauss, P. R., Fischer, P. B. "Single-domain magnetic pillar array of 35 nm diameter and 65 Gbits/in^2 density for ultrahigh density quantum magnetic storage" *J. Appl. Phys.* **76**, 6673-6675 (1994).

[18] Whitney, T. M., Jiang, J. S., Searson, P. C., Chien, C. L. "Fabrication and

Magnetic Properties of Arrays of Metallic Nanowires" *Science* **261**, 1316-1319 (1993).

[19] McHenry, M. E., Willard, M. A., Laughlin, D. E. "Amorphous and nanocrystalline materials for applications as soft magnets" *Progress in Materials Science* **44**, 291-433 (1999).

[20] Kueser, P. E., Pavlovic, D. M., Lane, D. H., Clark, J. J., Spewock, M. "Properties of Magnetic Materials for use in High-Temperature Space Power Systems", **1967**, NASA SP–3043.

[21] Chou, S. Y. "Patterned magnetic nanostructures and quantized magnetic disks " *Proc. IEEE* **85**, Issue 4, 652-671 (1997).

[22] Chen, Z., Zhan, Q. F., Xue, D. H., Li, F., Zhou, X., Kunkel H., Williams, G. "Mossbauer study of Fe-Co nanowires" *J. Phys. Cond. Matter.* **14**, 613-620 (2002).

[23] Zhan, Q. F., Chen, Z., Xue, D.H.; Li, F., Kunkel, H., Zhou, X. Z., Roshko, R., Williams, G. "Structure and magnetic properties of Fe-Co nanowires in self assembled arrays" *Phys. Rev. B* **66**, 134436 (2002).

[24] Fodor, P. S., Tsoi, G. M., Wenger, L. E. "Fabrication and characterization of $Co_{1-x}Fe_x$ alloy nanowires" *J. Appl. Phys.* **91**, 8186-8188 (2002).

[25] Metzger, R. M., Konovalov, V.V., Sun, M., Xu, T., Zangari, G., Xu, B., Benakli, M., Doyle, W.D. "Magnetic Nanowires in Hexagonally Ordered Pores of Alumina" *IEEE Trans. Magn.* **36**, 30 (2000).

[26] Arai, K. I., Wang, H.W., Ishiyama, K. "Magnetic properties of Co-Fe electrodeposited alumite films" *IEEE Trans. Magn.* **27**, 4906 (1991).

[27] Tang, S. L., Chen, W., Lu, M., Yang, S. G., Zhang, F. M., Du, Y. W. "Nanostructure and magnetic properties of $Fe_{69}Co_{31}$ nanowire arrays" *Chem. Phys. Lett.* **384**, 1-4 (2004).

[28] Pierce, J. P., Plummer, E. W., Shen, J. "Ferromagnetism in cobalt-iron alloy nanowire arrays on W(110)" *Appl. Phys. Lett.*, **81**, 1890-1892 (2002).

[29] Lee, G. H., Huh, S. H., Jeong, J. W., Kim, S. H., Choi, B. J., Ri, H.-C., Kim, B., Park, J. H. "Arrays of ferromagnetic FeCo and FeCr binary nanocluster wires" *J. Appl. Phys.* **94**, 4179-4183 **(**2003).

[30] Massalski, T. B. *Binary Alloys Phase Diagrams;* 2nd. Edition, ASM International, National Standard Reference Data System; 1990; Vol.2, pp. 1186-1187.

[31] Yoo, C. S., Söderlind, P., Cynn, H. "The phase diagram of cobalt at high pressure and temperature: stability of γ(fcc)-cobalt and new ε'(dhcp)-cobalt" *J. Phys.: Condens. Matter*, **Vol. 10**, 20, L311-L318 (1998).

[32] Terrones M. "Science and Technology of the Twenty-First Century: Synthesis, Properties and Application of Carbon Nanotubes" *Annu. Rev. Mater. Res.* **33**, 419-501 (2003).

[33] Helveg, S., Lopez-Cartes, C., Sehested, J., Hansen, P. L., Clausen, B. S., Rostrup-Nielsen, J. R., Abild-Pedersen, F., Norskov, J. K. "Atomic-scale imaging of carbon nanofiber growth" *Nature* **427**, 426-429 (2004).

[34] Sharma, R., Iqbal, Z. "*In situ* observations of carbon nanotube formation using environmental transmission electron microscopy" *App. Phys. Lett.* **84**, 990-992 (2004).

[35] Lopez-Urias, F., Munoz-Sandoval, E., Reyes-Reyes, M., Romero, A.H., Terrones, M., Moran-Lopez, J.L. "Creation of Helical Vortices during Magnetization of Aligned Carbon Nanotubes Filled with Fe: Theory and Experiment" *Phys. Rev. Lett.* **94**, 216102 (2005).

***EELS is different form Fe or Co alone. Please check. Check if Co is correct, the plot is different. From the inoiztion edges of Fe (708 eV) and Co (840 or 780 eV) specify ionizarion edge. Try to obtain differences and shifts of Fe and Co form FeCo EELS. The peaks look very different!! This is interesting. Please compare ionization edges!! Ask Molly and check other papers. MTM

3. Pyrolytic synthesis of long strands of large diameter SWNTs at atmospheric pressure

In this section, the synthesis of centimeter-long strands of single walled carbon nanotubes by the aerosol pyrolysis method is described. The experiment consists on the thermolysis of $FeCp_2$-ethanol solutions at temperatures ranging form 800 to 950 °C. The diameter of the produced nanotubes is proportional to the amounf of $FeCp_2$ in the solution or the increase in temperature. This method is advantageous because there is no need to use H_2, sulphur agents or vacuum.

3.1 Synthesis of single-walled carbon nanotubes by CVD method: An Overview

Carbon nanotubes (single- and multi-walled), considered as a novel forms of nanocarbon [1,2] have been subject of extensive research. In particular, SWNTs could behave as metals or semiconductors depending on the tube diameter and chirality (the orientation of the hexagonal rings with respect to the tubule axis, see chapter 1). Although SWNTs could now be produced using different techniques [3], there is still no control over the chirality and diameter. It is important to improve the synthesis and control the tube dimensions and chirality, even thus chemical methods have been able to separate semiconducting and metallic tubes [4,5].

SWNTs exhibit quantum confinement along the single-atom-thin tubule circumference. However their production appears to be more complicated when compared to that of MWNTs. Three main routes are now used to produce SWNTs: 1) arc discharge of graphite electrodes in the presence of metals (e.g. Ni, Co, Y) [2], 2) laser ablation of graphite-metal targets, and 3) chemical vapor deposition (CVD) of organic precursors over metal catalysts [3, 4-6]. These catalysts could be deposited in different ways onto substrates, so that the tubes grow from there. The most common methods for reacting these metal particles with carbon species are: i) by patterning metal particles on porous substrates via anchoring techniques (templating method) [3,4-7] and ii) by promoting in-situ chemical reactions in the gas phase (floating catalyst) [8-10].

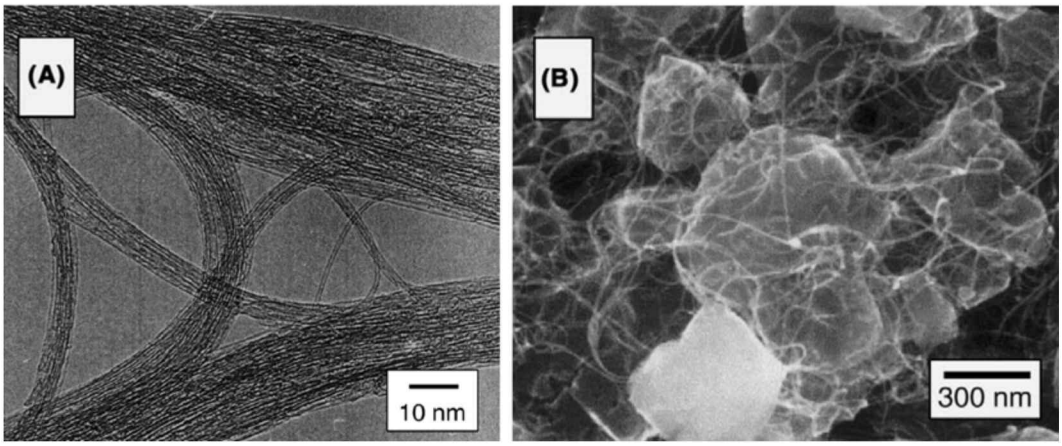

Fig. 3.1. *200 kV TEM image of pristine SWNTs synthesized by catalytic decomposition of ethanol over an Fe/Co mixture embedded in zeolite, at 800 °C. The SWNT bundles appear to be free of amorphous carbon and other impurities, without being purified. (b) Lower magnification SEM image of as grown SWNT material on zeolite surfaces (obtained from Maruyama's paper [13]).*

The CVD method is suitable for the large scale production of SWNTs and MWNTs, and has the advantage of permitting the use of solid, liquid and gaseous carbon precursors. It is also possible to produce doped carbon nanotubes with N or B,

when varying the CVD precursor [11,12]. Gaseous carbon sources are often preferred for SWNT production (*e.g.* methane, ethylene carbon monoxide). A significant step towards SWCNTs production from liquid carbon source was reported by Maruyama and co-workers [13]. They found the suitability of oxygenated organic molecules for SWCNT production. Using this particular method, SWNTs were grown from alcohols (MeOH, EtOH) by their thermal decomposition over metal catalysts (Fe and Co), at low pressures of about 5 Torr (see figure 3.1).

It was conjectured that OH radicals, produced during thermal decomposition, played a key role in removing amorphous carbon via the formation of gaseous CO and CO_2, and in inhibiting the growth of secondary layers (known as double-walled nanotubes DWNTs and MWNTs). This process also increased the life time of the catalyst, which is often deactivated by excess of amorphous carbon. Subsequently, Zheng et al. [14] used the same approach to produce cms-long SWNTs (see figure 3.2). However, long strands of SWNTs could also be produced using containing precursors that do not contain oxygen. In this context, Zhu et al. [15] used hexane/ferrocene/thiophene solutions at 1150°C along in conjunction with hydrogen, to synthesize SWNT bundles of several centimeters in length [7] (see figure 3.3). Later, Windle's group [16] managed to direct spin SWNT-bundles in continuous fibers by thermolyzing oxygen solvents together with ferrocene, in the presence of thiophene and hydrogen at 1200 °C (see figure 3.4).

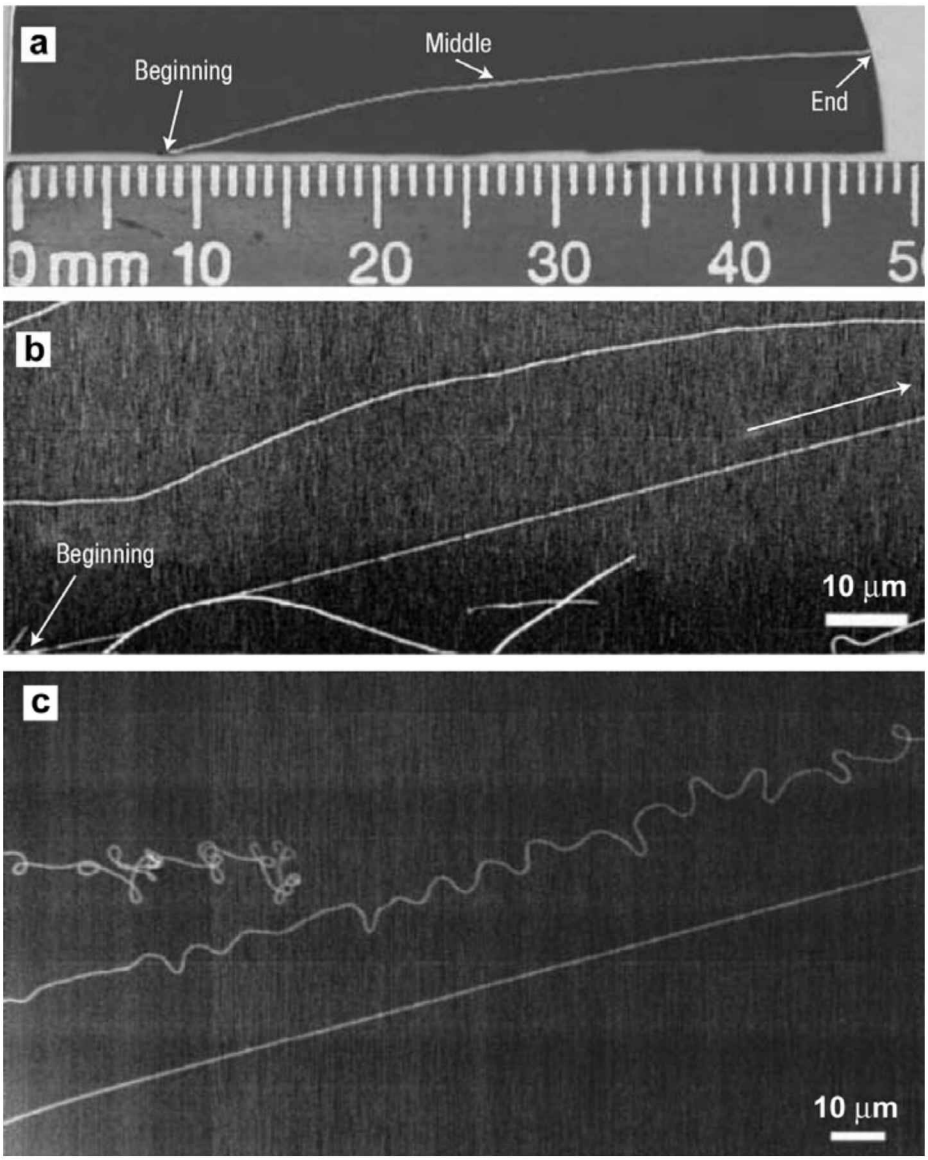

Fig. 3.2. *(a) SEM superimposed images depicting a 4-cm long SWNT rope placed on a Si substrate. (b) SEM image of the beginning segment of a straight SWNT rope. (c) SEM image of a SWNT rope that ended on the Si Substrate surface away form edges, exhibiting its wavy and tangled morphology; SWNT in the middle is wavy as well; SWNT rope at the bottom is straight and continues to grow to longer length (obtained from Zheng's paper [14]).*

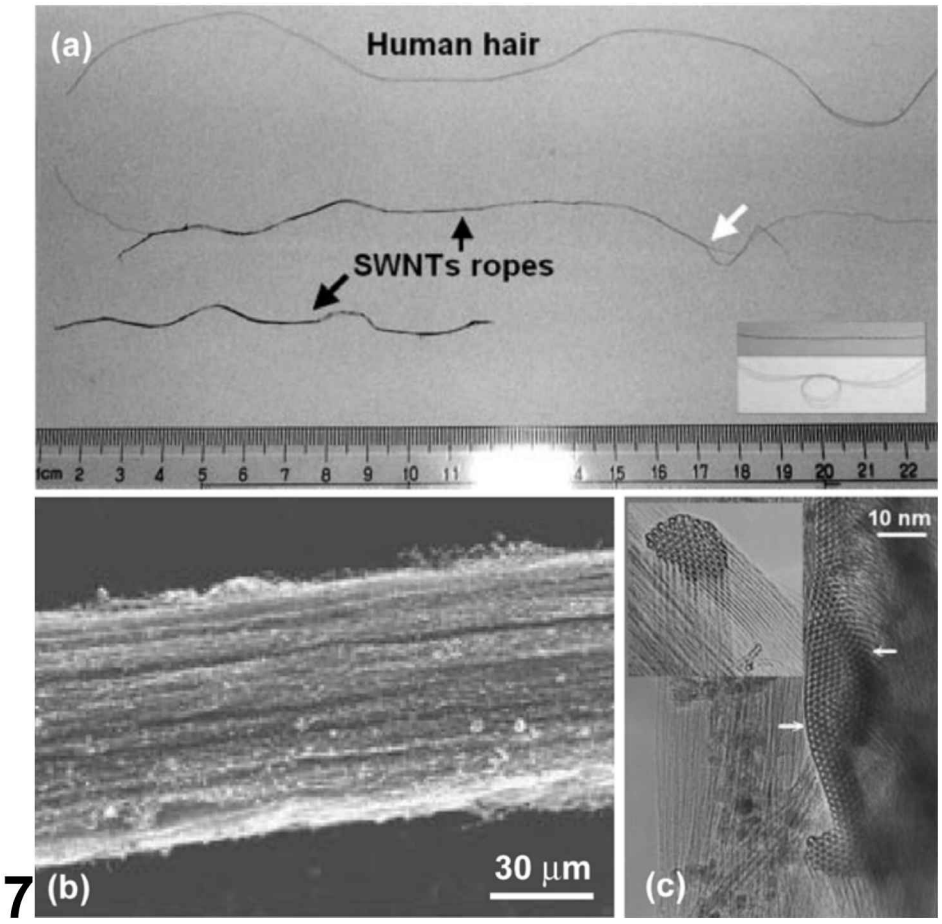

Fig. 3.3. *(a) Optical microscope image showing a comparison between a human hair and SWNTs strands of outstanding lengths (20 and 10 cm). SWNTs strands are composed by thinner ropes (0.3-0.5 nm diameter). The inset shows the high flexibility of SWNTs strands, where one strand is straightened and another one is tied in a knot without breaking. (b) Low-magnification SEM image of a long SWNTs strand. (c) HRTEM image of a SWNTs rope. Arrows indicate the hexagonal arrangement of individual nanotubes within the rope. Inset exhibits the cross section a SWNTs bundle (obtained from Zhu's paper [15]).*

Hata et al. [17] further developed the idea of using oxidizing agents during the CVD process in order to keep active the catalyst and avoid the formation of unwanted carbonaceous materials. These authors proposed that a controlled amount of water when feeding the reactor with hydrocarbons increased the yield of

aligned SWNT bundles on patterned substrates (see figure 3.5).

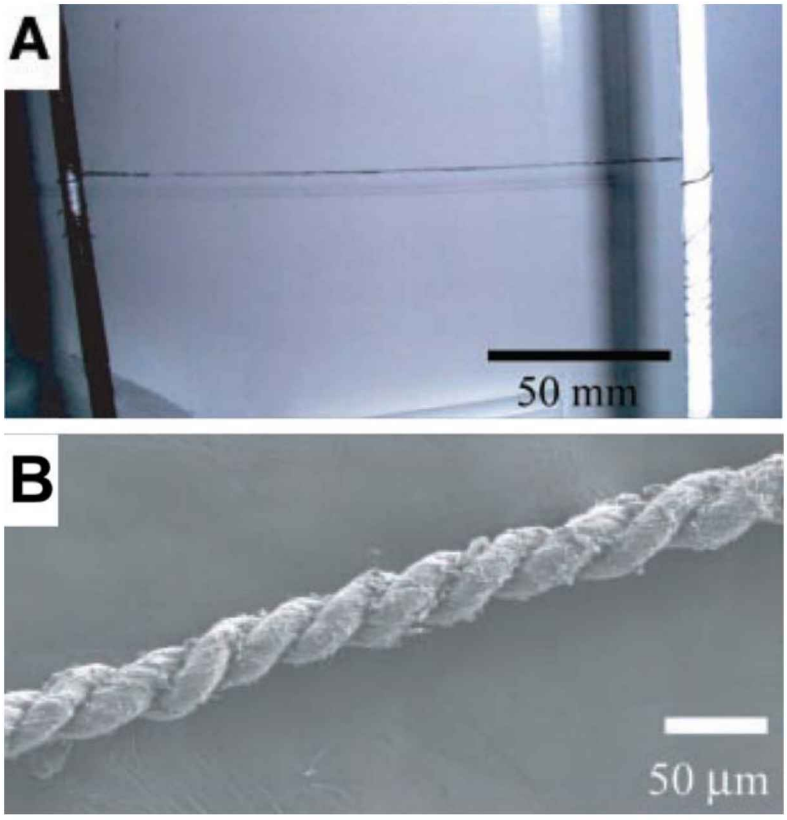

Fig. 3.4. *(a) SWNT strand being wounded from the left spindle onto the right spindle, which has outstanding length. (b) SEM image of a SWNT fiber which was twisted before being extracted form the furnace (obtained from Li's paper [16]).*

The production of macroscopic amounts of cm-long strands consisting of SWNT bundles, using an alternative route involving the spray pyrolysis ferrocene-ethanol solutions, is described in the following sections. This floating catalyst process is not carried out at low pressures, and does not require high pyrolytic temperatures or possible contaminating additives such as thiophene, water or H_2. However and more importantly, the SWNT material condensed outside the reaction zone (at lower temperatures than 950°C). Therefore, the use of a high temperature gradient caused by the high temperature cracking zone (inside the furnace) and the room

temperature zone (outside the furnace) is fundamental to produce SWNTs in this system.

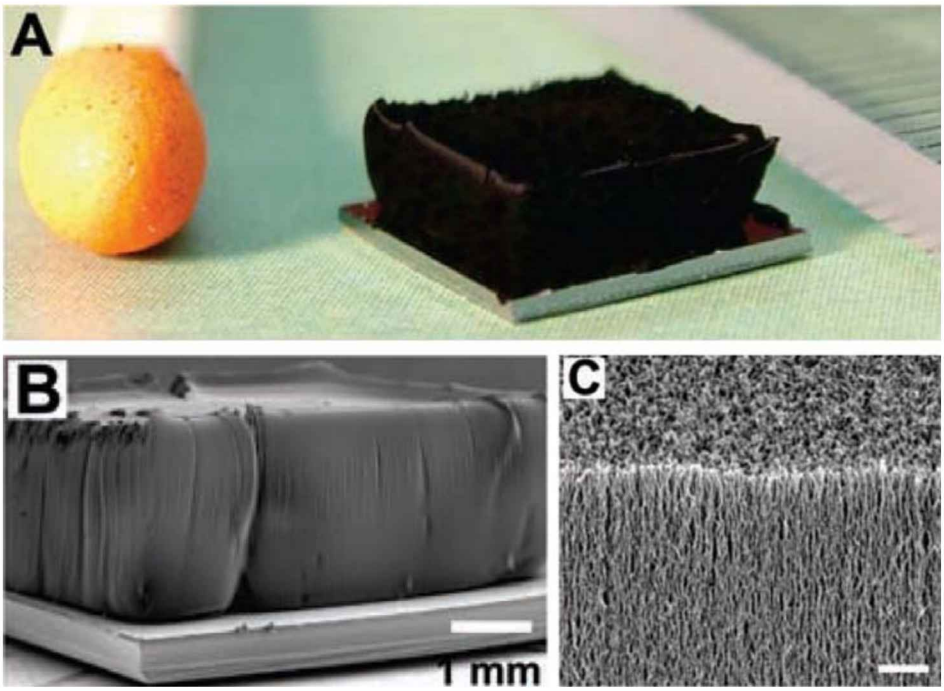

Fig. 3.5. *Aligned SWNT array grown with water-assited CVD. (a) Photograph of a 2.5-mm-tall SWNT array on a 7²mm silicon wafer. A matchstick on the left is shown for size reference. (b) SEM image of the array shown in (a). (c) Higher magnification SEM image form (b). Scale bar, 1 μm (obtained from Hata's paper [17]).*

3.2 Synthesis of SWCNTs by the aerosol pyrolysis of ferrocene:ethanol solutions

Solutions of ethanol (Aldrich 99.99%) - ferrocene ($FeCp_2$; Aldrich 99.97%) were prepared by dissolving different ferrocene ratios in (typically) 300cc of ethanol; subsequently all solutions were sonicated for 30 minutes (SonoPlus with tip MS73, Bandelin, power: 10%), and transferred to the reservoir of the sprayer. Solutions

containing 0.2, 0.4, 0.6, 0.8, 1.0, 1.25 and 1.5 wt.% of ferrocene were employed. The sprayer system used has been described in chapter 2 [18,19]. The reaction quartz tube was heated up to temperatures varying from 700 – 950 °C using a tubular furnace (40 cm-long).

The quartz tube was positioned 12 cm outside the furnace next to the sprayer. Once the furnace reached the desired reaction temperature, the alcohol-ferrocene solutions were turned into an aerosol, by a piezoelectric placed at the bottom of the solution container (see chapter 2 for details). The aerosol was carried inside the quartz tube using a high purity Ar flow of 0.5 - 1.0 L/min (Messer Griessheim 99.999% at 1 atm). The pyrolytic reactions were carried out for 30 minutes.

After 5-7 minutes of spraying the solutions, black treads could be seen in the quartz tube at the exit of the furnace. The length and the amount of these treads increased with time and after *ca*. 15 minutes, it was not possible to distinguish the single threads inside the tube but only a dark film coating the inner surface of the silica tube located outside the reaction zone (Fig. 3.6(a)). After the completion of the experiment, the tube and its contents were allowed to cool until they reached the room temperature under an Ar atmosphere. A black deposit was obtained inside the furnace (center of the reaction zone). This deposit was easily removed by scratching the inner surface of the tube (see movie located at http://materials.ipicyt.edu.mx/SWNT_growth/).

The dark film observed at the exit of the oven, was collected using a long metal tool (see movie located at http://materials.ipicyt.edu.mx/SWNT_growth/), as it is depicted in Figures 3.6b and c. The net could be extracted as a long strand by twisting the metal tool (< 12cm; Fig. 3.6d). It is important to note that the formation of this net ocurrs on the cold part of the reaction zone. The measured temperature

was of about 500 °C, when the oven was operated at 950 °C.

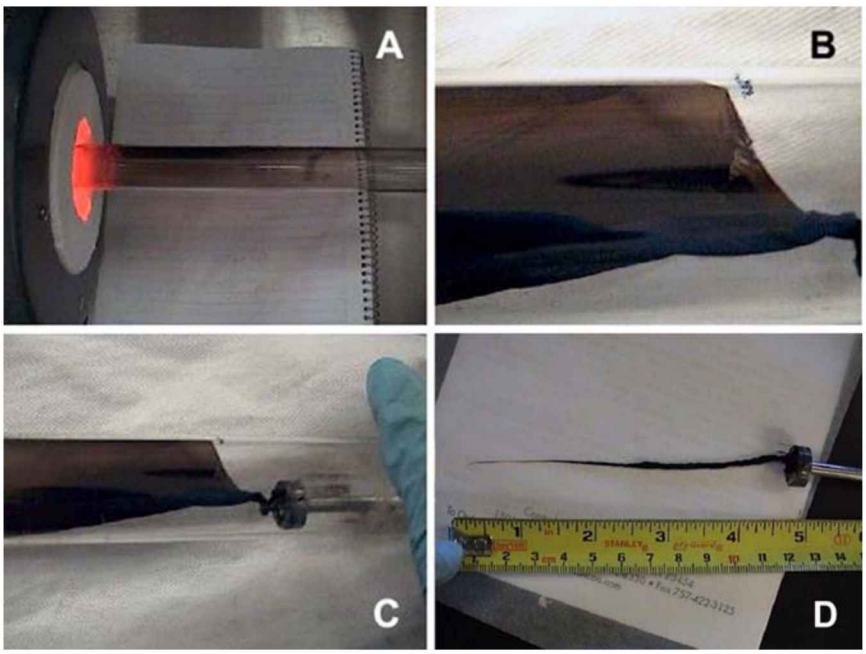

Fig. 3.6. *Photographs showing the formation and collection of SWNT material obtained after reacting ferrocene-alcohol at 800-950 °C. (a) Picture depicting the formation of a light black coating formed on the outside of the furnace, after 5 min of reaction; (b,c) Images showing the way the dark film could be easily removed by twisting a piece of wire, and (d) Picture revealing the long strand that can be obtained from these experiments. In this case, the strand was 12 cm long and consisted of SWNTs and Fe catalyst.*

3.3. Characterization of the SWCNTs produced by ferrocene:ethanol pyrolysis

The black deposits grown inside the furnace, and the strands collected from the outside were analyzed by scanning electron microscopy (SEM; JEOL JSM 6300F, equipped with a Noran instrument EDX detector and a FEI field emission XL-30). High resolution transmission electron microscopy (HRTEM) studies were carried

out on powders dispersed ultrasonically (5 min) in ethanol, and a few drops of the suspensions were transferred onto a 3 mm lacey carbon grid (300 mesh). For these HRTEM observations three microscopes were used: a JEOL JEM-2010 FEF instrument operated at 200 kV; a JEOL JEM 4000EX operated at 400kV; and a Philips CM20 operated at 200kV. Raman spectra on various products were obtained at laser excitation energies of λ=32 nm (2.33 eV) and λ=366 nm (1.96 eV) with a Kaiser Holo Lab 5000 system.

The hard deposit formed in the hot zone and the strands (web-like material) from the cold zone of the reaction tube were analyzed by SEM, HRTEM and Raman spectroscopy. Figure 3.7 depicts SEM micrographs taken from a sample prepared using 1 wt% ferrocene in alcohol. In particular, the material obtained form the reaction zone (heated at 950 °C), consists of thin multi-walled carbon nanbotubes (diameter <35 nm) and exhibits particles at the end of the tubes that were identified as Fe usind EDX analysis (Fig. 3.7 a-b).

The web-like strands exhibits a completely different microstructure when compared to the material obtained in the hot part of the furnace. The strand looks like a wrapped sheet of homogeneous material, as observed in the low magnification micrograph shown in Fig. 3.7(c). The edge of this "sheet", visible in Fig. 3.7(c), reveals a finer structure consisting of filaments bundled together; higher magnification magnifications of these areas clearly display networks of very thin and long filaments entangled together with spherical particles (Fig. 3.7(d)). Based on SEM observations, it is possible to conclude that MWNTs are grown inside the hot temperature zone and SWNT bundles conform the strand material. These suppositions were confirmed using TEM and Raman analyses.

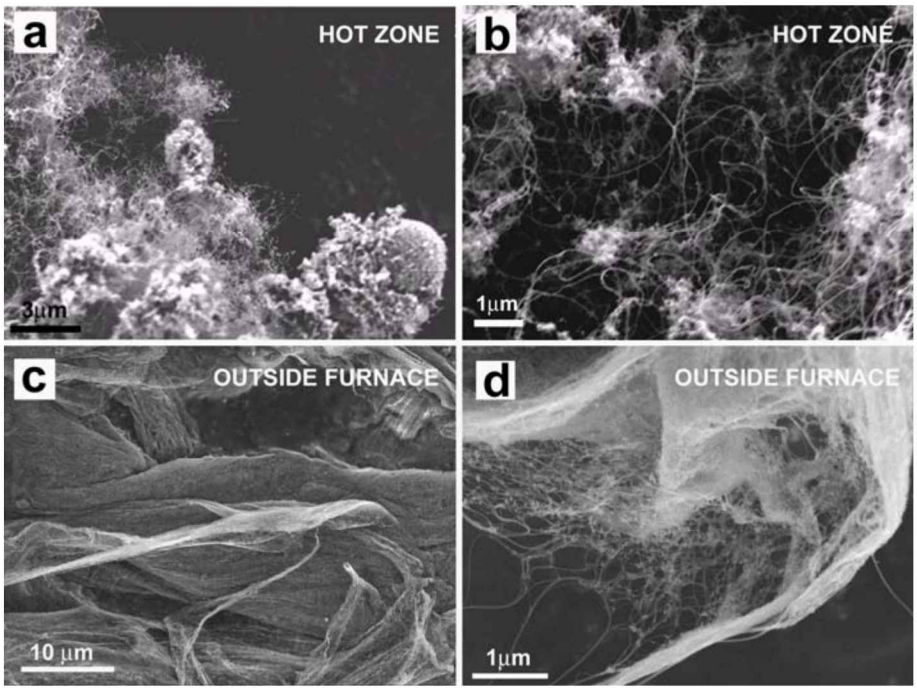

Fig. 3.7. *SEM images of (a,b) carbonaceous products collected in the high temperature region (when the furnace was operated at 950 °C), it is possible to observe filaments protruding from solid large particles; the filamentous material does not seem to be homogeneous, and high contrast regions could be observed at the ends of the filaments, attributed to Fe particles responsible of catalyzing the nanotube growth; (c,d) web-like material collected from the film deposited outside the hot zone; the material consists of entangled sheet-like material consisting of filaments and particles.*

The TEM micrograph shown in Figure 3.8(a) was obtained from the material collected in the hot zone of the reactor. Here, relatively thin (small diameter, OD 10-12nm) MWNTs were clearly distinguishable. A large number of 25-nm diameter metal particles was also present (consisting of Fe as confirmed by EDX measurements). It is interesting to note that these metal particles possess small diameters when compared to those obtained in MWNTs (30-50nm) prepared by ferrocene decomposition or the thermolysis of xylene-ferrocene solutions. Therefore, once more it was confirmed that the catalyst particle size is strongly

related to the outer MWNT diameter [6,20]. Some of the MWNTs were partially filled with Fe, and others contain metal particles at the ends, but not all; therefore both root-growth and tip-growth mechanism [20] are possible during the synthesis reported in this work.

It was never found SWNTs in the material obtained from the hot zone, thus indicating that SWNTs do not form at high temperatures. TEM studies on the web-like strands obtained form the cool part of the furnace revealed the presence of copious bundles of SWNTs as well as Fe particles. Higher magnification TEM images (Fig. 3.8(b)) shows the existence of SWNT bundles entangled to metal particles. The diameters of the Fe particles range from 2 to 25nm. These SWNTs are extremely long and it was very difficult to identify both extremes using TEM (Figure 3.9).

The best conditions for producing crystalline and clean SWNTs occurred at 950°C when pyrolyzing ferrocene concentrations of 1.25wt% in the ethanol solution. In addition, these tubes usually exhibited large diameters than those synthesized at lower temperatures, showing tubes up to 3.5 nm (Figure 3.8 and 3.9), and it is extremely difficult to find bundle cross-sections. Pyrolytic reactions carried out at 800°C revealed the presence of a large number of narrower tubes (0.9 – 1.4 nm). It is important to mention that the SWNT (web-like material) was hardly obtained outside the furnace at temperatures lower than 800°C and ferrocene concentrations below 0.6 wt%.

In order to get a better understanding about the growth of these SWNTs on the cold region, different types of nanotube materials were produced by varying the reaction furnace temperature from 800 to 950°C, using a fixed concentration of 1.2 wt% in EtOH (Fig. 3.9), and different ferrocene concentrations in the alcohol

solutions (e.g. 0.6, 0.8, 1.0, and 1.25 wt% of ferrocene). HRTEM and Raman spectroscopy were carried out on the products in order to identify diameter distributions, crystallinity and amorphous carbon content (Fig. 3.9).

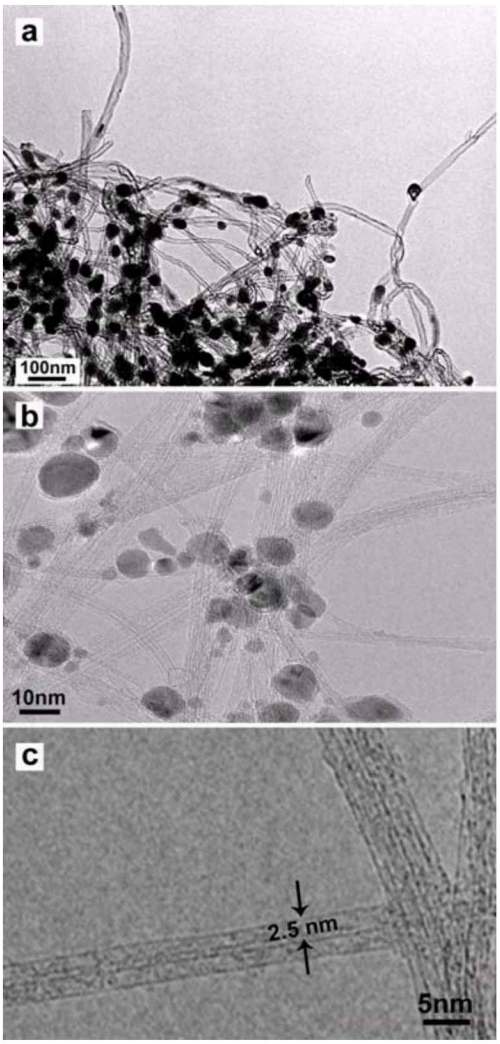

Fig. 3.8. *(a) TEM image of the material collected in the reaction zone (operated at 950 C), which consists of thin MWNTs (OD 10-35 nm). Fe particles can be clearly observed at the ends of some tubes as well as inside the tubes. The tubes are remarkably thin when compared to other types of tubes produced using different carbon precursors. (b) TEM images of the web-like material collected at the exit of the hot reaction zone (furnace operation maintained at 950 °C) revealing the presence of SWNT bundles and Fe particles; (c) higher magnification shows the SWNTs of relatively large diameter (2.5-3 nm).*

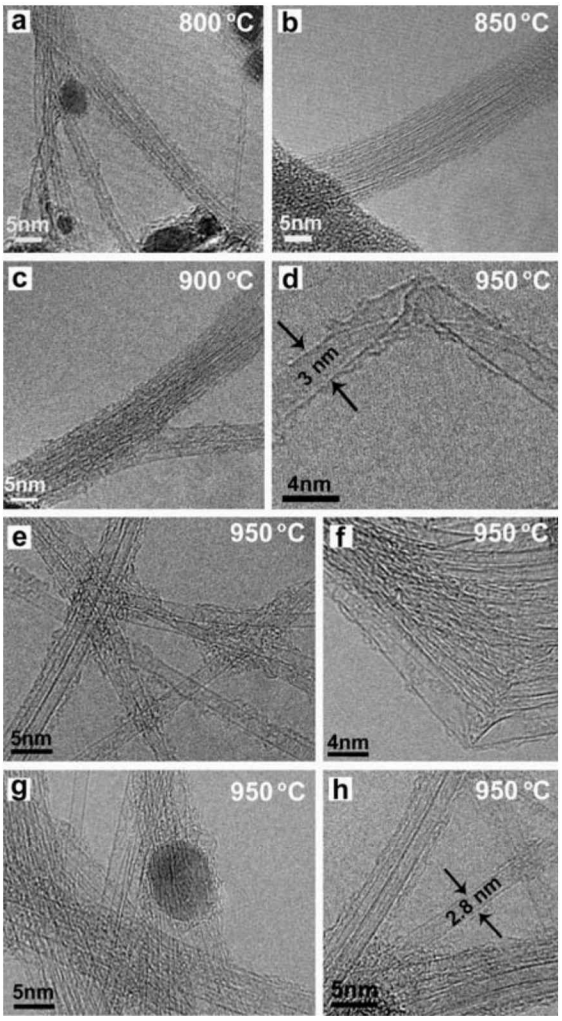

Fig. 3.9. *TEM images of the web-like material collected outside the furnace when reaction was carried out at: (a) 800 °C, (b) 850 °C, (c) 900 °C and (d-h) 950 °C. Note that as the temperature increases the diameter of the tubes also increases. It is possible to observe extremely large tubes of diameters ranging form 2.5 to 4 nm. In addition, the material appears to contain less amorphous carbon as the reaction temperature increases.*

In particular, Raman spectra of all samples of the strand-like (SWNTs) material obtained at different temperatures and ferrocene concentrations revealed multiple low frequencies associated with the radial breathing mode (RBM), which is inversely related to the tube diameter (Figure 3.10(a)). In addition, high frequencies could be also observed and these are associated with the G-band (*ca.* 1590 cm^{-1}), the

G'-band (*ca.* 2670 cm^{-1}), and a weak D-band (*ca.* 1340 cm^{-1}).

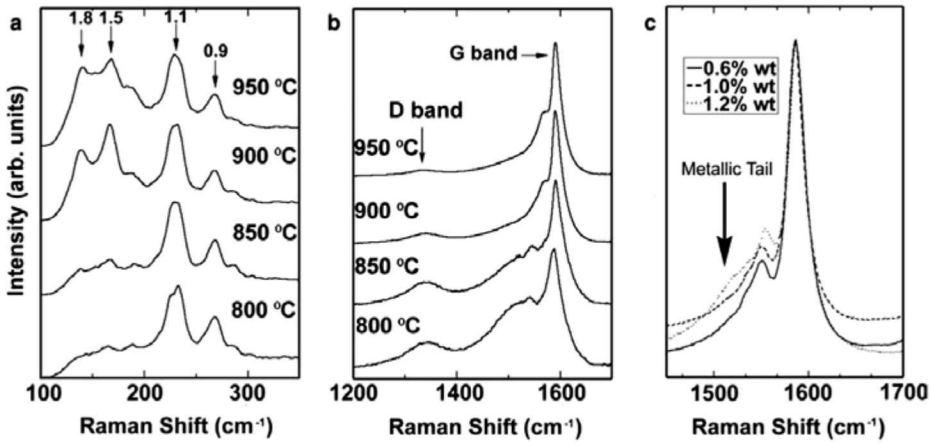

Fig. 3.10. *(a) Raman spectra in the RBM region, obtained using a 532-nm laser line on SWNT samples produced at different furnace temperatures using an alcohol solution containing 1.25 wt% of ferrocene (arrows indicate the diameters of the tubes found in the samples). As the temperatures increases, the RBM intensities corresponding to large diameter tubes (lower frequencies) increase. Note that there is not much difference between the sample obtained at 900 and 950 °C because nanotube diameters larger than 1.8 nm (usually observed using HRTEM), could not be detected in the spectrometer (e.g., frequencies below 100 cm^{-1}); (b) Raman spectra of the samples displayed in (a) showing the G-band (ca. 1550 and 1594 cm^{-1}) and D-band (ca. 1340 cm^{-1}) for different oven temperatures. The intensity of the D-band decreases as the temperature increases. This indicates that SWNT material with the highest degree of crystallinity was obtained when the furnace was operating at 950 C; (c) Raman spectra obtained using a 632 nm laser line on SWNT samples produced at furnace temperatures of 950 °C when pyrolyzing ferrocen-ethanol solutions containing different concentrations (0.6, 1.0 and 1.2 wt%). We found that a shoulder close to 1500 cm-1 (see arrow), which has been attributed to metallic tubes, increases in intensity as the ferrocene concentration increases.*

The RBM spectra shown in Fig. 3.10(a) indicate the presence of peaks below 250 cm^{-1} (usually associated with large diameter SWNTs), and smaller peaks appearing

above 250 cm^{-1}, consistent with narrow diameter nanotubes. Using the equation $\omega_{RBM} = 243/d_t$ [21], different diameters that depend on the thermolytic temperature and the ferrocene concentration were found.

In order to observe SWCNT diameter distribution, from the RBM when varying the reaction temperatures (figure 3.10(a)) for a 1.2 wt% ferrocene concentration, an excitation laser line of 532 nm was used. Clear intensities corresponding to large diameters of 1.8 nm (ω_{RBM} = 136 cm^{-1}) when the reaction occurred at 950 °C (inside the furnace). At 800 °C, the most common RBM signal was located at ω_{RBM} = 228 cm^{-1}, which is attributed to nanotubes of 1.1 nm. Larger temperatures caused a down shift in the RBM for the CVD grown SWNTs produced by Maruyama and coworkers [13], as can be observed in figure 3.11(a). These authors used an excitation wavelength of 488 nm for the Raman characterization and the estimated diameters that they reported ranged between 0.8 and 1.2 nm.

Regarding the crystallinity of the SWNT material, the intensity ratios between the D and G bands were analyzed (Figure 3.10(b)). As the D band becomes weaker, the material tends to be more crystalline. In particular, at pyrolytic temperatures of 950 °C a ratio of I_D/I_G = 0.08 was found, whereas at temperatures of 800, 850 and 900 °C, I_D/I_G corresponds to 0.32, 0.25 and 0.12, respectively. This indicates that the optimum crystalline material was obtained at 950 °C. Maruyama et al. [13] also found a decrease in the D band as they increased the reaction temperature (see figure 3.11(b)).

One could easily observe that as ferrocene concentration is increased, wider diameters start to dominate the sample and narrow tubes tend to disappear (not shown here). For example, when the ferrocene is added to alcohol at 1.2 wt%, the signal from 0.9 nm diameter tubes disappears and those located at diameters

corresponding to 1.4 are lowered in intensity, whereas the peaks for large diameter RBMs are increased and a new diameter gets prominent at 1.5 nm.

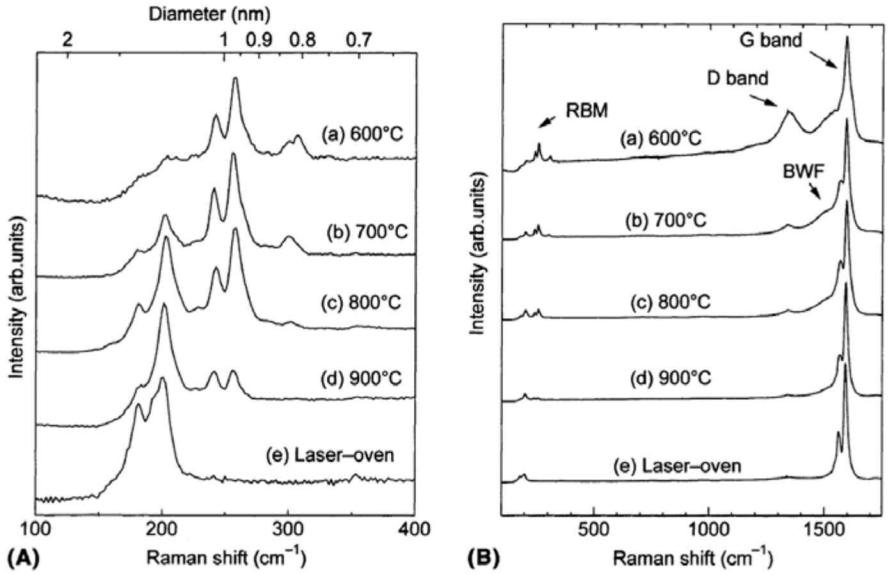

Fig. 3.11. *Raman spectra of pristine SWNTs, obtained with a 488-nm-excitation laser. (a) RBM region of the spectra obtained at different temperatures (600-900 °C). Spectrum of laser oven produced SWNts is shown for comparison. (b) G and D bands form SWNT spectra exhibiting their changes with temperature (obtained from Maruyama's paper [13]).*

It is noteworthy that the large diameter tubes observed by HRTEM of ca. 2 - 3.5 nm could not be observed because the Raman detector was not able to identify such low frequencies. However, a clear enhancement in the RBMs corresponding to nanotubes above 2 nm would be expected. It is important point out that double-walled carbon nanotubes (DWNTs) were never observed using HRTEM, and different diameters can not be attributed to concentric nanotubes. Interestingly, the tail located at *ca.* 1550 cm $^{-1}$, corresponding to metallic tubes, is enhanced considerably as the concentration of ferrocene increases to 1.2 wt% (Figure 3.10(c)). Therefore, ferrocene appears to have an influence on the production of metallic tubes of larger diameter.

3.4 Discussion and possible growth mechanism of SWCNTs produced by ferrocene: ethanol pyrolysis

It is believed that as $FeCp_2$ concentration is increased in the ethanol solution, larger Fe catalytic particles are generated. Since these catalytic particles determine the diameter of the SWNTs, tubes of large diameter are produced as the ferrocene concentration increases. In addition, as the diameter increases, the tubes tend to behave (at least locally) as graphene, thus metallic or semi-metallic contributions are significantly enhanced. A detailed study related to the metallicity needs to be carried out using electron diffraction in conjunction with Raman spectroscopy (the latter provided the spectrometer is able to identify wave numbers lower than $100cm^{-1}$).

Based on the previous results, a possible mechanism can be proposed, which accounts for the formation of SWNTs in these experiments. First, the carbon source is efficiently, cracked in the hot reaction zone and the formation of active catalyst clusters occurs. Subsequently, some of these Fe particles are attached on the wall of the reactor in order to act as a seed for nanotube growth (MWNTs), adopting the root-growth scenario. In the cooler zone (outside the furnace), SWNT growth forms possibly due to the condensation of the Fe clusters and the carbon species. In this context, it was observed that long black treads are generated in the cooler zone, and grow in the direction of the Ar flow. A similar growth mechanism has been discussed by Huang [7] for the fast heating CVD. Fe catalyst finds suitable conditions to promote SWNT growth only in a limited range of temperatures. Suitable temperature means that the metal particles possess the right dimensions [6]. However a higher temperature in the hot zone is necessary to generate extremely reactive species that able to condense as SWNT material with high crystallinity.

3.5 Conclusions

It has been demonstrated that SWNTs could be produced by pyrolyzing $FeCp_2$-alcohol solutions at 800 – 900°C, and are always deposited as a web-like material outside the reaction (at temperatures of ca. 500°C) that could be extracted as long strands. The method is novel and does not require the presence of thiophene, hydrogen or water in the solution. It was further demonstrated that the optimum conditions in our reactor for collecting high crystalline and long strands of SWNT bundles occurred at 950°C when using $FeCp_2$ concentrations of 1.25 wt% in ethanol. However, the average diameters of these tubes are relatively large (2 - 3.5 nm). As the temperature and the ferrocene concentration are reduced, the SWNT exhibit a large proportion of narrower diameters of *ca.* 1 nm. It is believed that this technique is a step forward, towards the production of SWNTs of various diameters with different electronic properties. However, further research is still needed along this direction.

References

[1] Oberlin, A., Endo, M., Koyama, T. "Filamentous growth of Carbon through benzene decomposition" *J. Cryst. Growth* **32**, 335-349 (1976).

[2] Iijma, S. "Helical Microtubules of Graphitic Carbon" *Nature* **354**, 56-58 (1991).

[3] Terrones M. "Science and Technology of the Twenty-First Century: Synthesis, Properties and Application of Carbon Nanotubes" *Annu. Rev. Mater. Res.* **33**, 419-501 (2003).

[4] Krupke, R., Hennrich, F., von Lohneysen, H., Kappes, M.M. "Separation of Metallic from Semiconducting Single-Walled Carbon Nanotubes" *Science* **301**, 344-347 (2003).

[5] Chen, Z., Du, X., Du, M.-H., Rancken, C.D. Cheng, H.-P., Rinzler, A.G. "Bulk Separative Enrichment in Metallic or Semiconducting Single-Walled Carbon Nanotube" *Nano Lett.* **3**, 1245 (2003).

[6] Moisala, A., Nasibulin, A.G., Kauppinen, E.I. "The role of metal nanoparticles in the catalytic production of single-walled carbon nanotubes-a review" *J. Phys. Condens. Matter* **15**, 3011-3035 (2003).

[7] Huang, L., Wind, S.J., O'Brien, S.P. "Controlled Growth of Single-Walled Carbon Nanotubes from an Ordered Mesoporous Silica Template" *Nano Lett.* **3**, 299-303 (2003).

[8] Endo, M. "Grow Carbon Fibers in the Vapor Phase" *Chem Technol.* **568** (1998).

[9] Nasibulin, A.G., Moisala, A., Brown, D.P., Jiang, H., Kauppinen, E.I. "A novel aerosol method for single walled carbon nanotube synthesis" *Chem. Phys. Lett.* **402**, 227 (2005).

[10] Nikolaev, P., Bronkowski, M.J., Bradley, R.K., Rohmund, F., Colbert, D.T., Smith, K.A., Smalley, R.E. "Gas-phase catalytic growth of single-walled carbon nanotubes from carbon monoxide" *Chem. Phys. Lett.* **313**, 91 (1999).

[11] Terrones, M., Jorio, A., Endo, M., Rao, A.M., Kim, Y.A., Hayashi, T.,

Terrones, H., Charlier, J.-C., Dresselhaus, G., Dresselhaus, M.S. "New direction in nanotube science" *Mater. Today* **7**, 30 (2004).

[12] Lozano-Castello, D., Kamalakaran, R., van Benthem, K., Phillipp, Y.J., Grobert, N., Rühle, M. "Preparation and characterisation of novel "sea-cucumber"-like structures containing carbon and boron" *Carbon* **42**, 2223-2231 (2004).

[13] Maruyama S, Kojima R, Miyauchi Y, "Low-temperature synthesis of high-purity single-walled carbon nanotubes from alcohol" *Chem. Phys. Lett.* **360**, 229-234 (2002).

[14] Zheng, L.X., O´Connell, M.J., Doorn, S.K., Liao, X.Z., Zhao, Y.H., Akhadov, E.A., Hoffbauer, M.A., Roop, B.J., Jia, Q.X., Peterson, D.E., Huang, S.M., Liu, J., Zhu, Y.T. "Ultralong single-wall carbon nanotubes" *Nature Materials* **3**, 673-676 (2004).

[15] Zhu, H.W., Xu, C.L., Wu, D.H., Wei, B.Q., Vajtai, R., Ajayan, P.M. "Direct Synthesis of Long Single-Walled Carbon Nanotube Strands" *Science* **296**, 884-886 (2002).

[16] Li, Y., Kinloch, I.A., Windle, A.H. "Direct Spinning of Carbon Nanotube Fibers from Chemical Vapor Deposition Synthesis" *Science* **304**, 276-278 (2004).

[17] Hata, K., Futaba, D.N., Mizuno, K., Namai, T., Yumura, M., Iijima, S. "Water-Assisted Highly Efficient Synthesis of Impurity-Free Single-Walled Carbon Nanotubes" *Science* **306**, 1362-1364 (2004).

[18] Mayne-L'Hermite, M., Armand, X., Porterat, D., Reynaud, C. "Pyrolysis od mixed aerosols: a versatile CVD-based process to produce clean and long aligned multi-walled carbon nanotubes" *Procedings of chemical vapor deposition-XVI and EUROCVD-14* **Vol. 2003-2008**, 549-56 (2003).

[19] Pinault, M., Mayne-L'Hermite, M., Reynaud, C., Pichot, V., Launois, P., Ballutaud, D. "Growth of multiwalled carbon nanotubes during the initial

stages of aerosol-assitedCCVD" *Carbon* **43**, 2968-2976 (2005).

[20] Ding, F., Rosén, A., Bolton, K. "The role of the catalytic particle temperature gradient for SWNT growth from small particles" *Chem. Phys. Lett.* **393**, 309 (2004).

[21] Jorio, A., Saito, R., Hafner, J.H., Lieber, C.M., Hunter, M., McClure, T., Dresselhaus, G, Dresselhaus, M.S. "Structural (*n*,*m*) Determination of Isolated Single-Wall Carbon Nanotubes by Resonant Raman Scattering" *Phys. Rev. Lett.* **86**, 1118-1121 (2001).

4. Synthesis of N-doped Multi Walled Carbon Nanotubes on Quartz Plates and Nanofoam Formation

4.1 Synthesis of arrays of aligned MWNTs and nanofoam formation: An Overview

add CPL paper on doping with nitrogen.

The achievement of growing aligned arrays of carbon nanotubes was pioneered by Terrones et al. [1]. These authors deposited a Co thin film on a silica substrate by thermal evaporation and, subsequently, etched that film with a laser pulse and a cylindrical lens, in order to create linear patterns. A 2-amino-4,6-dichloro-*s*-triazine compound was placed in one of the ends of a silica tube and the etched substrate was placed in the opposite end. The tube was introduced in a two stage furnace system under an Ar atmosphere and the temperature was then set to 1000 °C and 950 °C for the first and second furnaces, respectively. Aligned CN_x MWNTs grew on the patterned substrate, as shown in figure 1a, while the etched sections resulted free of the nanomaterial. TEM (see figure 1b) and HRTEM characterization performed on the sample revealed morphological features within these nanotubes, such as diameter (ranging between 30-50nm) and number of layers (about 60-80). These authors established that Co particles were responsible for nanotube growth, acting as catalyst; their presence at the ends of the CN_x MWNTs was determined by EDX analysis. Electron energy-loss spectroscopy (EELS) determined that the

nanomaterial was mainly composed by pure carbon, but a weak signal at 400 eV evidenced the presence of N (<2-5%), which these authors attributed to be generated during triazine compound decomposition.

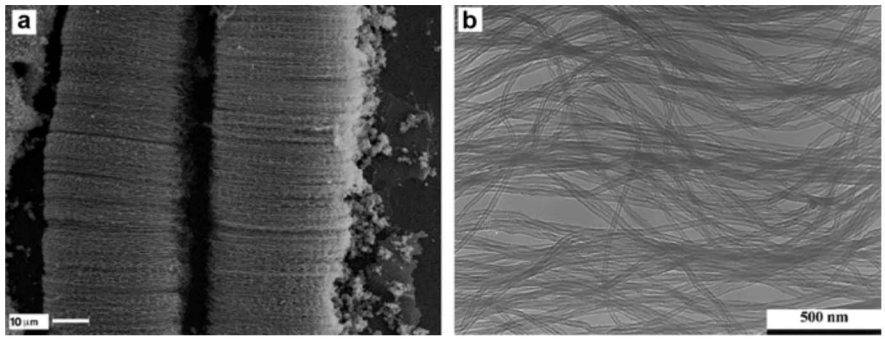

Fig. 1. *(a) SEM images showing the alignment of MWNTs bundles grown on a patterned SiO_x/Co etched substrate. Undesired material, such as polyhedral particles, is notably abscent. (b)TEM image of the as grown material, exhibiting carbon nanotube diameters, which range between 30-50nm (Images obtained from Terrones' manuscript [11]).*

Terrones' method [1] constituted an important advantage over other methods used for nanotube synthesis, such as arc discharge, catalytic pyrolysis of hydrocarbons and electrolysis, because polyhedral particles were notably absent within the sample.

Almost simultaneously, Li et al. [2] reported the large scale synthesis of aligned carbon nanotubes. These authors prepared a mesoporous silica substrate, containing Fe nanopaticles attached at the bottom of the pores, using a sol-gel process. A mixture of 9% of acetylene in nitrogen flowed over the substrate, at a temperature of 700 °C. This experiment resulted in the growth of aligned nanotubes of uniform lengths. SEM and HRTEM characterization of as grown samples are shown in figure 2. A uniform MWNT array is depicted in figure 2a, exhibiting a length of 50 µm. Carbon nanotubes had an average diameter of 30 nm and they

were 100 nm apart from each other. Because this distance was consistent with the spacing between porous in the silica substrate, and the nanotube diameters were similar to those of the pores, these authors speculated that MWNT growth was constrained for nanotube porous size and shape [2]. MWNTs exhibited a good degree of crystallinity (figure 2b).

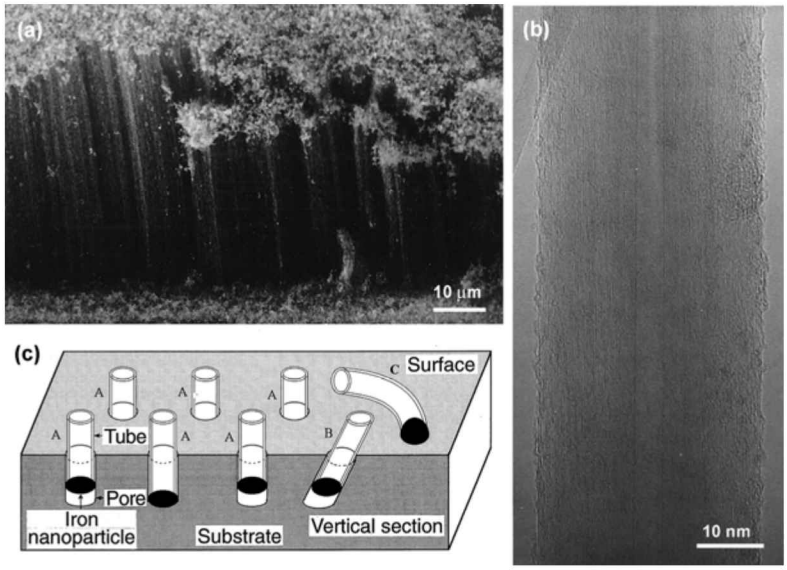

Fig. 2. *(a) SEM image of an aligned carbon nanotube array grown on a mesoporous silica substrate. The height of the array is 50 μm. (b) HRTEM image of a carbon nanotube of 30 nm in diameter. The MWNT exhibits a good graphitization. (c) Carbon nanotube growth model. Cylindrical pores within the silica substrate are mostly horizontal and Fe catalyst particles are found within these pores. Fe particles serve as catalyst for MWNTs growth (Images obtained from Li's manuscript [12]).*

Li and coworkers [2] proposed that MWNTs grew out form the Fe nanoparticles within the pores that serve as a template that restricted and conducted the aligned growth of MWNTs. Figure 2c depicts this growth model, where the cylindrical pores are mostly horizontal and Fe catalyst particles are found within these pores. These authors stated that Fe particles on the surface of the substrate (outside of

pores) could serve as catalyst for unaligned MWNTs growth.

Aligned MWCNTs arrays have a lot of potential applications. One of them, explored in the past, is the formation of bidimensional patterns of aligned nanotubes on quartz substrates, called nanofoams [3]. The formation of these patterns is triggered by the evaporation of organic solvents from the nanotube array. This self assembly phenomenon, could be used to infiltrate several substances in nanotube carpets, such as polymers, biological materials, and other solvents.

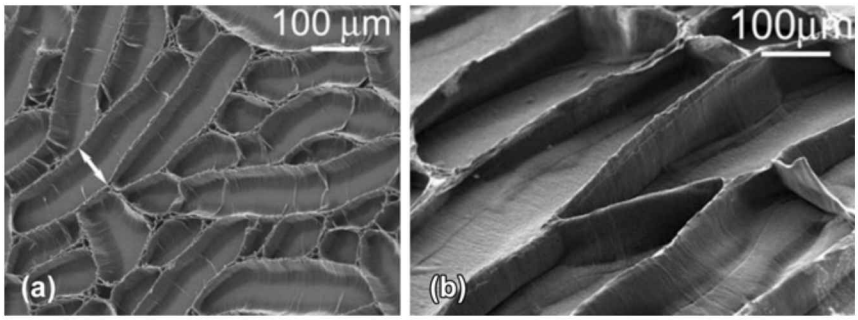

Fig. 3. *SEM images of self assembled cellular carbon nanotube foams. (a) Lateral view of a nanotube foam array, where the arrow depicts a cell width of 100 µm. (b) Higher magnification SEM image of (a), exhibiting flattened nanotubes at the bottom of the cellular cavities. (Images obtained from Chakrapani's manuscript [7]).*

Chakrapani and coworkers [3] reported an interesting phenomenon that occurs in MWNT aligned arrays when they interact with organic solvents. Capillary forces drive the assembly of two-dimensional structures named cellular carbon nanotube foams that are obtained by wetting oxidized carbon nanotube arrays with water, acetone, toluene, dimethylformamide, tetrahydrofluran and methanol. In particular, MWNT arrays of different lengths were grown onto SiO_2 substrates by the CVD process [4]. These authors thermolyzed a xylene/ferrocene solution in a tube furnace system, at 800 °C, under an Ar atmosphere. They reported a nanotube-

nanotube distance within the array of *c.a.* 50 nm [4]. As grown MWNT arrays were oxidized inside a glow discharge chamber with an oxygen plasma at room temperature [3]. Oxydized MWNT arrays were then deeped into a solvent and subsequently were allowed to dry under different humidity conditions [3].

Strong capillary forces present during the solvent evaporation lead to the compaction of the nanotube array and therefore, the formation of cellular carbon nanotube foams, which are depicted in figure 3 [3]. These cellular structures were reported by these authors to be stable, even after annealing in vacuum at 800 °C. Careful observations using an optical microscope provided more detail related to the formation of nanotube foams. Figure 4a depicts the first step occurring during the solvent evaporation, which is the formation of micro scale long cracks in several regions of the nanotube array; subsequently, these cracks slowly become wider, and nanotubes start compacting (figure 4b). The latter process is finished when the solvent is completely evaporated form the array; at this point, carbon nanotubes were bent to allow the formation of cellular structures (figure 4c).

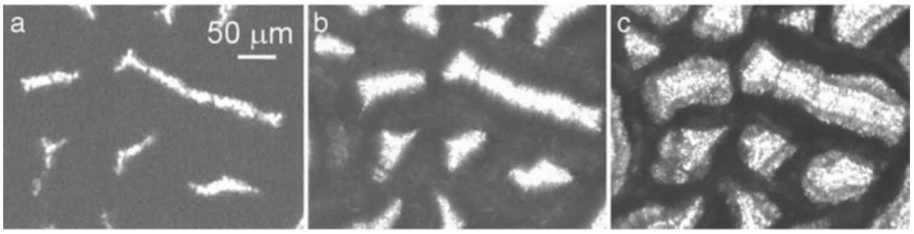

Fig. 4. *Optical microscope images of a nanotube array, obtained during evaporation of water. (a) Firstly, large cracks are formed within a short period of time. (b) In a different step of the cellular nanotube foam formation, compacting of carbon nanotubes takes place, while initial cracks become slowly larger. (c) Final stage of the nanotube foam, showing cellular cavities of different sizes (Images obtained from Chakrapani's manuscript [7]).*

Chakrapani and coworkers [3] established that the cellular foam formation is

caused by the differences between the air and solvent pressures, which are induced by surface tension effects. These authors were also capable of controlling the formation of cellular foams using nanotube arrays on previously patterned Si/SiO_x substrates [4]. Figure 5a exhibits one of these controlled foams, which alternates octagons and squares [3]. Figure 5b shows a schematic view of the original nanotube array that consisted of a nanotube film with evenly distributed holes [3].

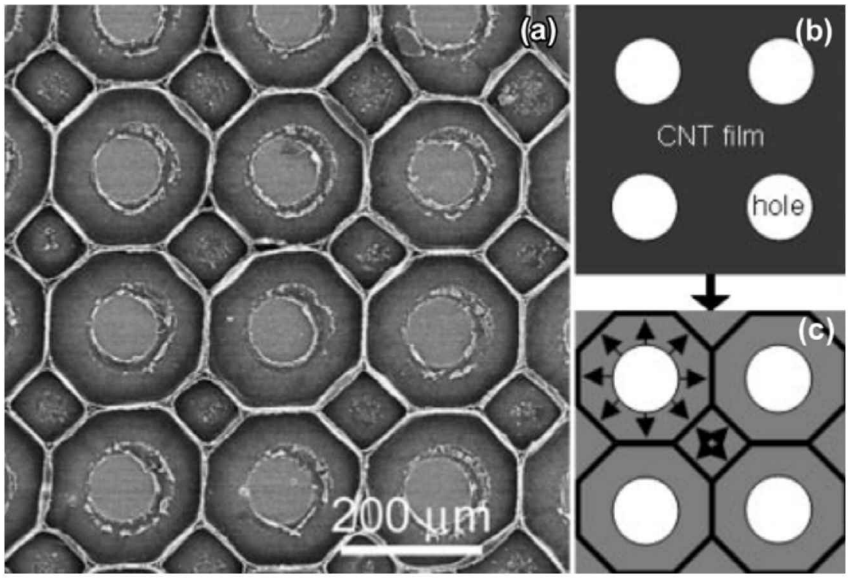

Fig. 5. *(a) SEM image of a controlled cellular carbon nanotube array, which alternates octagons and squares. The authors were capable of controlling the formation of cellular foams by using nanotube arrays grown on previously patterned Si/SiO_x substrates. (b) Schematic view of the original nanotube array that consisted of a nanotube film with evenly distributed 100 µm diameter holes. (c) Arrows depict the direction of compaction of carbon nanotube that generated the array shown in (a) (Images obtained from Chakrapani's manuscript [7]).*

Almost simultaneously, Liu et al [5] also reported the formation of what they called large-scale micropatterns of carbon nanotubes. These authors grew arrays of carbon nanotubes pyrolyzing iron pthalocyanine (FePc) at 900 °C. Individual nanotubes

were characterized by TEM and they exhibited a bamboo-like structure, due to the presence of nitrogen during the formation process. Figure 6 depicts the micropatterns formed in these nanotube arrays.

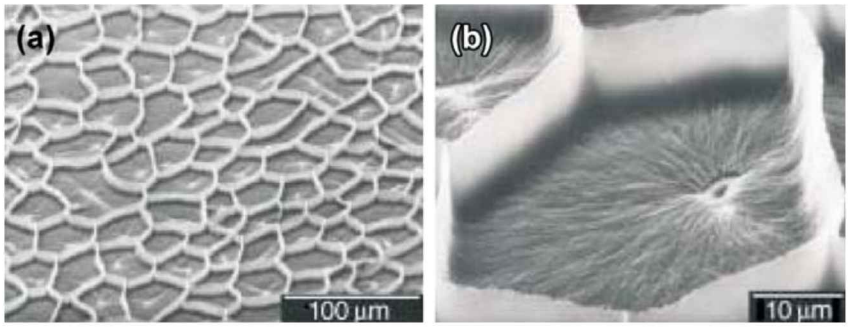

Fig. 6. *SEM images of large-scale micropatterns on carbon nanotubes arrays. (a) Low magnification image an array synthesized by the pyrolysis of iron pthalocyanine (FePc) at 900 °C. Average size of individual honeycomb ranges frim 30 to 60 µm. (b) Larger magnification SEM image an individual cellular vacancy (Images obtained from Liu's manuscript [9]).*

These authors explained the phenomenon of foam-like formation as a result of water capillary action [5]. The water goes into the free spaces between the aligned nanotubes until it reaches the hydrophilic quartz substrate guided by capillary forces. All the free spaces within the nanotube array are occupied by water and capillary action starts to reduce them. Capillary forces induce a hydrostatic dilation stress to the water, which was estimated by the authors to be in the MPa order, causing nanotubes to flatten. These authors also established that because the hydrostatic dilation stress is lower in low density nanotube region when compared to higher density areas, therefore the nanotubes collapse forming walls between the two regions of lower density. Using this principle, these authors etched surfaces with regular vacancies within the nanotube array, prior the formation of the cellular patterns, in order to control that process [5]. Figure 7 exhibits three

different patterns with a predefined cell, defined by artificial etching, and a series of additional free cells. The distance between holes is responsible for the amount of free cells formed; when this distance decreases, free vacancies are less frequent (figure 7b), until it reaches a limit value, where the cells arrays copy the artificially created vacancy array (figure 7c). CONFUSING mtm

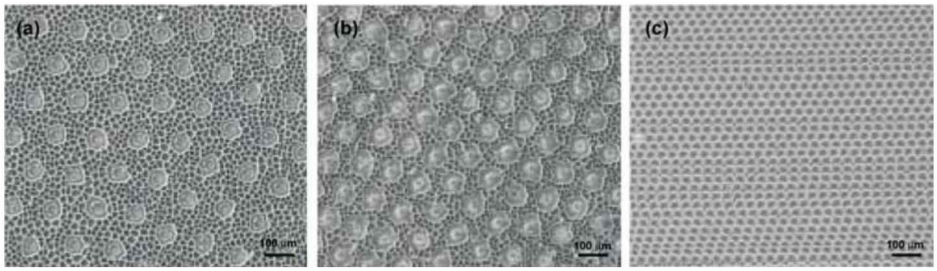

Fig. 7. *SEM images of three different patterns defined by artificial etching. (a) Pre-etched hole inter-distance is 150 microns. The distance between artificially created holes is responsible for the amount of free cells formed. (b) Cellular carbon nanotube foam from a pre-etched array. Distance between holes was 100 μm. (c) A limit value for the distance between holes was reached. Holes were etched with a distance of 30 μm. The assembly of free cells is restricted here (Images obtained from Liu's manuscript [9]).*

Correa-Duarte et al. [6] reported the first application of cellular carbon nanotube foams. These authors studied the growth of mouse fibroblast cell line L929 on a micropatterned MWNT array, which helped the cell adhesion and resulted to be suitable for cell proliferation. Aligned MWCNTs grown on silicon substrates were acid treated (1:3 nitric:sulfuric acid) to generate carboxylic groups and produce the nanotube foams by capillary and tensile forces. Three different nanotube foams are depicted in figure 8, which were formed with MWNT arrays of different lengths. Fibroblast cells were cultured onto previously sterilized MWNT scaffolds for 1 or 7 days and SEM was used to determine cell proliferation and morphology.

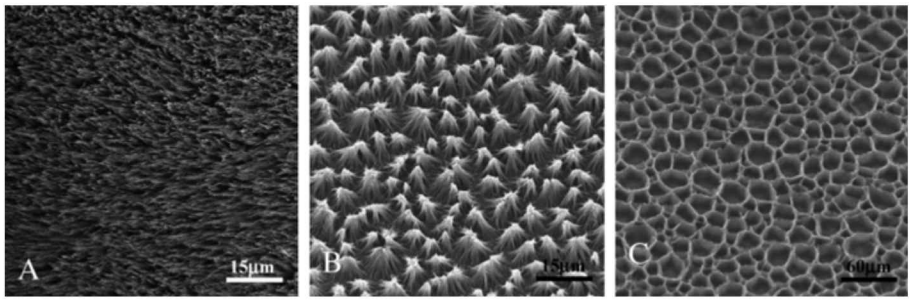

Fig. 8. *SEM images of acid treated aligned MWCNTs grown on silicon substrates that produce nanotube foams by capillary and tensile forces. (a) Aligned MWNT array. (b) Pyramidal-like structure, whit a 3 microns base plane. (c) Cross linked cellular foams (Images obtained from Correa-Duarte's manuscript [10]).*

Figure 9 exhibits two cell cultures, after one and seven days of incubation. The majority of the cell were added to the MWNT surfaces after one day of incubation; some were attached to the wall of nanotube foams and others were found at the bottom of cavities (see inset in figure 9a). After 7 days of incubation, a cell layer almost completely covered the nanotube array, as can be seen in figure 9b. These authors did not report and increase in cell proliferation caused by nanotubes, and they did not find a cytotoxic effect either [6].

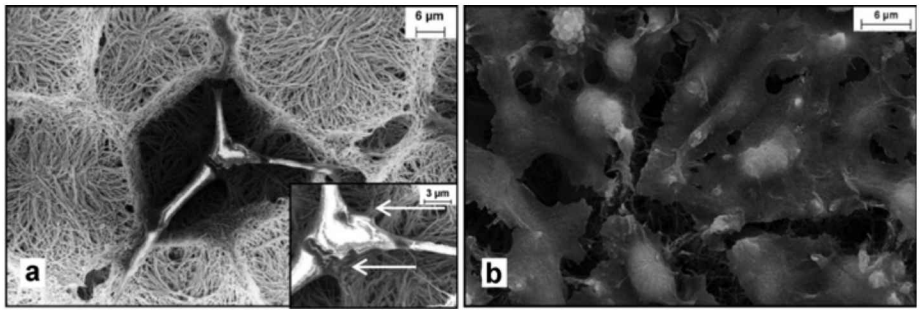

Fig. 9. *SEM images of L929 mouse fibroblasts cell cultures. (a) Culture after one day of incubation. The majority of the cells was added to the MWNT surfaces; some cells were attached to the wall of nanotube foams and others were found at the bottom of cavities (see inset). (b) After 7 days of incubation, a cell layer almost completely covered the nanotube array (Images obtained from Correa-Duarte's manuscript [10]).*

In the following sections, the growth of nitrogen doped MWNT arrays is described, as well as the formation of nanotube (doped and undoped) foams with different features such as size, form and interconnectivity.

4.2 Synthesis of aligned MWNT and CN_x MWNT arrays

Aerosol pyrolysis method (see chapter 2) was used for growing pure carbon MWNTs and CNx MWNTs on quartz plates. For the synthesis of MWNTs, ferrocene ($FeCp_2$) was mixed with toluene (C_7H_8) at a concentration of 2.5% by weight. 300 ml of this solution were placed into a container; a piezoelectric placed at the bottom of this container vibrated ultrasonically and turned the solution into a mist. A quartz tube supported the individual quartz plates that served as substrates for nanotube growth. An Ar flow of 3.71 l/min carried the produced mist into a two furnace system to be pyrolyzed at a temperature of 800 °C. The experiment was carried out for 15 min.

The synthesis of CNx MWNTs on quartz plates was carried out using the same experimental set up but with different parameters. Here, the toluene was replaced for benzylamine (C_7H_9N) that served for both carbon and nitrogen source. The temperature used for the production of N doped nanotubes was 850 °C, slightly higher than the one used for synthesizing pure carbon nanotubes. Reaction time and Ar flow were 15 min and 3.71 l/min, as in the MWNT case. A third type of nanotube array was synthesized mixing benzylamine-ferrocene and toluene-ferrocene in a 1:1 ratio. Experimental parameters were the same as those described for the synthesis of CNx MWNTs with pure a benzylamine-ferrocene solution.

After the reaction was carried out, furnaces were allowed to cool to room temperature and the individual quartz plates were extracted form the quartz tube for their characterization.

4.3 Characterization of as grown MWNT and CN_x MWNT arrays

Pure carbon MWNT and CNx MWNT arrays were characterized by SEM, EDX, thermo gravimetric analysis (TGA), nuclear reaction analysis technique (NRA) and particle induced X-ray emission (PIXE). Figure 10 depicts SEM characterization of representative samples of MWNT arrays. Their lengths range from 200 to 500 μm, and a high magnification image exhibits the alignment of the nanotubes within the array (see figure 10b). MWNT images showed a little amount of undesired material, mainly amorphous carbon deposited on the top surface of the nanotube arrays and, besides this, the sample was clean. Figure 10c exhibits a SEM image of a nanotube array surface, where the presence of amorphous carbon is evident. A small amount of nanotubes was scratched from the quartz substrate, to observe the bottom of the arrays. Figure 10d shows a bottom view of a MWNT bundle. Nanotubes produced using a mixed solution appeared to have a much smaller lengths (~20 microns) when compared to MWNTs and CNx MWNTs synthesized with pure benzylamine-ferrocene solution (not shown).

In figure 11, SEM images of CNx MWNT arrays grown on quartz are shown. Well aligned CNx MWNTs are exhibited at low magnification, in figure 11a. The length of N doped nanotubes varies from 80 to 300 μm. The alignment of the array is depicted in a high magnification image (see figure 11b). For comparison between figures 10b and 11b, it is clear that pure carbon MWNTs are slightly larger in

diameter (50 – 70 nm) when compared to CNx MWNTs (40 - 60 nm). A little amount of amorphous carbon was present on the top of the CNx MWNT arrays, as happened for the case of pure carbon MWNTs (see figure 11c). Finally, a bottom view of a CNx MWNT bundle is presented in a high magnification image (see figure 11d). Iron particles attached to the majority of nanotube caps support the thesis that carbon nanotubes grow through the "base growth mechanism" proposed for carbon filaments synthesis, almost 30 years ago [7].

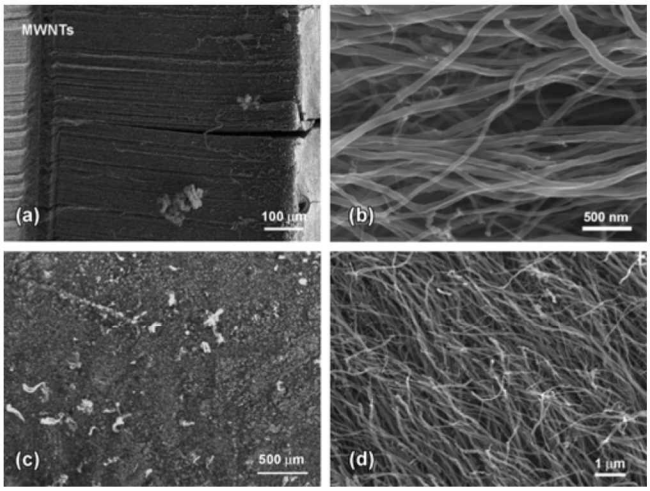

Fig. 10. *SEM images of pure carbon MWNT arrays. (a) Array composed for very long MWNTs (500 µm). (b) High magnification SEM image of (a), showing the alignment of the nanotubes within the array. (c) Top view of a nanotube array showing a little amount of deposited amorphous carbon. (d) Bottom view of a nanotube bundle.*

Figure 12 and 13 exhibit EDX spectra from bulk samples of MWNTs and CNx MWNTs, respectively. Kα C energy, which is located at 0.282 keV, was detected in both spectra. Synthesis of both MWNTs and CNx MWNTs was catalyzed by Fe nanoparticles, and EDX confirmed the presence of Fe, showing a signal at 6.403 keV, in both spectra. A roughly calculation performed by the software for this particular spectra indicated that the Fe content within these samples corresponds to less than 1%, by weight. Particularly, Fe content in MWNT samples was reported to

be 4.3 %wt, while CNx MWNT array contained 3.24 %wt. Oxygen was also detected at both EDX spectra, at 0.523 keV, and its weight percentage was calculated to be 4.13 and 4.26 for MWNTs and CNx MWNTs, respectively. Figure 13 depicts the presence of an additional signal, very weak and almost completely embedded within the carbon pick, corresponding to Kα N. The signal is located at 0.329 keV and the software calculated a 5.96%wt of nitrogen within the sample. This calculation is outstanding because in most cases, the signal associated with N gives an estimated of 2 – 3%wt within CNx MWNTs.

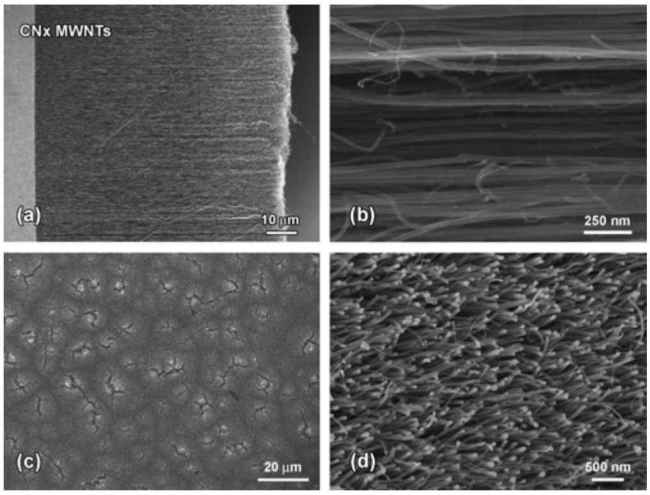

Fig. 11. *SEM images of CNx MWNT arrays on a quartz substrate. (a) Low magnification image exhibiting the length of CNx MWNTs (80 μm). (b) High magnification SEM image showing the outstanding alignment of the nanotubes within this array. (c) Top view of the nanotube array, showing an amorphous carbon layer. (d) Bottom view of a nanotube bundle were Fe catalyst particles are clearly present.*

TGA analysis of MWNTs and CNx MWNTs is shown in figure 14. Samples were thermolyzed in air at a temperature up to 800 °C, with a constant increase of 5 °C/min. The main weight lost of the MWNT sample (figure 14a) takes place at c. a. 550 °C, as depicted for the calculated first derivative (red line). Direct comparison of this data with CNx MWNTs TGA curve (figure 14b). It is clear that CNx MWNTs

are much more unestable to temperature, while pyrolyzed in air atmosphere. The calculated first derivative has its maximum in 423°C, a temperature lower than the corresponding from MWNTs, for more than 100 °C. The weight percentage residues from TGA analysis were 2.93wt% for CNx MWNTs and 2.86 wt% for CNx MWNTs. This evidences that Fe content within both types of nanotubes is comparable.

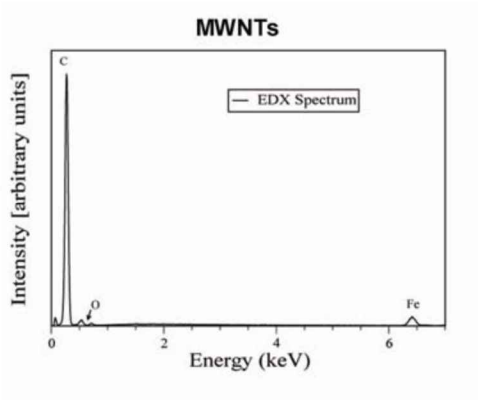

Fig. 12. *EDX spectrum obtained from a MWNT bulk sample. Carbon edge, located at 0.282 keV dominates de spectrum. The signal corresponding to Fe (see arrow) localizes at 6.4 eV, whereas the O signal (see arrow) appears at 0.523 keV and the carbon signal at 0.282 keV. Fe weight percent amount within the sample was roughly determined to do be 4.3; 3.24 wt % was found in the sample.*

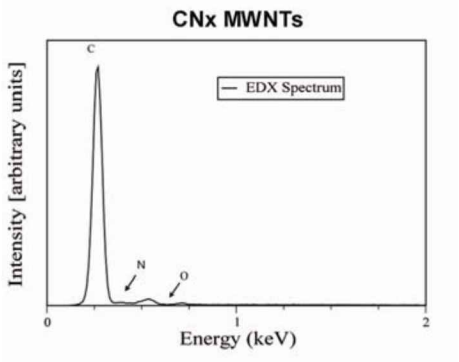

Fig. 13. *EDX spectrum obtained from a CNx MWNT bulk sample. The signal corresponding to Fe was exhibited in the spectrum at 6.4 eV (not shown). O signal (see arrow) appears at 0.523 keV and the carbon signal at 0.282 keV. Additionaly, a very weak N signal was detected at 0.392 keV.*

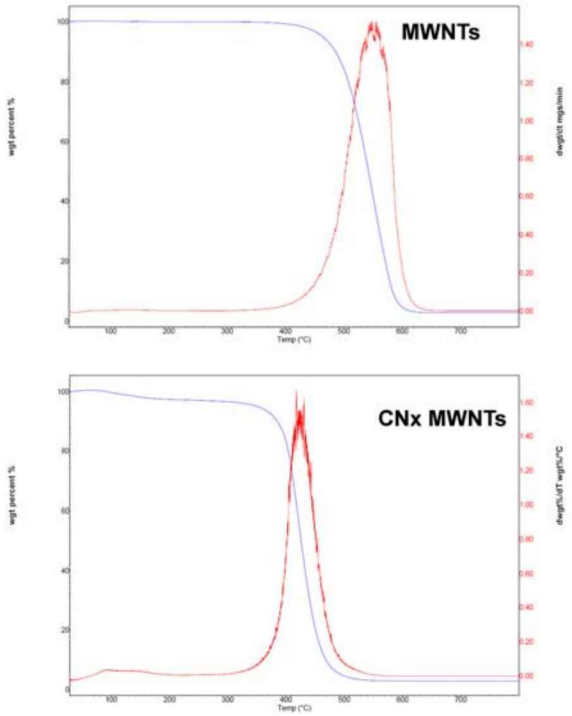

Fig. 14. *TGA analysis plots of MWNTs and CNx MWNTs thermolyzed in air, at a temperature of 800 °C. (a) The maximum of the first derivative (red line) of the weight percentage curve is located at 550 °C. (b) The first derivative has its maximum in 423°C, lower temperature when compared to MWNTs' curve derivative. The weight percentage residues from TGA analysis were 2.93wt% for CNx MWNTs and 2.86 wt% for CNx MWNTs.*

Nuclear reaction analysis (NRA) was used as an additional technique to determine a more accurate value of the N content on CNx MWNT samples. A deuterio 0.96 MeV beam was used in the analysis, which generated a nuclear reaction. Protonic particles generated from this reaction were detected and plotted in Figure 15. Two separated nuclear reactions were generated to measure 14N(d,p)15N and 16O(d,p)17º. SIMNRA software was used to simulate experimental curves superimposed with experimental data. It is important to remark that this technique is not invasive and sample damage occurred by electron beam in other techniques,

such as EELS or EDX, is avoided. Figures 15a and 15 b correspond to calibrations made with Si_3N_4 and SiO_2, respectively, for comparison with CNx MWNTs sample's data. Figures 15c and 15d plot the actual data obtained from CNx MWNTs, and the analysis. Nitrogen and Oxygen atomic percentage was determined as a function of sample layer thickness. Results indicated that a first layer of 21000x10^{15} at/cm^2 contained 3.4 wt% of N and 3.2 wt% of O. A second layer of a bulk thickness only reported 0.5 wt% of N, therefore, the majority of the nitrogen within this sample was located at the first layer. Oxygen concentration within this second bulk layer was 4.0 wt%. Data depicted in figure 15d served to determine a single bulk layer concentration of N, O and C, to be 4.0, 1.0 and 95.0 wt%, respectively.

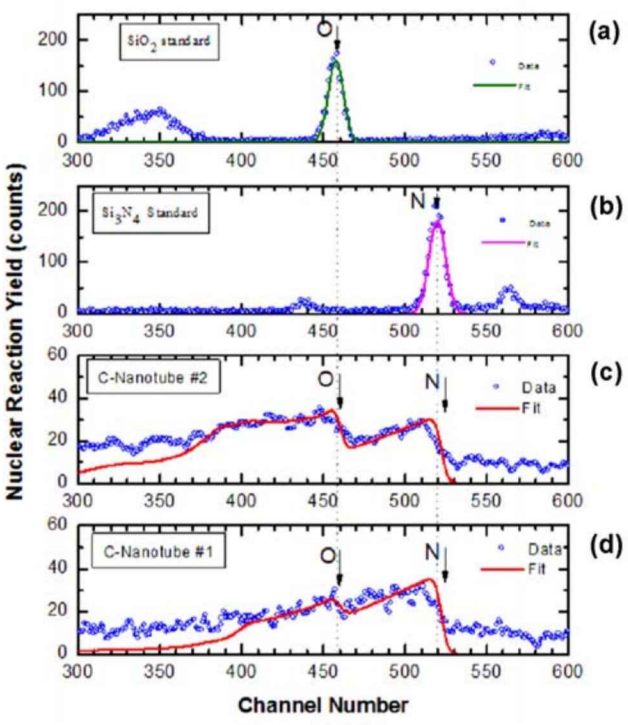

Fig. 15. *Nuclear reaction analysis (NRA) performed in CNx MWNT samples. (a) Calibrations experiment made carried out with SiO_2 and (b) Si_3N_4. (c) - (d) Plotted data form two NRA experiments with two samples of CNx MWNTs, coming from different batches. Calculation indicate a N 3.4 wt% and 4.0 wt% for each case.*

In figure 16 particle induced X-ray emission (PIXE) was used to determine the exact amount of Fe within a CNx MWNT bulk sample. In these experiments, a highly energetic proton beam was directed to the sample causing core shell excitation. X-ray emission driven for that excitation was used to determine the Fe content of the sample. An obtained value of 5.0 wt% of Fe was determined from the experiment. Figure 16 also exhibits a Mg signal, located at 1.254 keV. The amount of Mg within the sample was 0.05 wt%, and it could be attributed to glassware contamination introduced into the CVD system while handling the benzylamine-ferrocene solution.

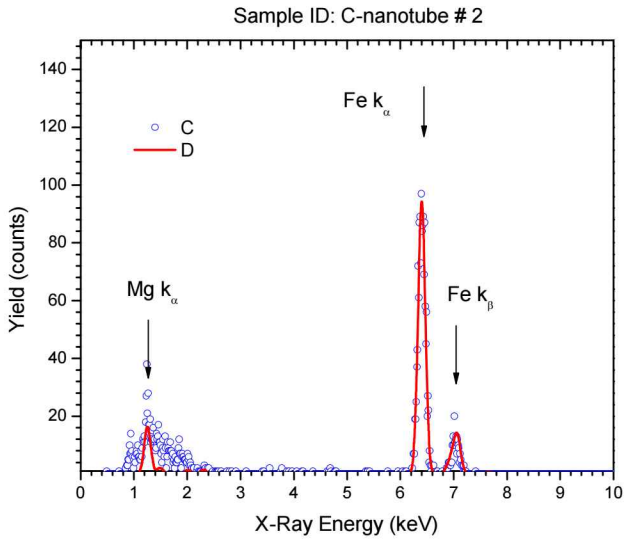

Fig. 16. *Particle induced X-ray emission (PIXE) data, used to determine an Fe 5.0 wt% within a CNx MWNT bulk sample. Kα Fe signal is located at 6.403 keV. A weak Mg signal, located at 1.254 keV is also present in the spectrum.*

4.4 Surface oxidation of carbon nanotube arrays

In the previous section, an extensive characterization of MWNT and CNx MWNT arrays was described. In particular, the presence of undesired amorphous carbon (figures 11 and 12) on top of nanotube arrays was eliminated following an

oxidation procedure. Nanotube arrays were placed into a glow discharge chamber at room temperature. The chamber was operated at a pressure of 500 - 650 militorrs and an O plasma was generated. This oxidation treatment was carried out for 15 to 40 minutes, depending on the amorphous carbon layer thickness. Further SEM characterization of the oxidized samples was performed (not shown).

4.5 Formation of cellular carbon nanotube foams

Oxidized undoped MWNT and CNxMWNT arrays were deeped into acetone for *c.a.* 60 seconds. Wetted nanotube arrays where extracted from the solvent container and were allowed to dry under ambient conditions. The organic solvent penetrated the interspaces of the nanotube arrays and, as established in previous work [3,5-6], capillary forces driven the compaction of individual nanotubes from lower density regions to higher density regions. SEM characterization of those arrays is shown in figures 17-19.

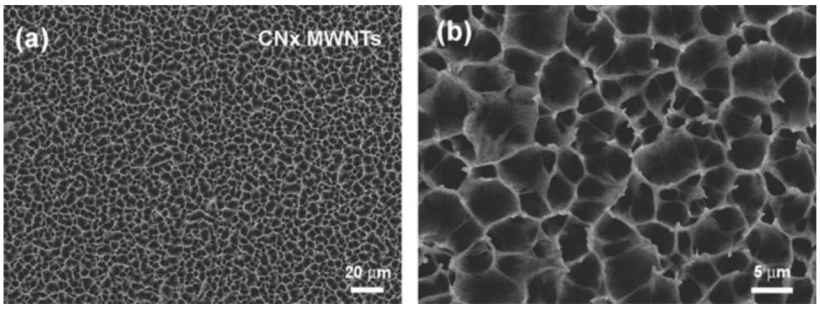

Fig. 17. *SEM images of cellular-like foam patterns formed from short arrays of CNx MWNTs -grown from a mixed solution of ferrocene in toluene and benzylamine (a) Low magnification image of the cellular CNx MWNT foams. (a) Cell-like units formed during solvent evaporation have varied sizes (1 to 10 µm) and a polygonal morphology.*

SEM images of cellular-like foam patterns formed from short arrays of CNx

MWNTs -grown with toluene and benzylamine (see section 3.2 for details)- are depicted in figure 17. Cell-like units formed during solvent evaporation have varied sizes (1 to 10 μm) and a polygonal morphology, as can be seen in figure 17b. Wall thickness appears to be uniform along the nanotube array. This is what Chakrapani and coworkers recalled as a two dimensional nanotube foam array, which consist on interconnected cellular-like cavities formed by the compaction and bending of nanotubes.

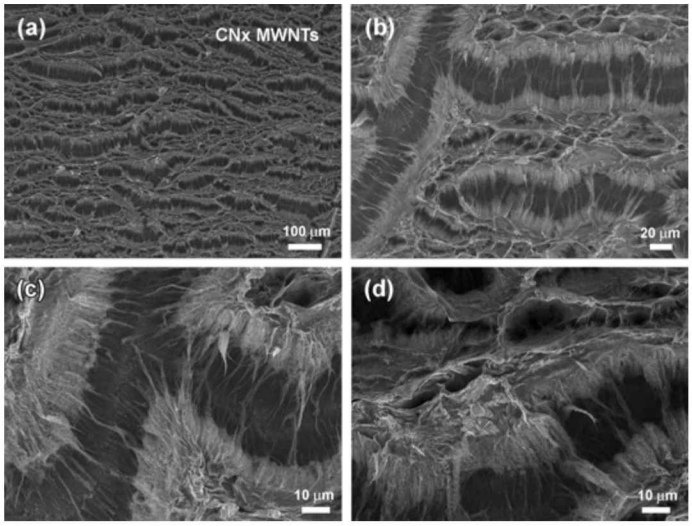

Fig. 18. *SEM images of a cellular CNx MWNT foam. (a) Low magnification image of labyrinth-like foam, with defined pathways up to 800 μm in lenght; the width of these long interconnected cavities ranges from 25 to 50 μm (b) Higher magnification SEM image of the foam. (c) Detail of elongated open cell vacancies. (d) High magnification image the foam, where a secondary foam pattern with much smaller cells is depicted.*

A more complex nanotube foam is depicted in figure 18. CNx MWNTs of approximately 150 μm formed a labyrinth-like foam, with defined pathways up to 800 μm in lenght; the width of these long interconnected cavities ranges from 25 to 50 μm (see figure 18a). CNx MWNTs located within these pathways constituted a secondary foam pattern of much smaller cell-like foam. Individual vacancy's sizes

ranged form 5 to 40 μm (see figure 18b-d). Bending of CNx MWNTs appears to be much more pronounced for the labyrinth-like foam formation when compared to the rest of the array, where density of nanotubes is too high to allow the formation of well defined cell-like cavities.

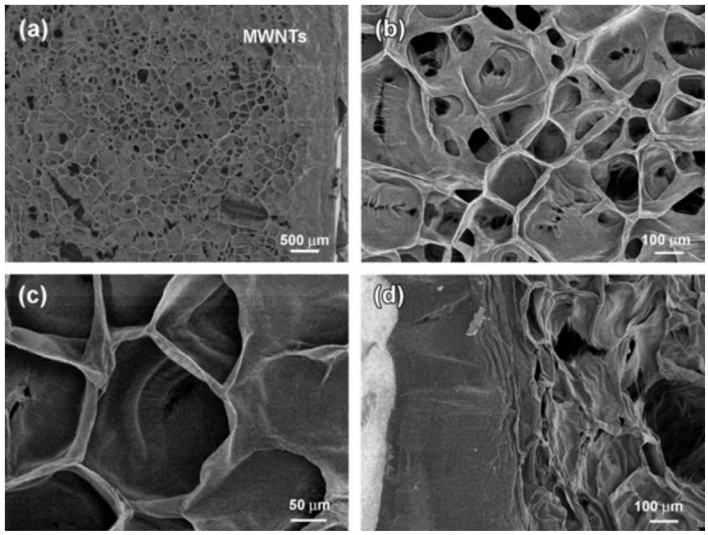

Fig. 19. *SEM images of three dimensional MWNTs cellular foam on quartz. (a) Low magnification image showing the bulk features of the foam. (b) SEM image of the array, where several hundred microns sized polygonal cells are observed. These large cells usually contain smaller sized cells at upper heights. (c) High magnification image, exhibiting details of big cells. (d) Lateral view of the foam showing its length (~400 μm).*

500 μm long undoped MWNTs constitute the array depicted in figure 19. These long nanotubes promote the formation of an opened three dimensional foam. Several microns sized polygonal cells posses were observed within this nanotube foam. These large cells usually contain smaller sized cells at upper heights (see figure 19b). Nanotube foams showed in figures 17 and 18 allways exhibited the quartz substrate at the bottom of each cavity. This is in contrast with the foam exhibited in figure 19, which depth does not reach the substrate in all cases as shown in figure 19d. A very important feature that characterizes this foam is the

morphology of the cells' walls. In contrast with nanotubes obtained with shorter tubes reported in this chapter or in previous work [3,5-6], these walls resemble an extended fabric that does not posses the rigidity to remain vertical and bends in diverse fashions. During SEM characterization, the stage was tilted to obtain another perspective of the nanotube foam, which is shown in figure 19d. The length of the nanotubes that conform the array is clearly appreciated in that panel to be ~400 μm. Several wide but short cells are also observed in this figure.
A surface portion of this type of array is constituted for inclined or bended nanotubes, which do not exhibit clear cell-like cavities, probably because they do not have enough depth.

In order to avoid the plasma oxidation of nanotube arrays before nanotube formation, carbon tape was placed on top of the array and pressed hardly against to the surface of the mat. Nanotube arrays where pilled of from the quartz substrate and their caps were now exposed (see figure 10 and 11). The new surface is now very flat and regular, with absolute absence of an amorphous carbon layer that can stop the penetration of the solvent in the interspaces of the array. As reported for Kaur and coworkers [8], the compaction of nanotubes during pattern formation is strongly correlated with the substrate where the nanotubes stand. Droplets of acetone were placed on the surface of the pilled off nanotubes and were allowed to dry in ambient conditions.

Figure 20 shows images of compacted pure carbon MWNTs and CNx MWNTs on carbon tape. Long MWNTs bended towards a preferential direction and compacted forming rounded cellular like cavities of 100 microns in size (figure 20a and b). The polygonal feature of other nanotube foams (see figure 17 and 19) is not present in this array. CNx MWNTs on carbon tape that were exposed to acetone formed a patterned similar to that of CNx MWNTs on quartz (see figure 17). Large elongated

cavities having lengths of up to 500 microns and widths of c.a. 100 microns resulted from the drying process, which exposed the carbon tape substrate (figure 20c). Large sections between these elongated cells exhibited small and superficial cavities; their morphology is neither rounded nor polygonal (figure 20d). These small cells are not well defined and their interconnectivity and little depth are formed with flattened CNx MWNTs.

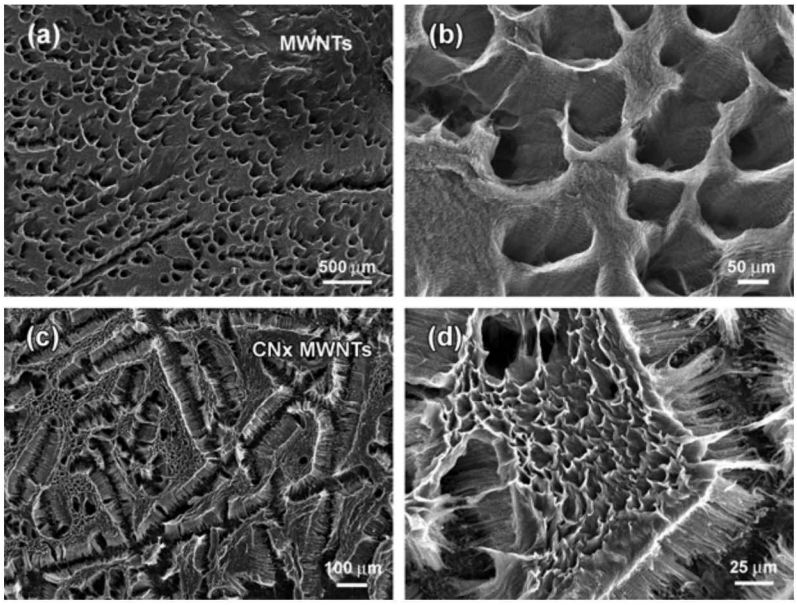

Fig. 20. *SEM images of compacted pure carbon MWNTs and CNx MWNTs on carbon tape. (a) Long MWNTs bended towards a preferential direction and compacted forming rounded cellular like cavities of 100 microns in size. (b) Higher magnification SEM image showing the morphology of nanotube foams. (c) CNx MWNTs on carbon tape that were exposed to acetone formed a patterned similar to that of CNx MWNTs on quartz. Large elongated cavities with 500 μm in length and 100 μm in widths are depicted in this low magnification SEM image. (d) Detail of sections between elongated cells, which exhibit small and superficial cavities.*

4.6 Interaction of self standing nanotube arrays with organic solvents

In section 3.2, the synthesis of nanotubes on quartz plates was described. Carbon nanotube growth takes place inside a quartz tube that acts as substrate for a large amount of nanotubes. This sample is scratched from the inner walls of the quartz tube and a portion of the obtained nanomaterial consists on self standing macroscopic nanotube arrays, called flakes. In this section, the interaction of organic solvents and nanotube flakes is explored.

Drops of toluene, acetone, methanol, among other organic solvents wetted CNx MWNT and undoped MWNT flakes. The solvent wetted the nanotube array and the evaporation process takes place. Carbon nanotubes flakes bended towards a preferential direction. SEM characterization of those samples showed that nanotubes remain aligned after interacting with solvents, though the nanotube array is not flat (not shown).

Samples evolution was followed in an optical microscope. An interesting effect was observed during solvent evaporation: nanotube flakes jumped from the glass microscope slide. Movies of the process are provided to the reader. The process of CNx MWNTs interacting with acetone is documented in movie 3.1. Interaction of CNx MWNTs and methanol is shown in movie 3.2. Undoped MWNTs were also tested and movie 3.3 exhibits their interaction with acetone, whereas movie 3.4 shows the effect of MWNT wetting by methanol. The forces generated from the interaction of nanotubes with the solvent are predicted to be very large.

Free standing nanotube arrays shrink after their interaction with organic solvents

but remained aligned. The observed strong reaction of nanotube flake jumping, driven by an interaction with solvents envisages that these arrays could be suitable for applications as natural actuators.

4.7 Discussion and Conclusions

The interaction of organic solvents with doped and undoped carbon nanotubes was reported in this chapter. Multiwalled nanotube arrays grown on quartz have been rearranged to constitute nanotube foams. The formation process of the nanotube foams is outstanding for its simplicity. Self assembly processes have been used widely in material sciences to achieve diverse goals in an easier, cheaper and more controllable manner. The basics of the cellular pattern formation in nanotube arrays after its interaction with organic solvents have been explained in the past [3,5]. Strong capillary forces caused that free spaces within the nanotube array becomed rearranged, resulting in the nanotube foam self assembly formation.

Nanotube arrays synthesized with floating catalyst CVD methods could generate arrays with a large variety of densities. Density of nanotube arrays is a key parameter during foam formation. Not only the average value of inter-nanotube distances, but the nanotube distribution within the array distances is important. Prepatterned nanotube arrays assist the control of cell pattern, but different nanotube foams can be obtained form nanotube arrays that have not been patterned.

Several parameters are crucial during the formation of foams, such as nanotube length [3]. Chakrapani and coworkers [3] reported that the average cell width grows with height of nanotube film. These authors plotted this data from 20 to 200 microns. Arrays of much longer MWNTs formed nanotube foams, with very

different fashions when compared to those of Chakrapani. The size of the nanotube cells increased with the length, according to the results presented in this chapter, which is consistent with Chakrapani's predictions.

Substrate adhesion to individual nanotubes could also have importance, as well as its hydrophilicity or hydrophobicity. Different substrates modify completely the foam formation in pre-patterned MWNT arrays [8].

The formation of carbon nanotube foams with different nitrogen doping levels has been described. Amorphous carbon layer on top of some pristine MWNT arrays could be thick and plasma oxidation would not be enough for removing that undesired material. Solvents cannot penetrate the array if such a layer of amorphous carbon is present (it is highly hydrophobic). Straightness of nanotubes within the arrays could also play an important role. Ideally, MWNTs are perfectly normal to the SiOx substrate and parallel to each other. Proposed models for explaining nanotube foam formation are partially based in their perpendicularity. If that perpendicularity is reduced, foam self formation would be affected.

Interaction of solvents and nanotubes themselves would be studied deeply in the future. Nanotube flakes, especially those conformed for CNx MWNTs, appeared to have a stronger response when interacting with acetone and that could be due to the presence of N within external graphitic layer. The strong forces involved in the nanotube array shrinkage and lifting could be applied for building a natural actuator. Though, once the nanotube flake is wetted, it bends and does not recover its original conformation.

Large cellular patterns could have a wide variety of applications. Polymer solutions could be infiltrated between free interspaces of nanotube arrays, to constitute a

strong nanocomposite. The alignment of nanotubes within that nanocomposite could give interesting properties to the composite, besides the fact that the problem of dispersing carbon nanotubes in aqueous solutions would be avoided. Biocompatibility of CNx nanotube will be discussed in the following chapters. Evidence of cellular CNx MWNTs biocompatibility would be provided. Therefore, CNx MWNT foams have could be tested for its application in cell culture, following the pioneer research reported by Correa Duarte, et al. [5].

References

[1] Terrones, M., Grobert., N., Olivares, J., Zhang,J. P., Terrones, H., Kordatos, K., Hsu, W. K., Hare, J. P., Townsend, P. D., Prassides, K., Cheetam, A. K., Kroto, H. W., Walton, D. R. M. "Controlled production of aligned-nanotube bundles" *Nature* **388**, 52-55 (1997).

[2] Li, W. Z., et al "Large synthesis of aligned carbon nanotubes" *Science* **274**, 1701-1703 (1996).

[3] Chakrapani, N., Wei, B. Q., Carrillo, A., Ajayan, P. M., Kane, R. S. "Capillarity-driven assembly of two-dimensional cellular carbon nanotube foams" *PNAS* **101**, 4009-4012 (2004).

[4] Wei, B.Q, Vajtai, R., Jung, Y., Ward, J., Zhang, R., Ramanath, G., Ajayan, P.M. "Assembly of Highly Organized Carbon Nanotube Architectures by Chemical Vapor Deposition" *Chem. Mater.* **15**, 1598-1606 (2003).

[5] Liu, H., Li, S., Zhai, J., Li, H., Zheng, Q., Jiang, L., Zhu, D. "Self-Assembly of Large-Scale Micropatterns on Aligned Carbon Nanotube Films" *Angew. Chem. Int. Ed.* **43**, 1146-1149 (2004).

[6] Correa-Duarte, M.A., Wagner, N., Rojas-Chapana, J., Morsczeck, C., Thie, M., Giersig, M. "Fabrication and Biocompatibility of Carbon Nabotube-Based 3D Networks as Scaffolds for Cell Seeding and Growth" *Nano Lett.* **4**, No. 11, 2233-2236 (2004).

[7] Terrones, M. "Science and Technology of the Twenty-First Century: Synthesis, Properties and Application of Carbon Nanotubes" *Annu. Rev. Mater. Res.* **33**, 419-501 (2003).

[8] Kaur, S., et al. *In preparation* (2006).

5. Biocompatibility and Toxicological Studies of Carbon Nanotubes Doped with Nitrogen

A comparison of the toxicological effects between pure carbon multi-walled nanotubes (PCMWNTs) and N-doped multi-walled carbon (CN_x) nanotubes is presented in this chapter. In particular, different doses of nanotubes were administered in various ways to mice: nasal, oral, intratracheal and intra-peritoneal. It was found that when PCMWNTs were injected directly into the mouse's trachea, the mouse could die by dyspnea depending on the PCMWNTs doses. However and more interestingly, CN_x nanotubes never caused the dead of any mouse. CN_x nanotubes were far more tolerated by the mice when compared to PCMWNTs. Extremely high concentrations of CN_x nanotubes administrated directly into the mice's trachea only induced granulomatous inflammatory responses. Importantly, all other routes of administration did not induce signs of distress or tissue changes on any treated mouse. It is concluded that CN_x nanotubes are less harmful than PCMWNTs or SWNTs and might be more advantageous for bioapplications.

5.1 Toxicology studies of SWCNTs and pure carbon MWNTs in mammals and living tissue: A Review

Carbon nanoscience and technology has developed very rapidly over the last decade following the identification [1,2] and bulk production [3,4] of carbon

nanotubes. Due to the remarkable mechanical, thermal and electronic properties of carbon nanotubes [5], numerous applications have been conceived. For example, carbon nanotubes could be used as gas sensors [6-7], field emission sources [8], polymer composite fillers [9], protein immobilizers [10], filters [11], electronic components [5,8], etc. However, a crucial issue, which needs to be addressed before nanotube-based components are commercially available, is toxicity. If nanotubes are used in novel products, they are likely to get in contact with the human body through the skin and ocular surfaces, and access the inner organs through the respiratory and digestive tracts. During manufacture, carbon nanotubes may enter the respiratory airways of the workers, and accumulate in the lungs. If nanotubes are used as fillers in food packaging products, they could reach the stomach and intestines of the consumers. If cosmetics and bio-filters are developed using nanotubes, they will certainly get in contact with the human skin. Therefore, additional toxicological studies of these carbon nanomaterials need to be carried out. In 2003 Colvin [12], reviewed some potential environmental risks of nanosized materials, including nanoparticles, carbon nanotubes and fullerenes. He pointed out that environmental effects of nanomaterials, and especially carbon-based, should be an important research subject.

Lam et al. [13] reported for the first time the pulmonary toxicity of SWNTs in two-month-old male mice. These authors used the intratracheal instillation as a route to deliver the nanomaterial into the mice's lungs using three different doses: 0, 0.1 and 0.5 mg per mouse (30 g of body weight). In order to make this study as complete as possible, they used three different samples of SWNTs; two of them were HiPco synthesized [14], one raw and the other purified, and the third type was pristine arc discharge SWNT sample [5]. Besides using three different nanotube samples, they instilled carbon black (as negative control) and quartz (as positive control). They sacrificed the animals after 7 or 90 days of instillation. The authors also estimated

the amount of metal particles in their samples. From their findings it is important to point out that raw HiPco nanotubes contained 26.9 % Fe by weight and arc discharge nanotubes contained 25.99 % Ni by weight, whereas purified HiPco nanotubes contained only 2.14 % of Fe by weight.

One of the most surprising results from that report [13] was the death of 5 of the 9 mice treated with the high dose of the arc discharge SWNTs. The authors remarked that before dying, the mice suffered lethargy, inactivity and lost of body weight (two of the mice died within one week post treatment). The surviving animals from the 90 days group, instilled with the high dose of arc discharge nanotubes, lost about 27% of body weight, and started gaining it after one week. Neither purified nor pristine HiPco SWNTs caused body weight losses.

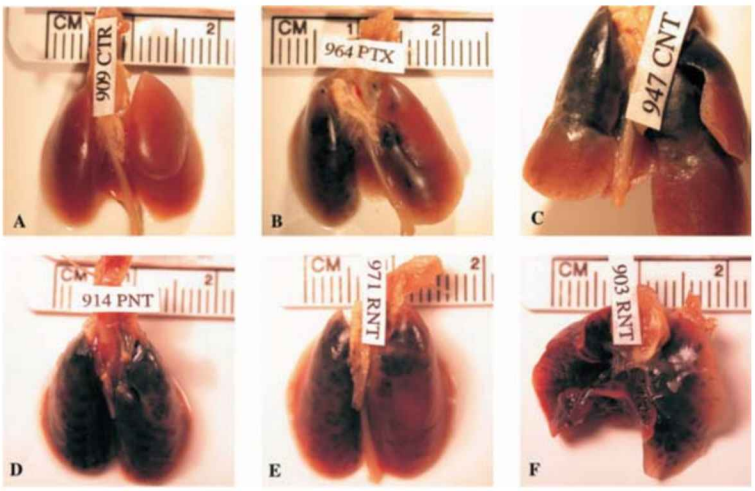

Fig. 5.1. *Photographs of mice's lungs instilled with the high dose of carbon nanotubes or carbon black (0.5 mg per mouse of 300 mg). Mice were euthanized 90 days after single treatment. (a) Serum control; (b) Carbon black; (c) The portions of the lung receiving arc discharge produced SWCNTs, had abnormal appereance; (d) Particle distribution of purified HiPco SWCNTs was even; (e) Clusters of black pigment probably correspond to granulomas induced for the presence of pristine HiPco SWCNTs; (f) Dorsal view of (e) (Images obtained from Lam's manuscript [24]).*

The external appereance of the lungs was carefully analyzed by Lam and coworkers. Figure 5.1(a) exhibits the lungs from the control experiment (treated with harmless serum), and it is used for comparison with the lungs from treated mice (figure 5.1b-f). Evident damage was observed in lungs of mice treated with arc discharge and raw HiPco after 90 days post treatment (figure 5.2e-f). Particularly, arc discharge nanotubes induced granulomes 7 and 90 days post treatment only with the high dose (0.5 mg of SWNT); it is important to remark that some of these granulomes were found in the interstisium and not only in the alveolar space (figure 5.2d). Both purified and pristine HiPco SWCNTs also caused granulomes at both doses and after 7 or 90 days of instillation (figure 5.2e-f). Carbon black present between the lungs can be appreciated in figure 5.2(b). However, quartz was much more harmful than carbon black; it induced granulome aggregates surrounded by lymphocytes (see figure 5.2c). Non carbon black neither quartz resulted aggressive to the lung tissue, as observed for SWNTs (figure 5.2).

Warheit et al. [15], reported a comparative pulmonary toxicity study of SWNTs in rats. They intratracheally instillated 1 – 3 μm quartz particles (silica), 1.4 nm diameter laser ablated SWNTs, 3-10 μm graphite particles and 0.8- 3.0 μm carbonyl iron particles into eight-week-old rats. The authors performed cytotoxicity studies (chemotaxis and proliperation studies) and lung morphological studies. The doses used for this research were 1 and 5 milligrams per kilogram of rat body weight (mg/kg).

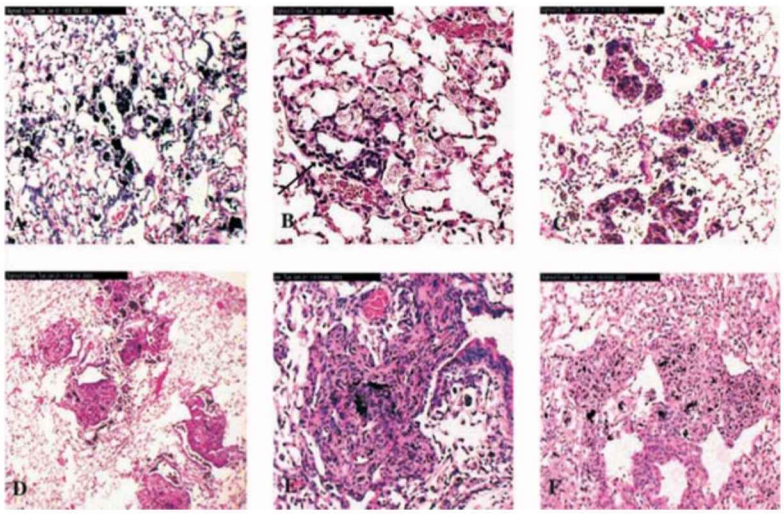

Fig. 5.2. *Lung tissue of mice sacrificed 90 days after a single instillation with 0.5 mg of carbon black (b), quartz (c), arc discharge produced SWCNTs (d), pristine HiPco SWCNTs (e) or purified HiPco SWCNTs (PNT) (f) per mouse. (a) Control experiment (b) Carbon black is present in lungs scattered in alveoli; (c) The arrow shoes lymophocytessurrounding quartz particles contained in macrophages; (d) Arc discharge nanotubes are trapped into granulomes; (e) Pristine HiPco SWCNTs induced granulomas; (f) Higher magnification of a granuloma induced for pristine HiPco SWCNTs, and (f) a large granuloma exhibiting necrosis. Magnifications varied form 40 to 200X (Images obtained from Lam's manuscript [24]).*

The administration of the high dose of SWNTs into rats produced the dead of 15% of the population within 24 hours, although, the authors argued that this mortality was mainly an artifact of the highly electrostatic nature of the tubes, which do not disperse and block mechanically the upper airways. SWNTs induced the formation of multifocal granulomes in lungs, surrounding the nanomaterial with mononuclear cells (figure 5.3a and b). Cytotoxicity studies revealed that quartz was toxic while SWNTs were not. For instance, alveolar macrophages exposed to quartz particles lost motility, which is a sign of deficiency in the cell function. Iron carbonyl and graphitic particles instilled groups did not differ form the control

experiments. The authors concluded that nanotubes do not follow the regular "toxic paradigm" of other dusts such as asbestos and quartz.

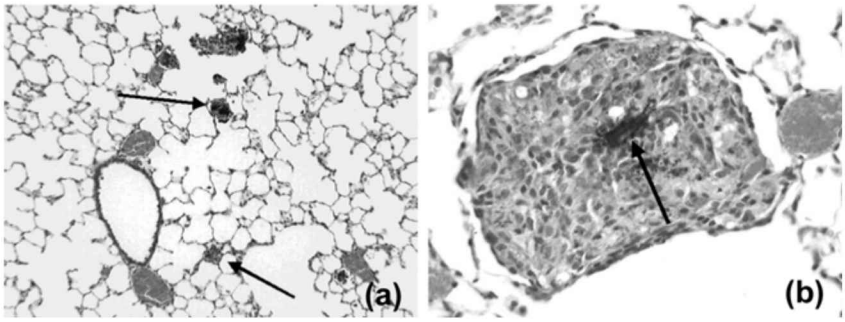

Fig. 5.3. *(a) Image of lung tissue from a rat instilled with 1 mg/kg single-wall carbon nanotubes, after one week post treatment; arrows indicate the early development of lesions surrounding the instilled SWCNT and a diffuse pattern of single-wall carbon nanotube particulate deposition in the lung (Magnification 100X). (b) Image of lung tissue of a rat instilled with the same dose as in figure (a) but after 1 month post treatment; the arrow points a mononuclear multifocal granuloma that surrounds nanotube material (Magnification 400X). (Images obtained from Warheit's manuscript [12]).*

Hat-stacked carbon nanofibers (H-CNFs) have also been tested for their toxicological effects in biological tissue. Yokoyama and coworkers [16], reported an *in vivo* toxicicy study of H-CNFs, where the carbonaceous nanomaterial was implanted in subcutaneous tissue of rats. H-CNFs exhibited diameters between 30 and 100 nm and a from 0.1 to 1 μm in length. A group of eight 6-week-old male rats were anesthetized and clusters of H-CNFs were implanted in row incisions made in the thoracic region. After 1 and 4 weeks these authors sacrificed rats and obtained subcutaneous tissue for histological and TEM analysis. The authors reported the observation of clusters of H-CNFs surrounded by macrophages, foreign gigant cells and mesenchymal cells, that formed granulomes after 1 week post of implantation (figure 5.4). TEM images revealed the presence H-CNFs inside and the outside cells. Some H-CNFs were found inside macrophages and others within phagocytes

(see arrows in figure 5.5). Particularly, after 4 weeks of treatment, the observed phagocytes had many vacuoles. Severe inflammatory responses such as unprogrammed cell death through disease or injury (necrosis) were not reported.

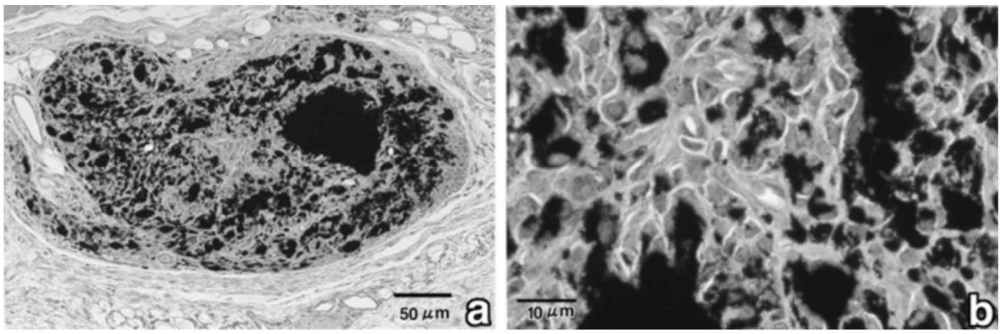

Fig. 5.4. *Histology cuts of CNFs implanted in the subcutaneous tissue. (a) One week post treatment: granulation tissue covering CFS aggregates. (b) High magnification of (a). Several mesenchymal cells and macrophages appeared surrounding CNFs. (Images obtained from Yokoyama's manuscript [26]).*

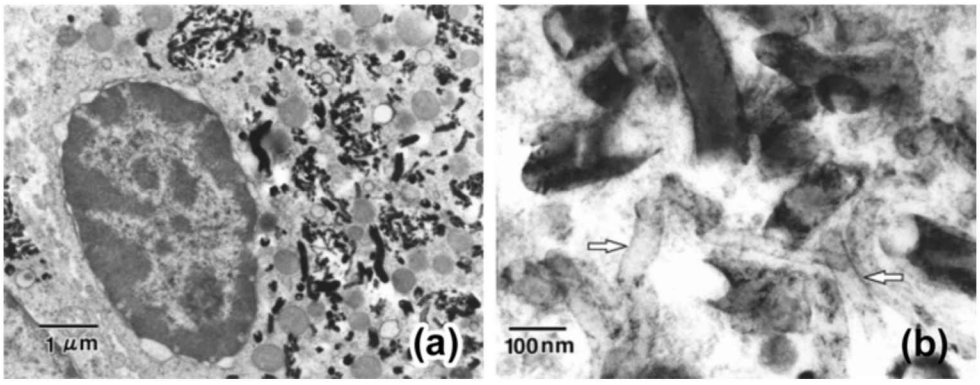

Fig. 5.5. *TEM micrographs of CNFs implanted in the subcutaneous tissue of rats, after 4 weeks post treatment. (a) CNFs were observed in macrophage cytoplasm, close to the cell nucleous. (b) Higher magnification TEM image of CNFs inside macrophages; arrows indicate some CNFs that became translucent (Images obtained from Yokoyama's manuscript [26]).*

Sato et al. [17] carried out a comparative cytotoxicity study of MWNTs with different lengths (220 and 825 nm). The tests were performed *in vivo* and *in vitro* (with THP-1 cells). Six male rats were anesthetized and 0.1 mg of MWNTs samples were implanted into bilateral incisions made in the thoracic region. Histological examination revealed inflammatory response induced by 825 nm MWNTs, which was generally more pronounced than that caused by 220 nm MWNTs (figure 5.6). Nanotubes appeared surrounded by a granulation tissue with macrophages, body giant cells and firbroblasts. Macrophages were able to wrap short nanotubes but long nanotubes were less frequently found inside these cells. TEM characterization also showed the presence of short and long nanotubes inside macrophages. Short nanotubes were usually found inside lysosomes whereas long nanotubes were in the cytoplasm, not covered by a membrane (figure 5.7). The results did not show a toxic response of THP-1 cells for the *in vitro* case.

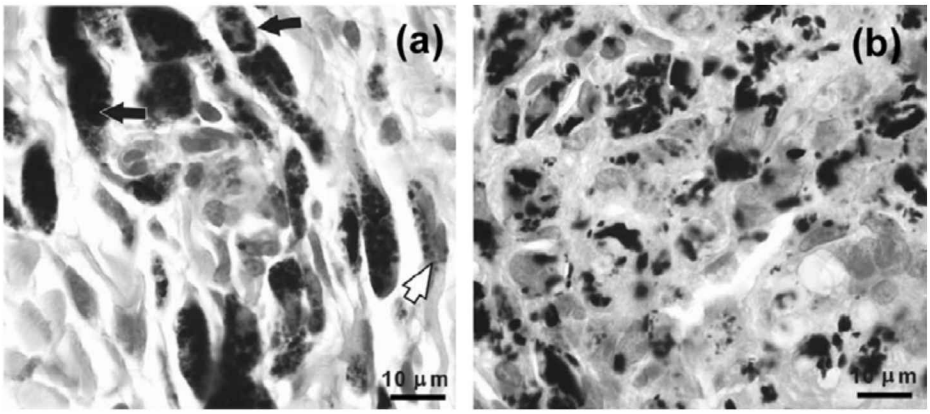

Fig. 5.6. *TEM images of urine samples obtained form mice treated with functionalized SWCNTs and MWCNTs. The urine samples were centrifuged. (a) and (b) Functionalized SWNT obtained from the supernatant. (Scale bars 500 nm). (c) – (e) Functionalized MWNT obtained from the supernantant. (f) – (h) Functionalized MWNT in the precipitate. (Scale bars for (c)-(h) 100 nm) (Images obtained from Singh's manuscript [25]).*

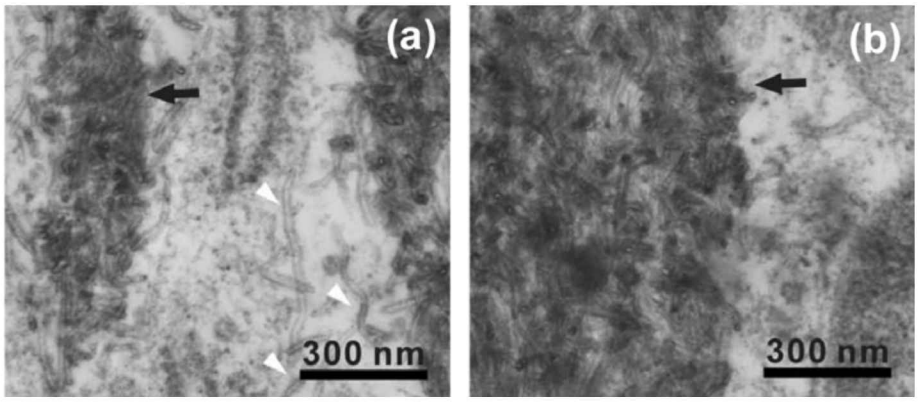

Fig. 5.7. *Histology of 220 nm and 824 nm SWNCTs implanted in the subcutaneous tissue of rats, 4 weeks post treatment. (a) Most of the 220 nm SWCNTs were observed in macrophage cells, pointed by black arrows, and fibroblasts, pointed with withe arrows. (b) 828 nm SWCNTs also caused inflammatory responses in the inoculated tissue. There were no differences in the degree of the tissue damage after one or four weeks. All scale bars are 10 μm. (Images obtained from Sato's manuscript [28]).*

Subsequently, Singh et al. [18] injected radioactively marked SWCNTs and MWCNTs in mice's blood stream, and analyze their behavior and clearance pathway. Six- to eight-week-old female mice were injected via tail vain with 60 μg of SWCNTs and were sacrificed after 30 minutes, 3 and 24 hours and the blood, muscles, bones, skin, heart, lungs, liver, kidneys and spleen were analyzed. The authors reported the highest concentration of SWCNTs in the kidney of the animal after 30 minutes, but this concentration decrease rapidly after 3 hours. This suggests that the clearance pathway is renal excretion. 400 mg of functionalized SWCNT or MWCNTs were injected through the same via and urine was analyzed after 18 hours. TEM characterization of urine samples revealed a dense presence of SWCNTs (figure 5.8a-b) and MWCNTs (figure 5.8c-h). Therefore, the clearance mechanism of nanotubes from blood was confirmed to be renal excretion. This report provided the first pharmacokinetic data after the administration of carbon

nanotubes, where the blood clearance rates of the two types of SWNTs have a blood circulation half-life of c.a. 3.5 hours.

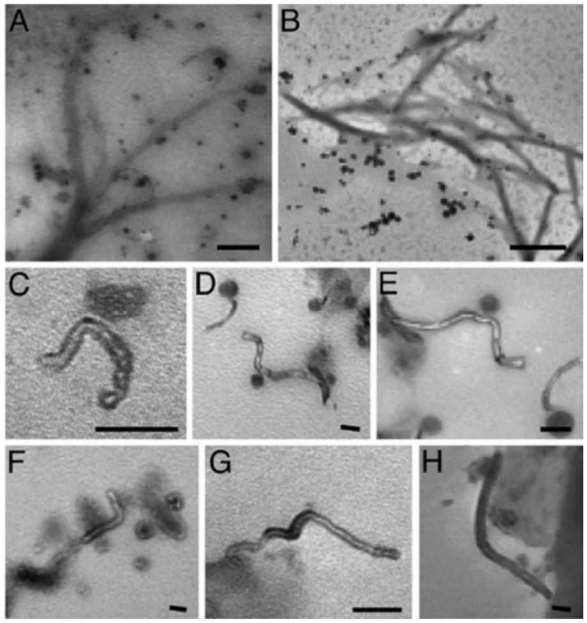

Fig. 5.8. *TEM micrographs of 825 nm SWCNTs implanted in the subcutaneous tissue, 4 weeks post treatment. (a) The black arrow points an aggregate of SWCNTs. Their typical structure was also observed in the cytoplasm, as it is noticed by the arrowheads. (b) The black arrow indicates an aggregate of 825 SWCNTs observed in the cell cytoplasm, which was not covered by membrane. All scale bars are 300 nm. (Images obtained from Sato's manuscript [28]).*

Previous work carried out by Oberdörster and coworkers [19] reported the translocation of inhaled ultrafine ^{13}C particles to secondary organs in rats. Animals exposed to nanoparticles were sacrificed after 1 to 7 days post treatment, and isotope ratio mass spectroscopy detected ^{13}C in secondary organs such as lung, cerebrum, cerebellum and olfactory bulbs.

It should be emphasized that the most common technique for producing bulk amounts of pure carbon nanotubes is based on the chemical vapor deposition route

(CVD), which consists on pyrolyzing organic molecules (*e.g.* CH_4, C_6H_6, C_2H_2, etc) over a metal catalyst (*e.g.* Ni, Co, Fe) in an inert atmosphere [4]. More recently, a new type of carbon nanotubes, known as CNx nanotubes, has been reported [20]. These tubes are characterized by the bamboo-type morphology (Fig. 5.9c,d), and contain N atoms embedded in the hexagonal carbon network at different ratios (1 – 10 at %). Interestingly, the nitrogen is bonded to the carbon atoms in two fashions: i) pyridine-type N, in which each N atom is bonded to two carbon atoms; these type of doping creates cavities within the side wall of the tube (Fig. 5.9a), and ii) Substitutional N, which corresponds to N atoms bonded to three carbon atoms (Fig. 5.9a). Since N contains an additional electron when compared to C, CN_x nanotubes are expected to be metallic [21-22]. Moreover, the N groups increase the reactivity on graphene walls when compared to pure carbon nanotubes, which are basically inert. Due to this enhanced surface reactivity, CNx nanotubes have been used as fast responsive sensors [23], efficient and intense field emission sources [24], PS- and epoxy-composites [25], protein [10] and nanoparticle immobilizers [26], etc. In addition, the incorporation of cyanide groups is plausible, and if so, these tubes could be lethal. Therefore CN_x nanotubes, which are more reactive than pure carbon nanotubes with the possibility of being hazardous and lethal, need to be studied from the toxicological standpoint.

As discussed above, intratracheal injection of single-walled carbon nanotubes (SWNTs) results in the death of the treated mice [13] and rats [15], suggesting that they could be hazardous to humans. However, no information is available on the toxicity of multi-walled carbon nanotubes doped with nitrogen (CN_x MWNTs). CN_x nanotubes could be industrially produced for the manufacture of novel biochemical products. However, strict biosafety measures need to be developed for the production and processing of these nanotubes into new materials. In the following sections, toxicological studies of CN_x MWNTs and pure carbon multi-

walled nanotubes (MWNTs) on mice are presented. It will be demonstrated that when using extremely high doses of CN_x nanotubes (e.g. 5mg/kg), no lethal effects are observed on the mice, which is in contrast to previous reports using SWNTs [13,15].

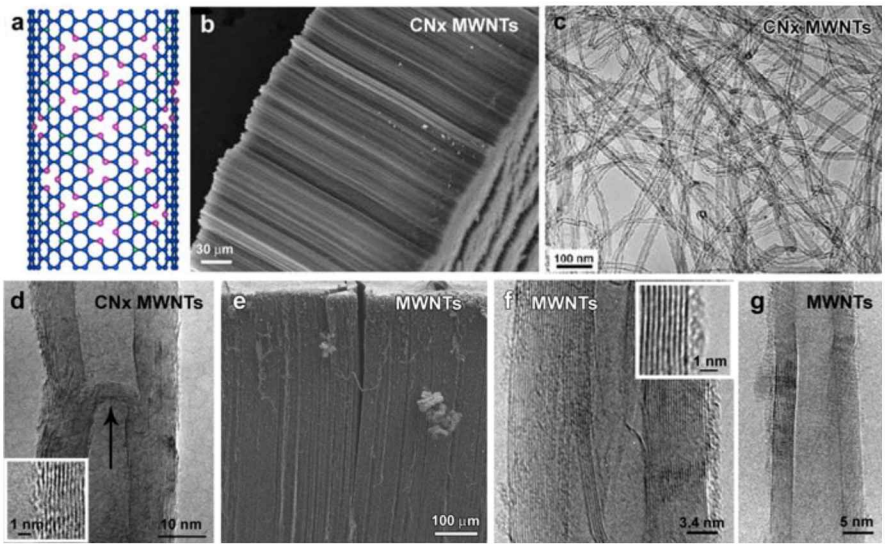

Fig. 5.9. *(a) Molecular model CN_x nanotube indicating the two types of N-groups attached on the tube surface, pyridine-type N, in which each N atoms is bonded to two carbon atoms (see pink vertices) and subtitutional N, which corresponds to N atoms covalently liked to C atoms (see green vertices); (b) SEM image of a typical nanotube carpet grown in the CVD experiments, showing tubes with average diameters of (30-50 nm) and lengths of several microns (100-300 mm); (c) TEM image of a CN_x nanotube showing the overall morphologies and compartmentalized structure of the tubes (bamboo-type); (d) HRTEM image of an individual tube exhibiting bamboo-type compartments; see arrow pointing the edge of one compartment. The inset shows a higher magnification image of the graphitic planes of the CN_x MWNT. (e) SEM image of PCMWNTs. (f)-(g) HRTEM images of two different types of MWNTs with different diameter showing the excellent degree of crystallinity (note that the graphene planes are straight and parallel, see inset in f).*

5.2 In vivo instillation of CNxMWNTs and MWCNTs in mice: Nanotube production and suspension preparation

Two types of multiwalled carbon nanotubes have been synthesized in this study: pure carbon MWNTs and CN_x MWNTs. The CVD process was used involving organic solvents as the carbon source in conjunction with ferrocene ($FeCp_2$), which is used as a catalyst. Solutions containing 2.5 wt% of ferrocene in toluene (C_7H_8) were sprayed using an abrupt Ar pressure difference [27]. This generated spray was introduced into a quartz tube heated to 850 ^oC in the presence of Ar. Note that the SiO_x tube served as substrate for growing the nanotubes. This method has been described in chapter 1. In order to produce CNx nanotubes (Figs. 5.9b-c), the toluene was exchanged by benzylamine (C_7H_9N) [28]. The nanotube growth proceeded for 15 minutes, using an argon flow of 3.7 l/min. The nitrogen content within these CN_x MWNTs has been determined using nuclear reaction analysis, and the samples treated contained ca. 2 - 4wt% (for more details see chapter 4). It should be emphasized that higher nitrogen concentrations cannot be obtained using the experimental parameters indicated above. Both types of pristine nanotubes contained between 2 and 2.5 wt% of Fe (usually encapsulated in the tubes).

Scanning electron microscopy (SEM) images of as produced MWNTs and CN_x MWNTs are shown in figures 5.9b and 5.9e. At these magnifications, structural differences between the two samples are not evident. In particular, MWNTs are usually longer than CN_x MWNTs; their lengths are up to 500 μm (Fig. 5.9e), whereas the CN_x MWNTs' maximum length only reaches the value of 300 μm (Fig. 5.9b). High resolution transmission electron microscopy (HRTEM) images exhibit

the bamboo-like structure for CN_x MWNTs (see arrow in Fig. 5.9d). For comparison, Figs. 5.9f and 5.1g show HRTEM images of undoped MWNTs. The degree of crystallinity within the graphene cylinders for MWNTs (undoped) is higher when compared to CN_x MWNTs (Figs. 5.9d-f). In addition, it can be observed that CN_x MWNTs possess a rougher surface than pure carbon MWNTs (see insets from Fig. 5.9d & f) caused by the presence of pyridinic nitrogen. In general, CN_x tubes exhibit average diameters of 20-40 nm, whereas MWNTs could display slightly larger diameters (< 50nm). Additionally, CN_x nanotubes are shorter and could break easily under sonication due to the bamboo-like structure.

Pristine carbon nanotubes agglomerate easily due to strong van der Waals interations. Therefore, chemical treatments need to be carried out in order to increase their reactivity and solubility [29]. The followed oxidation procedure has been described by Jiang and coworkers [26]. In particular, 200 mg of nanotubes (doped or undoped) were mixed with 20 ml of a H_2SO_4:HNO_3 (3:1) solution. Suspensions were treated for 2 hours in an ultrasonic bath, and filtered to obtain the solid material. Before filtering process, deionized water was added, in a volume of 250 ml. A second filtration was carried for neutralizing the products, after adding 200 ml of NaOH, 0.01 M. The solids were dispersed in phosphate-buffered saline (PBS) in order to obtain homogenous and stable suspensions.

The latter suspensions were subsequently administrated to the mice in different ways (see below). It should be emphasized that the acid treatment of nanotubes modifies their surface, creating four types of functional groups: hydroxyl, carboxyl, carbonyl and sulfate [26]. These groups are hydrophilic, therefore, the nanotubes were successfully dispersed in PBS after the acid treatment. The chemical functionalization of nanotube surfaces was carried out in order to obtain homogenous nanotube suspensions so that they could be administrated easily to

mice in different ways, thus avoiding agglomeration and warranting reproducibility.

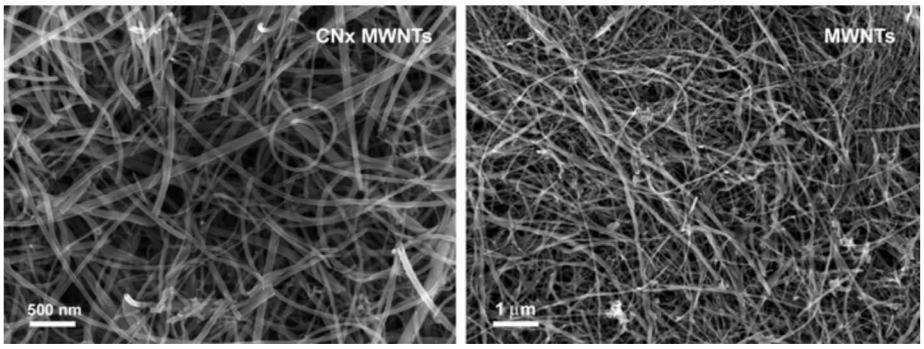

Fig. 5.10. *SEM image of acid treated (a) CNx MWNTs and (b) PCMWNTs dispersed in PBS. Notice that the nanotubes have lost their original bundle conformation.*

SEM images of the two suspensions are shown in figure 5.10. Not significant differences between the samples were noticed from these SEM micrographs. For instance, the length of both types of nanotubes seems to be alike.

We should stress that similar functionalization approaches have been followed by other groups when performing cell viability tests with carbon nanotubes and experiments regarding their usage as cell transporters (17,30-33). For example, Cui and coworkers (30) reported the experimental encapsulation of DNA inside MWCNTs using similar functionalization approaches. In addition, SWCNT functionalized suspensions have also been introduced into human promyelocytic leukemia (HL60) cells, by Kam and coworkers (31). Viability studies revealed that a biotin-SA-SWCNTs conjugate and functionalized SWCNTs were both innocuous (31). The same research group also used functionalized SWCNTs as intracellular protein transporter (32).

For the toxicity assays, male inbred CD1 mice (C.129S2-*Cd1tm1Gru*, 4 weeks old) were purchased from The Jackson Laboratory (Maine, USA), and housed in

wirebottomed cages with controlled light/dark cycles. Mice were maintained under pathogen-free conditions and provided with food and water ad libitum, in compliance with the guidelines of the institution's Ethical Committee. Groups of 10 mice received a single dose of 1, 2.5 or 5 mg/kg of CN_x nanotubes (doped) in PBS via nasal, oral, intratracheal or intraperitoneal routes. Other groups of mice received identical treatments (50-150 µl in volume) with undoped MWNTs. Individual doses, in volumes of 20-150 µl, were administered intranasally by instillation using a micropipette; orally using a plastic cannula; and intratracheally (after anesthesia) and intraperitoneally using insulin syringes (27G). Groups of 5 mice, receiving identical volumes of PBS through each route of administration, served as non treated controls.

For comparison, another group of 10 mice was injected intratracheally with 2 mg/kg of sepharose (in 50 µl of PBS), a well known inducer of pulmonary injury. Two mice from each treated group and one from the control groups were sacrificed 24 h, 48 h, 72 h, 7 days and 30 days after post-treatment. After necropsy, lungs, liver, intestines, spleen and heart were carefully examined for tissue changes associated with toxicity; the lungs from the mice treated intranasally and intratracheally were exposed, fixed by intratracheal instillation with 10% formaldehyde in PBS, embedded in paraffin, sectioned and stained with hematoxylin-eosin for histological examination. Serum samples were obtained from all the animals one day before sacrifice, and used to evaluate some biochemical parameters that reflect the physiological status of some vital organs: levels of glucose, creatinine, amylase, alanine aminotransferase (ALT), total protein, albumin, globulins and cholesterol, determined using commercially available kits and always following the instructions from the manufacturer (DCL Reactives, USA).

5.3 Responses induced by oral and intraperitoneal routes

Administration of PC MWNTs or CN_x nanotubes to CD1 mice by oral and intraperitoneal routes did not induce distress or local tissue responses in the dose and time ranges evaluated in this study. Biochemical studies were unrewarding. In mice challenged orally, aggregates of nanotubes were identified in the feces after 24 h. These mice did no show signs of intestinal occlusion or diarrhea. During autopsy, the intestines were free of nanotube aggregates or inflammatory lesions. Mice challenged by the intraperitoneal route, revealed aggregates of nanotubes dispersed between the intestinal loops without evidence of inflammation or tissue damage and internal organs such as liver, lungs, spleen, kidney and heart appeared normal. Glucose, amylase, cholesterol, electrolytes, and other biochemical parameters in serum of challenged and control mice were within normal limits.

5.4 Responses driven by carbon nanotube instillation through the mice's respiratory tract

Two experimental approaches were undertaken to analyze the effects of both types of nanotubes in the respiratory tract. First, the nanotubes were administered by nasal instillation in PBS at different concentrations: 1, 2.5 and 5 mg/kg; using a single administration or a daily dose for a week. Neither mortality nor clinical signs of distress were noticed in the treated mice. At all times and with all doses, histologic examination of lung tissue sections failed to reveal deposition of nanotubes and there were no inflammatory changes noticed. Possibly, the mucosa was able to trap and expel the nanotube material. For this reason, both types of

nanotubes were directly instilled into the trachea of the mice using the same doses mentioned above, in a single administration (see below).

5.4.1 Effects of intratracheal instillation of CN_x MWNTs

Again, the mice challenged with CN_x MWNTs resulted in no mortality, even with the highest dose of 5 mg/kg, and more interestingly the weight, external appearance and behavior of mice remained unchanged. During autopsy, macroscopic examination of heart, liver, spleen and intestines did not reveal any adverse effect in all mice challenged with the different doses. No macroscopic evidence of CN_x MWNTs deposition was observed in lungs of mice receiving 1 mg/kg (Fig. 5.11a). However, lung deposition of carbon material was evident in the lungs of the mice receiving 2.5 or 5 mg/kg (Fig. 5.11b), whereas changes were not detected in other organs.

Histologically, the lungs of mice instilled with 1 mg/kg of CNx MWNTs appeared normal at all experimental times; nanotube deposition was not observed neither in the lungs nor in the hylar lymph nodes. In mice challenged with 2.5 mg/kg, bronchioles containing small aggregates of CN_x MWNTs in close contact with the epithelium were observed, but without evidence of epithelial damage or inflammation 48 h, 72 h and one week post-challenge. After one month, a tiny mononuclear cell granuloma was observed in the lung of one mouse without evidence of nanotubes. Draining lymph nodes were also free of nanotubes or granulomatous reaction.

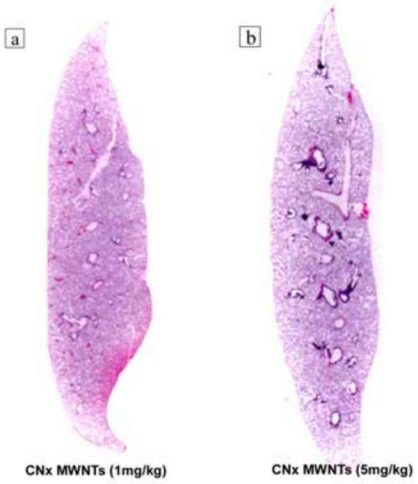

Fig. 5.11. *Progressive pulmonary lesions caused by intratracheal instillation of CN_x MWNTs to CD1 mice. The panels show hematoxylin-and eosin-stained lung sections from mice treated with CNx MWNTs at 1 mg/kg for 24 h (a) and 5 mg/kg for 24 h (b). Original magnifications were taken at 2X.*

In contrast, histological examination of lungs from mice challenged with 5 mg/kg of CN_x nanotubes at the different times, revealed a sequential process of tissue invasion and inflammation. At 48 h and 72 h post-challenge, nanotube aggregates were found in the lumen of small and medium size bronchi (Fig. 5.12a). Frequently, the epithelial cells were cuboidal or flattened and, in segments of the bronchiolar wall, they were absent (Fig. 5.12a). The wall of some bronchioles was completely disrupted and nanotube aggregates were seen in the neighboring interstitium surrounded by a granulomatous reaction containing macrophages, lymphocytes, fibroblasts and collagen deposition, which were also abundant in the peribronchiolar interstitium (Fig. 5.12b). The draining lymph nodes were hyperplasic without evidence of CNx nanotube deposits. At later times (7 and 30 days) reactive fibrosis was observed in the peribronchiolar interstitium. After 7 days of the challenge, lesions were observed throughout the lungs caused by CN_x MWNTs aggregates disrupting the bronquial epithelium and causing extensive papillomatous hyperplasia with hypercromatic nuclei and pleomorphic cells. The

damage was associated with intense mononuclear infiltration (lymphocytes and macrophages) and fibroblastic proliferation (Fig. 5.12c). After one month, the mucosa of many bronchioli was extensively eroded in areas in contact with nanotube clumps and, occasionally, small granulomas were observed in the lung interstitium (Fig. 12d). The hylar draining lymph nodes did not exhibit nanotube deposition or inflammatory changes (data not shown).

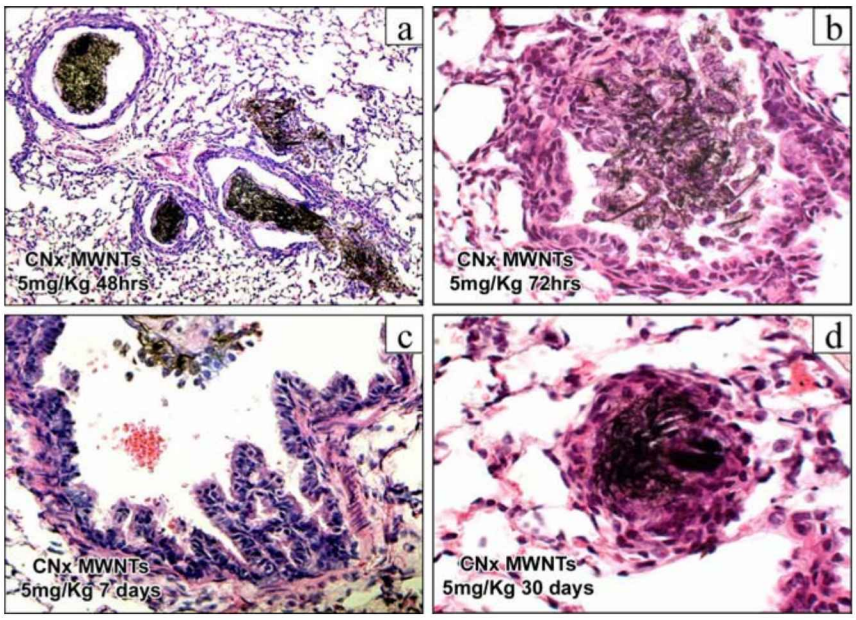

Fig. 12. *Representative micrographs of hematoxilin-eosin stained lung sections illustrating the pathologic changes observed in mice challenged intratracheally with 5 mg/Kg CN_x MWNTs. Mice were sacrificed after challenge at 48h (a), 72 h (b), 7 days (c) and 30 days (d). The lumina of several bronchioles was occupied by compact aggregates of nanotubes (a), some of them adhered to the bronchiolar mucosa. There were not inflammatory changes in the interstitium. A nanotubes aggregate was observed in a small-size bronchiole which had penetrated the wall, infiltrating the neighboring lung interstitium, inducing a mononuclear cell infiltrate (b). Papillary hyperplasia of the lining epithelium of a small-size bronchiole that contains nanotubes (c); cell nuclei are pleomorphic and hyperchromatic. At 30 days nanotubes were surrounded by macrophages forming an interstitial granuloma (d).*

5.4.2 Effects of intratracheally instilled MWCNTs

A different result was witnessed in mice receiving pure MWNTs by the intratracheal route. After a single dose of 1, 2.5 and 5 mg/kg of nanotubes, 30, 60 and 90% of mice immediately died, respectively. In these mice, signs of pulmonary distress, mainly dyspnea, were observed. Macroscopic evidence of MWNTs deposition was observed in the lungs of mice at all doses as multiple black tiny dots scattered throughout the lung tissue; however, the level of deposition was proportional to the dose (Figs. 5.13 a, b and c). Microscopic analysis of lung tissue from mice that survived a challenge with 1 mg/Kg MWNTs, showed no lung changes at early stages (24 and 48 h). After 15 days of treatment, granulomatous inflammatory reaction in the lumen of the bronchi was occasionally observed (Figure 5.14 a). Globet cell hyperplasia was found in numerous small bronchi containing adhered clumps of nanotubes and multiple granulomas were also observed in the lung interstitium (Figure 5.14 b).

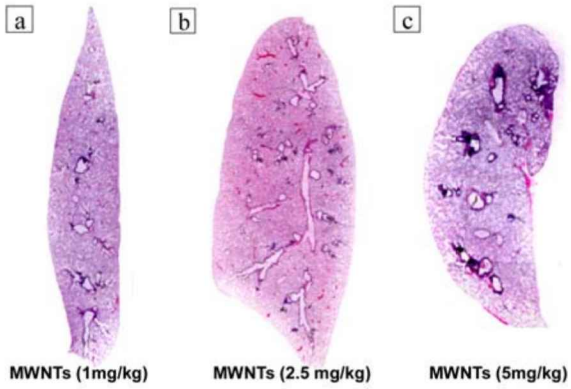

Fig. 5.13. *Progressive pulmonary lesions caused by intratracheal instillation of PCMWNTs (undoped nanotubes) to CD1 mice. The panels show hematoxylin-and eosin-stained lung sections from mice treated with PCMWNTs at 1 mg/kg for 24 h (a); 2.5 mg/kg for 24 h (b); 5 mg/kg for 24 h (c). The number of bronchioles of small to large size occupied by MWNTs and the magnitude of the deposition is related to the amount of nanotubes instillated into the lungs. With 5 mg/Kg dose the majority of the bronchioles are involved (c).*

Occasionally it was observed a segmentary disruption of the bronchial epithelium, with invasion of the interstitium by the nanotubes. Those pathological changes started earlier on mice treated with 2.5 mg/kg MWNTs. At 24 h, numerous bronchioli with MWNTs aggregates in close contact with a flattened epithelium were observed. After 48 h, atypical hyperplasia with nuclear polymorphism and hyperchromatism was observed in most bronchi containing nanotubes. In some bronchi and bronchioles partial loss of the lining epithelium was witnessed; in their lumen and the surrounding interstitium, intense mononuclear inflammatory reaction and numerous polymorphonuclear cells were frequently observed. After 72 h and 7 days of the challenge, pathological changes were similar to those observed at 48 h (data not shown). Additional changes were observed in the mice that survived to 1 and 2.5 mg/Kg nanotube challenges. An intense inflammatory infiltrate composed by polymorphonuclear leukocytes and some eosinophils was also observed around these bronchioles. It was frequent to observe bronchioles with MWNTs aggregates that had broken the bronchiolar wall and infiltrated the interstitium, a change associated with intense inflammatory reaction composed by macrophages, lymphocytes and few eosinophils (Fig. 5.14 c). Multiple granulomas in the lung interstitium were also observed, an effect already seen with the lowest dose (Figure 5.14 b). As observed with CN_x MWNTs at late experimental times, atypical hyperplasia of the bronchiolar epithelium was observed (Fig. 5.14 c). An interesting finding was the globet cell hyperplasia detected in numerous small bronchioles (Fig. 5.14 d). This effect was not observed with CN_x MWNTs. As mentioned above, most animals receiving 5 mg/kg of MWNTs by intratracheal route immediately died or were moribund; these mice were autopsied at 24 and 48 h and the lungs processed for histologic examination. Most of the bronchi were occupied by compact nanotube aggregates forming a pellicle closely adhered to the lining epithelium (Fig. 5.14 e-f), a change that was not observed with CN_x MWNTs. Frequently, the lumen of the bronchioli was almost completely occupied by the

MWNTs clumps, causing intense erosion of the epithelium and rupture of the bronchial wall (Fig. 5.14 e).

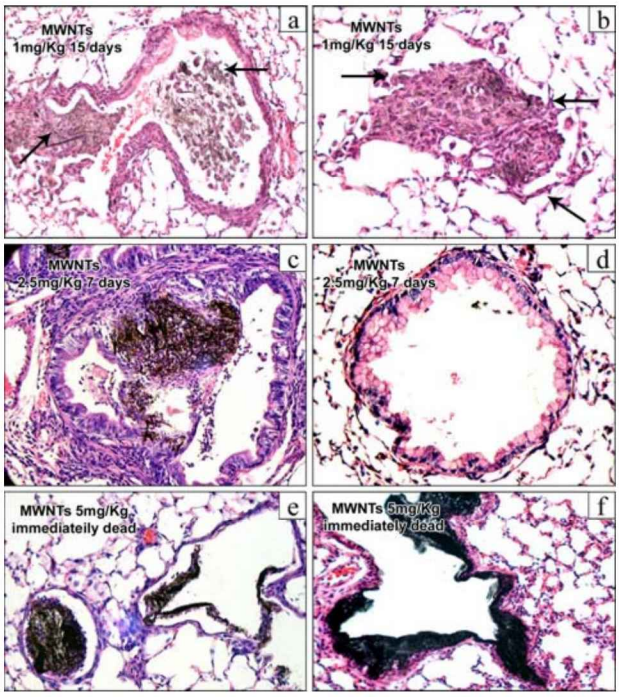

Fig. 5.14. *Pulmonary hematoxylin-and eosin-stained sections from CD1 mice challenged by the intratracheal route with 1.0 (a-b), 2.5 (c-d) and 5 mg/kg (e-f) of pure MWNTs (undoped nanotubes). Lungs were obtained from mice that immediately died (e-f) or mice sacrificed at 7 days (c-d) and 15 days after challenge (a-b). (a) Granulomatous inflammatory reaction observed in the lumen of the bronchi. (b) Granulomas present in the lung interstitium. (c) A small–size bronchiole showing a compact PCMWNTs aggregate occupying the lumen, breaking the bronchiolar wall and eliciting intense mononuclear inflammation. Papillary hyperplasia of lining epithelium is also observed. (d) Globet cell hyperplasia observed in a small bronchiole in the absence of nanotubes. (e) Two large bronchioles occupied by PCMWNTs aggregates; the lumina of several bronchioles were occupied by compact aggregates of nanotubes, some of them adhered to the bronchiolar mucosas. There are not inflammatory changes in the interstitium. (f) Micrograph of a small bronchiole showing PCMWNTs forming a pellicle firmly adhered to the bronchiolar wall; the aggregate has penetrated the wall infiltrating the neighboring lung interstitium inducing a mononuclear cell infiltrate.*

Figure 5.15 b shows a very different toxic response driven by a positive control for comparison with responses caused by CNx MWNTs and PC MWNTs; sephadex was directly instilled into mice's trachea. Lungs from sephadex- treated mice presented a diffuse inflammatory response (figure 5.15b). For comparison, figure 5.15 a shows an image from a negative control (instilled with pure PBS), where there lungs appeared healthy, without evidence of any toxic response.

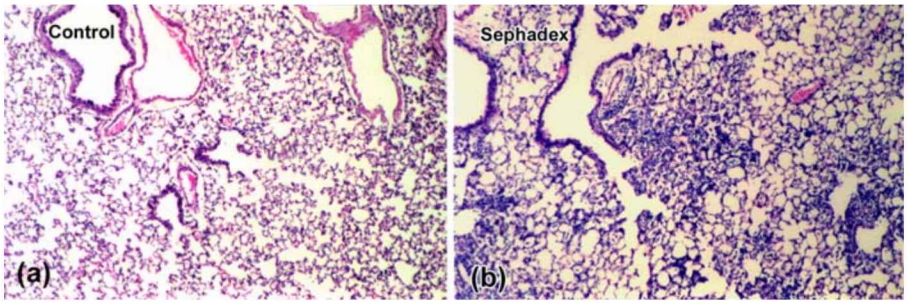

Fig. 5.15. *(a) Lung tissue from a control experiment. (b) Image of a lung intratracheally instilled with 2 mg/Kg of sephadex. This was used as a positive control; the image depicts a diffuse inflammatory response. (Magnification 10X).*

5.5 Discussion and Toxicological Mechanisms of Nanotubes

According to their lethality, the pathologic changes associated with the administration of PCMWNTs were different and more severe than those observed with the CN_x MWNTs. Signs of respiratory insufficiency as well as histological analysis of the lungs suggested that a mechanical obstruction of bronchi by clumps of PCMNTs could be responsible of mice death, because they adhere to epithelial cell surface. CN_x MWNT do not induced this effect and are frequently seen in the lumen of bronchioli. The tendency of nanotubes (both CN_x and PCMWNTs) to form aggregates was observed with all administration routes, and this is likely due

to their electrostatic properties [34]. However, PCMWNTs are more likely to form large agglomerates when compared to CN_x, which could be better dispersed in different media.

Both types of nanotubes induce erosion and disruption of the bronchi epithelium at different levels, concomitant with a mononuclear inflammatory reaction. PCMWNTs when used at 5 mg/kg concentrations, also induced the arrival of eosinophils, an immune cell involved in allergy and fibrosis, suggesting that PCMWNTs, in contrast to CNx nanotubes could induce allergic inflammation when they are inhaled. Besides, both types of tubes induced an abnormal increase in the number of bronchiolar epithelial cells (epithelial hyperplasia); this change, however, was more frequent in the mice challenged with the PCMWNTs and it appeared at earlier times, even if the bronchioli showed an apparent absence of nanotubes (see figure 5.14 d). Granulomas and fibrogenesis were seen at late stages with both types of nanotubes, as described in previous nanotubes toxicological studies [13,15]. However for MWNTs, these responses were more numerous than those observed with the highest CN_x dose.

It is important to compare the results described above with previous toxicology studies performed with other forms of carbon besides nanotubes. Environmental concerns have derived in the toxicity study of several materials that are present in mines. In 1999, Fan et al. [35] described toxicity and cytotoxicity studies of brown coal dusts. The samples were collected from two coal mining places and were milled manually to obtain particle sizes <5 μm. X-ray fluorescene and atomic absorption determine that the samples contained Zn, Ni, Ca, Al, Cu, Co, Cd, Cr, Mn, V, Ba, Mg and Ti. They performed cell viability tests with alveolar macrophages from rats. The study included a comparison of quartz cytotoxicity, as

a negative control. They found that the viability of cells was affected by the presence of brown coal dusts.

Carbon black (CB) has been the target of several toxicology studies as well. Researches started to worry about smaller sized particles contained in this material. In 2004, Barlow et al. [36] performed a comparative chemotaxis study with carbon black nanopartices of 260 and 14 nm in size. Fetal bovine serum (FBS) was exposed to carbon black and to antioxidants such as *tert*-butyl hydroperoxide (*t*BHP), Trolox and nacystelin. Ultrafine carbon black (14 nm particles) induced macrophage migration. Nanoparticles co-exposed with Trolox or nacystelin (antioxidants) did not induced significant macrophage migration, suggesting that the chemotactic factor generation was driven for oxidation caused by the nanoparticles.

Yamawaki and Iwai [37], reported a cytotoxicity study of carbon black (CB) in human vascular endothelial cells (ECs). The motivation of this researach was the linkage between particulate matter (PM) and cardiovascular diseases, such as atherosclerosis. ECs were incubated with CB particles (250 μm) in different concentrations. By TEM, it was possible to describe structural changes in the cell and the presence of CB particles inside vacuoles. There was also reported an increase in lactate dehydrogenase (LDH) delivery, which is a marker of cell death and injury of the plasma membrane. CB had an antiploriferative effect on ECS as well. Therefore, these authors concluded that carbon black causes cytotoxic injury and inflammation and inhibits cell growth in ECs.

It should be emphasized that the highest nanotube concentration used in these studies (e.g. 5 mg/kg) is difficult to be inhaled or ingested by the human body. During nanotube processing, it is likely that nanotubes could be inhaled, however in such cases, the CN_x tubes tend to be agglomerated in bundles or carpet-like

morphologies (see figures 5.9b and 5.9e) that could be easily trapped by the mucosa avoiding the delivering of these nanomaterial to the lungs. Nevertheless, masks and strict measures need to be taken during handling and production of nanotubes. If the nanotubes are embedded in a polymer matrix (e.g. reinforced packaging products) or a metal (reinforced materials), it would be extremely difficult for the tubes to detach and therefore, the concentrations that could be exposed to the human body would be much lower than those used in the present toxicological studies. With such low concentrations, and in particular for CN_x nanotubes, no inflammatory effect in the body cells, skin and organs, neither intestinal occlusion nor diarrhea are expected.

The plausible formation of cyanide groups driven by the interaction of CN_x MWNTs and the mice did not occur. On the contrary, the presence of nitrogen in the graphitic network could be the reason for the CN_x MWNTs to be less injurious to a living organism. Amino groups are expected to be present on the surface of the CN_x tubes. It is therefore possible that these amino groups may be the reason for expecting a better biocompatibility on the CN_x tubes when compared to pure carbon MWNTs (undoped). The two types of tubes (Figure 5.9) exhibit clear structural differences. For example, MWNTs display a high degree of crystallinity and therefore are more robust. This crystallinity results in stronger van der Waals interactions and the MWNTs tend to aggregate easily. Therefore, PCMWNTs will agglomerate faster and would create large clumps that result in the dead of the mice by dyspnea. On the contrary, CN_x nanotubes posses a bamboo-like structure with a rougher surface, exhibiting weaker van der Waals interactions, that result in the formation of less agglomerates causing much less damage to the mice´s lungs (e.g. they are definitely better dispersed than pure MWNTs). In addition, MWNTs do not break easily when compared to CN_x nanotubes. This mechanical enhancement in MWNTs could also increase the damage in the mice tissue and

therefore become more hazardous because they damage the epithelium. Finally, the Fe content within both types of treated tubes is similar (ca. <0.5wt%), and it is possible to discard the presence of Fe as the trigger for toxicity.

It is clear that PCMWNTs cause the dead of 30% of the mice when using the smallest dose (1 mg/kg), 60% when 2.5 mg/kg were administered to the mice, and 90% with the highest dose (5 mg/kg). In this context, Lam's work [13] reported the death of 5 of the 9 mice treated with a dose of 0.5 mg of arc discharge SWNTs; the mice had a body weight of 30 g, thus the dose administered was 16.6 mg/kg. In addition, Warheit and coworkers [15] reported 15% of dead rats with intratracheal instillation of 5 mg/kg of SWNTs. From a direct comparison between SWNTs toxicity assays [13,15] and this work, it can be established that PCMWNTs appear to be more harmful to mice than SWNTs, whereas CN_x MWNTs are less harmful.

It is important to note that the present study involved only one type of CNx nanotubes containing between 2-4 wt% of N. However, further studies dealing with different N concentration (e.g. > 4wt%) are required, although these samples cannot be easily prepared.

5.6 Conclusions

In this chapter, toxicological effects of different types of carbon nanotubes and especially between PCMWNTs and N-doped multi-walled carbon (CN_x) nanotubes were described and compared. The tubes were administered in different ways to mice: nasal, oral, intratracheal and intra-peritoneal. It has been found that either PCMWNTs or CN_x nanotubes injected into the mouse's trachea induce granulomatous inflammatory responses when extremely high nanotube doses are administrated. These tubes also caused the obstruction of small and medium-size

bronchioles, and damaged the bronchiolar wall that resulted in lung inflammation. However, CN_x nanotubes were far more tolerated by the mice when compared to PCMWNTs. In particular, intratracheal injection of up to 5mg/kg of CN_x tubes did neither caused the dead of the mice nor induced visible signs of distress on the animals, in contrast to the lethal effects of similar doses of MWNTs or SWNTs [15] administered to mice through the same via. All other routes of administration did not induce signs of distress or tissue changes on treated mice. It is concluded that CN_x nanotubes are thus more biocompatible than MWNTs or SWNTs and might be more advantageous for practical applications (also see chapter 5).

In summary, CN_x nanotubes are not toxic to mice when administered at doses ≤ 1 mg/Kg; however, when high concentrations (e.g. 5 mg/kg) are directly inoculated into the trachea of mice, they result in bronchial epithelial erosion and an acute inflammatory response. At this concentration, when the CN_x tubes invaded lung interstitium, the response evolved after 30 days post-challenge to the formation of granulomas, small and fibrous nodules that isolate and confine the nanotubes. However, the exposition of the lower respiratory tract to this amount of nanotubes seems to be unrealistic in normal conditions, since, even when individuals inhaled such a dose of CN_x nanotubes, much of them will be retained and expulsed by the mucus and cilia of the upper respiratory tract.

Because none of these studies with CN_x tubes resulted in the death of the mice, it is believed that CN_x nanotubes would be more biocompatible when compared to other types of nanotubes (e.g. single-walled, multiwalled, double-walled, etc), thus suggesting that these types of nanotubes could now be tested in biological systems such as drug and antigen delivery (immunological adyuvants) as well as infectious agents inhibitors. Finally, it should be emphasized that these tests are the first of its

kind, and further studies with other animals besides mice, with longer life times, should be now carried out.

References

[1] Iijima, S. "Helical microtubules of graphic carbon" *Nature* **354**, 56-58 (1991).

[2] Oberlin, A., Endo, M., Koyama, T. "Filamentous growth of carbon through benzene decomposition" *J. Cryst. Growth* **32**, 335-349 (1976).

[3] Ebbesen, T. W., Ajayan, P. M. "Large-scale synthesis of carbon nanotubes" *Nature* **358**, 220-222 (1992).

[4] Endo, M. "Grow carbon fibers in the vapor phase" *Chem. Tech.* **568**-576 (1988)

[5] Terrones, M. "Carbon nanotubes: synthesis and properties, electronic devices and other emerging applications" *International Materials Reviews* **49**, 325-377 (2004).

[6] Wong, S.S., Joselevich, E., Woolley, A.T., Cheung, C.L., Lieber, C.M. "Covalently functionalized nanotubes as nanometre-sized probes in chemistry and biology" *Nature* **394**, 52-55 (1998).

[7] Kong, J., Franklin, N.R., Zhou, C.W., Chapline, M.G., Peng, S., Cho, K.J., Dai, H.J. "Nanotube molecular wires as chemical sensors" *Science* **287**, 622-625 (2000).

[8] Baughman, R.H., Zakhidov, A.A., De Heer, WA. "Carbon nanotubes – the route toward applications" *Science* **297**, 787-792 (2002).

[9] Harris, P.J.F. "Carbon nanotube composites" *Int. Mater. Rev.* **49** (1), 31-43 (2004).

[10] Jiang, K.Y., Schadler, L.S., Siegel, R.W., Zhang, X.J., Zhang, H.F., Terrones, M. "Protein immobilization on carbon nanotubes via a two-step process of diimideactivated amidation" *J. Mater. Chem.* **14**, 37-39 (2004).

[11] Viswanathan, G., Kane, D.B., Lipowicz, P.J. "High efficiency fine particulate filtration using carbon nanotube coatings" *Adv. Mater.* **16**, 2045-2049 (2005).

[12] Colvin, V.L. "The potential environmental impact of engineered nanomaterials" *Nature Biotechnology* **21**, No. 10, 1166-1171 (2003).

[13] Lam, C.-W., James, J.T., McCluskey, R., Hunter, R.L. "Pulmonary Toxicity of Single-Wall Carbon Nanotubes in Mice 7 and 90 Days after Intratracheal Instillation" *Toxicol. Sci.* **77**, 126-134 (2004).

[14] Alvarez, W.E., Kitiyanan, B., Borgna, A., Resasco, D.E. "Synergism of Co and Mo in the catalytic production of single-wall carbon nanotubes by decomposition of CO" *Carbon* **39**, 547-558 (2001).

[15] Warheit, D.B., Laurence, B.R., Reed, K.L., Roach, D.H., Reynolds, G.A.M., Webb, T.R. "Comparative Pulmonary Toxicity Assessment of Single-wall Carbon Nanotubes in Rats" *Toxicol. Sci.* **2004**, 77, 117-125.

[16] Yokoyama, A., Sato, Y., Nodasaka, Y., Yamamoto, S., Kawasaki, T., Shindoh, M., Kohgo, T., Akasaka, T., Uo, M., Watari, F., Tohji, K. "Biological Behavior of Hat-Stacked Carbon Nanofibers in the Subcutaneous Tissue in Rats" *Nano Lett.* **5**, No. 1, 157-161 (2005).

[17] Sato, Y., Yokoyama, A., Shibata, K-I, Akimoto, Y., Ogino, S-I, Nodasaka, Y., Kohgo, T., Tamura, K., Akasaka, T., Uo, M., Motomiya, K., Jeyadevan, B., Ishiguro, M., Hatakeyama, R., Watari, F., Tohji, K. "Influence of length on cytotoxixity of multi-walled carbon nanotubes against human acute monocytic leukemia cell line THP-1 *in vitro* and subcutaneous tissue of rats *in vivo*" *Mol. BioSyst.* **1**, 176-182 (2005).

[18] Singh, R., Pantarotto, D., Lacerda, L., Pastorin, G., Klumpp, C., Prato, M., Bianco, A., Kostarelos, K. "Tissue biodistributionand blood clearance rats of intravenously administered carbon nanotube radiotracers" *PNAS* **103**, 3357-3362 (2006).

[19] Oberdorster, G., Sharp, Z., Atudorei, V., Elder, A., Gelein, R., Kreyling, W., Cox, C. "Translocation of inhaled ultrafine particles to the brain" *Inhalation Toxicology* **16**, 437-445 (2004).

[20] Terrones, M., Grobert, N., Zhang, J. P., Terrones, H., Olivares, J., Kordatos, K., Hsu, W. K., Hare, J. P., Prassides, K., Cheetham, A. K., Kroto, H. W., Walton, D. R. M. "Formation of aligned carbon nanotubes catalysed by laser-etched cobalt thin films" *Chem. Phys. Lett.* **285**, 299-305 (1998).

[21] Czerw, R., Terrones, M., Charlier, J.C., Blasé, X., Foley, B., Kamalakaran, R., Grobert, N., Terrones, H., Tekleab, D., Ajayan, P.M., Blau, W., Rühle, M., Carroll, D.L. "Identification of electron donor states in N-doped carbon nanotubes" *Nanolett.* **1**, 457-460 (2001).

[22] Terrones, M., Grobert, N., Terrones, H. "Synthetic routes to Nanoscale $B_xC_yN_z$ architectures" *Carbon* **40**, 1665-1684 (2002).

[23] Villalpando-Páez, F., Romero, A., Muñoz-Sandoval, E., Martínez, L.M., Terrones, H., Terrones, M. "Fabrication of Vapor and gas sensors using films of aligned CNx nanotubes" *Chem. Phys. Lett.* **386**, 137-143 (2004).

[24] Doytcheva, M., Kaiser, M., Reyes-Reyes, M., Terrones, M., de Jonge, N. "Electron emission from individual nitrogen-doped multi-walled carbon nanotubes" *Chem. Phys. Lett.* **396**, 126-130 (2004).

[25] Dehonor, M., Varlot-Masenelli, K., González-Montiel, A., Gauthier, C., Cavaillé, J.Y., Terrones H., Terrones, M. "Nanotube brushes : polystyrene grafted covalently on CNx nanotubes by nitroxide-mediated radicalpolymeriazion" *Chem. Comm.* **42**, 5349-5351 (2005).

[26] Jiang, K.Y., Eitan, A., Schadler, L.S., Ajayan, P.M., Siegel, R.W., Grobert, N., Mayne, M., Reyes-Reyes, M., Terrones, H., Terrones, M. "Selective attachment of gold nanoparticies to nitrogen-doped carbon nanotubes" *Nano Lett.* **3**, 275-277 (2003).

[27] Mayne, M. Grobert, N., Terrones, M., Kamalakaran, Rühle, M., Walton, D. R. M., Kroto, H. W., Walton, D. R. M. "Pyrolytic production of aligned carbon nanotubes from homogenously dispersed benzene-based aerosols" *Chem. Phys. Lett.* **338**, 101-107 (2001).

[28] Terrones, M., Kamalakaran, R., Seeger, T., Rühle, M. "Novel nanoscale gas containers: encapsulation of N_2 in CN_x nanotubes" *Chem.Commun.* **23**, 2335-2336 (2000).

[29] Ham, H.T., Choi, Y.S., Chung, I.J. "An explanation of dispersion states of single-walled carbon nanotubes in solvents and aqueous surfactant solutions using solubility parameters" *J. Colloid. & Inter Sci.* **286**, 216-223 (2005).

[30] Cui, D., Ozkan, C.S., Ravindran, S., Kong, Y., Gao, H. "Encapsulation of Pt-labelled DNA Molecules inside Carbon Nanotubes" *MCB* **1**, 113-121 (2004).

[31] Kam, N.W.S., Jessop, T.C., Wender, P.A., Dai, H. "Nanotube Molecular Transporters: Internalization of Carbon Nanotube-Protein Conjugates into Mammalina Cells" *J. Am. Chem. Soc.* **126**, 6850-6851 (2004).

[32] Kam, N.W.S., Dai, H. "Carbon Nanotubes as Intracellular Protein Transporters: Generality and Biological Functionality" *J. Am. Chem. Soc.* **127**, 6021-6026 (2005).

[33] Nimmagadda, A., Thurston, K., Nollert, M.U., McFetridge, P.S. "Chemical modification of SWNT alters *in vitro* cell-SWNT interactions" *J. Biomed. Mater. Res. Part A* **76A**, 614-625 (2006).

[34] Che, R.C., Peng, L.M., Wang, M.S. "Electron side-emission from corrugated CNx nanotubes" *Appl. Phys. Lett.* **85**, 4753-4755 (2004).

[35] X. Fan, B. Zhao, X. Han, L. Yao "Studies on Cytotoxic Effects of Brown Coal Dusts" *J. Occup. Health* **41**, 43-44 (1999).

[36] Barlow, P.G., Donaldsn, K., MacCallum, J., Clouter, A., Stone, V. "Serum exposed to nanoparticle carbon black displays increased potential to induce macrophage migration" *Toxicology Letters* **155**, 397-401 (2005).

[37] Yamawaki, H., Iwai, N. "Mechanisms Underlying Nano-Sized Air-Pollution Mediated Progression of Arterosclerosis" *Cir. J.* **70**, 129-140 (2006).

6. Interaction between amoebas and undoped MWNTs and CN_x MWNTs.

In this chapter, a cell viability study of amoeba cells (*Entamoeba histolytica*) was performed. Pure carbon MWCNTs and CN_x MWNTs were incubated with amoeba cells in different doses (form 0.1 to 100 *m*g/ml). Cell cultures were characterized by SEM and TEM. Nanotube uptake mechanism is discussed. It is demonstrated that CN_x MWNTs are innocuous to amoebas, while MWNTs were lethal. This new result encourages further studies testing CN_x nanotubes as drug deliveries and cell transporters. MWNTs exhibited an amoebicidal condition, which could be exploited and tested further to develop a new drug that could replace Metronidazole, currently used against amoebiasis.

6. 1 Cytotoxicity of carbon nanomaterials

Molecular Biology has been related to nanotechnology after the implementation of polymerase chain reaction (PCR) devices in biology laboratories. This relationship has had an important progress, according to Bogunia-Kubik and Sugisaka [1]. These authors established that different kinds of nanoparticles could be used as carriers of therapeutical molecules or even as drug delivery matrices. Liposomes have been widely used for these proposes but their performance can be substantially improved by nanomaterials [1]. Considering the growing interest towards development of nanotechnology and all the research going on world wide on nanosciences, it is essential to promptly attend a vital issue related to this new science field: Toxicology. One of the first reports pointing out this issue was carried out by Borm [2], in 2001. He basically encouraged researchers to focus on health

risks of nanomaterials and reviewed toxicology research on particulate matter (PM). He mentioned the importance of the epidemiological evidences, which suggest that fine (2.5 μm particles) and ultrafine (0.1 μm particle) particles could contain the most toxic components of PM, due to an effect of their small sizes. He also remarked the phenomenon of translocation of ultrafine particles, from lungs to blood stream, as a cause of serious diseases because of their effects on heart and vessel walls.

Service [3], reported in 2003 various investigations carried out towards the assessment of nanomaterials toxicity. He briefly described the work of Lam [4] and Warheit [5], who inoculated SWNTs intratracheally in mice and rats, respectively; both studies concluded that SWNTs are able to damage the lungs, even more severely than carbon black. Service also commented on Oberdörster's work [6], which consisted in a comparative toxicological study of polytetrafluoroethylene (PTFE) particles of 20 and 130 nm in mice, using intranasal via; in this study, mice treated with 20 nm sized particles died quickly, while the animals treated with 130 nm PTFE nanoparticles survived. In the same year, Colvin [7] reviewed some potential environmental risks of nanosized materials, including nanoparticles, carbon nanotubes and fullerenes. He pointed out that the environmental effects of nanomaterials should become an important research subject.

Toxicology studies in mammals provide very valuable information on the effects of certain nanomaterials, such as nanotubes. Because of the wide potential bio-applications of nanomaterials [8], it is also very important to know their effects in living cells. In this context, Shvedova et al. [9] exposed human epidermal kerationocytes (HaCaT) to pristine SWCNTs. They used different nanotube concentrations ranging from 0.06 to 0.24 mg/ml. The incubation time was varied as well. Cytotoxicity and oxidative stress was detected in treated cells by the

formation of free radicals, loss of cell viability and dramatic reduction in Vitamin E levels, among others.

Lymphocytes (B-cells) were incubated with carbon nanotubes bonded to peptides by Bianco and Prato [10]. Because this nanomaterial did not drive immune response in B-cells, they promoted the organic functionalization of carbon nanotubes to use them as nanotools for biological applications. They also reported an extrordinary solubility of 50 mg/ml of carbon nantubes in chloroform.

Bianco's group reported for the first time that funtionalized carbon nanotubes can cross the cell membrane [11]. They covered SWCNTs with peptides and cultured them with human 3T6 (which grow adherently as monolayer) and murine 3T3 fibroblasts (standard fibroblast cell line). They performed confocal microscopy in the treated cells and found that nanotubes were inside in the cytoplasm or cellular nucleus. Because they could not observe differences in the SWCNTs uptake from 4 to 37ºC, they discarded the endocytosis pathway, which is a temperature affected process.

In 2004, Bianco and coworkers [12], reported the effective usage of carbon nanotubes as plasmid DNA gene deliver. They used ammonium-functionalized single and multi walled carbon nanotubes, and put them in contact with mammalian HeLa cells (that do not age) for a period of 90 minutes. They characterized these cells with transmission electron microscopy and found that the carbon nanotubes had been introduced into the cell, preferentially cell nucleus, by an unknown mechanism. They suggested that nanotubes could spontaneously cross the cell membrane. Subsequently, they attached DNA plasmids on functionalized SWCNTs, at different concentrations an incubated them with HeLa cells. Gene expression increased when using SWCNTs as transporters of DNA

molecules, compared to DNA alone.

The interaction of plasmid DNA with three different types of chemically functionalized carbon nanotubes, was studied by Singh et al [13]. These authors demonstrated that those nanotubes were able to condensate DNA. Therefore, they support the idea of creating a carbon nanotube-based gene transfer vector.

Molecular dynamic simulations performed by Gao and co-workers [14], showed that a single stranded DNA chain can be inserted into the hollow cavity of a SWCNT. The movement is very rapid (around 500 ps) and it is driven by van der Waals and hydrophobic forces. Cui and coworkers [15], reported for the first time the experimental encapsulation of DNA inside MWCNTs. Double stranded DNA was previously attached to Pt nanoparticles and then was spontaneously introduced to MWCNTs. This study denied the statement made by Guo et al. [16], who tried to encapsulate Pt-labelled DNA molecules into carbon nanotubes with no success.

Gao's group have reported more research on nanotoxicology. They studied changes in the efficiency of polymerase chain reaction (PCR) by adding SWCNTs [17]. This effect was previously reported for Mg^{2+} ions. They performed PCR experiments with several different concentrations of SWCNTs, ranging form 0 to 5.28 μg/ml. There is a critical SWCNTs concentration at which the PCR products are more abundant, even in the absence of Mg^{2+}. These authors suggest that SWCNTs could be acting as receptors of electrons, thus increasing the activity of the Taq enzyme. In another publication, these authors tested cytotoxicity of pristine SWCNTs on human embryo kidney cells (HEK293) [18]. Their results showed inhibition in cell viability and cell adhesion, in a time and concentration dependent manner. Interestingly, nanotubes induced the arrest of the first step in the cell cycle (where

cells produce RNA and synthesizes proteins, called G1), and cell apoptosis in the HEK293 cells. These authors also found that cells can mobilize active responses such as the secretion of proteins that isolate cells attached to nanotubes. This finding itself could have important applications in medicine.

Correa Duarte et al [19] proposed a different application for carbon nanotubes in cell culture. Here, aligned MWCNTs grown on silicon substrates were acid treated and annealed to produce three dimensional arrays, previously called nanofoams by Chakrapani et al [20]. The formed micro cavities, which sizes range between 5 and 60 microns, are successfully used as scaffolds for cell seeding and growth.

Fluorescent SWCNTs were introduced into human promyelocytic leukemia (HL60) cells, by Kam and coworkers [21]. They confirmed the presence of SWCNTs inside the membranes and cytoplasms of cells by confocal microscopy. The functionalized nanotubes were treated with biotin-LC-PEO-amine and fuoresceinated streptavidini (SA) and subsecuently incubated with HL60 cells. SA was successfully introduced into the cell by an endocytosis pathway. Viability studies were also performed and both the biotin-SA-SWCNTs conjugate and functionalized SWCNTs appeared to be innocuous.

The same research group used functionalized SWCNTs as intracellular protein transporter [22]. They proposed the endocytosis pathway as the cellular mechanism for nanotubes uptake. Human epidermal keratinocytes (HEK) were incubated with pristine bamboo structured MWCNTs in different concentrations and periods of time [23]. The nanotubes were synthesized in presence of ammonia, therefore they are nitrogen-doped and that explains their morphology. The cells were characterized by TEM to show intracellular localization of MWCNTs. Cell viability decreased as the concentration of nanotubes in the culture media increased, which

ranged from 0.1 to 0.4 mg/ml. The authors measured the release of proinflammatory cytokine interleukin 8 (IL-8), as an early marker of biological response, which also increased with the amount of nanotubes and incubation time. Thus, they reported cellular irritation driven by these MWCNTs.

A recent publication from Nimmagadda et al. [24], shows the effect of pristine and chemically functionalized SWCNTs on fibroblasts (from the standard 3T3 cell line) after 3 days of incubation. Their hypothesis was that the contaminants present in SWCNTs suspensions are the real cause of reduction in cell viability and not the SWCNTs themselves. Reduction on viability cell was present in every test, but the functionalization did reduce the toxic effects of the nanomaterial.

Sayes et al [25], performed a C_{60} cytotoxixity test in human dermal fibroblasts (HDF) and human liver carcinoma cells (HepG2). The study was performed *in vitro* with pristine and functionalized (fullerenes). The concentration of C_{60} molecules tolerated by cells increased up to 7 orders of magnitude when using water soluble fullerenes. They reported oxidative damage to cell membranes as a possible cause of cell death.

A comparative cytotoxicity study was performed by Jia and coworkers [26]. They tested SWCNTs, MWCNTs, C_{60} and quartz particles in alveolar macrophages and observed different toxicity grades for each material. Here, SWCNTs were the most toxic, followed by MWCNTs, quartz and C_{60}. The assessment of cytotoxicity was determined by an assay based on the mitochondrial dehydrogenase activities and is called MTT reduction experiment.

Subsequently, Sato et al. [27], performed a comparative cytotoxicity study of MWCNTs with different lengths (220 and 825 nm). The tests were carried out both

in vivo and *in vitro*, using human acute monolytic leukemia cells (line THP-1). The results showed almost no difference in response of THP-1 cells for the *in vitro* case. They found some qualitative differences when analyzing histological cuts of tissue, from the *in vivo* experiments. In particular, they found that the longer the nanotube, the worse the tissue damage.

Different and new nanomaterials have been recently tested for their cytotoxiciy. Tohji's group [28], reported in 2005 an acid/ultrasonic treatment on hat-stacked carbon nanofibers (H-CNFs), which controls their length and solubility in water. These authors found that the functionalization of the nanostructure surface is very important for its biocompatibility. The same year and for the first time, Yokoyama and coworkers [29], reported an *in vivo* toxicicy study of H-CNFs. The carbonaceous nanomaterial was implanted in subcutaneous tissue of rats. After 1 and 4 weeks they sacrificed some animals and obtained histological cuts of treated tissue for TEM analysis. They found H-CNFs surrounded by macrophages, foreign gigant cells and mesenchymal cells. Some were found inside macrophages and other phagocytes. They did not find a severe inflammatory response in the inoculated tissue, such as necrosis or degeneration.

Metallic nanoparticles have been also tested for cytotoxicity. Cheng et al [30] reported a new method for the production of stable Fe_3O_4 colloidal suspensions, which were structurally and magnetically characterized. These authors pointed out the importance of developing synthesis methods for producing superparamagnetic materials that are biocompatible, which could be used in magnetic resonance imaging (a new contrast agent). They also performed a viability test in whit human blood cells (hemoglobin, Cos-7), and after 4 hours of incubation, it resulted in no significant changes in viability when comparing with the control.

In 2005, Uo and collaborators [31] reported for the first time on the cytotoxicity of metal-encapsulating carbon nanocapsules (MECNCs). These researchers tested the nanomaterial in rat fibroblasts and alveolar macrophages, and determined cell viability, alterations in the proliferation rate within 4 days and studied the release of cytokines such as TNF-α, IL-1β and M-CSF. The results indicated that the presence of MECNCs reduce the cell viability and the proliferation rate in a time and concentration dependant manner.

Lee et al [32] described the formation of nanotubular structures of a very uniform diameter and wall size. These were not carbon nanotubes, but cylindrical structures with diameter in the range nanometers. Their formation resulted from the reaction products from the synthesis of a secondary amine HBr salt. The nanotubes were put in contact with *Escherichia Coli* K12 and from that their bactericidal nature was discovered. At certain concentrations of bacteria and nanotubes, the solution changed its color after the cells death.

Environmental concerns have derived in the toxicity study of several materials that are present in mines. In 1999, Fan et al [33], described toxicity and cytotoxicity studies of brown coal dusts. They performed cell viability tests with alveolar macrophages from rats. The study included a comparison of quartz cytotoxicity, as a negative control. They found that the viability of cells was affected by the presence of brown coal dusts. Carbon black (CB) has been the target of several toxicology studies as well. Researches have now started to worry about smaller sized particles of this material. In 2004, Barlow et al [34], performed a comparative chemotaxis study with carbon black nanopartices of 260 and 14 nm. Fetal bovine serum (FBS) or an antioxidant were exposed to the particles, and the treated serum induced macrophage migration, at the highest doses when using the 14 nm particles. When FBS and antioxidant were exposed together to FBS, this did not

induced significant macrophage migration, suggesting that the chemotactic factor generation was driven by oxidation due to the nanoparticles.

More recently, Yamawaki and Iwai [35], reported a cytotoxicity study of carbon black (CB) in human vascular endothelial cells (ECs). The motivation of this researach was the linkage between particulate matter (PM) and cardiovascular diseases, such as atherosclerosis. ECs were incubated with CB particles (250 μm) in different concentrations. TEM provides a possible way to describe ultrastructural changes in the cell and the presence of CB particles inside vacuoles. These researches also reported an increase in lactate dehydrogenase (LDH) delivery, which is a marker of cell death and injury of the plasma membrane. CB had an antiploriferative effect on ECS as well.

In 2004, Oberdörster and coworkers [36] reported the translocation of inhaled ultrafine ^{13}C particles to brain after inhalation. The ^{13}C nanoparticles were exposed to rats for 6 hours. Animal were sacrificed at different times, ranging form 1 to 7 days, and isotope ratio mass spectroscopy determined the presence of ^{13}C in lungs, cerebrum, cerebellum and olfactory bulbs.

Recently, Singh et al. [37] have administrated chemically functionalized SWCNTs and MWCNTs into the blood stream of mice. Carbon nanotubes were provided with a radioactive isotope for imagine proposes and this allowed to detect the excretion of all the nanomaterial in TEM characterized urine.

6. 2 Amoeba structure

Entamoeba histolytica is a protozoan parasite with a simple life cycle, which oscillates between the infective phase or cyst and the invasive phase or trophozoite. The

latter is the mobile and invasive form of the parasite and its diameter ranges between 10 and 50 μm. The trophozoite is mononuclear, pleomorphic and reproduces through binary fission [38]. The cytoplasm is conformed by ectoplasm (clear and refractile) and endoplasm (contains abundant vacuoles). *E. histolytica* cytoskeleton is conformed by microfilaments joined to the plasmatic membrane. Their movement originates form an anaerobic conversion of glucose and pyruvate in ethanol and CO_2. This movement is mediated for pseudopodia emissions, which are cytoplasmatic protrusions that can be formed in any point on the organism surface; the ectoplasm flows to form pseudopodia, followed by the endoplasm (see figure 6.1).

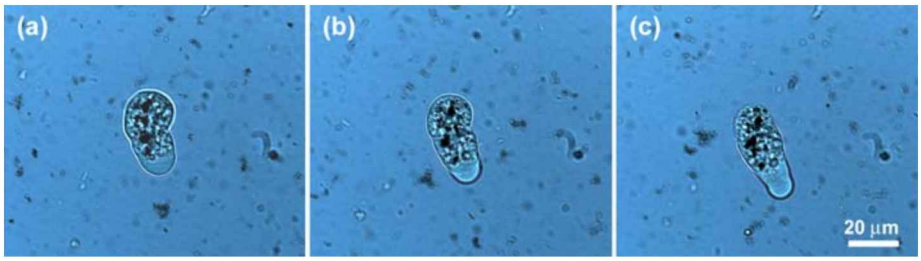

Fig. 6.1. E. histolytica *movement is mediated for pseudopodia emissions, which are cytoplasmatic protrusions that can be formed in any point on the organism surface. (a) Pseodopodia starts forming. (b) Ectoplasm flows to form pseudopodia. (c) Endoplasm starts moving towards pseudopodia.*

Trophozoites are able to condense and form round or oval masses, with a very thin wall (a few μm), known as immature cysts or pre-cysts. Pre-cysts suffer two nuclear divisions, so they produced four nuclei constituting a mature cyst, with morphology similar to that of the immature cysts and 10-20 μm in diameter [38]. They possess a refractile wall 0.5 μm thick. The most important feature that mature cysts exhibit is the presence of a ketine covering which fortifies the parasite against the environment. It is important to mention that human beings are the only natural hosts of *E. histolytica*.

We should stress that infections caused by *E. histolytica* start when ingesting mature cysts in food or water contaminated with human feces. Cysts survive the strong acids form the stomach due to their ketine covering and travel until they reach the low part of thin intestine, where they lost their covering and liberate a thetranuclear amoeba. At this point, the amoeba duplicates their nuclei and fragments forming eight small amoebas, called metacystic amoebulas that migrate to the thick intestine, where they turn into mature trophozoites and multiplicate by binary fission. When trophozites invade the colon adhere to mucosa and epithelial layers, where they feed themselves with bacteria and cellular rests. This is the case for the non pathogen species, known as *Entamoeba dispar*. In the majority of the cases *E. histolytica*, know as the pathogen species, damage the intestinal epithelial surface and penetrate to mucosa, causing intestinal amoebiasis or dysentery. In rare cases, *E. histolytica* is capable to migrate invade any other human organ, such as liver, lung, skin and even brain. For both the non-pathogen and pathogen cases, trophozites become cysts and are eliminated in feces. These cysts could be available in the environment for weeks or months, depending on the environmental conditions.

Amoebiasis is one of the most frecuent infections in humans and it is cataloged as the third cause of death for parasite related illnesses, following malaria and esquistosomiasis [39]. Even when *E. histolytica* is distributed world wide, amoebiasis represents an important health risk in particular regions, where food and water hygienic conditions are unattended. It is estimated that about 10% of total population suffers symptoms of this illness. There are some features related to the transmission of *E. histolytica*, such as:

- Low social-economical conditions
- Overcrowding/stacking

- Contaminated food, due to inadequate techniques of irrigation and fertilization
- Lack of hygiene in food processing and cleaning
- Inadequate deposition and elimination of feces
- Lack of sewers and drains
- Inadequate treatment and insufficient administration of water

Invasive amoebiasis is one of the most important problems for the public health, reaching an incidence of 50% in certain areas of developing countries; the most affected are Asia, Africa and Central America. In Mexico, serological studies indicate that more than 8% of the population has suffered for amoebiasis and there are about 10000 to 30000 deaths every year for this cause. This data put amoebiasis as the first cause of death for parasite infections in Mexico [40,41].

Efforts toward the development of a vaccine against *E. histolytica*, have not succeeded so far. The treatment of amoebiasis is pharmacological [40], administrating medication of different groups: a) those that act in the intestinal lumen, such as quinolines, diloxanide, puromycin sulfate and quinfamide; b) tissular amoebicidals, such as emetine, dehydroemetine and chloroquine; c) those that act in both levels, such as metronidazole and its derivatives.

Metronidazole (MTZ) in its native form is practically inactive. When it is metabolized inside susceptible organisms becomes active, enters the cells for passive diffusion and, for the reductive action of ferredoxine or flavodoxine enzymes, transforms its nitro group and activates to a nitro-radical, which is cytotoxic. MTZ results in the formation of N-hydroxyethyl of oxalic acid and acetamide; therefore, it has been postulated that the action mechanism of the pharmaco is through the elimination of the reductive potential of microorganisms.

Even thus MTZ is very effective, the interest in new alternatives in treatment of this illnesses has been recently increased, specially due to the *in vitro* generation of mutant trophozites that resist high concentrations of MTZ (40 μM) for continuos exposition to the pharmaco. Simultaneously, and due to the indiscriminated usage of MTZ for automedication [41], metronidazole resistant parasites have been found *in vivo*. This resistant phenomenon has been observed in parasitosis such as giardiasis, trichomoniasis and amoebiasis [42]. Therefore, the development of new antiparasites drugs besides MTZ is very important.

In this research, regular undoped (pure carbon) MWCNTs and nitrogen-doped MWCNTs (CN_xMWNTs) were incubated with amoeba cells in different doses (form 0.1 to 100 *m*g/ml). A detailed cell viability study was performed, monitoring the cultures for 45 hours. When the cells were incubated with CN_xMWNTs, they survived and there were no changes in their behavior or morphology. Most of the amebas' population died after 8 hours of incubation with undoped MWCNTs (100 *m*g/ml). Samples were also characterized by Optical Microscopy, Scanning Electron Microscopy (SEM) and Transmission Electron Microscopy (TEM). As a result of these investigations, it was found out that the amoebas were able to uptake CNTs; phagocytosis could be the mechanism. These results imply that CN_xMWNTs could be biocompatibile and that they could be tested for their useage in various applications, such as drug delivery systems.

6. 3 CNx MWNTs and undoped MWNTs incubation with *E. histolytica*

Two different kinds of multi walled carbon nanotubes (MWCNTs) were synthesized using the same method, chemical vapor deposition (CVD), with

organic solvents as the carbon source and ferrocene $FeCp_2$ as the catalyst. With these two components, a solution was made and placed into a reservoir. From here, the solution was atomized by a difference of pressure and the generated aerosol was introduced into a quartz tube, serving as a substrate for the reaction, at 800 or 850 ºC, using a tubular furnace. This method was previously described by Mayne, M. et al [43]. For undoped MWCNTs the used solvent was toluene (C_7H_8) and the reaction temperature was 800 ºC. For nitrogen doped multi walled carbon nanotubes (CNxMWNTs), the solvent employed was benzylamine (C_7H_9N), at a temperature of 850 ºC. The reactions were carried out during 15 minutes, using an argon flow of 3.7 l/min.

It is well known that pristine carbon nanotubes are not soluble. Several methods have been proposed in the past to generate uniform disperssions [44-46]. In this work, we performed a mild oxidation treatment with the carbon nanotubes. This procedure was previously described by Jiang, et al [47]. Here, 200 mg of nanotubes were added into 20 ml of an acid solution made of H_2SO_4:HNO_3, 3:1. After 2 hours of ultrasonic disperssion, the solution was mixed with 250 ml of double deionized water (DDW) and filtered. In order to neutralize the carbon material, a second filtration was carried out, adding 200 ml of NaOH, 0.01 M. Nanotubes were dried in air and, finally, suspended in phosphate buffer solution (PBS). The prepared suspension contained 1 mg of multi walled nanotubes per 1 ml of PBS.

The culture medium used for these studies was TYI-S-33, which contains 600 ml of deionized water, 1 g of potassium phosphate (dibasic), 0.6 g of potassium phosphate (monobasic), 2 g of sodium chloride, 20 g of casein digest peptone, 10 g of yeast extract, 10 g of glucose, 1 g of L-Cysteine Hydrochloride, 0.2 g of ascorbic acid and 1 ml of ferric ammonium citrate (brown form). This suspension's pH is adjusted to 6.8 using NaOH 1N and autoclaved for 15 min at 121 °C with a 15 lbs

pressure. 1 x 10^5 trophozoites in 0.5 ml of TYI-S-33 culture medium were incubated at 37°C with 0.5 ml of prepared nanotube dissolutions, obtaining final concentrations of 0.1, 1.0, 5.0, 10.0, 20.0, 50.0 and 100.0 μg per 1 ml, which was the total volume of the culture. These cultures were observed at 2, 4, 6, 8, 24 and 45 hours post-treatment.

Trypan blue dye exclusion method was used to determine cell viability. At each point of time, the trophozoites were resuspended and 100 μl of the cultures were removed. The samples were centrifuged for 3 min at 3000 rpm and the supernatant was removed. Subsequently, the amoebas were resuspended in trypan blue (0.4% is saline solution), and samples were ready for being observed with an optical microscope. One drop of the dyed solution was placed on the surface of precleaned glass slides and these were taken to the optical microscope (Nikon TMS-F). The percentage of died trophozoites was determined by counting the number of stained cells in 100 trophozoites.

Transmission Electron Microscopy (TEM) characterization was carried out on some of the samples as well. Amoebas were incubated with the CNxMWNTs and CVD produced MWCNTs in the way described above, for 90 minutes and 16 hours. Cell cultures of amoebas and carbon nanotubes were fixed in a Karnovsky solution (Karnovsky, 1965) with no Ca, at pH 7.4. Subsequentlly, they were post fixed with 1% of osmium tetroxide (OsO4) in a Zatterqvist (Zetterqvist, 1956) buffer, and were included in Epon 812. 60-90 nm sections were dyed with Uranyl acetate and lead citrate and placed in Au TEM grids. TEM characterization was carried out in a Jeol JEM 1010, operated at 80 kV and a Jeol JEM-100CX, operated at 80 and 100 kV.

Scanning Electron Microscopy (SEM) was performed with a field emission Philips FEG-XL30, operated at 2 keV. The fixed nanotube-cell solution was pipetted onto a

holy carbon grid and dried in air.

6. 4 Characterization of amoeba samples

Figure 6.2 depicts a bar graphic of the cell viability study performed with CN_x MWNTs in amoebas. Using different concentrations, up to 100 μg/ml, nanotubes were tested for 45 hours. There were not significant changes in viability, compared with control experiments. Amoebas appeared to tolerate the presence of CN_x MWNTs in their culture medium, even after 24 and 45 hours, some CN_x MWTNs-amoeba samples exhibited higher cell viability percentages when compared to the control experiment. The mobility and shape of amoebas was not altered by the presence of CN_x MWNTs, as far as it could be appreciated in the optical microscope.

A completely different reaction is shown in Figure 6.3. Here, the bar graphic of viability, for the case when undoped MWCNTs were incubated with amoebas. After 2 and 4 hours of incubation, the cell viability slightly decreases in a dose-manner, compared to the control. After 6 hours of incubation, there is significant decrease in cell viability for the higher concentrations (50 and 100 μg/ml) of MWCNTs. At 24 and 45 hours, there were a high number of dead cells, much more than 50% for the concentrations of 10, 20 and 50 μg/ml; the highest concentration practically eliminated all the cells.

By optical microscopy, we were able to observe amoebas interacting with agregates of CNTs. At that resolution (40x, 100x), it is not possible to observe isolated nanotubes, but one could obtain valuable information form these observations.

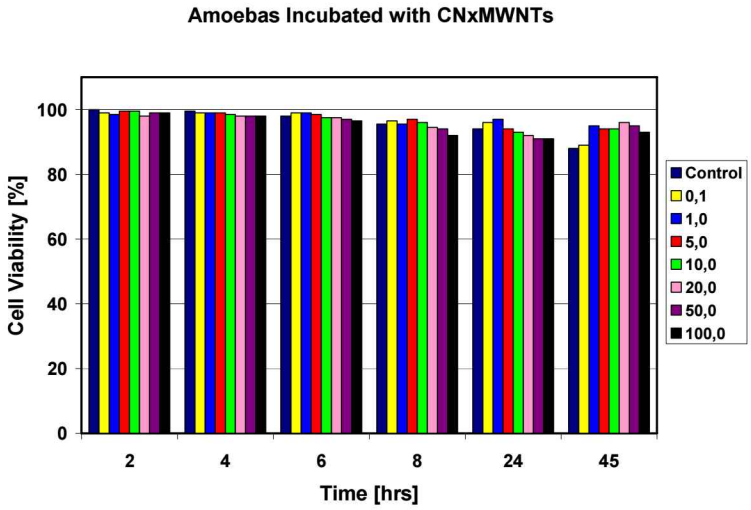

Fig. 6.2. *Cell viability of* E. histolytica *cells incubated with CNx MWNTs. Dark blue color is associated with the control experiment, where pure PBS was added to the cell medium. Yellow color is associated with the lowest concentration used (0.1 μg) while black is linked to the highest concentration (100 μg). Cell viability decreases with time naturally, as can be observed in the column corresponding to 24 hours.*

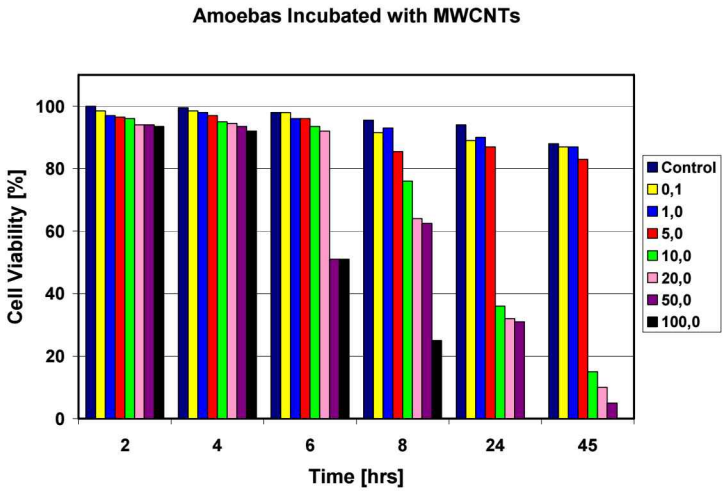

Fig. 6.3. *Cell viability of* E. histolytica *cells incubated with undoped MWNTs. A dose of 100 mg drastically reduces cell viability after 6 hours of incubation and results absolutely lethal after 24 hours. Low concentrations, such as 0.1, 1.0 and 5.0 μg, did not exhibit important effects.*

Figure 6.4 shows images of living amoebas, as they look under the optical microscope. They were incubated with CNxMWNTs for 45 minutes (figure 6.4(a)) and 22 hours (figure 6.4(b)). There were no significant differences in cell viability between these two samples, and we did not observe structural changes in cell morphology either. In both images, it is possible to notice black agglomerates inside the cells (see arrows). It is not possible to determine weather these are carbon nanotubes or not, but it is a fact that those spots are not present in the control sample (not shown here). Therefore, it is highly likely that these agglomerates consist of nanotubes.

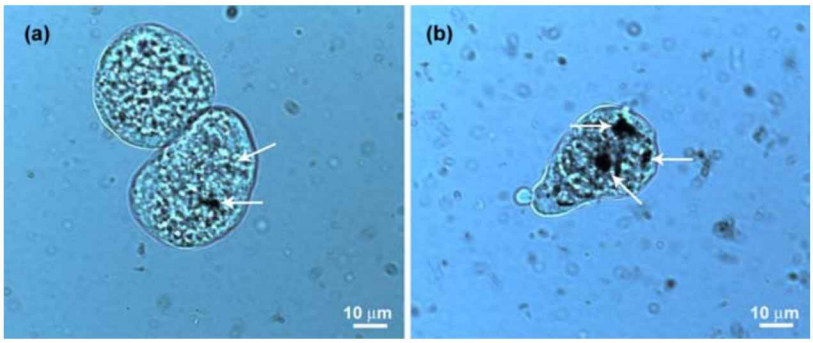

Fig. 6.4. *Living amoebas incubated with CNxMWNTs for (a) 45 minutes and (b) 22 hours. In both images it is possible to see black agglomerates inside cells (see arrows). It is not possible to determine weather these are carbon nanotubes or not, but it is a fact that those spots are not present in the control sample.*

In figure 6.1, a sequence of three images of the same amoeba is shown. The sample was incubated with CNxMWNTs for a period of 22 hours. This amoeba also reveals black spots in the cytoplasm, which could be associated to carbon nanotubes. This figure also illustrates very clearly a "pseudopodia". In figure 6.1(a), at the bottom of the cell, there is a region that looks clearer than the rest of the cell and it grows, as can be seen in the following figures. This is the cell mechanism that helps the cell's motion and can also help during to uptake nutrients. The pseudopod grows for a brief period of time; subsequently the cell membrane contracts in that region and

the pseodopod disappears.

During the characterization with optical microscopy, one of the objectives was to capture an amoeba during phagocytosis. We observed several cells when they were close to bundles of carbon nanotubes, waiting for the cell to incorporate that bundle into the cytoplasm. Unfortunately, this phenomenon never happened during our observations, on the contrary, the amoeba seemed to be moving away from carbon nanotube bundles. Movie 1 shows a clear example of this phenomenon that was observed several times. In this case, a bundle of CN_x MWNTs is attached to the cell membrane at its lowest part. The cell then develops several pseudopods and moves to the top of the visual field. The bundle of nanotubes remains close to the cell, so it continues its movement in the opposite direction of the bundle. Once the cell arrived to the limits of the frame, the glass slide was moved to continue the observation of this cell. Subsequently, the cell advanced, but it never gets rid of the nanotube bundle. The cell of reference corresponds to the sample of amoebas incubated with CN_x MWNTs during 22 hours.

Amoebas are capable of forming what is recalled as "phagocytical mouth", which is another feature that characterizes these cells. These are tubular cavities that amoebas develop in order to feed themselves. Movie 2 shows some amoeba cells that have been incubated with MWCNTs during two hours. The amoeba at the center of the frame exhibits two phagocytical mouths, and after a short period of time, it is possible to observe four of them. As pseudopodia, a phagocytical mouth develops and disappears after. At this magnification, it is not possible to observe the phagocytocis, but this nutrient mechanism is presented as a possible mechanism of nanotubes uptake. In addition, in movie 2 we also observed two amoebas whose membranes are attached to bundles of MWCNTs, and they repeat the behavior observed in movie 1; they move away form nanotube bundles. This is

a clear example of the phagocytosis mechanism, which only occurs in certain specialized cells, such as amoebas.

Movie 3 displays two very interesting phenomena. At the beginning, it seems there are two cells in that movie, but there is actually only one that is divided in two very well defined poles, which are joined together by a thread-like cell membrane. That thread grows in length, resembling a mitosis mechanism (cell division). This does not ocurr; on the contrary, the two sections of the amoeba get close together until they integrate a unified cell again. The right side of Movie 3 shows another situation. Here, the cell membrane appears to involve an object which cannot be seen at this magnification, and incorporates it into the cytoplasm, forming a new vacuole. This happened twice when observing this particular amoeba. Thus demonstrating that the endocytosis mechanism ocurrs in our observations.

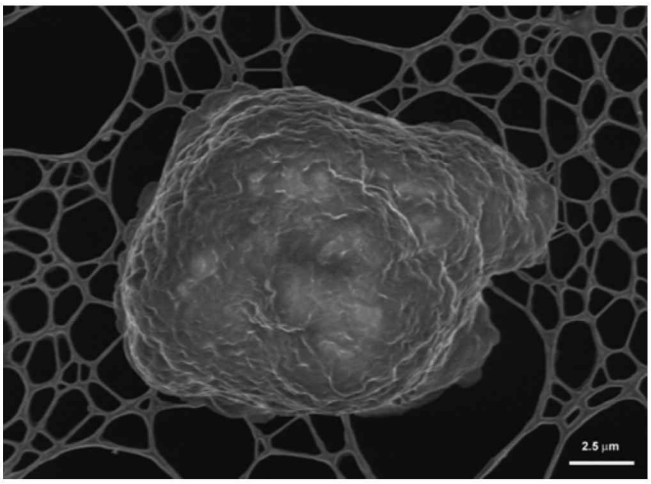

Fig. 6.5. *SEM image of a fixed amoeba cell.*

The results presented so far indicate that carbon nanotubes interact with amoeba cells directly or indirectly, and that can have a negligible effect, depending on the kind of carbon nanotube. If the amoeba cell is capable of intake carbon nanotubes is an important issue. For that reason, we carried out transmission electron

microscopy to characterize the interior of the treated cells.

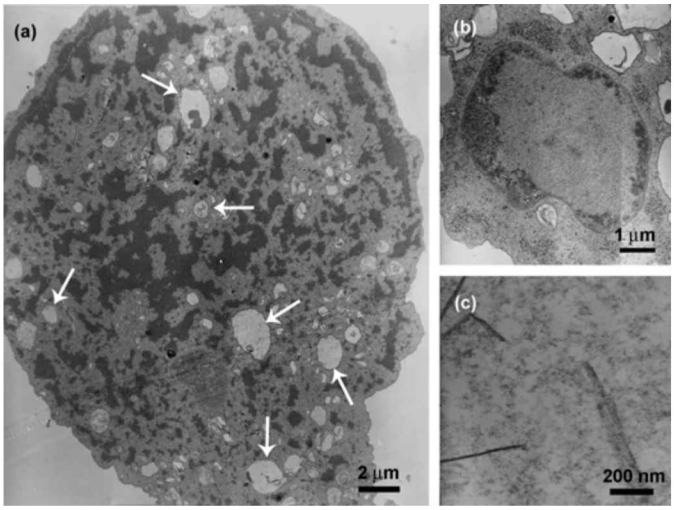

Fig. 6.6. *TEM images of amebas from a control experiment. (a) Typical TEM image of an amoeba that exhibits different sized vacuoles inside its cytoplasm (see arrows) (b) Nucleus of an amoeba. (c) Cylinder-like structures in cell cytoplasm that could resemble carbon nanotubes.*

Figure 6.5 shows an SEM image of an amoeba treated with CN_x MWNTs. Unforutunately, this technique did not revealed the carbon nanotubes. In figure 6.6, three different TEM images of amebas are shown. They represent the control experiment, in which the amoeba was kept away from carbon nanostructures. Figure 6.6(a) depicts a typical TEM image of an amoeba. Their size ranges from a few microns up to 50 µm, but the most common value is around 20 µm. One can observe a well defined cell membrane in most cases, and different sized vacuoles inside the cytoplasm (Figure 6.6(a), arrows). The TEM grids are prepared from microtome slices in a random way. Sometimes it was possible to observe a very well defined nucleus of the amoeba, as shown in figure 6.6(b). There are some cylinder-like structures present in cells free of nanotubes (Figure 6.6(c)). It was necessary a very detailed study of TEM images because the cylinder-like structures

inherent to cells could resemble carbon nanotubes.

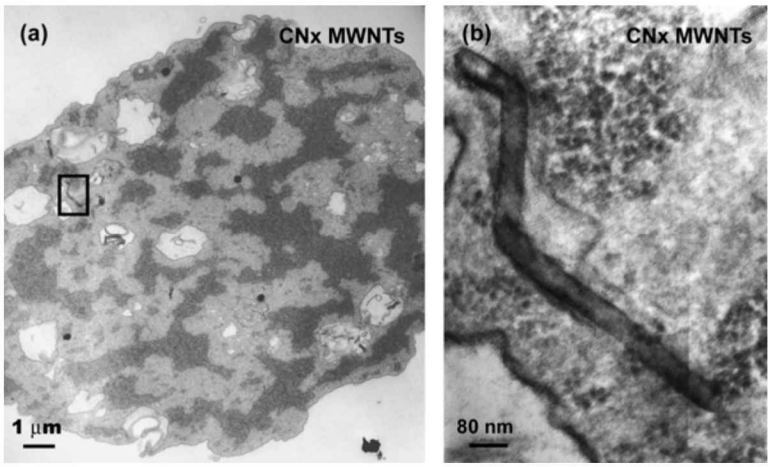

Fig. 6.7. *TEM images of an ameba that was previously incubated with CNxMWNTs, during 16 hours. (a) A small amoeba containing carbon nanotubes in its cytoplasm. (b) Inset form (a), showing a very small length CNxMNT.*

Figure 6.7(a) depicts a small amoeba that was previously incubated with CNxMWNTs during 16 hours. Closer inspection of the cytoplasm reveals the presence of carbon nanotubes, as it can be observed in the inset (figure 6.6(b)). It is important to notice the very small length of the CNxMNT in this figure (*c.a.* 1 µm); a feature which appears in several nanotubes observed inside cells.

Figures 6.8 and 6.9 were taken form cells incubated with CNxMWNTs for 16 hours. In figure 6.8 we can observe a cell section with a large density of CNxMWNTs. The inset (figure 6.8(b)) shows us a CNxMWNT that appears to be partially in the cytoplasm of the cell and partially inside a vacuole. This could be a transitory state going in or out the vacuole. In figure 6.9 one can observe several CNxMWNTs inside a vacuole. Again, it is notorious the reduced length of the nanotubes, some of them a few hundred nanometers only (*e.g.* 500 nm). In this micrograph the bamboo structure of the CNxMWNTs is clearly observed (arrows).

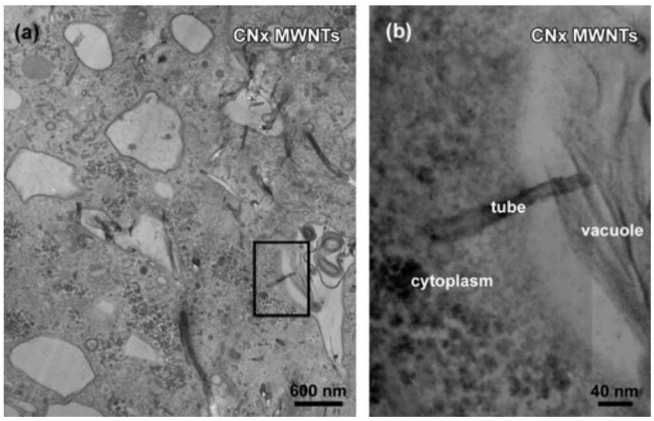

Fig. 6.8. *TEM images of cells incubated with N doped MWNTs for 15 hours. (a) low magnification image of the cellular cytoplasm, exhibiting several carbon nanotubes. (b) Inset from (a), which shows a CNx MWNT placed partially in the cytoplasm of the cell and partially inside a vacuole. This could be a transitory state going in or out the vacuole.*

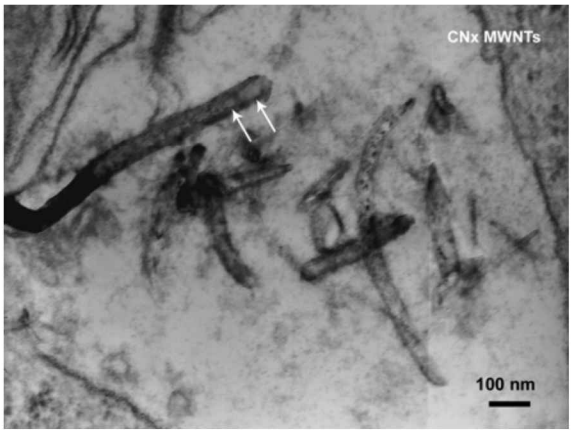

Fig. 6.9. *TEM image form a sample of cells incubated with N doped MWNTs for 15 hours. Several CNx MWNTs can be seen inside a vacuole. The reduced length of the nanotubes is notorious. In this micrograph, the bamboo structure of CNxMWNTs is clearly seen (some bamboo-like compartments are pointed with arrows).*

The observations made in amoebas incubated with undoped MWCNTs are presented in the next images. Figure 6.10 depicts an isolated short MWCNT inside the vacuole of a cell previously incubated with the nanomaterial for 90 minutes. The inset shown in figure 6.10(b) allows to observe that carbon nanotube more clearly and it is even possible to appreciate two iron nanowires inside the hollow

cavity of this MWCNT (see arrows in figure 6.10), which is a common feature in these nanotubes.

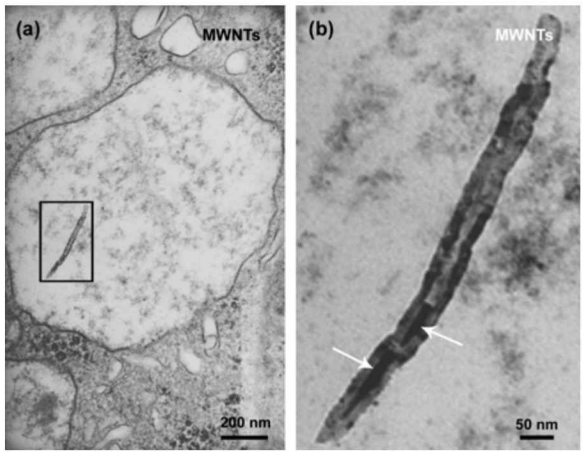

Fig. 6.10. *TEM images from amoebas incubated with undoped MWCNTs for 90 min. (a) Low magnification image of an isolated short MWCNT inside a vacuole. (b) Inset from (a) that shows more clearly the carbon nanotube; it is possible to appreciate two tiny iron nanowires inside the hollow cavity of this MWCNT (see arrows), which is a common feature in these nanotubes.*

In figure 6.11,TEM images of an ameba incubated with MWNTs for 90 minutes are shown. The low magnification image depicts a large region of the cell that contains various MWCNTs, either inside or outside vacuoles. The presence of MWCNTs within the cell at this early stage of incubation shows that amoebas do not need many hours to phagocyte carbon nanotubes; we cannot see important changes in viability at these early stages (see figure 6.3). In a particular, section of the cell membrane (figure 6.11(a)) indicated by an arrow, it is possible to observe a few carbon nanotubes that apparently are being introduced into the cell. It seems that the membrane is forming a vacuole and introducing the nanotubes at the same time. This could be a mechanism for the carbon nanotube uptake. Because the cell contains varipus tubular features, it is difficult to clearly identify carbon nanotubes. Therefore, dark field imaging was used to identify the graphitic networks of

nanotubes. For example, figures 6.11(b) and 6.11(c) revealed the high contrast dark field images showing the (002) graphite planes of nanotubes.

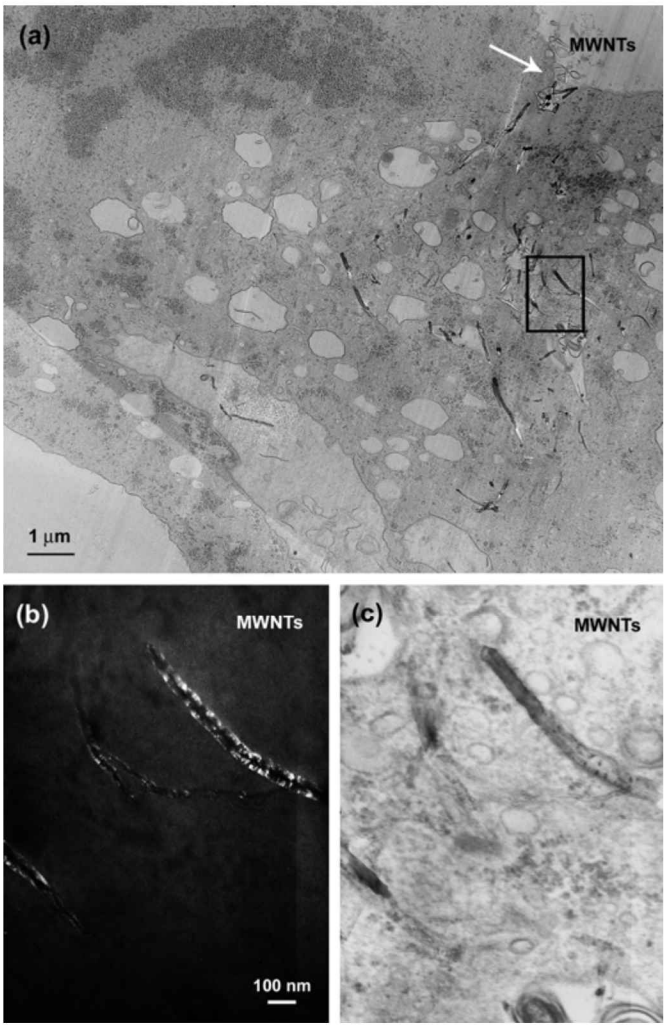

Fig. 6.11. *TEM images of an ameba incubated with MWNTs for 90 minutes. (a) Low magnification image that depicts a large region of the cell that contains many MWCNTs, either inside or outside vacuoles. The presence of MWCNTs within the cell at this early stage of incubation proves that cell can phagocyte carbon nanotubes in a few hours. In the section of the cell membrane indicated by an arrow, it is possible to observe a few carbon nanotubes that apparently are being introduced into the cell. It seems that the membrane is forming a vacuole and introducing the nanotubes at the same time. (b) Dark field image of a particular region form (a) showing the presence of a carbon nanotube. (c) Bright field image of (b). Scale bar is the same as in (b).*

Figure 6.12 shows TEM images of amebas incubated with MWNTs for 16 hrs. The presence of carbon nanotubes within the cytoplasm of the cell is noted, but is more clearly seen in the inset (figure 6.12(b)). It is noteworthy the very small length of that particular nanotube (*e.g.* 200 nm). Figure 6.13(a) shows the dark field image of two MWNTs (undoped) embedded in the cytoplasm of an amoeba cell. In comparison with the bright field image (figure 6.13(b)), the nanotubes are more defined. It is important to notice again the length of the nanotubes. In this case we can see a very small nanotube (not more than 200 nm in length).

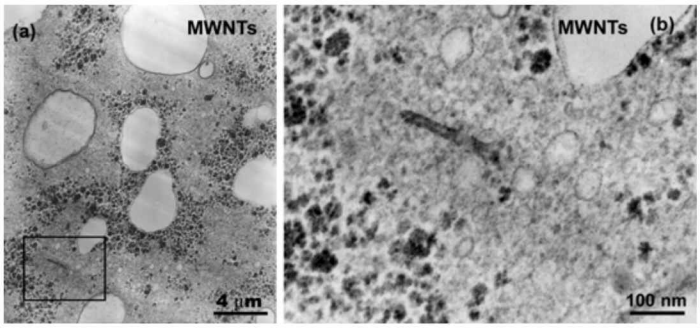

Fig. 6.12. *TEM images of amebas incubated with MWNTs for 16 hrs. (a) Low magnification image of vacuoles. (b) Inset shows a short MWNT in within the cytoplasm. section.*

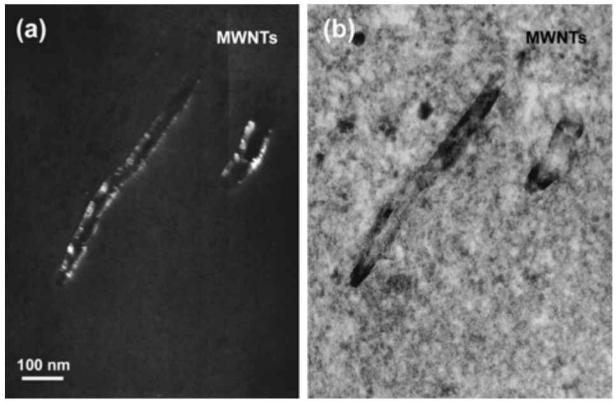

Fig. 6.13. *High magnification TEM images of amebas incubated with MWNTs for 16 hrs. (a) Dark field image of two carbon nanotubes embedded in the cytoplasm of an amoeba cell. (b) Bright field image of (b). A very small aspect ratio nanotube (not more than 200 nm in length) can be seen.*

6. 5 Discussion and Conclusions

Undoped MWNTs (pure carbon) used in this study resulted lethal for the amoebas at concentrations of 100 μg/ml. Incubation of amoebas with CN_x MWCNTs did not resulted in a reduction of cell viability; however, the cell viability slightly increased for all used concentrations after 45 hours of treatment. Therefore, CNxMWNTs are biocompatible with amoebas, whereas MWCNTs are not.

Cells incubated with MWCNTs and CNxMWNTs characterized by TEM or optical microscope did not exhibit morphological deformation or structural changes when compared to the control experiment. Both types of carbon nanotubes are capable of entering into the cytoplasm and vacuoles of amoebas. We observed phagocytical mouths, pseudopodia, and even the clear formation of intracellular vesicles or vacuoles when an amoeba was ingesting. All these are signs of phagocytosis (nanotube uptake).

Nanomaterials suspensions in PBS are not the same in the studied cases. The two different kinds of carbon nanotubes were treated with the exact same protocol, but they are chemically different and it was clear that CN_x MWNTs were more soluble than MWNTs. The chemical reactivity of CNxMWNTs, provided by the presence of substitutional and pyridinic nitrogen atoms in the graphitic layers contributes to the solubility of these nanostructures [47]. On the other hand, MWNTs are more crystalline and that results in stronger van der Waals interactions, that promote the agglomeration of the tubes. This surface condition could also be related to the results of this study, being better solubility part of the biocompatible features associated with CN_x MWNTs.

In this chapter we have demonstrated that CN_x MWNTs appeared to be innocuous

to amoebas, while MWNTs were lethal. These discovered features of nanotubes have important implications. In the first place, CN_x MWNTs are more biocompatible than undoped MWNTs, like it was described in chapter 5. This new result encourages further studies testing CNx nanotubes as drug deliveries and cell transporters. On the other hand, MWNTs exhibited their amoebicidal condition, which could be exploited and tested further to develop a new drug that could replace Metronidazole.

6. 6 Future Work

Besides MWCNTs and CNxMWNTs gown at IPICyT Nanostructures Laboratory, we tried arc discharge grown MWCNTs, boron doped MWCNTs (BCx MWNTs) and hat stacked carbon nanofibers (H-CNFs).

Table 1 refers to the interaction of arc discharge grown MWCNTs with amoeba cells.

TABLE 1	2 hours	4.5 hours	6.5 hours	8 hours	24 hours
Mass [μg]	Viability %	Viability %	Viability %	Viability %	Viability %
0.1	100	100	100	92	90
1.0	100	97	99	85	64
10.0	100	88	92	80	20
100.0	99	24	0	40	0
Control	100	96	98	99	95
Control PBS	100	99	97	98	96

Table 2 refers to the interaction of BCx MWNTs with amoeba cells.

TABLE 2	2 hours	4.5 hours	6.5 hours	8 hours	24 hours
Masa [μg]	Viability %	Viability %	Viability %	Viability %	Viability %
0.1	100	99	93	98	70
1.0	98	97	93	95	60
10.0	96	96	82	88	20
100.0	95	94	80	16	0
Control	100	96	98	99	95
Control PBS	100	99	97	98	96

Table 3 shows the cell viability when they interacted with hat stacked carbon nanofibers.

TABLE 3	2 hours	4.5 hours	6.5 hours	8 hours	24 hours
Masa [μg]	Viability %	Viability %	Viability %	Viability %	Viability %
0.1	100	98	95	97	80
1.0	100	97	92	92	65
10.0	99	99	94	80	30
100.0	96	94	24	15	0
Control	100	96	98	99	95
Control PBS	100	99	97	98	96

The result obtained from these experiments is very clear: none of these structures resulted biocompatible with amoeba cells.

These experiments were carried out in the exact same conditions described previously, but they were only performed once. It remains as future work to verify

if they are reproducible and to perform the complete optical and electron microscopy characterization of these samples.

References

[1] Bogunia-Kubik, K., Sugisaka, M. "From molecular biology to nanotechnology and nanomedicine" *BioSystems* **65**, 123-138 (2002).

[2] Borm, P.J.A. "Particle Toxicology: from coal mining to Nanotechnology" *Inhalation Toxicology* **14,** 311-324 (2002).

[3] Service, R. "Nanomaterials Show Signs of Toxicity" *Science* **300,** 243 (2003).

[4] Lam, C.-W., James, J.T., McCluskey, R., Hunter, R.L. "Pulmonary Toxicity of Single-Wall Carbon Nanotubes in Mice 7 and 90 Days After Intratracheal Instillation" *Toxicol. Sci.* **77**, 126-134 (2004).

[5] Warheit, D.B., Laurence, B.R., Reed, K.L., Roach, D.H., Reynolds, G.A.M., Webb, T.R. "Comparative Pulmonary Toxicity Assessment of Single-wall Carbon Nanotubes in Rats" *Toxicol. Sci.* **77**, 117-125 (2004).

[6] Johnston, C.J., Finkelstein, J.N., Mercer, P., Corson, N., Gelein, R., Oberdorster, G. "Pulmonary effects induced by ultrafine PTFE particles" *Toxicology And Applied Pharmacology* **168**, 3, 208-215 (2000).

[7] Colvin, V.L. "The potential environmental impact of engineered nanomaterials" *Nature Biotechnology* **21**, 1166-1171 (2003).

[8] Martin, C.R., Kohli, P. "The emerging field of nanotube biotechnology" *Nature Reviews Drug Discovery* **2**, 29-37 (2003).

[9] Shvedova, A.A., Castranova, V., Kisin, E.R., Schwegler-Berry, D., Murray, A.R., Gandelsman, V.Z., Maynard, A., Baron, P. "Exposure to Carbon Nanotube Material: Assessment of nantoube Cytotoxicity using human keratinocyte cells" *Journal of Toxicology and Environmental Health, Part A,* **66**, 1909-1926 (2003).

[10] Bianco, A., Prato, M. "Can Carbon Nanotubes Be Considered Useful Tools for Biological Applications?"*Adv. Mater* **15**, 1765-1768 (2003).

[11] Pantarotto, D., Briand, J.P., Prato, M., Bianco, A. "Translocation of bioactive

peptides across cell membranes by carbon nanotubes" *Chem. Commun*. 16-17 (2004).

[12] Pantarroto, D., Singh, R., McCarthy, D., Erhardt, M., Briand, J.P., Prato, M., Kostarelos, K., Bianco, A. "Functionalized Carbon Nanotubes for Plasmid DNA Gene Delivery" *Angew. Chem*. **116**, 5354-5358 (2004).

[13] Singh, R., Pantarotto, D., McCarthy, D., Chaloin, O., Hoebeke, J., Partidos, C.D., Briand, J.P., Prato, M., Bianco, A., Kostarelos, K. "Binding and Condensation of Plasmid DNA onto Functionalized Carbon Nanotubes: Toward the Construction of Nanotube-Based Gene Delivery Vectors" *J. Am. Chem. Soc*. **127**, 4388-4396 (2005).

[14] Gao, H., Kong, Y., Cui, D., Ozkan, C.S. "Spontaneous Insertion of DNA Oligonucleotides into Carbon Nanotubes" *Nano Lett*. **3**, No. 4, 471-473 (2003).

[15] Cui, D., Ozkan, C.S., Ravindran, S., Kong, Y., Gao, H. "Encapsulation of Pt-labelled DNA Molecules inside Carbon Nanotubes" *MCB* **1**, 113-121 (2004).

[16] Guo, Z.J., Sadler, P.J., Tsang, S.C. "Immobilization and visualization of DNA and proteins on carbon nanotubes" *Adv. Mater*. **10**, 702-703 (1998).

[17] Cui, D., Tian, F., Kong, Y., Titushikin, I., Gao H. "Effects of single-walled carbon nanotubes on the polymerase chain reaction" *Nanotechnology* **15**, 154-157 (2004).

[18] Cui, D., Tian, F., Ozkan, C.S., Wang, M., Gao, H. "Effect of single wall carbon nanotubes on human HEK293 cells" *Toxicology Letters* **155**, 73-85 (2005).

[19] Correa-Duarte, M.A., Wagner, N., Rojas-Chapana, J., Morsczeck, C., Thie, M., Giersig, M. "Fabrication and Biocompatibility of Carbon Nabotube-Based 3D Networks as Scaffolds for Cell Seeding and Growth" *Nano Lett*. **4**, 2233-2236 (2004).

[20] Chakrapani, N., Wei, B.Q., Carrillo, A., Ajayan, P.M., Kane, R.S.

"Capillarity-driven assembly of two-dimensional cellular carbon nanotube foams" *PNAS* **101**, 4009-4012 (2004).

[21] Kam, N.W.S., Jessop, T.C., Wender, P.A., Dai, H. "Nanotube Molecular Transporters: Internalization of Carbon Nanotube-Protein Conjugates into Mammalina Cells" *J. Am. Chem. Soc.* **126**, 6850-6851 (2004).

[22] Kam, N.W.S., Dai, H. "Carbon Nanotubes as Intracellular Protein Transporters: Generality and Biological Functionality" *J. Am. Chem. Soc.* **127**, 6021-6026 (2005).

[23] Monetiro-Riviere, N.A., Nemanich, R. J., Inman, A.O., Wang, Y.Y., Riviere, J.E. "Multi-walled carbon nanotube interactions with human epidermal keratinocytes" *Toxicology Lett.* **155**, 377-384 (2005).

[24] Nimmagadda, A., Thurston, K., Nollert, M.U., McFetridge, P.S. "Chemical modification of SWNT alters *in vitro* cell-SWNT interactions" *Journal Of Biomedical Materials Research Part A* **76A**, 614-625 (2006).

[25] Sayes, C.M., Fortner, J.D., Guo, W., Lyon, D., Boyd, A.M., Ausman, K.D., Tao, Y.J., Sitharaman, B., Wilson, L.J., Huges, J.B., West, J.L., Colvin, V.L. "The Differencial Cytotoxicity of Water-Soluble Fullerenes" *Nano Lett.* **4**, 1881-1887 (2004).

[26] Jia, G., Wang, H., Yan, L., Wang, X., Pei, R., Yan, T., Zhao, Y., Guo, X. "Cytotoxicity of Carbon Nanomaterials: Single-Wall Nanotube, Multi-Wall Nanotube, and Fullerene" *Environmental Science & Technology* **39**, 1378-1383 (2005).

[27] Sato, Y., Yokoyama, A., Shibata, K-I, Akimoto, Y., Ogino, S-I , Nodasaka, Y., Kohgo, T., Tamura, K., Akasaka, T., Uo, M., Motomiya, K., Jeyadevan, B., Ishiguro, M., Hatakeyama, R., Watari, F., Tohji, K. "Influence of length on cytotoxixity of multi-walled carbon nanotubes against human acute monocytic leukemia cell line THP-1 *in vitro* and subcutaneous tissue of rats *in vivo*" *Mol. BioSyst.* **1**, 176-182 (2005).

[28] Sato, Y., Shibata, K-I, Kataoka, H., Ogino, S-I, Bunshi, F., Yokoyama, A., Tamura, K., Akasaka, T., Uo, M., Motomiya, K., Jeyadevan, B., Hatakeyama, R., Watari, F., Tohji, K. "Strict separation and evaluation of water-soluble hat-stacked carbon nanofibers for biomedical application and their high biocompatibility: influence of nanofiber-surface functional groups on cytotoxicity" *Mol. BioSyst.* **1**, 142-145 (2005).

[29] Yokoyama, A., Sato, Y., Nodasaka, Y., Yamamoto, S., Kawasaki, T., Shindoh, M., Kohgo, T., Akasaka, T., Uo, M., Watari, F., Tohji, K. "Biological Behavior of Hat-Stacked Carbon Nanofibers in the Subcutaneous Tissue in Rats" *Nano Lett.* **5**, 157-161 (2005).

[30] Cheng, F.Y., Su, C.H., Yang, Y.S., Yeh, C.S., Tsai, C.Y., Wu, C.L., Wu, M.T., Shieh, D.B. "Characterization of aqueous dispersions of Fe_3O_4 nanoparticles and their biomedical applications" *Biomaterials* **26**, 729-738 (2005).

[31] Uo, M., Tamura, K., Sato, Y., Yokoyama, A., Watari, F., Totsuka, Y., Tohji, K. "The Cytotoxicity of Metal-Encapsulating Carbon Nanocapsules" *Small* **1**, 816-819 (2005).

[32] Lee, S.B., Koepsel, R., Stolz, D.B., Warriner, H.E., Russell, A.J. "Self-Assembly of Biocidal Nanotubes from a Single-Chain Diacetylene Amine Salt" *J. Am. Chem. Soc.* **126**, 13400-13404 (2004).

[33] Fan, X., Zhao, B., Han, X., Yao, L. "Studies on Cytotoxic Effects of Brown Coal Dusts" *J. Occup. Health* **41**, 43-44 (1999).

[34] Barlow, P.G., Donaldsn, K., MacCallum, J., Clouter, A., Stone, V. "Serum exposed to nanoparticle carbon black displays increased potential to induce macrophage migration" *Toxicology Lett.***155**, 397-401 (2005).

[35] Yamawaki, H., Iwai, N. "Mechanisms Underlying Nano-Sized Air-Pollution Mediated Progression of Arterosclerosis" *Cir. J.* **70**, 129-140 (2006).

[36] Oberdorster, G., Sharp, Z., Atudorei, V., Elder, A., Gelein, R., Kreyling, W., Cox, C. "Translocation of inhaled ultrafine particles to the brain" *Inhalation*

Toxicology **16**, No. 6-7, 437-445 (2004).

[37] Singh, R., Pantarotto, D., Lacerda, L., Pastorin, G., Klumpp, C., Prato, M., Bianco, A., Kostarelos, K. "Tissue biodistribution and blood clearance rates of intravenously administered carbon nanotube radiotracers" *PNAS* **103**, 3357-3362 (2006).

[38] Martínez-Palomo, A. "Amibiasis. México" Editorial Médica Panamericana, 1989.

[39] Walsh, J.A. "Problems in recognition and diagnosis of amebiasis: estimation of the global magnitud of morbitidity and mortality" *Rev Infect Dis* **8**, 228-237 (1986).

[40] Conde-Bonfil, M.C., De la Mora-Zerpa, C. "Entamoeba histolytica: a standing threat" *Salud Pública Mex* **34**, 335-341 (1992).

[41] Samarawickrema, N.A., Brown, D.M., Upcroft, J.A., Thammapalerd, N., Upcroft, P. "Involvement of superoxide dismutase and piruvate ferredoxin oxidorreductase in mechanisms of metronidazole resistance in *Entamoeba histolytica*" *Antimicrob Agents Chemother* **40**, 833-40 (1997).

[42] Hanna, R.M., Dahniya, M., Badr, S.S., El-Betagy, A. "Percutaneous catheter drainage in drug-resistant amoebic liver abscess" *Trop Med Int Health* **5**, 578-581 (2000).

[43] Mayne, M., Grobert, N., Terrones, M., Kamalakaran, R., Rühle, M., Kroto, H.W., Walton, D.R.M. "Pyrolytic production of aligned carbon nanotubes from homogeneously dispersed benzene-based aerosols" *Chem. Phys. Lett.* **338**, 101-107 (2001).

[44] Ham, H.T., Choi, Y.S., Chung, I.J. "An explanation of dispersion states of single-walled carbon nanotubes in solvents and aqueous surfactant solutions using solubility parameters" *Journal Of Colloid And Interface Science* **286**, 1, 216-223 (2005).

[45] Perepichk, D.F., Wudl, F., Wilson, S.R., Sun, Y., Schuster, D.I. "The

dissolution of carbon nanotubes in aniline, revisited" *Journal Of Materials Chemistry* **14**, 2749-2752 (2004).

[46] Curran, S.A., Ajayan, P.M., Blau, W.J., Carrol, D.L., Coleman, J.N., Dalton, A.B., Davey, A.P., Drury, A., McCarthy, B., Maier, S., Strevens, A. "A Composite form Poly(*m*-phenylenevinylene-*co*-2,5-dioctoxy-*p*-phenyleneviny-lene) and Carbon Nanotubes: A Novel Material for Molecular Optoelectronics" *Adv. Mater.* **10**, 1091-1093 (1998).

[47] Jiang, K.Y., Eitan, A., Schadler, L.S., Ajayan, P.M., Siegel, R.W., Grobert, N., Mayne, M., Reyes-Reyes, M., Terrones, H., Terrones, M. "Selective Attachment of Gold Nanoparticles to Nitrogen-Doped Carbon Nanotubes" *Nano Lett.* **3**, 275-277 (2003).

7. Conclusions and Perspectives

Synthesis, characterization and applications of carbon based nanostructures have been described in detail. The experimental aerosol pyrolysis approach taken to synthesize those nanostructures has been put in perspective, and their advantages (such as versatility and low cost) over different CVD systems used in the past for other research groups have been discussed. Several variations of the experimental parameters have been explored and novel nanotube structures have been synthesized and characterized. FeCo single crystalline nanowires were successfully encapsulated inside MWNTs, with outstanding magnetic properties. Cellular foam-like nanotube arrays were self assembled in a simple and controllable process. SWNTs were synthesized with the same aerosol pyrolysis method, in the absence of sulphur, hydrogen or vacuum.

The synthesis of high aspect ratio ferromagnetic nanostructures is currently one of the approaches to achieve larger density for magnetic storage devices. Although, one of the problems is the immediate oxidation of such structures when get into contact with ambient conditions. Synthesis of carbon nanotubes filled with ferromagnetic elements or alloys overcomes this problem. This material could represent a competitive low cost for producing novel magnetic hard drives. In a common device, each bit of information is stored in several magnetic grains, with different grain sizes and that causes noise during reading. On the contrary, a monocrystalline nanowire possesses only 2 quantized directions, which diminishes the noise during reading. Each nanowire could be use to store one bit of information, therefore, encapsulated nanowires could exhibit high available storage densities at low cost. The results of this research were published in Nano Letters and Solid State Communications journals [1,2].

A wide variety of advantages of the known carbon nanotube synthesis methods develop everyday, towards the optimization of chirality and diameter control, and reducing the costs while keeping quality. The production method for the synthesis of high yields of SWNTs (pyrolyzing ferrocene:ethanol solutions) stated in chapter 3, represents an important advantage over other CVD methods previously described. The synthesis method does not involve the usage of sulphur or hydrogen, and besides that, experiments are carried out at atmospheric pressures. It confirms that these structures can grow at atmospheric pressure, with relatively low temperatures. HRTEM observations exhibited the preferential growth of large diameter nanotubes when temperatures were larger than 850 ^{o}C were used. These results were accepted for publication in Chemical Physics Letter journal [3].

Self assembly methods are very important because represent the natural and easiest way to achieve the synthesis of a given nanomaterial, with desired morphologies and distributions. In this context, the single step production of aligned carbon nanotubes (PCMWNTs and CN_x MWNTs) constituted a huge step forward. Applications of microscopic arrays containing nano-components have been studied in the past. The natural pattern formation of cellular foam-like structures using aligned nanotubes was reported in chapter 4 and the possible applications were discussed.

Although novel nanomaterias such as carbon nanotubes and metallic nanowires have been proposed for developing various applications, so far their toxicity tests have not been conclusive and the lack of proper material safety data sheets (MSDS) of these structures persists. Fortunately, this thesis also studied detailed toxicity assays of MWNTs and CN_x MWNTs in mice and amoeba cells.

Along this line, pure carbon MWNTs and CN_x MWNTs were instilled to mice through 4 different routes: oral, intranasal, intraperitoneal and intratracheal. The highest nanotube concentration used corresponded to 5mg/kg of the body weight and did not induce any irregular behavior in mice or sign of toxicity using the three first routes. Unfortunately, intratracheal instillation of MWNTs caused death of mice by asphyxia at the highest PCMWNT concentration, and severe inflammatory responses and signs of toxicity were triggered. However, CN_x MWNTs did not cause the death of any mouse, but at high concentrations produced granulomas and inflammatory responses, less severe than those induced by PCMWNTs. The less harmful effect of CNx MWNTs is remarkable and suggests that these materials could be tested for bio-applications. This results were published in Nano Letters journal [4].

Entoamoeba Hystolitica, commonly know as amoeba) was incubated with undoped MWNTs and CN_x MWNTs at different concentrations and incubation times. Again, CN_x MWNTs showed signs of better biocompatibility because they did not produce a decrease in cell viability, whereas undoped MWNTs kill the cells after a few hours. It is important to remark that those biocompatibility studies are the first of their kind in Mexico and it is hoped that this work stimulates further medical research related to nanostructures.

7.1 Future Work

7.1.1 Synthesis of high density FeCo nanowires inside MWNTs

In chapter 2, the synthesis and characterization of FeCo nanowires inside MWNTs was described. An exact determination of the amount of nanowires inside nanotubes would be useful for the understanding of the magnetic properties detected. Besides the results presented, Electron Holography studies are currently underway in collaboration with Prof. David Smith's group, at Arizona State University. A complete characterization of the magnetic properties of arrays by SQUID measurements should be also carried out. Theoretical characterization of preferentially oriented FeCo nanowires within different density arrays would be very helpful. Diameter and length of nanowires could be varied and magnetic responses could be predicted. Experimental parameters such as concentration of ferrocene and cobaltocene in the solution, reaction times, testing of different carbon sources (solvents) and Ar flow could be varied and optimized in order to modify the average size of nanowires and spacing.

7.1.2 Synthesis of combined nanotube cellular foams

Both PCMWNT and CN_x MWNT foams, formed with PCMWNT arrays were magnetically characterized, at room temperature. It was expected a variation of the coercive field (Hc) after the foam formation. Figure 7.1 plots the variation of Hc with different samples and also with the change in the orientation of the applied magnetic field. At room temperature, the magnetic signal did not modify. In the future, these arrays of nanotubes could be tested for changes in their magnetic properties at low temperatures.

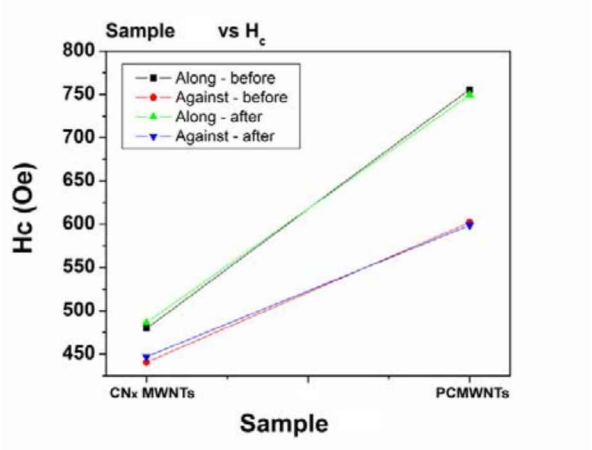

Fig. 7.1. *Variation in the coercive field from CN_x MWNTs and PCMWNT foams. The original length of the arrays was 250 μm for CN_x MWNTs and 450 μm for PCMNTs. Measurements were taken at room temperature.*

Synthesis of multilayer arrays of carbon nanotubes have been described in the literature. One experiment is carried out, and an aligned array of nanotubes is produced; subsequently, another experiment can be performed using the same substrate and one can obtain one array of carbon nanotubes on top of the other. 3 layered PCMWNT arrays have been obtained, as well as PCMWNT-CN_x MWNT arrays, and Figure 7.2 shows representative SEM images of such materials.

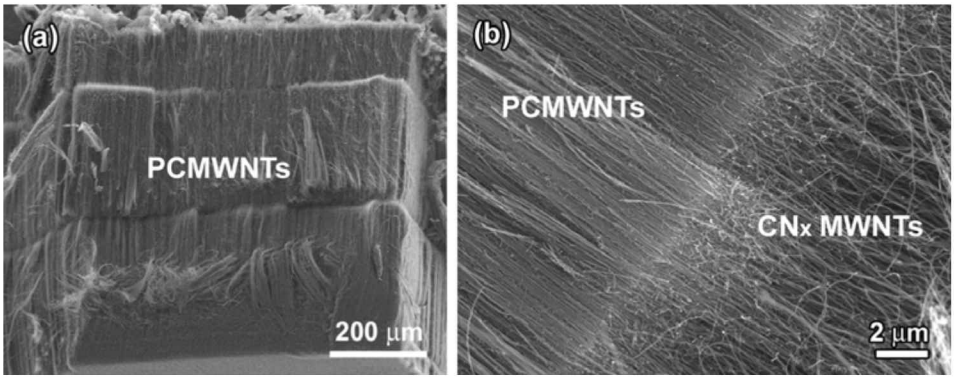

Fig. 7.2. *SEM images of multilayer arrays of MWNTs. (a) A three layer array of PCMWNTs, with different lengths. (b) SEM image of the interface between a PCMWNT-CN_x MWNT array.*

It would be very interesting to study the behavior of such a layered array, in terms of its compaction level and foam morphology.

Growth of CN_x MWNT arrays on pre-patterned Si/SiOx substrates is currently underway. Is now important to compare to compare the nanotube foams formed using CN_x MWNTs with those formed with PCMWNTs. Figure 7.3 shows a SEM image of CN_x MWNT arrays on Si/SiO_x prepatterned substrate, which grew selectively. Multilayer growth of nanotube arrays over pre-patterned substrates and their corresponding foams would be also interesting to characterize.

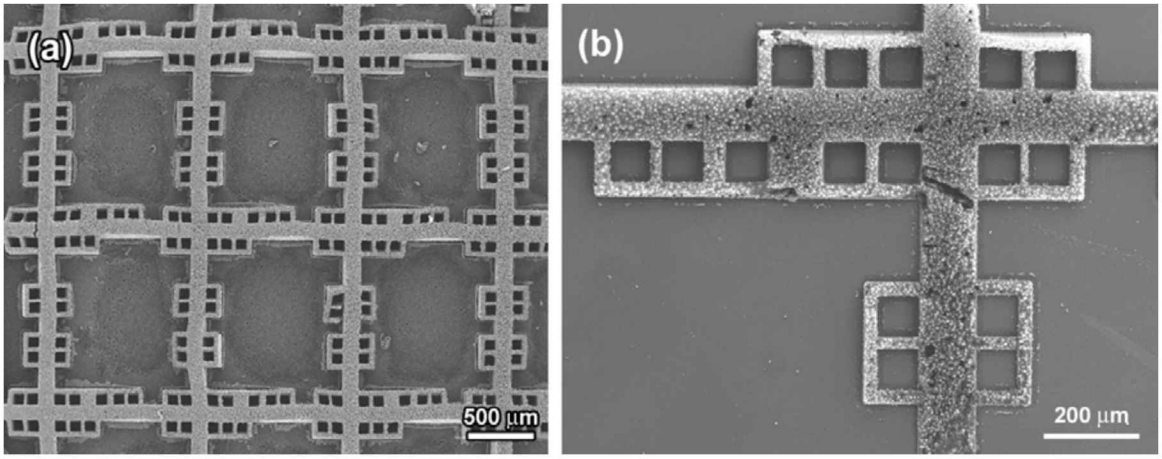

Fig. 7.3. *SEM images of CN_x MWNTs grown on pre-patterned Si/SiO_x substrates. (a) Low magnification image of the patterned CN_x MWNTs array. (b) Higher magnification SEM image.*

7.1.3 Long term toxicity studies of PCMWNTs and CNx MWNTs on mice

Nasal, oral and intraperitoneal instillation of both PCMWNTs and CN_x MWNTs did not affected mice in the concentrations tested. However, it is necessary to

increase these concentrations, even if it is one or more orders of magnitude, until 50% of the tested population dies. These data are required for a complete MSDS of the produced nanotubes.

As described in chapter 5, the intratracheal instillation of PCMWNTs caused the death of 30, 60 and 90% of mice population, for 1, 2.5 and 5 mg/kg concentrations. CNx MWNTs, on the contrary, did not cause the death any mouse at any concentration. The studies were performed with a single administration of nanotubes and different times were tested, up to one month. Longer times should be tested now, because one cannot discard the appearance of other long-term toxic effects. Another very interesting experiment would be the chronic exposure to nanotubes, which could trigger responses different to effects observed in a single administration. Other mammals could be used for these toxicity studies, such as rats or other with longer life times.

7.1.4 Understanding of the N role in biocompatibility of CNx MWNTs with *E. Hystolitica*

When amoebas were incubated with both pure carbon PCMWNTs and CNx MWNTs, the observed responses driven were opposed: CN_x MWNT did not reduced cell viability whereas PCMWNTs killed the cells. Speculations about the causes of this surprising result have been discussed in chapter 6. However, further experiments should be now carried out in order to elucidate clearly the effect of N in cells. Nanomaterials citotoxicity is a growing field and a brief review of its advances to date has been discussed in section 6.1. Molecular biology techniques could be used to test the delivery of toxic-associated substances by the cell and that would provide more information of the toxicity mechanism. Also, CN_x MWNTs

could be tested as virus inhibitors, to assist cancer treatment, or evaluate their usage as gene delivery transporters.

Other nanomaterials such as hat stacked carbon nanofibers and boron doped MWNTs have been tested for viability with *E. hystolitica*. However, experiments should be repeated at least twice. Other nanostructures could be tested for viability, such as SWNTs or nitrogen doped SWNTs, in order to compare their toxicological effects.

7.1.5 Fabrication of composite fibers by Electrospinning technique

Polymer-MWNT solutions were electrospunned in order to produce nanofibers composites. Several polymers were used, such as polypropylene, polystyrene, polyurethane, among others. Both types of nanotubes (PCMWNTs and CNs MWNTs) were suspended in THF. In the other hand, PP, PS or PU were dissolved in THF, in concentrations ranging form 5 to 10 wt%. Polymer solutions and nanotube dispersions were mixed in different ratios, to obtain nanotube concentrations of 1 to 3 wt%. Experimental parameter such as voltage, distance between the needle and rate were varied. Figure 7.4 depicts an example of the obtained fibers. For that case, the polymer used was polypropylene, at 10 wt%, and 1% CNx MWNTs were added.

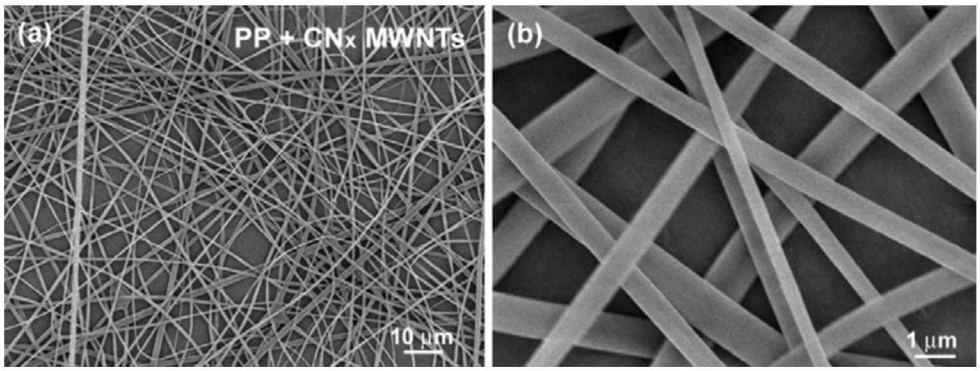

Fig. 7.4. *SEM images of composite fibers, synthesized form initial THf-PP-CN_x MWNTs solutions with the electrospinning technique. (a) Low magnification image shows the uniformity of the produced fibers. (b) Higher magnification image exhibits fibers diameter, ranging from 0.2 to 1 μm.*

Higher concentrations of nanotube in the initial solution should be now tested. Morphological differences between PCMWNTs-polymer and CNx MWNTs-polymer fibers were not noticed at the concentrations testes. Electric characterization of these samples could also be interesting.

References

[1] Elías A.L., Rodríguez-Manzo J.A., McCartney M.R., Golberg D., Zamudio A., Baltazar S.E., Lopez-Urías F., Munoz-Sandoval E., Gu L., Tang C.C., Smith D.J., Bando Y., Terrones H., Terrones M., "Production and characterization of single-crystal FeCo nanowires inside carbon nanotubes" *Nano Lett.* **5(3)**, 467-472 (2005). ***Highlighted by Nano Letters***

[2] H. Terrones, F. López-Urías, E. Muñoz-Sandoval, J. A. Rodríguez-Manzo, A. Zamudio, A. L. Elías, M. Terrones, "Magnetism in Fe-based and Carbon Nanostructures: Theory and Applications" *Solid State Sciences* **8**, 303-320 (2006).

[3] F. Lupo, J. A. Rodríguez-Manzo, A. Zamudio, A.L. Elías, Y. A. Kim, T. Hayashi, M. Muramatsu, R. Kamalakaran, H. Terrones, M. Endo, M. Rühle, M. Terrones, "Pyrolytic synthesis of long strands of large diameter single-walled carbon nanotubes at atmospheric pressure in the absence of sulphur and hydrogen" *Chem. Phys. Lett. 410, 384-390* (2005).

[4] J. C. Carrero-Sánchez, A. L. Elías, R. Mancilla, G. Arrellín, H. Terrones, J. P. Laclette, M. Terrones, "Biocompatibility and Toxicological studies of Carbon Nanotubes Doped with Nitrogen" *Nano Lett.*, web release July 7th, 2006.

NANO LETTERS

2005
Vol. 5, No. 3
467−472

Production and Characterization of Single-Crystal FeCo Nanowires Inside Carbon Nanotubes

A. L. Elías,[†] J. A. Rodríguez-Manzo,[†] M. R. McCartney,[‡] D. Golberg,[§] A. Zamudio,[†] S. E. Baltazar,[†] F. López-Urías,[†] E. Muñoz-Sandoval,[†] L. Gu,[‡] C. C. Tang,[§] D. J. Smith,[‡] Y. Bando,[§,||] H. Terrones,[†] and M. Terrones*[,†,||]

Advanced Materials Department, IPICYT, Camino a la Presa San José 2055, Col. Lomas 4 sección, San Luis Potosí, 78216, México, Department of Physics and Astronomy and Center for Solid State Science, Arizona State University, Tempe, Arizona 85287-1504, Advanced Materials Laboratory, National Institute for Materials Science, Namiki 1-1, Tsukuba, Ibaraki 305-0044, Japan, and International Center for Young Scientists (ICYS), National Institute for Materials Science, Namiki 1−1, Tsukuba, Ibaraki 305-0044, Japan

Received December 9, 2004; Revised Manuscript Received January 13, 2005

ABSTRACT

We describe the synthesis of novel monocrystalline FeCo nanowires encapsulated inside multiwalled carbon nanotubes (MWNTs). These FeCo nanowires exhibit homogeneous Fe and Co concentrations and do not contain an external oxide layer due to the presence of insulating nanotube layers. The method involves the aerosol thermolysis of toluene–ferrocene–cobaltocene solutions in inert atmospheres. The materials have been carefully characterized using state-of-the-art high-resolution transmission electron microscopy (HRTEM), electron-energy-loss spectroscopy (EELS), scanning electron microscopy (SEM), energy-dispersive X-ray analysis (EDX), electron diffraction, HREELS–STM elemental mapping, X-ray powder diffraction, and SQUID magnetometry. We noted that the formation of FeCo alloys occurs at relatively low pyrolytic temperatures (e.g., 650–750 °C). These single-crystal nanowires, which have not been reported hitherto, always exhibit the FeCo (110) plane parallel to the carbon nanotube axis. The FeCo nanomaterials have shown large coercive fields at room temperature (e.g., 900 Oe). We envisage that these aligned ferromagnetic nanowires could be used in the fabrication of high-density magnetic storage devices and magnetic composites.

Periodic arrays of ferromagnetic nanostructures could be used in the fabrication of high-density magnetic storage devices.[1] In the past, it has been demonstrated that Fe-filled carbon nanotubes exhibit large magnetic coercivities at room temperature (e.g., 430 Oe),[2] greater than those associated with Ni and Co nanowires.[3] However, FeCo alloy nanowires offer an attractive alternative for magnetic data storage since they could exhibit even larger coercive fields at room temperature.[4] Due to robustness, FeCo alloys are also useful for high-temperature magnetic applications (e.g., high-temperature space power systems,[5] wiring materials for audio and radio frequency transformers, magnetic bearings, magnetomechanical actuators, etc.). Nanowire arrays may have significant potential in magnetic data storage devices (quantized magnetic disks) due to their size and anisotropic behavior, which permits the use of smaller bit size (one per nanowire), thus increasing the attainable recording density.[6] In this communication, we describe the production and characterization of aligned MWNTs filled with monocrystalline FeCo nanoalloys. The preparation method involves the aerosol thermolysis of C_7H_8−$FeCp_2$−$CoCp_2$ solutions at temperatures ranging from 600 to 800 °C in an Ar atmosphere. The materials were characterized using HRTEM, EELS, SEM, EDX, XRD, and magnetometry. The FeCo materials exhibited large magnetic coercivities at room temperature (e.g., 928 Oe). Elemental mapping studies revealed homogeneous distributions of Fe and Co within the nanowires. To the best of our knowledge, the production of monocrystalline FeCo nanowires has never been previously reported. We believe that these FeCo nanomaterials could also be used in the fabrication of sensitive magnetic sensors and magnetic inks for xerography.

In the past, different groups have tried to produce $Fe_{(1-x)}Co_x$ nanowires of different stoichiometry. Most production methods were based on the use of templates such as

* Corresponding author. E-mail: mterrones@ipicyt.edu.mx.
[†] IPICYT.
[‡] Arizona State University.
[§] National Institute for Materials Science.
[||] ICYS.

10.1021/nl0479583 CCC: $30.25
Published on Web 01/28/2005

Available online at www.sciencedirect.com
SCIENCE DIRECT®
Chemical Physics Letters 410 (2005) 384–390
CHEMICAL PHYSICS LETTERS
www.elsevier.com/locate/cplett

Pyrolytic synthesis of long strands of large diameter single-walled carbon nanotubes at atmospheric pressure in the absence of sulphur and hydrogen

F. Lupo [a], J.A. Rodríguez-Manzo [b], A. Zamudio [b], A.L. Elías [b], Y.A. Kim [c], T. Hayashi [c], M. Muramatsu [c], R. Kamalakaran [a], H. Terrones [b], M. Endo [c], M. Rühle [a], M. Terrones [b,*]

[a] *Max-Planck-Institut für Metallforschung, Heisenbergstrasse 3, D-70569 Stuttgart, Germany*
[b] *Advanced Materials Department, IPICYT, Camino a la Presa San José 2055, Col. Lomas 4a. sección, San Luis Potosí 78216, México*
[c] *Faculty of Engineering, Shinshu University, 4-17-1 Wakasato, Nagano-shi 380-8553, Japan*

Received 15 April 2005; in final form 30 April 2005
Available online 22 June 2005

Abstract

We describe the synthesis of cm-long strands consisting of single-walled carbon nanotube ropes. The method involves the thermolysis of ferrocene ($FeCp_2$)–alcohol solutions under an Ar atmosphere at 800–950 °C. The tubes within strands could exhibit large diameters (2–3.5 nm OD) in high yields by either increasing the ferrocene concentration in the alcohol solution or by increasing the pyrolysis temperature. We noted that the nanotube material with the highest degree of crystallinity was produced at 950 °C, and as the ferrocene concentration in the alcohol solution increases (e.g., 1.2 wt%), the tubes tend to be metallic. This method appears to be simple, safer and more efficient than others reported in the literature because it does not require vacuum, sulphur agents, relatively high temperatures or large amounts of H_2.

1. Introduction

Carbon nanotubes (single- and multi-walled), considered as a novel form of nanocarbon [1,2], have been subject of extensive research for their possible applications due to their outstanding mechanical and electronic properties [3]. In particular, single-walled carbon nanotubes (SWNTs) could behave as metals or semiconductors depending on the tube diameter and chirality (the orientation of the hexagonal rings with respect to the tubule axis). Although SWNTs could now be produced using different methods [3], there is still no control over the chirality and diameter. Recent chemical methods have been able to separate semiconducting and metallic tubes [4,5]. However, it is important to improve the synthesis and control the tube dimensions and chirality. This account adds new insights into the production of SWNTs using a simple and less hazardous technique, able to synthesize nanotubes of large diameter exhibiting a larger proportion of metallic tubes.

Single-walled nanotubes are more attractive from the nanoscience point of view because they behave differently when compared to multi-walled carbon nanotubes (MWNTs). SWNTs exhibit quantum confinement along the single-atom-thin tubule circumference. However, their production appears to be more complicated when compared to that of MWNTs. Three main routes are now used to produce SWNTs: (1) arc discharge of graphite electrodes in the presence of metals (e.g., Ni, Co, Y), (2) laser ablation of graphite-metal targets,

* Corresponding author. Fax: +52 444 834 2040.
E-mail address: mterrones@ipicyt.edu.mx (M. Terrones).

0009-2614/$ - see front matter © 2005 Elsevier B.V. All rights reserved.
doi:10.1016/j.cplett.2005.05.116

Decorated nanotubes

DOI: 10.1002/smll.200500348

Efficient Anchoring of Silver Nanoparticles on N-Doped Carbon Nanotubes**

*Adalberto Zamudio, Ana L. Elías, Julio A. Rodríguez-Manzo, Florentino López-Urías, Geonel Rodríguez-Gattorno, Fabio Lupo, Manfred Rühle, David J. Smith, Humberto Terrones, David Díaz, and Mauricio Terrones**

Carbon nanotubes exhibit fascinating electronic and mechanical properties. Soon after their identification by Iijima,[1] carbon nanoscience developed rapidly and various experimental researchers started to confirm these unique properties.[2] In addition, carbon nanotubes (CNTs) can be used as catalytic supports, in which metal particles are anchored to the surfaces of the tubes. These coated tubes have also be employed as fast responsive sensors or templates for generating metallic nanowires.[3] In order to establish a uniform coverage of metal particles on the surfaces of pure carbon nanotubes, it is necessary to activate the graphitic surface of the tubes, which is extremely inert. Therefore, nanotube surfaces need to be functionalized using different acid treatments to create carboxylic (–COOH), carbonyl (–C=O) and hydroxyl (–OH) groups, that are able to link different metal clusters.[4] Unfortunately, these acid treatments reduce considerably the mechanical and electronic performance of the tubes due to the introduction of large numbers of defects. However, nitrogen-doped multi-walled carbon nanotubes (CN_xMWNTs) contain nitrogenated sites (substitutional and pyridinic nitrogen) that are chemically active. Therefore, it should be possible to avoid functionalization processes that use strong acid treatments, and attach metal particles onto the CN_xMWNTs.

In this account, we describe three different methods to anchor Ag nanoparticles (2–10 nm in diameter) on CN_xMWNTs using a chemical route that does not require any acid treatment. High-resolution transmission electron microscopy (HR-TEM) and scanning electron microscopy (SEM) images reveal uniform coverage of Ag nanoparticles (NPs) on the surfaces of the CN_xMWNTs. These small particles could be attached covalently via the nitrogenated groups located on the nanotube surfaces. It is important to mention that the Ag NPs attached to the CN_x nanotubes are able to withstand ultrasonic treatments. The new Ag–CN_x material could be used as bactericides, novel catalytic supports, sensors, and as nanoelectronic systems with enhanced electrical conductivity.

When nanotubes are coated with metals, wetting becomes an important issue. In this context, Dujardin, et al.[5] reported that it is possible to wet narrow-diameter multi-walled nanotubes (e.g., <20 nm outer diameter) when the surface tension of the metals is $<200\ mN\,m^{-1}$. Recently, it has been demonstrated that the performance of nanotube-based sensors could be improved if metal particles such as Pd and Al were anchored to the tubes.[6–8] Zhao and coworkers[8] calculated the effects of Al_{13} clusters deposited on the surface of nanotubes, and found a considerable increase of electronic states around the Fermi level. The latter could be related to an enhancement of the chemical reactivity on the tube surface. Therefore, these systems could be used to detect low concentrations of NH_3 molecules efficiently.[7]

Jiang et al.[9] activated the surface of CN_xMWNTs with a mixture of nitric and sulfuric acid. Subsequently, polyelectrolyte was added and adsorbed on the surfaces of the nanotubes by electrostatic interaction with the carboxylic sites. Gold particles were then successfully attached to the surfaces of the CN_xMWNTs. These reactive sites allowed a uniform deposition of Au clusters along the nanotubes.

This account reports a novel approach that allows Ag clusters to be anchored on the surfaces of CN_x nanotubes. The method does not require any acid treatment and promotes an attachment of Ag particles during the reduction of the metallic salts. We synthesized Ag NPs with different average diameters (2–10 nm) by the reduction of a silver/2-ethylhexanoate complex ([Ag-ethex]) or $AgNO_3$, in two different solvents (DMSO and DMF) using, in some cases, sodium citrate tribasic dihydrate ($Na_3Cit{\cdot}2\,H_2O$) as a stabilizer. Subsequently, CN_xMWNTs were added to the Ag NPs suspensions, which resulted in the generation of a uniform silver particle coating on the tube surfaces. It is important to note that when undoped nanotubes were mixed with these Ag suspensions, a poor coating of tubes was observed.

N-doped multi-walled carbon nanotubes were obtained by aerosol thermolysis of solutions of ferrocene in benzylamine ($PhCH_2NH_2$–$FeCp_2$) at 850 °C in an Ar atmosphere.[10] Pure carbon MWNTs were produced in a similar way but by using solutions of ferrocene in toluene (C_7H_8–

[*] A. Zamudio, A. L. Elías, J. A. Rodríguez-Manzo, Dr. F. López-Urías, Prof. H. Terrones, Prof. M. Terrones
Advanced Materials Department, IPICYT
Camino a la Presa San José 2055, Col. Lomas 4ª Sección
San Luis Potosí 78216 (Mexico)
Fax:(+444) 834-2040
E-mail: mterrones@ipicyt.edu.mx
Dr. G. Rodríguez-Gattorno, Dr. D. Díaz
Facultad de Química, Universidad Nacional Autónoma de México
Coyoacán, México DF, 04510 (Mexico)
Prof. D. J. Smith
Department of Physics and Astronomy and
Center for Solid State Science
Arizona State University, Tempe, AZ 85287-1504 (USA)
Dr. F. Lupo, Prof. M. Rühle
Max-Planck-Institut für Metallforschung
Heisenbergstrasse 3, 70569 Stuttgart (Germany)

[**] This work was also sponsored by CONACYT-México grants: E-43662-F (D.D.), 45762 (H.T.), 45772 (M.T.), 41464-Inter American Collaboration (M.T.), 42428-Inter American Collaboration (H.T.), 2004-01-013/SALUD-CONACYT (M.T.), PUE-2004-CO2-9 Fondo Mixto de Puebla and PhD Scholarships (A.Z., J.A.R.M., A.L.E.). We also thank the Max-Planck-Gesellschaft, DFG Grant No. Ru342/11-2, Nanocomp HPRN-CT-2000-00037 (F.L.) and NSF DMR-030342 (DJS) for financial support. The authors are also grateful to K. Hahn, D. Ramírez González, Grisel Ramírez Manzanares, and Lisette Noyola for technical assistance.

Available online at www.sciencedirect.com
SCIENCE DIRECT
Solid State Sciences 8 (2006) 303–320
Solid State Sciences
www.elsevier.com/locate/ssscie

Magnetism in Fe-based and carbon nanostructures: Theory and applications

H. Terrones, F. López-Urías, E. Muñoz-Sandoval, J.A. Rodríguez-Manzo, A. Zamudio, A.L. Elías, M. Terrones *

Advanced Materials Department, IPICYT, Camino a la Presa San José 2055, Col. Lomas 4ª Sección, San Luis Potosí 78216, Mexico

Available online 2 March 2006

Abstract

We demonstrate that it is possible to encapsulate ferromagnetic nanowires of Fe, FeCo and FeNi inside carbon nanotubes via chemical vapor deposition methods. These wires exhibit extremely high coercive fields when compared with the bulk phases. We review the state-of-the art characterization carried out on these novel wires and discuss the importance of having aligned arrays of carbon nanotubes filled with ferromagnetic materials, towards the development of novel magnetic storage devices. In this context, we will show from the experimental and theoretical stand points, that the wire shape, aspect ratio and inter-wire distances play a crucial role in the fabrication of novel storage components. In addition, we theoretically show that pure carbon nanostructures such as carbon nanotori, perforated fullerenes and nanoporous graphitic structures, exhibiting negative Gaussian curvature introduced by the presence of non-hexagonal rings, behave as strong paramagnets experiencing large magnetic moments when an external magnetic field is applied. The latter results could explain some of the magnetic properties observed experimentally in carbon nanofoams and polymerized C_{60} phases. We envisage that magnetism in different families of nanostructures will be playing a key role in the development of emerging technologies in the present century.

1. Introduction

Undoubtedly, the most fruitful technological advances and outstanding scientific research achievements took place during the last century. Carbon science has also advanced very rapidly. For example, the structural identification of crystalline graphite by J.D. Bernal in 1924, subsequent developments of carbon alloys such as spheroidal graphite (SG) cast iron in the 1940s and the development of carbon fibers in the 1950s. However, in the mid-1980s the discovery of a third carbon allotrope, Buckminsterfullerene (C_{60}), by Kroto, Curl, Smalley, and co-workers initiated a novel field now known as carbon nanoscience and nanotechnology. In the early 1990s, elongated cage-like carbon structures (known as nanotubes) were identified. This achievement provided a significant impetus related to the synthesis of carbon and ferromagnetic nanostructures that will be certainly involved in the development of novel electronic and material technologies.

Since carbon nanotubes consist of hollow cylinders (either individual or concentric), it is possible to introduce metals inside their core. In 1992, it was predicted [1] that open nanotubes might act as 'molecular straws' capable of absorbing dipolar molecules by capillary action. In this context, it is clear that the introduction of 'foreign' materials, such as metals, their carbides, oxides and even proteins is possible and may alter significantly their conducting, electronic or mechanical behavior.

During the last decade, it was demonstrated that the thermolysis of organic precursors over Co and Ni substrates [2,3], or organometallic compounds containing Fe [4,5], leads to multiwalled carbon nanotubes (MWNTs) filled with these metals (Fig. 1). For example, Fe nanowires encapsulated by carbon nanotubes exhibit high magnetic coercivities (e.g., 430–2100 Oe) when compared to the bulk phase (e.g., 60 Oe). Therefore, these nanowires could have important implications in the development of quantized magnetic disks using arrays of aligned carbon nanotubes filled with Fe [6]. The novel disks would permit the use of a smaller bit size (one per nanowire; Fig. 2), thus increasing the attainable recording density. Film structures of this kind, based on single-domain elements, could exhibit the best available storage densities (e.g., 65 Gb/in^2) [7]. However, theoretical and experimental studies related to

* Corresponding author. Tel.: +52 (444) 834 2039; Fax: +52 (444) 834 2040.
E-mail address: mterrones@ipicyt.edu.mx (M. Terrones).

1293-2558/$ – see front matter
doi:10.1016/j.solidstatesciences.2006.02.006

Available online at www.sciencedirect.com
SCIENCE DIRECT®
Chemical Physics Letters 424 (2006) 345–352
CHEMICAL PHYSICS LETTERS
www.elsevier.com/locate/cplett

Synthesis and characterization of long strands of nitrogen-doped single-walled carbon nanotubes

F. Villalpando-Paez [a], A. Zamudio [e], A.L. Elias [e], H. Son [b], E.B. Barros [f], S.G. Chou [d], Y.A. Kim [a], H. Muramatsu [g], T. Hayashi [g], J. Kong [b], H. Terrones [e], G. Dresselhaus [b], M. Endo [g], M. Terrones [e,*], M.S. Dresselhaus [b,c]

[a] *Department of Materials Science, Massachusetts Institute of Technology, Cambridge, MA 02139-4307, USA*
[b] *Department of Electrical Engineering and Computer Science, Massachusetts Institute of Technology, Cambridge, MA 02139-4307, USA*
[c] *Department of Physics, Massachusetts Institute of Technology, Cambridge, MA 02139-4307, USA*
[d] *Department of Chemistry, Massachusetts Institute of Technology, Cambridge, MA 02139-4307, USA*
[e] *Advanced Materials Department, IPICYT, San Luis Potosí 78216, Mexico*
[f] *Department of Physics, Universidade Federal do Ceara, Fortaleza 60455-760, Brazil*
[g] *Faculty of Engineering, Shinshu University 4-17-1 Wakasato, Nagano-shi 380-8553, Japan*

Received 21 March 2006; in final form 13 April 2006
Available online 29 April 2006

Abstract

We describe the synthesis of N-doped single-walled carbon nanotubes (N-SWNTs), that agglomerate in bundles and form long strands (<10 cm), via the thermal decomposition of ferrocene/ethanol/benzylamine (FEB) solutions in an Ar atmosphere at 950 °C. The amount of benzylamine in the solution was varied from 0% to 26% by weight. Using Raman spectroscopy, we noted that as the N content is increased in the starting FEB solution, the growth of large diameter tubes is inhibited. We observed that the relative electrical conductivity of the strands increases with increasing nitrogen concentration. Thermogravimetric analysis (TGA) showed novel features for highly doped tubes that are related to chemical reactions on N sites.

1. Introduction

Carbon nanotubes are well known for their exceptional mechanical and electrical properties. Since their identification by Iijima [1] in 1991, researchers have conducted numerous experiments and simulations aimed at understanding their intrinsic characteristics. However, most of the work has involved pure carbon nanotubes. When a foreign atom is inserted in the nanotube lattice, the nanotube symmetry is altered and its structure and properties consequently change [2]. This was first confirmed experimentally by Stephan et al. [3] by the successful doping of carbon nanotubes with boron and nitrogen using arc discharge methods. Boron [4–7] and nitrogen [8–14] atoms are the most conveniently used dopants, and because of their small atomic size, they have a reasonable probability to enter the nanotubes lattice. Boron and nitrogen, respectively, serve as p- or n-type dopants to nanotubes. Nevertheless, other elements like cobalt [15], potassium [16], silicon [17], phosphorous [18] and oxygen [19], may also be able to 'dope' the tubes and to modify their properties.

If carbon nanotubes are to be used as future building blocks in nanocomposites and nanoelectronic devices, it is imperative to fine tune their wall reactivity, mechanical strength and electronic band gap by controlling the amount of foreign atoms inserted into the tube lattices. In the semiconductor industry, the synthesis of p- and n-type materials is crucial. Therefore, from an applications standpoint, it is important to be able to carefully control the insertion of different dopants into nanotubes.

* Corresponding author.
E-mail address: mterrones@ipicyt.edu.mx (M. Terrones).

0009-2614/$ - see front matter © 2006 Elsevier B.V. All rights reserved.
doi:10.1016/j.cplett.2006.04.074

NANO LETTERS

xxxx
Vol. 0, No. 0
A−H

Biocompatibility and Toxicological Studies of Carbon Nanotubes Doped with Nitrogen

J. C. Carrero-Sánchez,† A. L. Elías,‡ R. Mancilla,† G. Arrellín,† H. Terrones,‡ J. P. Laclette,*,† and M. Terrones*,‡

Instituto de Investigaciones Biomédicas, Universidad Nacional Autónoma de México, Cd. Universitaria, 04510, México, D.F., and Advanced Materials Department, IPICYT, Camino a la Presa San José 2055, San Luis Potosí 78216, México

Received March 10, 2006; Revised Manuscript Received June 7, 2006

ABSTRACT

In this report, we compare the toxicological effects between pure carbon multiwalled nanotubes (MWNTs) and N-doped multiwalled carbon (CN_x) nanotubes. Different doses of tubes were administered in various ways to mice: nasal, oral, intratracheal, and intraperitoneal. We have found that when MWNTs were injected into the mice's trachea, the mice could die by dyspnea depending on the MWNTs doses. However, CN_x nanotubes never caused the death of any mouse. We always found that CN_x nanotubes were far more tolerated by the mice when compared to MWNTs. Extremely high concentrations of CN_x nanotubes administrated directly into the mice's trachea only induced granulomatous inflammatory responses. Importantly, all other routes of administration did not induce signs of distress or tissue changes on any treated mouse. We therefore believe that CN_x nanotubes are less harmful than MWNTs or SWNTs and might be more advantageous for bioapplications.

Carbon nanoscience and technology has developed very rapidly over the past decade following the identification[1,2] and bulk production[3,4] of carbon nanotubes. Because of the remarkable mechanical, thermal, and electronic properties of carbon nanotubes,[5] numerous applications have been conceived. For example, carbon nanotubes could be used as gas sensors,[6,7] field-emission sources,[8] polymer composite fillers,[9] protein immobilizers,[10] filters,[11] electronic components,[5,8] and so forth. However, a crucial issue, which needs to be addressed before nanotube-based components are commercially available, is toxicity. If nanotubes are used in novel products, then they are likely to get in contact with the human body through the skin and ocular surfaces and access the inner organs through the respiratory and digestive tracts. During manufacture, carbon nanotubes may enter the respiratory airways of the workers, and accumulate in the lungs. If nanotubes are used as fillers in food packaging products, then they could reach the stomach and intestines of the consumers. If cosmetics and bio-filters are developed using nanotubes, then they will certainly get in contact with human skin. Therefore, additional toxicological studies of these carbon nanomaterials need to be carried out. Previous reports have demonstrated that intratracheal injection of single-walled carbon nanotubes (SWNTs) results in the death of the treated rats[12] and mice,[13] suggesting that they could be hazardous to humans. However, no information is available on the toxicity of multiwalled carbon nanotubes doped with nitrogen (CN_x MWNTs); these tubes have demonstrated to have numerous potential applications.[14−20] In this report, we compare the toxicological effects of two different types of carbon nanotubes, namely, MWNTs and N-doped multiwalled carbon (CN_x) nanotubes. The tubes were administered in different ways to mice: nasal, oral, intratracheal, and intraperitoneal. We have found that MWNTs injected into the mouse's trachea induce severe granulomatous inflammatory responses. Undoped MWNTs also caused the obstruction of small and medium-size bronchioles and damaged the bronchiolar wall that resulted in lung inflammation. However, CN_x nanotubes were far more tolerated by the mice when compared to MWNTs. In particular, intratracheal injection of up to 5 mg/kg of CN_x tubes neither caused the death of the mice nor induced visible signs of distress on the animals, in contrast to the lethal effects of similar doses of MWNTs or SWNTs[12,13] administered to mice or rats through the same route. All other routes of administration of CN_x and MWNTs did not induce signs of distress or tissue changes on the treated mice. We envisage that CN_x nanotubes could be more biocompatible when compared to MWNTs or SWNTs and might be more advantageous for practical applications.

* To whom correspondence should be addressed. E-mail: laclette@biomedicas.unam.mx; mterrones@ipicyt.edu.mx.
† Instituto de Investigaciones Biomédicas, Universidad Nacional Autónoma de México.
‡ Advanced Materials Department, IPICYT.

10.1021/nl060548p CCC: $33.50
Published on Web 07/07/2006